UNIVERSITÀ DEGLI STUDI DI PAVIA

DOTTORATO IN SCIENZE CHIMICHE E FARMACEUTICHE

XXIX CICLO

CHIRAL COPPER COMPLEXES AS TYROSINASE BIOMIMETIC SYSTEMS

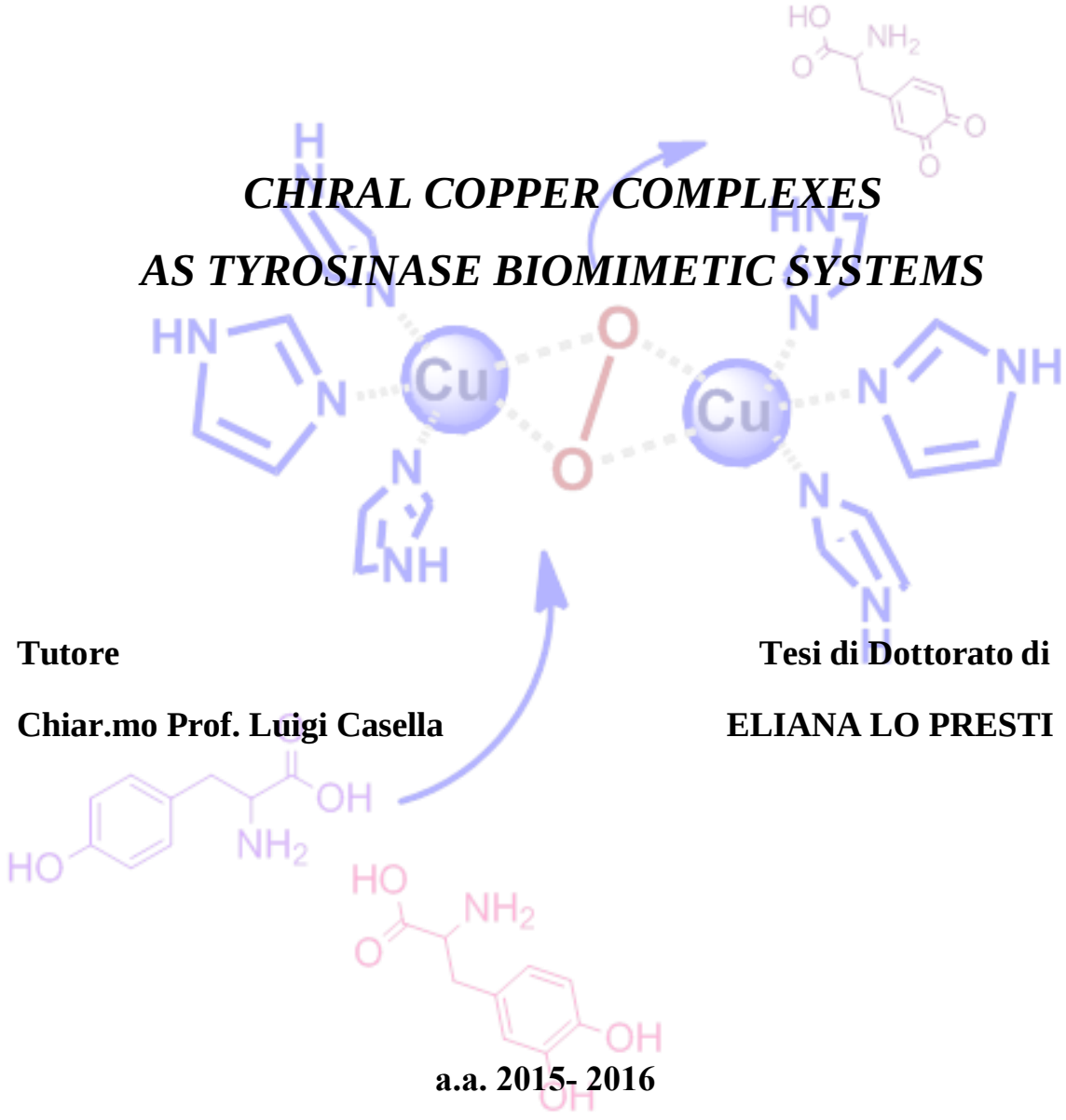

Tutore

Chiar.mo Prof. Luigi Casella

Tesi di Dottorato di

ELIANA LO PRESTI

a.a. 2015- 2016

UNIVERSITÀ DEGLI STUDI DI PAVIA

DOTTORATO IN SCIENZE CHIMICHE E FARMACEUTICHE

XXIX CICLO

Coordinatore: Chiar.mo Prof. Mauro Freccero

CHIRAL COPPER COMPLEXES AS TYROSINASE BIOMIMETIC SYSTEMS

Tutore

Chiar.mo Prof. Luigi Casella

Tesi di Dottorato di

ELIANA LO PRESTI

a.a. 2015- 2016

Index

Chapter 1. Introduction

1. Introduction

The oxidation of different kinds of C-H bonds represents a continuous challenge in organic chemistry. From the industrial point of view, catalytic oxidation reactions are fundamental for the transformation of petroleum stocks to exploitable source of energy or other higher oxidation state molecules (alcohols, aldehydes, carboxylic acids, etc...). Common trend is to use oxygen as primary oxidant, because of its large availability and reduced cost and toxicity. In the majority of cases, however, fine chemistry preferred to carry out oxidation reactions with the stoichiometric use of hazardous reagent, such as dichromate, permanganate or other heavy metals, whose waste are difficult to dispose. This expensive and environmental non-friendly approach is going, however, to be replaced by a more atom-economic approach. The use of catalysts in oxidation reactions could act both on the *E*-factor (waste per kg of product) and on the disposal of waste, as the reusability of the catalyst itself decreases this problem. Catalysis, as a young and partially explored field, suffers of different problems. Many catalytic reactions are not as efficient as the traditional counterparts and in many cases expensive and toxic metals are required (platinum, rhodium, palladium, etc...). Catalytic oxidations can be classified in three main categories. Catalytic oxygen transfer reactions are those in which an oxygen molecule reacts with the substrate, supported by the presence of a metal catalyst. In free radical oxidation, instead, the chain reactions are initiated by the

radical decomposition of alkyl hydroperoxides. The third category includes oxidations of substrates coordinated by a metal ion, in which the initial form of the catalyst is in many cases regenerated with the participation of dioxygen. In billion years of evolution, Nature has developed enviable and extremely efficient catalysts for different reactions, the enzymes. Enzymatic reactions benefit of both high efficiency and regio- and stereo-selectivity and from here starts the interest of chemists to implement these characteristics in non-natural reactions. Natural selection brought to simplify as much as possible the architecture of these systems, and made the choice of using the most available elements. In the enzymes whose active site includes metal ions, the commonly found metals are same of the commonly available in Nature, for example iron, zinc and copper. Iron and copper in particular offer a variety of accessible and less common oxidation states, that make them very good candidates for oxidation reactions. Enzymes represent a valid alternative to traditional organic synthetic methods and a convenient solution to problems related to oxidation reactions. Dioxygen is the most common oxidation source in Nature, and in biological systems it is mainly transported by protein or managed by enzymes. Many copper-containing enzymes belongs to the class of oxidation enzymes and can be distinguished by the mechanism of interaction with dioxygen.

Due to their exquisite selectivity in oxidation reactions, many metal enzymes start to become a favorite source of inspiration for bioinorganic chemists who wanted to translate this natural efficiency to smaller synthetic compounds.[1] In the last three decades the investigation of the role of metals in biological systems provided deeper knowledge, elucidating the role and mechanisms in which they are employed. From this starting point, many efforts have focused on devising synthetic analogues of the active site of these metal enzymes, capable to activate molecular oxygen (Figure 1.1). In the field of copper enzymes, due to their interesting activity, many enzymes represent a continuous source of inspiration for bioinorganic chemists.

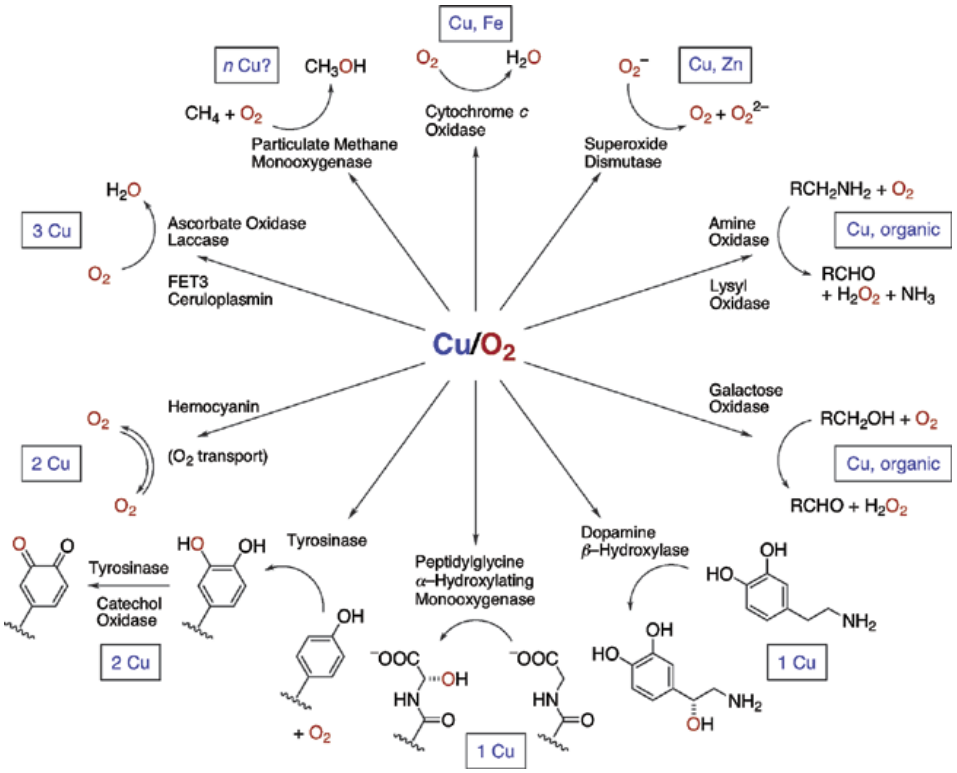

Figure 1.1- Examples of oxygen-activation and transport promoted by copper-containing proteins and enzymes.

1.1. Copper oxygenases

Oxygenase enzymes, belonging to the class of oxidoreductases, include enzymes that can transfer an oxygen atom from molecular oxygen to a substrate. There are two main types of oxygenases:

1) Monoxygenases, also known as mixed function oxidases, that transfer one oxygen atom to the substrate, while the other is reduced to water.

2) Dioxygenases, or oxygen transferases, that incorporate both oxygen atoms of dioxygen into the initial substrate to obtain the product.

1.1.1. Monoxygenases: Dopamine β-hydroxylase (DBH)

Dopamine β-hydroxylase, also known as dopamine monoxygenase is the enzyme involved in the biosynthesis of noradrenaline from dopamine.[2]

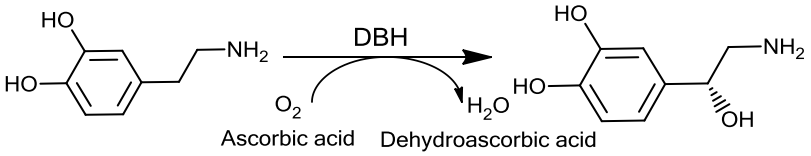

Scheme 1.1- Benzylic hydroxylation of dopamine to obtain norepinephrine, promoted by DBH.

DBH is a glycoprotein that requires ascorbic acid as cofactor to exercise its function. The active site of DBH, one per subunits of enzyme, consists of a type 2 copper site in which one copper ion (Cu_H) is coordinated to three histidine residues, while the second one (Cu_M) is coordinated to two histidine and a methionine. These two copper centers do not act in the same way. From spectroscopic studies and structural studies on PHM catalytic core, which shows high sequence homology with DBH catalytic core, it was possible to elucidate that Cu_M is the copper site implicated in the binding of dioxygen, while Cu_H is the site of electron transfer from ascorbate.

DBH is a membrane-bound enzyme, so norepinephrine is the only neurotransmitter that is synthesized inside vesicles. Due to its the peculiar position, DBH structure has only been recently solved.

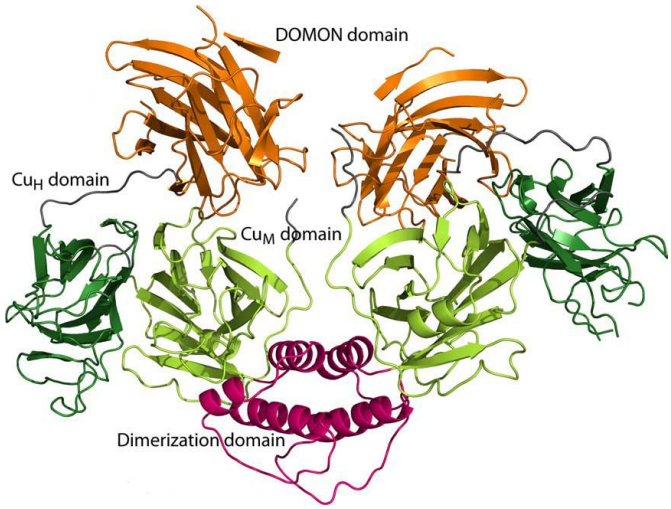

Figure 1.2- Crystal structure of human DBH, adapted from [2]

1.1.1.1. Dopamine β-hydroxylase biomimetic systems

The activation of the benzylic position of dopamine promoted by DBH has aroused the interest of many research groups. The group of Réglier, for example, studied the

benzylic oxygenation of 2-aminoindane derivatives, compared with the oxidation performed by DBH (Scheme 1.2).[3]

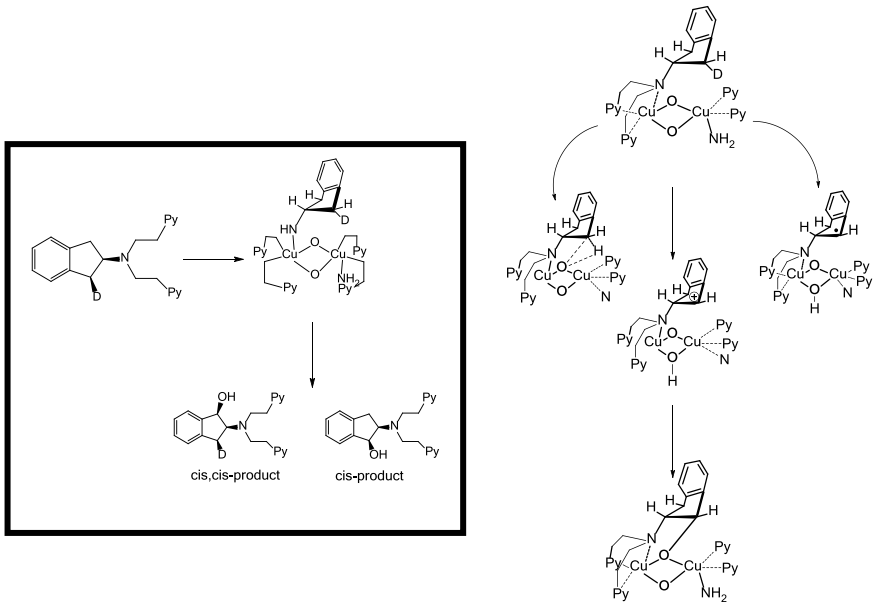

Scheme 1.2-Left: kinetic isotope effect on oxidation of 2-aminoindane derivtives; Right: oxidation of 2-aminoindane derivatives promoted by Règlier's biomimetic system, adapted from [3].

Règlier and coworkers demonstrated, differentiating the benzylic positions by labeling with deuterium (Scheme 1.2-left), that the reaction occurs following a stereospecific pathway with retention of configuration and a deuterium kinetic isotope effect was also determined. In both enzymatic and biomimetic reactions, a radical two-step process was involved.

1.1.2. Monoxygenases: Peptidylglycine α-amidating monooxygenase (PAM)

PAM is a bifunctional enzyme, as it mediates first the hydroxylation of the C-terminal glycine extended pro-hormone, followed by a N-C cleavage to give the active form of the hormone and glyoxylic acid as byproduct.[4]

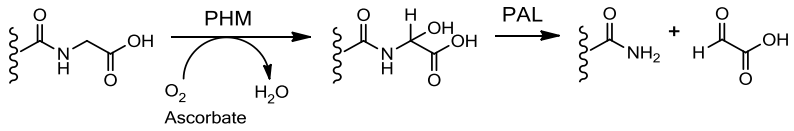

Scheme 1.3.-Enzymatic mechanism of peptidylglycine α-amidating monooxygenase. The first step is promoted by the pure monoxygenase domain PHM, while the N-C cleavage is mediate by the lyase PAL moiety.[4]

PAM has two well defined and distinguished domains, responsible of the double activity of this enzyme, PHM and PAL. PHM is responsible of the hydroxylation step of the C-terminal glycine extended pro-hormone, while PAL acts as lyase enzyme and catalyzes the C-N cleavage to give the active hormone in the amide form. The hydroxylation reaction, promoted by PHM, is a two-electron oxidation of the substrate, coupled to the reduction to water of one oxygen atom, while the second atom is incorporated in the substrate. This behavior makes only the PHM moiety acting like a monooxygenase. The reaction is accomplished by the presence of ascorbate; two of the electrons for the O_2 reduction, in fact, come from the substrate while the the second pair is provided by ascorbate, converted to dehydroascorbate. The active site of PHM consists of a type 2 copper complex; the not-coupled dinuclear site presents a solvent-accessible 11 Å cleft, that seems to play a fundamental role in the enzymatic turnover.

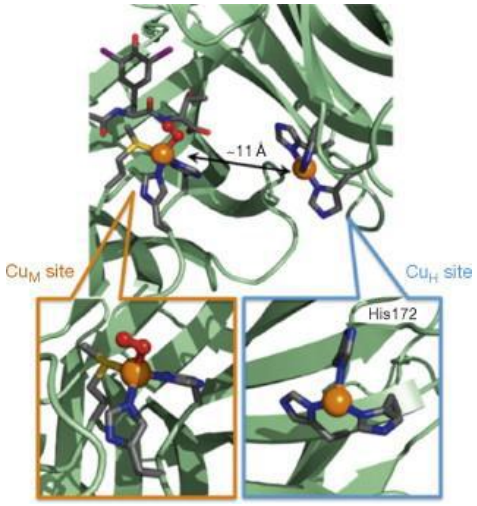

Figure 1.3- The active site of PHM. Bottom left: The Cu_M site exhibiting dioxygen binding in an end-on fashion. Bottom right: Expanded view of the electron-transfer Cu_H site (PDB code: 1SDW).

As in DBH, in PHM the copper sites are differentiated for both coordination surrounding and activity. Cu_H is the copper ion deputed to electron transfer, receiving the two electrons from ascorbate oxidation, while Cu_M is the moiety responsible for dioxygen binding. Cu_H is surrounded by two or three histidine residues, while Cu_M is bound to two hisidines, a methionine and a molecule of water. The potential role of methionine is to accommodate the change of oxidation state of copper during the catalytic cycle, stabilizing the reduced form of the metal and preventing from copper lost. In support of this hypothesis, studies identified a reduction of the distance Cu-S_{Met} from 2.4 Å to 2.24 Å, accompanied by the loss of the coordinated water. Relevant insight on the nature of the reactive oxygen species implicated in PHM catalytic cycle has been recently achieved by the resolution of a crystal structure obtained by Amzel's group. The dioxygen-derived species, most likely superoxide, is bound to the Cu_M site in an end-on fashion, with a Cu-O-O angle of 110° and a O-O distance of 1.23 Å. Regarding the nature of the species directly responsible for the oxidation, the commonly accepted hypothesis has been formulated by Klinman.[5]

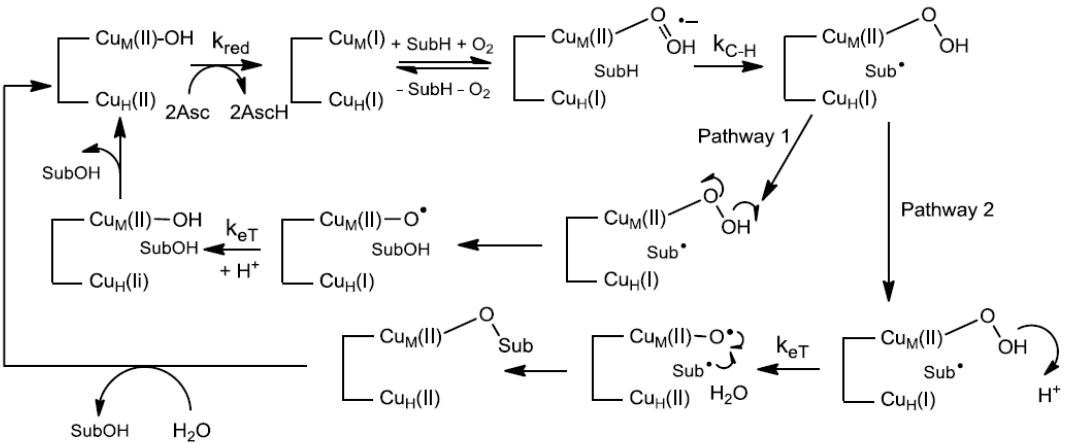

Scheme 1.4- Mechanism of PHM proposed by Klinman[5]

Klinman proposed a hydrogen-atom abstraction/transfer (HAT), followed by a double pathway mechanism that implicate either an hydroxyl transfer to form the product, followed by the electron transfer, or an electron transfer with subsequent protonation and heterolytic cleavage of O-O bond, followed by the radical coupling reaction of the substrate with a Cu-O species.

1.1.2.1. PHM bioinspired systems

Regio- and stereoselective oxidation of C-H bonds represents an appealing goal for bioinorganic chemists, so several attempts to mimic the activity of enzymes which perform selective C-H functionalization were done. Synthetic small molecules able to activate oxygen can provide interesting information about the Cu/O_2 intermediates involved in the enzymatic catalytic cycle (Cu(II)-O_2, Cu(II)-OOH, or high valent copper(III)-oxo complexes). Only few synthetic models were found to be able to replicate PHM activity (Scheme 1.5).[6,7,8,9,10]

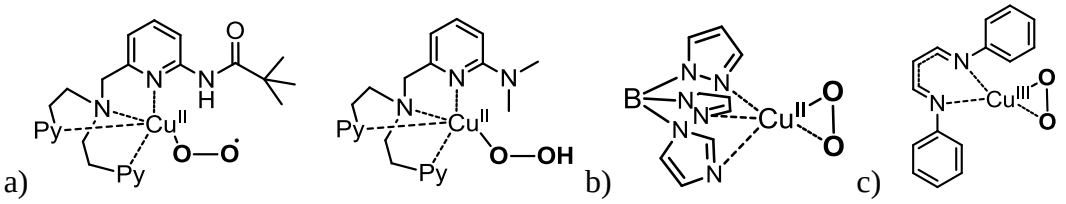

Scheme 1.5- Biomimetic systems for PHM enzyme as peroxo-(c), superoxo- (b), hydroperoxo-copper species (a).

Fujisawa et al. [7] characterized a superoxo-Cu complex with dioxygen bound in a side-on fashion, exploiting an anionic tris(pyrazolyl)borate ligand (Scheme 1.5-b), that was found to oxidize ethylbenzene (99 % of yield) in presence of tert-butylhydroperoxide as radical initiator and O_2 as oxidizing agent.

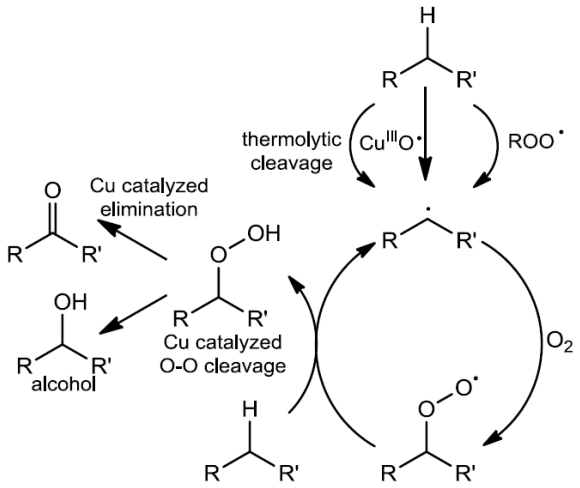

Scheme 1.6- General proposed mechanism for alkane oxidation

The catalytic cycle is initiated by hydrogen abstraction promoted by the superoxo complex, generating an alkylic radical, which reacting with molecular dioxygen provide the peroxo-alkylic radical species. In the propagation reaction, the highly-reactive alkyl-peroxide extracts an hydrogen atom from another alkane, to give the hydroperoxide intermediate that can follow the Cu-catalyzed elimination way to give the ketone or undergo O-O bound scission to provide the alcoholic product (Scheme 1.6). Similar conditions were tested on cyclohexane, whose oxidation products are important intermediate in caprolactame synthesis, providing 2-cyclohexan-1-one and 2-cyclohexane-1-ol with 87 % of yield in mild condition.[8] This oxygen mediated procedure could represent an efficient alternative to commercial processes, as the normally used harsh conditions compromize regioselevtivity, also providing over-oxidation products and peroxidic by-products. By the way, nowadays, a stereo-controlled C-H functionalization under mild conditions represents a challenge, although few copper catalysts were found to provide both good conversion and high selectivity.[11,12,13,14]

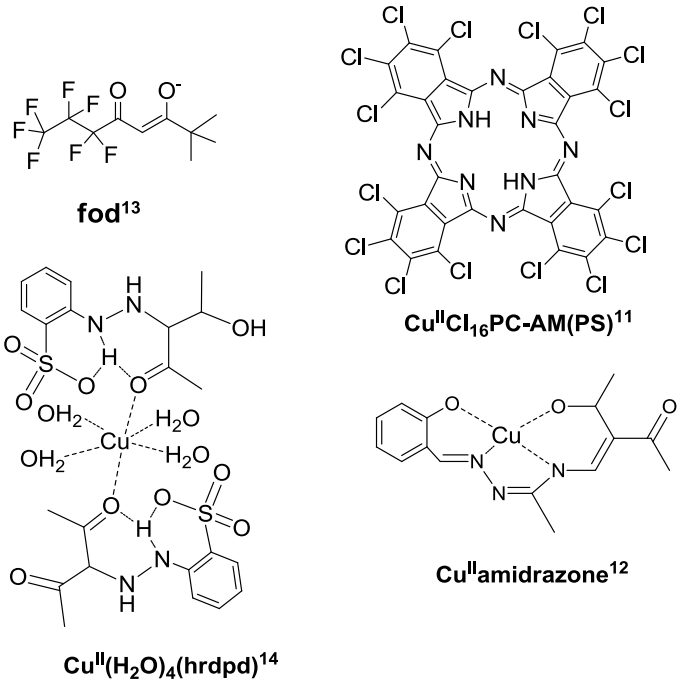

Scheme 1.7- Series of efficient mononuclear copper complexes for C-H oxidation promoted by oxygen.

1.1.3. Monoxygenases: Galactose oxidase

Galactose oxidase (GAO) is the enzyme responsible for catalyzing the stereospecific oxidation of a wide range of primary alcohols to aldehydes, coupled with the reduction of molecular oxygen to hydrogen peroxide.[15] It is an extracellular enzyme, secreted by the *Dactylium dendroides*, and it possesses a peculiar mononuclear copper site that catalyze the two electron transfer reaction during the oxidation. In the active site of galactose oxidase, copper is coordinated to two tyrosine (Tyr 272 and Tyr 496) and two histidines (His 496 and His 581), while a fifth coordination position is occupied by a molecule of water (Figure 1.4). X-ray data are limited to the inactive form of the enzyme, and show a trigonal bipyramidal geometry, with the long axis aligned with the coordinated solvent molecule. The catalytic activity, as alcohol oxidation ad oxygen reduction are both two-electron processes, could be interpreted as dihydrogen transfer. In biological systems, this kind of transfer involves a cofactor, such as flavines or nicotinamides. Galactose oxidase does not contain any of these cofactors and utilizes a free radical-coupled copper complex to perform the reaction.[16] The crystal structure at 1.7 Å resolution, reported by Ito et al.[15a] elucidates interesting and unique features of the active site. Tyr 272, directly implicated in the coordination of copper, was found to be bound to the sulphur atom of Cys 228. This peculiar bond seems to have the character of a partial double bond, extending the aromatic system, as the C_β of cysteine lies on the same plan of the tyrosine aromatic ring. This post-translational modification identifies the real redox-active site in the protein, as it forms a stabilized free radical upon oxidation in mild conditions. Further stabilization of the free radical complex may come from the outer sphere tryptophan residue (W290), that perhaps shields the Tyr-Cys dimer from interaction with the solvent.

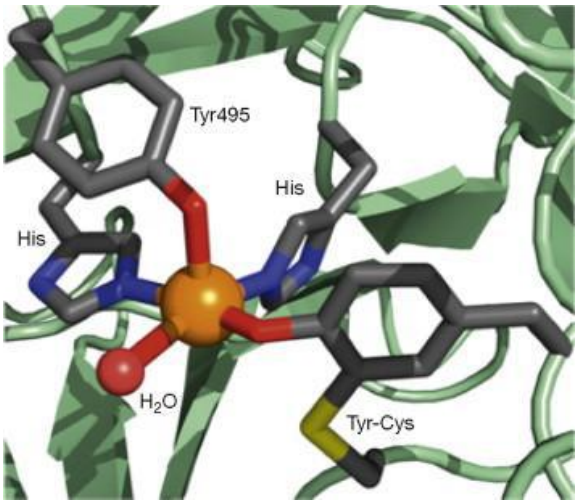

Figure 1.4- X-ray structure of GAO active site in its inactive form. Copper(II) coordination to the Tyr-Cys cofactor is highlighted in the figure.

The catalytic reaction can be formally divided into two separated reduction and reoxidation reactions, consistent with a ping-pong mechanism (Scheme 1.8). The reduction step involves the reaction of the free radical-Cu^{2+} complex with the primary alcohol (the process is governated by k_{red} as rate constant) to give the aldehyde. In the second step, the reduced form reacts with dioxygen to generate the metal-radical complex accompanied by the formation of hydrogen peroxide (k_{ox} is the rate constant).

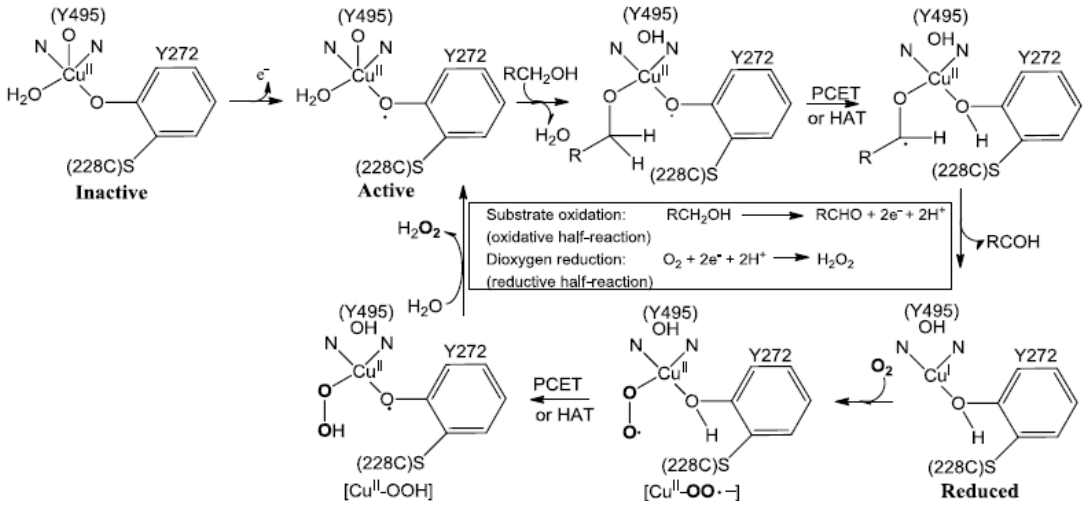

Scheme 1.8- Schematic representation of the overall catalytic process governed by GAO.

Resolution of the X-ray structure of the inactive form of galactose-oxidase shows the active site consisting of a mononuclear copper complex, in which the copper ion is

coordinated to two histidine residues, two tyrosines and an exogenous water molecule, to give a square pyramidal complex. A key factor in this structure is represented by the thioether crosslink between Tyr and Cys. In accord with the mechanism proposed in Scheme 1.8, in the active form of GAO, Tyr272 is oxidized to generate a Cu-phenoxyl radical species, responsible for alcohol oxidation in the oxidative half-step of the catalysis. In the reduction half-step, instead, a Cu-OO• is generated by binding of Cu(I) to O_2 and this intermediate provide hydrogen abstraction from the tyrosyl-hydroxyl group of Tyr-Cys cofactor, to give a Cu(II)-OOH plus tyrosyl radical. Release of H_2O_2 and proton transfer from the axial Tyr-OH to the Cu(II)-OOH regenerates the Cu(II)-tyrosyl radical moiety.

1.1.3.1. Galactose oxidase biomimetic systems- Alcohol oxidation

Studies of alcohol oxidation with molecular oxygen as oxidant, combined with the possibility to have further insight in the mechanism of GAO, inspired the synthesis of biomimetic analogues. Copper-catalyzed alcohol oxidation pathways can be summarized in four different main paradigms, differentiated by the hydrogen abstraction mechanism.

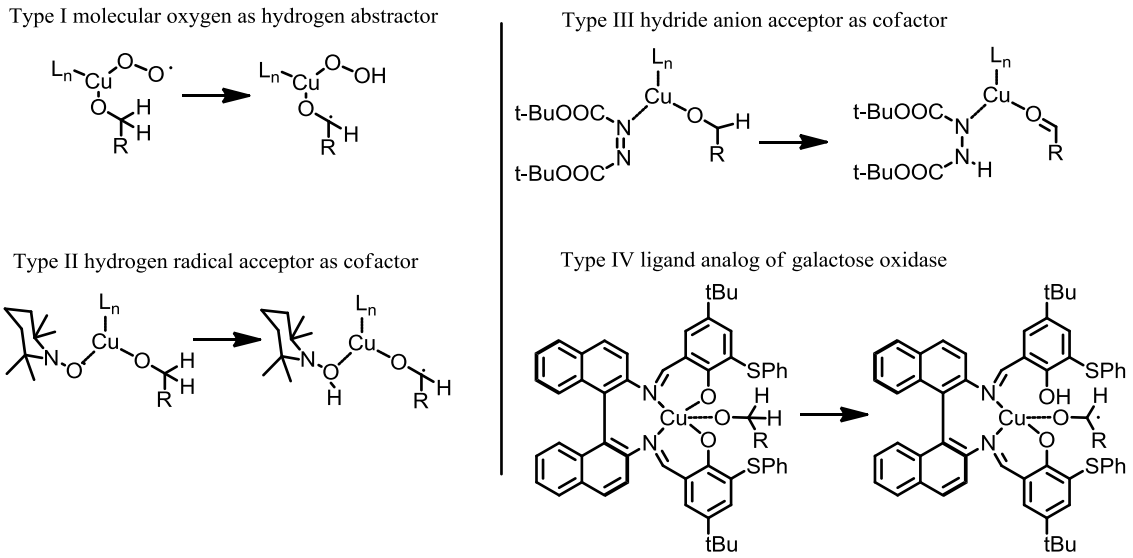

Figure 1.5- Four proposed mechanisms for hydrogen abstraction promoted by GAO biomimetic systems.

In Type I mechanism, Cu-coordinated molecular oxygen abstracts hydrogen atom from the coordinated alcohol, but the absence of co-oxidant implies the reaction conditions to

be forced, causing over-oxidation in many cases.[17] Mechanism II, proposed by Semmelhack,[18] exploits a radical acceptor (TEMPO) to provide hydrogen abstraction, while mechanism III, pioneered by Markò,[19] involves hydride acceptor as co-factor. Type IV mechanism is the most related to GAO activity, as the hydroxyl radical for hydrogen abstraction is provided by the ligand itself. Impressive functional group tolerance in many alcohol oxidation was found. The use of chiral ligand for homogenous copper catalysts can also provide interesting results in discriminating alcohol oxidation. For example, $Cu(OTf)_2$ coordinated to BINAM ligand, using TEMPO as co-factor exhibits capability in kinetic resolution of diaryl methanol, enantio-enriching the starting alcohol (Scheme 1.9).[20]

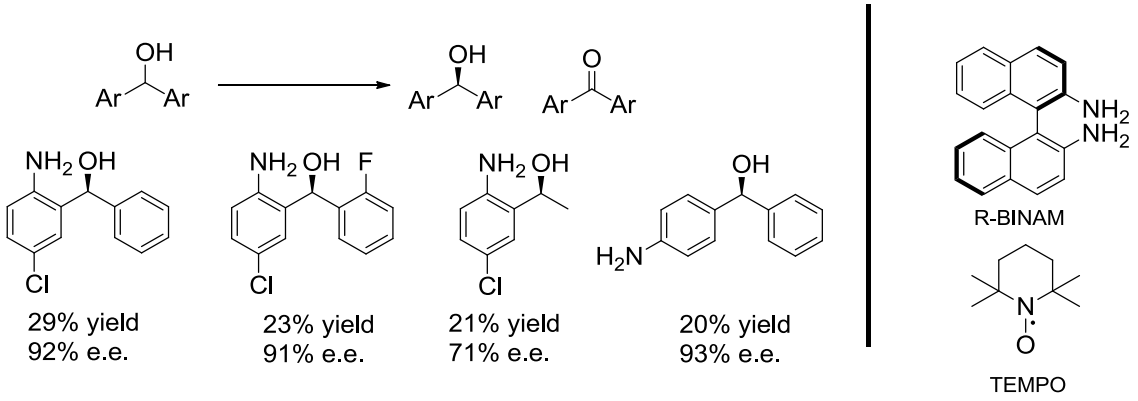

Scheme 1.9- Kinetic resolution mechanism of diaryl alcohols promoted by homogeneous Cu-BINAM complex in presence of TEMPO as radicalic co-factor.

1.1.4. Monoxygenases: Tyrosinase

Melanin is a biopolymer ubiquitously diffused in animal and vegetal world, and involved in all kinds of biological pigmentation processes, from the color of hair to the browning of fruits. It exerts also a role of protection from UV and ionizing radiation, quenching potential by harmful reactive oxygen species.

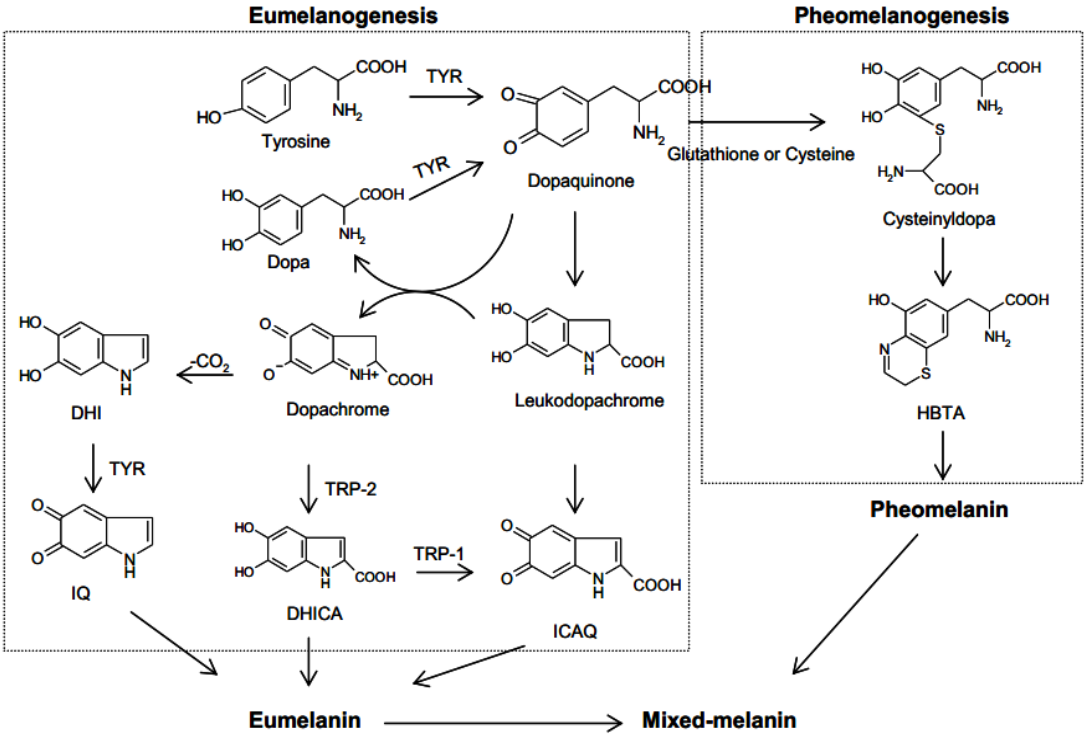

Scheme 1.10- Melanogenesis pathway, initiated by tyrosinase and followed by non-enzymatic polymerization.

Tyrosinase is the enzyme responsible for the initial step of melanogenesis, as it catalyzes the oxidation of both L-dopa and L-tyrosine to L-dopaquinone.[21] This peculiar type 3 copper enzyme is so able to perform two types of activity, the two electron oxidation of a catechol to *ortho*-quinone (catecholase activity) and an oxygen atom insertion into the aromatic C-H bond of a phenol, with subsequent oxidation to give the *ortho*-quinone (monophenolase activity).[22] Oxygen-labeling studies by Mason indicated that the oxygen atom incorporated into L-DOPAquinone originates from dioxygen.[23] Quinones, due to their intrinsic high reactivity, undergo an intramolecular Micheal-addition reaction to generate cycloDOPA. CycloDOPA is then oxidized by another molecule of L-DOPAquinone, to give DOPAchrome, which decomposes preferentially into 5,6-dihydroxyindole (DHI), *via* decarboxylation, or to 5,6-dihydroxyindole-2-carboxylic acid (DHICA) *via* tautomerization. These two dihydroxyindoles are then oxidized enzymatically by tyrosinase, or catechol oxidase, or nonenzymatically by L-DOPAquinone before autopolymerizing, forming eumelanin (Mason-Raper pathway). Eumelanin represents the most significant part of natural melanins, while pheomelanin are much less abundant. Pheomelanin derives from intermolecular Michael addition of cysteine to DOPAquinone, giving cysteinyl-DOPA derivatives, which after oxidation by

another molecule of DOPAquinone generate cyclic benzothiazine, that subsequently follows a polymerization chain to generate pheomelanin. The active site of type 3 enzymes (tyrosinase, catechol oxidase and hemocyanin) consists of a dinuclear copper complex in which each copper ion is coordinated to three histidine residues. The enzyme assumes three different form during the catalytic cycle, deoxy ($[Cu(I)_2]^{2+}$), oxy ($[Cu(II)_2\text{-}O_2]^{2+}$) and met (two Cu(II) ions bridged by an hydroxyl group). Oxygen is bound in a side-on $\mu\text{-}\eta^2\text{:}\eta^2$ fashion, with Cu-Cu distance of 3.6 Å and a O-O distance of 1.4 Å, as shown by the analysis of X-ray data on tyrosinase.[21]

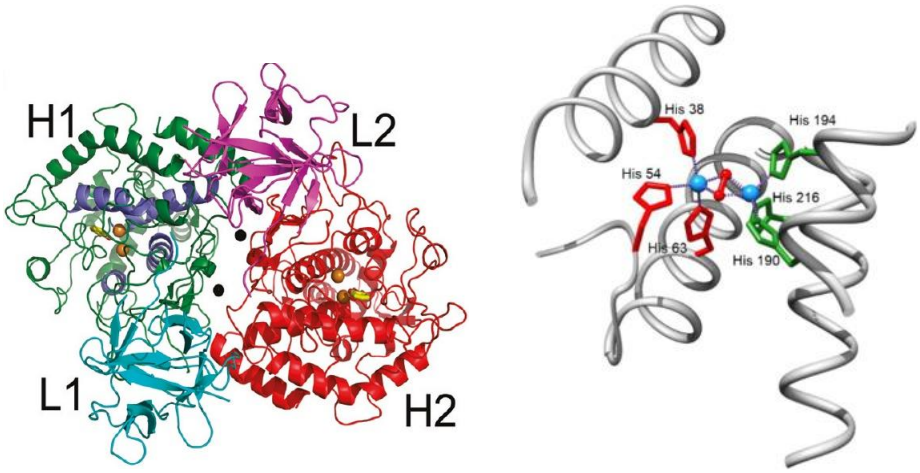

Figure 1.6- Left- Tyrosinase from *Agaricus Bisporus*;[24] Right: oxy-form of the active site of tyrosinase from the bacterium *S. castaneoglobisporus.*[25]

This peculiar peroxo-Cu(II) complex exhibits specific spectroscopic features, with an intense absorption band centered at 345 nm (ε~18000 $M^{-1}cm^{-1}$), attributable to peroxo→Cu(II) charge transfer transitions. The catalytic cycle of tyrosinase can be so schematize by considering two interpenetrating reaction pathways (Scheme 1.11).

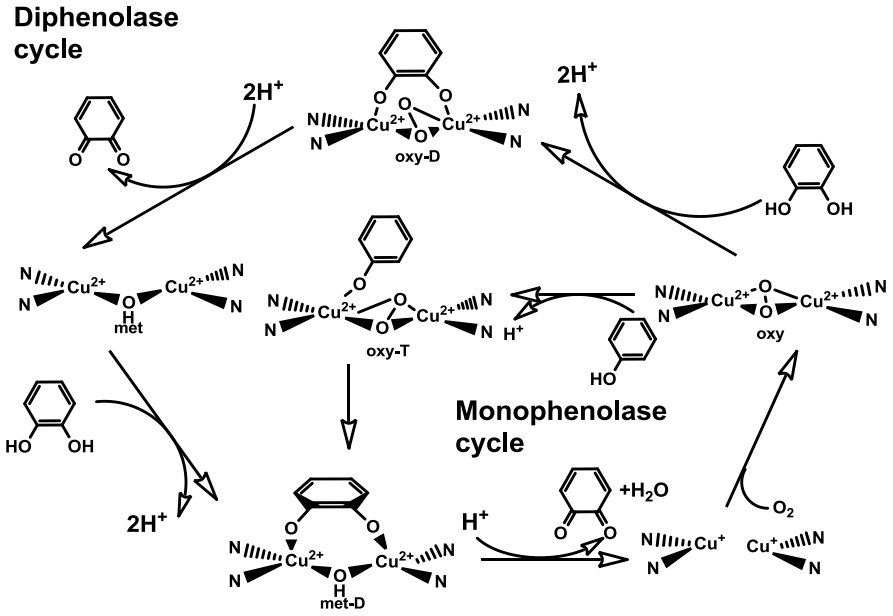

Scheme 1.11- Catalytic cycle of tyrosinase. Inner cycle: monophenolase activity. Outer cycle: dipheolase activity.

In the diphenolase activity (Scheme 1.11-outer pathway), the met-form of the enzyme oxidizes a molecule of catechol to quinone, reducing the enzyme to deoxy form that binds molecular oxygen. The resulting oxygenated intermediate is then able to oxidize a further molecule of catechol. In essence, it consists in a four-electrons reduction of oxygen to water, split in two discrete two-electron steps, without production of hydrogenperoxide. Monophenolase activity, instead, starts from the deoxy form of the enzyme, that binds molecular oxygen in a side-on peroxo fashion. The resulting complex, generates a ternary intermediate, whose structure has never been characterized, that is able to oxygenate the bound phenol, oxidizing it to quinone with reduction of oxygen to water. Dissociation constant of the Cu(II)-peroxo complex was estimated to 16.5−66 μM,[26] falling in the range of binding affinity of oxygen transporter hemocyanin. Different hypothesis on the nature of the intermediates involved in the catalytic cycle were formulated. By considering experimental X-ray data, Yoshizawa and coworkers recently formulated an hypothesis that involves the presence of a phenoxyl radical as intermediate, generated by H-abstraction from the protonated phenol. In enzymatic system, the phenoxyl radical remains inside the enzymatic pocket, so O-O cleavage is possible to provide the radical oxygenated intermediate able to oxygenate the phenol (Scheme 1.12).[25]

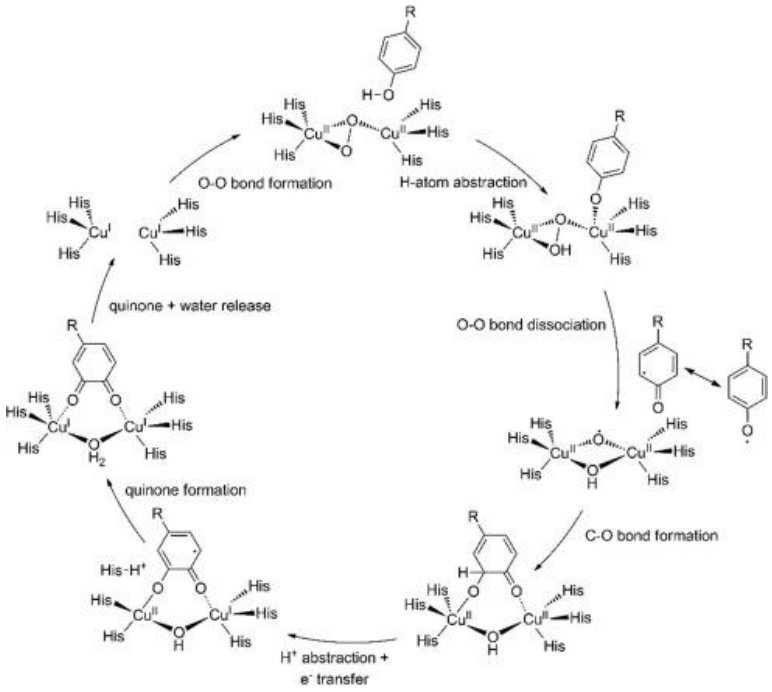

Scheme 1.12- Proposed mechanism for monophenolase cycle involving the formation of a phenoxyl radical intermediate, adapted from [25].

In biomimetic systems, the phenoxyl radical is not retained by the copper complex, but it "escapes", following a C-C coupling pathway rather than oxygenation.

Decker and coworkers supported the hypothesis that an asparagine and a glutamate residues in the enzymatic pocket deprotonate the starting phenol. The role of the active site proximal residues is enforced by Fishman and coworkers, who attribute an effective part in activation of a water molecule, that finally acts as internal base for the system, warranting the key-role of deprotonation of the phenolic substrate (Scheme 1.13). The difference in oxidation activity of catechol oxidase and tyrosinase has been recently proposed to reside in the presence of these two amino acid residues. A polyphenol oxidase from wine leave, which exhibits only catecholase activity, was modified *via* point mutation of a glycine to an asparagine, and it was found to promote oxygenation of external phenols.

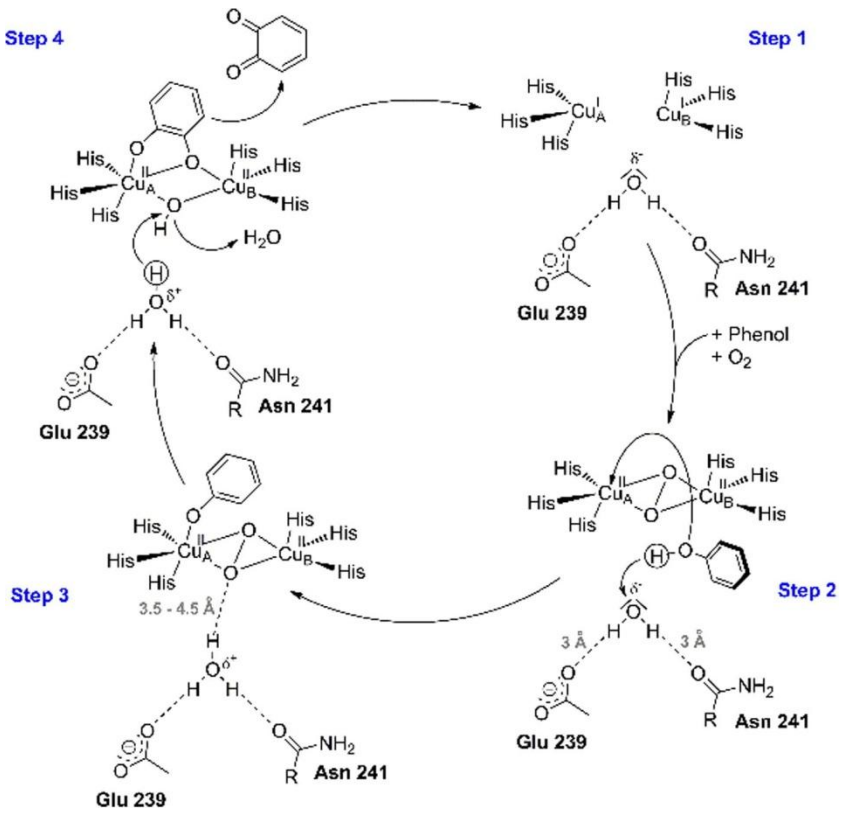

Scheme 1.13- Proposed catalytic cycle, considering the role of asparagine and glutamate residues in the deprotonation of the phenol, adapted from [25].

This proposed mechanism is consistent with the monophenolase activity promoted by several small-molecule models, which require the presence of a base (for example triethylamine) to allow monoxygenation of phenols.

1.1.4.1. Tyrosinase biomimetic models

Due to the specific activity of tyrosinase, the aim to mimic the enzyme features, by synthetic modeling the structure of the active site, fascinated bioinorganic chemists for long years. Biomimetic systems for tyrosinase could be substantially divided into systems able to catalyze simple catechol oxidation (catecholase activity) and systems which are also able to perform oxygen-mediated phenol oxygenation (monophenolase activity).

Catecholase activity, due to the low oxidation potential of the substrates (Scheme 1.14), was chosen in most of cases as preliminary elective mean to test the effective biomimetic activity of various model complexes. Several mononuclear and dinuclear copper complexes were synthesized with this aim.

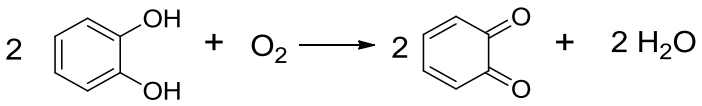

Scheme 1.14- Catecholase activity

Tyrosinase-like activity promoted by mononuclear copper complexes assumed that two mononuclear units associate themselves generating an adequate dinuclear site.[27] Experimental evidences have outlined that dinuclear complexes are more efficient and reactive than mononuclear congeners. The reason could be found in a pre-optimization of the Cu-Cu distance given by the correct structure of the ligand, which could favor the interaction between the dinuclear site and the catecholic substrates. Therefore, dinuclear and trinuclear complexes have aroused an increasing interest in synthesis. Efforts in synthesis were particularly directed toward chiral polydentate ligands for copper.[27] Despite from the difficulties that arise from the synthesis of these polydentate nitrogen ligands, the increased stability and possibility to take advantage of an additional anchoring site played a key role in the choice. My research group was so far interested in synthesizing these models for catecholase activity (Figure 1.7), testing the stereodifferentiating capability toward the oxidaton of chiral catechols. In most cases, the discrimination focused on the substrate-complex "affinity" rather than the oxidation rate.

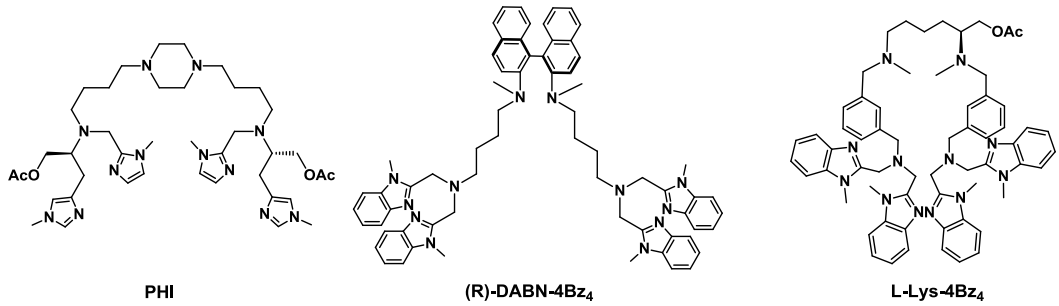

Figure 1.7- Trinucleating chiral ligands synthesized by my research group.

While catecholase activity was found to be relatively easy to mimic, only a few models were found to be able to perform oxygenation of external phenols exhibiting a genuine tyrosinase-like mechanism.[25] The first model able to hydroxylate phenols was conceived by Bulkowski in 1984,[29] and exploited a cyclic dinucleating tetramine ligand for Cu(I). With 100 equivalents of phenols and 200 equivalents of triethylamine as base, this

system was able to produce 18 equivalent of *ortho*-quinone from the corresponding starting phenol.

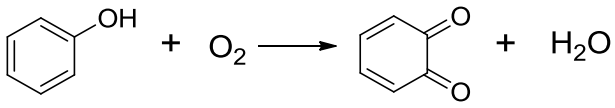

Scheme 1.15- Monophenolase activity

Under Bulkowski's conditions, a system consisting of a Cu(I) complex with BiPh(impy)$_2$, designed by Règlier and coworkers in 1990,[30] promoted the oxidation of 2,4-ditertbutyl phenol to 3,5-ditertbutyl quinone with a turn over number (TON) of 16. Later, my research group reported a tetrabenzimidazole dinucleating ligand for copper, labeled as L66, that was found to perform stoichiometric as well as catalytic oxidation of external phenols. Unlike the other mentioned complexes, L66 shows a peculiar behavior when oxygenation of phenols is performed at room temperature. The main isolated product, in fact, is attributable to Michael addition derived from the attack of the not reacted phenol in the obtained quinone.[31] In addition, it is the only biomimetic system reported so far where dioxygen binding in the absence of phenol is fully reversible. Therefore, it is currently the "best" synthetic model reproducing the binding and reactivity characteristics of the enzyme.

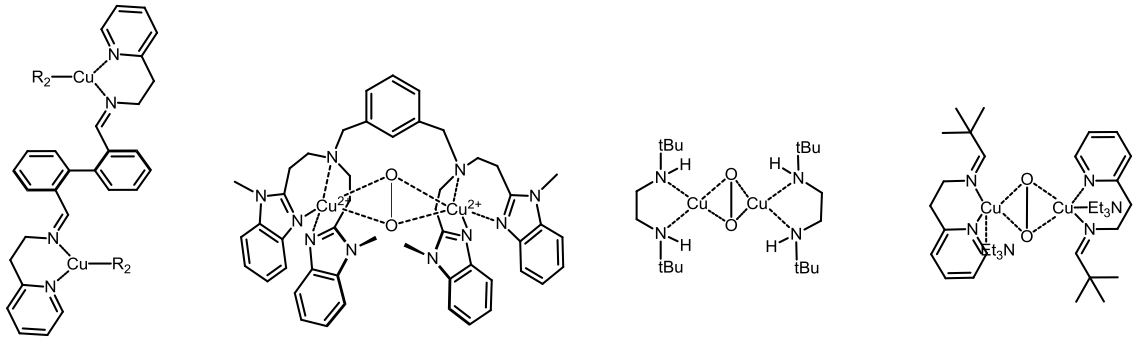

Figure 1.8- Biomimetic systems able to reproduce tyrosinase-like monoxygenation of phenols. From left to right: Règlier et al.; Casella et al.; Stack et al.; Tuczek et al.

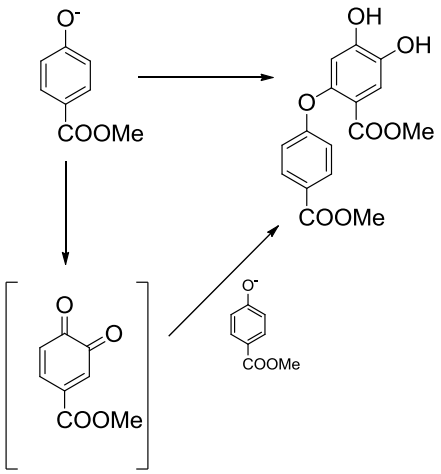

Scheme 1.16- Oxidation of 4-carbomethoxy phenolate promoted by Cu_2L66 in non-reducing conditions.

In 2005, Stack et al. presented another complex,[32] based on mononucleating diamine ligand, able to promote monophenolase activity. This generates a stable μ-η^2:η^2-peroxo dicopper(II) complex upon exposure to air oxygen at -120 °C. Another catalytic model for this activity was later proposed by Tuczek et al. in 2010, based on $L_{py}1$ ligand (Figure 1.8),[33] that was found to catalyze the oxidation of 2,4-ditertbutyl phenol to 3,5-ditertbutyl quinone with a TON of 22. In 2013, Herres-Pawlis and coworkers synthesized a room temperature stable μ-η^2:η^2-peroxo dicopper(II) complex able to catalyze the oxidation of several phenolic compounds, based on tripodal pyrazolyl ligands.[34] The key factor is represented by the possibility to trap the reactive Cu_2O_2 intermediate, responsible for phenol oxidation. All these previously reported systems based their activity on the support of external bases to promote the deprotonation of the starting phenols. Lumb and coworker, instead, reproduced monophenolase activity based on DBED ligand, using a slight overstoichiometric amount of base, that in this case acts as a Brønsted base.[35]

1.2. Reactivity of Cu-O_2 complexes with different fashion binding modes.

In the last two decades, bioinorganic chemists focused their efforts in identification of the nature of the reactive intermediates involved in the enzyme reactions. Copper(I)-dioxygen chemistry has so intensively flourished, as the nuclearity and the coordination chemistry in the enzyme active site bear several features. Hemocyanin, as oxygen carrier in arthropodal and molluscan hemolymph, was known to generate a reversible

Cu(I)-O_2 complex, so identification of the structure of this intermediate functioned as starting point. In the enzymes, oxygen, after coordination to copper, undergoes formal reduction to superoxo (O^{2-}), peroxo (O_2^{2-}) and O-O bond cleavage. The nature of the Cu-O_2 complex is, therefore, the mediator of the oxidation reaction involving the substrates. Recent advances in the clarification of the nature of these complexes make possible to sort them in reactivity groups, distinguishing them into electrophilic and nucleophilic "alternative oxidants".

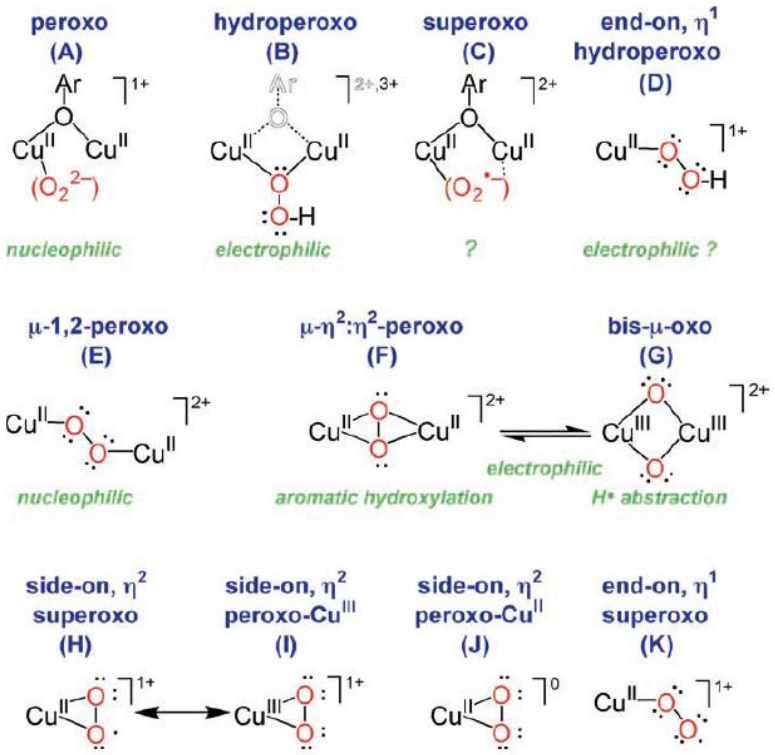

Figure 1.9- Different Cu(I)-O_2 intermediates, classified on their reactivity toward substrates, adapted from [36].

The μ-η^2:η^2-peroxodicopper(II) complex (F) was the first to be identified in its involvement in a synthetic system (Fujisawa and, later, from Kitajima[37,38]), subsequently it was confirmed also for oxy-hemocyanin, tyrosinase[21] and catechol oxidase.[39] This intermediate was considered the reactive complex performing enzymatic phenol hydroxylation. Experimental evidences of the bis-μ-oxo-dicopper(III) species were, instead, not found in nature, even if it could be considered the mediator for hydroxylation of methane performed by methane monooxygenase (p-MMO).[40] Hydroperoxo-copper entities, in their mononuclear and dinuclear fashions, are

speculated to be involved in the C-H hydroxylation reactions performed by dopamine-β-hydroxylase and peptitylglycine α-hydroxylating monooxygenase.[41,42]

1.2.1. Comparison between nucleophilic and electrophilic Cu-O_2 species

Binuclear peroxo-dicopper(II) complexes were the first adducts to be fully characterized. Originally, these systems were stabilized at low temperature (below -80 °C) in organic solvents, but later room temperature stable congeners have been found. Karlin and coworkers focused on the identification of the nature of these systems, involving them in well-defined reactions.[43,44,45]

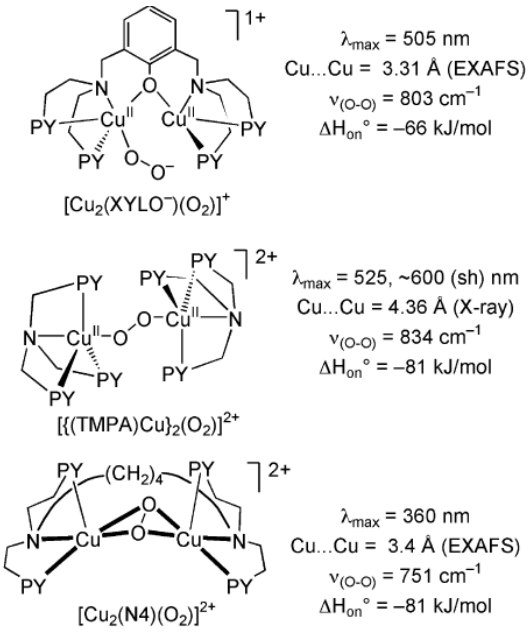

Figure 1.10- Synthetic Cu-O_2 intermediates studied by Karlin.

The dinuclear copper complex $[Cu^{II}_2(XYLO^-)(O_2)]^+$ was identified to have copper ions bonded to a peroxo ligand. Its basic and nucleophilic nature has been elucidated by monitoring the reaction with triphenylphosphine. It was found that this complex releases O_2 and binds PPh_3 rather than performing oxidation of the phosphine. The intermediate could also be protonated to generate a μ-1,1-hydroperoxo complex. Similar reactivity is shown by the mononuclear Cu(TMPA) complex. For $[Cu_2(N4)(O_2)]^{2+}$, reaction with PPh_3 afforded $O=PPh_3$, showing a reversed reactivity with respect to those previously described. This nonbasic, electrophilic nature of the side-on μ-η^2:η^2-peroxo dicopper(II) complex, also lately reported by Stack and coworkers, has been further

demonstrated in reactions of greater interest, as it was found to be able to mediate hydroxylation of phenols and other arenes.

1.2.2. Dynamic equilibrium between side-on peroxo-dicopper(II) and bis-μ-oxo-dicopper(III) complexes

Binuclear copper-containing enzymes, as tyrosinase and catechol oxidase, typically adopt a μ-η^2:η^2-peroxo side-on fashion in coordination of oxygen, but more recently a novel binding motif has been characterized. It consists of a peroxo complex in which the O-O bond is fully cleaved, rationalized assuming a Cu(III) oxidation state. Bis-μ-oxo dicopper(III) complex exhibits typical spectroscopic and structural features, coupled with a peculiar reactivity. Small energetic differences suggest a low energy barrier between these two isoelectronic forms, that appeared to be in dynamic equilibrium. This equilibrium is mostly ruled by the donating nature of the ligand, solvents, concentration, counterions and other experimental conditions. The first evidence of the bis-μ-oxo dicopper(III) complex has been highlighted by Tolman group,[46] while later Itoh et al. exploited this complex to perform dopamine-β-hydroxylase-like activity in benzylic hydroxylation reactions.[47] Karlin and coworkers also showed a dynamic equilibrium between the side-on peroxodicopper(II) and bis-μ-oxodicopper(III) species with the use of R-MePY2 tridentate ligands.[48,49]

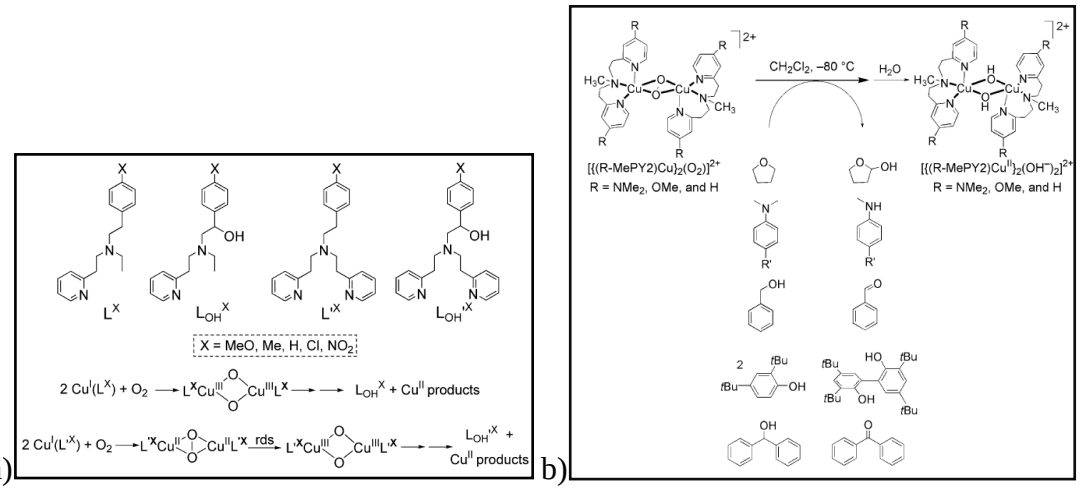

Figure 1.11- a) Example of benzylic hydroxylation performed bis-μ-oxo complex, by Itoh at al.; b) Oxidation reaction performed by Cu_2O_2 complex from Karlin et al.

1.3. Chiral copper complexes as biomimetic tyrosinase systems

High enzymatic eficiency of tyrosinase in catalyzing oxidation of catechols and phenols is accompanied by an intrinsic regio and, overall, stereoselectivity. The driving force of the capability to discriminate toward oxidation of chiral substrates resides in the spatial organization and coordination properties of the donating coordination units. Several attempts to mimic the tyrosinase coordination environment have been made in the past few years, but most of the reported models did not have the specific characteristics to enable enantio-discrimination. My research group developed several octadentate chiral ligand for two or three copper ions, and the resulting complexes were found to catalyze enantio-discriminating oxidation of chiral catechols, as previously reported. Octadentate ligands for copper, for example PHI, take advantage of the potential presence of a third coordination site, gaining in stability and efficiency, but in most cases the ligands required time-spending and poorly efficient synthetic strategies. With the aim to replicate a more faithful model, with the possibility to simplify the synthetic strategies, hexadentate chiral nitrogen ligands, able to host two copper ions, were, therefore, devised.

References

1- V. Mahadevan, R. J. M. Klein Gebbink, T. Daniel, P. Stack, *Curr. Opin. Chem. Biol.* **2000**, 4, 228–234.

2- Vendelboe, P. Harris, Y. Zhao, T. S. Walter, K. Harlos, K. El Omari, H. E. M. Christensen, *Sci. Adv*., **2016**.

3- (a) I. Blain, M. Giorgi, I. De Riggi and M. Réglier, *Eur. J. Inorg. Chem.*, **2001**, 205; (b) I. Blain, M. Pierrot, M. Giorgi and M. Réglier, *C. R. Acad. Sci., Ser. IIc: Chim.*, **2001**, 4, 1.

4- (a) S. T. Prigge, A. S. Kolhekar, B. A. Eipper, R. E. Mains and L. M. Amzel, *Science*, **1997**, 278, 1300; (b) S. Jaron and N. J. Blackburn, *Biochemistry*, **1999**, 38, 15086.

5- J. P. Klinman *J. Biol. Chem.* **2006**, 281, 3013–3016.

6- R. L. Peterson, R. A. Himes, H. Kotani, T. Suenobu, L. Tian, M. A. Siegler, E. I. Solomon, S. Fukuzumi, K. D. Karlin, *J. Am. Chem. Soc.* **2011**, 133, 1702–1705.

7- K. Fujisawa, M. Tanaka,Y. Morooka, Y. N. Kitajima *J. Am. Chem. Soc.* **1994**, 116, 12079–12080.

8- C.Cramer, W.Tolman *Acc. Chem. Res.* **2007**, 40, 601–608.

9- S.Yamaguchi, S. Nagatomo, T. Kitagawa, Y. Funahashi, T. Ozawa, K. Jitsukawa, H. Masuda, *Inorg. Chem.* **2003**, 42, 6968–6970.

10- D.Maiti, D.-H. Lee, K. Gaoutchenova, C. Würtele, M.C. Holthausen, A.A.N. Sarjeant, J. Sundermeyer, S. Schindler, K.D. Karlin, *Angew. Chem. Int. Ed*. **2008**, 47, 82–85.

11- P. Karandikar, M. Agashe, K. Vijayamohanan, A. Chandwadkar *J. Appl. Catal., A* **2004**, 257, 133.

12- N.V. Gerbeleu, S.S. Palanciuc, Y.A. Simonov, A. Dvorkin, P.N. Bourosh, M.T. Reetz, V.B. Arion, K. Töllner, *Polyhedron* **1995**, 14, 521.

13- D.H.R. Barton, S.D. Beviere, D.R. Hill, *Tetrahedron* **1994**, 50, 2665.

14-M.N. Kopylovich, A.C.C. Nunes, K.T. Mahmudov, M. Haukka T.C.O. Mac Leod, L.M.D.S. Martins, M.L. Kuznetsov, J.L. Pombeiro, *Dalton Trans.* **2011**, 40, 2822.

15- (a) N. Ito, S. E .V. Phillips, C. Stevens, Z. B.Ogel, M. J. McPherson, J. N. Keen, K. D. S.Yadav, P. F. Knowles, *Nature*, **1991**, 350, 87. (b) N. Ito, S. E. V. Phillips, K. D. S. Yadav, P. F. Knowles, *J. Mol. Biol.* **1994**, 238, 704.

16- J.W. Whittaker, *Archives of Biochemistry and Biophysics* 433, **2005**, 227–239.

17- A. M.Sakharov, I. P. Skibida, *J. Mol. Catal.*, **1988**, 48, 157.

18- M. F. Semmelhack, C. R. Schmid, D. A Cortés, C.S. Chou, *J. Am. Chem. Soc*. **1984**, 106, 3374.

19- (a) I. E.Marko, P. R.Giles, M. Tsukazaki, S. M. Brown, C. Urch., *Science*, **1996**, 274, 2044; (b) I. Markò, P.R. Giles, M. Tsukasaki, I. Chelle -Regnaut, A. Gautier; S.M. Brown; C.J. Urch *J. Org. Chem*. **1999**, 64, 2433.

20- S. Mannam, G. Sekar, *Tetrahedron: Asymmetry*, **2009**, 20, 497.

21- E. I. Solomon, U.M. Sundaram, T.E. Machonkin, *Chem. Rev.* **1996**, 96, 2563–2605.

22- S. Yamazaki, S. Itoh, *J. Am. Chem. Soc.* **2003**, 125, 13034–13035.

23- H. S. Mason, W. L. Fowlks, E. Peterson, *J. Am. Chem. Soc.* **1955**, 77, 2914.

24- Ismaya, W.T., Rozeboom, H. J., Weijn, A., Mes, J. J., Fusetti, F., *Biochemistry* 2011, 50, 5477–5486.

25- J.N. Hamann et al., *Coordination Chemistry Reviews*, **2016**, in press.

26- (a) Rodriguez-Lopez, J. N., Fenoll, L. G., Garcia-Ruiz, P. A., Varon, R., Tudela, J., Thorneley, R. N. F., Garcia-Canovas, F., *Biochemistry*, **2000**, 39, 10497; (b) A. B. P. Lever , B. S. Ramaswamy , S. R. Pickens, *Inorg. Chim. Acta*, **1980**, 46, 59–61; (c)T. R. Demmin , M. D. Swerdloff , M. M. Rogic , *J. Am. Chem. Soc.* **1981**, 103,5795–5804; (d) D. Bolus , G. S. Vigee, *Inorg. Chim. Acta*, **1982**, 67, 19–25; (e) M. Réglier , C. Jorand, B. Waegell, *J. Chem. Soc. Chem. Commun.*, **1990**, 1752–1755; (f) M. R. Malachowski, L. J. Tomlinson, M. G. Davidson, M. J. Hall, *J. Coord. Chem.*, **1992**, 25, 171–174; (g) R. Wegner, M. Gottschaldt, H. Görls, E.-G. Jäger, D. Kemm, *Chem. Eur. J.*, **2001**,7, 2143–2157. (h) E. Monzani, L. Quinti, A. Perotti, L. Casella, M. Gullotti, L. Randacchio, S. Geremia, G. Nardin, P. Faleschini, G. Tabbi, *Inorg. Chem.* **1998**, 37, 553–562; (i) E. Monzani, G. Battaini, A. Perotti, L. Casella, M. Gullotti, L. Santagostini, G. Nardin, L. Randacchio, S. Geremia, P. Zanello, G. Opromolla, *Inorg. Chem.*,**1999**, 38, 5359–5369.

27- G. Battaini, M. De Carolis, E. Monzani, F. Tuczek, L. Casella, *Chem. Commun.*, **2003**, 726–727.

28- (a) L. Santagostini, M. Gullotti, R. Pagliarin, E. Bianchi, L. Casella, E. Monzani, *Tetrahedron: Asymmetry* **1999**, 10, 281. (b) M. C. Mimmi, M. Gullotti, L. Santagostini, A. Saladino, L. Casella, E. Monzani, R. Pagliarin, *J. Mol. Catal. A: Chem.* **2003**, 204-205, 381-389. (c) L. Santagostini, M. Gullotti, R. Pagliarin, E. Monzani, L. Casella, *Chem. Commun.,* **2003**, 2186. (d) M. C. Mimmi, M. Gullotti, L. Santagostini, G. Battaini, E. Monzani, E. R. Pagliarin, G. Zoppellaro, L. Casella, *Dalton Trans.*, **2004**, 2192. (e) M. Gullotti, L. Santagostini, R. Pagliarin, A. Granata, L. Casella, *J. Mol. Catal. A,* **2005**, 235, 271. (f) F. G. Mutti, G. Zoppellaro, M. Gullotti, L. Santagostini, R. Pagliarin, K. K. Andersson, L. Casella., *Eur. J. Inorg. Chem.,* **2009**, 554.

29- J. E. Bulkowski, US Patent, 4545937 (1984).

30- M. Réglier, C. Jorand, B. Waegell, *J. Chem. Soc., Chem. Commun*, **1990**, 1752.

31- L. Casella, E. Monzani, M. Gullotti, D. Cavagnino, G. Cerina, L. Santagostini, R.Ugo, *Inorg. Chem.* **1996**, *35*, 7516-7525.

32- L.M. Mirica, M. Vance, D.J. Rudd, B. Hedman, K.O. Hodgson, E.I. Solomon, T.D.P. Stack, *Science*, 308, **2005,** 1890.

33- M. Rolff, J. Schottenheim, G. Peters, F. Tuczek, *Angew. Chem. Int. Ed.,* 49, **2010**, 6438.

34- A. Hoffmann, C. Citek, S. Binder, A. Goos, M. Rübhausen, O. Troeppner, I. Ivanovic -Burmazović , E.C. Wasinger, T.D.P. Stack, S. Herres-Pawlis, *Angew. Chem. Int. Ed.*, 52, **2013**, 5398

35- K.V.N. Esguerra, Y. Fall, J.P. Lumb, *Angew. Chem. Int. Ed.*, 53, **2014**, 5877.

36- L. Q. Hatcher, K. D. Karlin, *J Biol Inorg Chem*, **2004**, 9: 669–683.

37- N. Kitajima , K. Fujisawa, Y. Moro-oka, K. Toriumi, *J Am. Chem Soc*,**1989**, 11, 8975–8976.

38- N. Kitajima, Y. Moro-oka , *Chem Rev*, **1994**, 94, 737–757.

39- C. Gerdemann, C. Eicken, B. Krebs, *Acc Chem Res*, **2002**, 35, 183–191.

40- S. I. Chan, K. H. C. Chen, S. S. F. Yu, C. L. Chen, S. S. J. Kuo, *Biochemistry*, **2004**, 43, 4421–4430.

41- J. P. Evans, K. Ahn, J. P. Klinman, *J Biol Chem* , **2003**, 278, 49691–49698.

42- S. T. Prigge, R. E. Mains, B. A. Eipper, L. M. Amzel, *Cell Mol Life Sci*, **2000**, 57, 1236–1259.

43- K. D. Karlin, P. L. Dahlstrom, S. N. Cozzette, P. M. Scensny, J. Zubieta, *J Chem Soc Chem Commun*, **1981,** 881.

44- K. D. Karlin, Y. Gultneh, J. C. Hayes, R. W. Cruse, J. W. McKown, J. P. Hutchinson, J. Zubieta, *J Am Chem Soc*, **1984**, 106, 2121– 2128.

45- M. S. Nasir, B. I. Cohen, K. D. Karlin, *J Am Chem Soc*, **1992**, 114, 2482–2494.

46- (a) E. A. Lewis, W. B. Tolman, *Chem Rev*, **2004**, 104, 1047–1076; (b) S. Mahapatra, J. A. Halfen, W. B. Tolman, *J Am Chem Soc*, **1996**, 118, 11575–11586.

47- S. Itoh, M. Taki, H. Nakao, P. L. Holland, W. B. Tolman, L. Jr. Que, S. Fukuzumi, *Angew Chem Int Ed*, **2000**, 39, 398–400.

48- C. X. Zhang, H-C. Liang, E-i Kim, J. Shearer, M. E. Helton, E. Kim, S. Kaderli, C. D. Incarvito, A. D. Zuberbu¨ hler, A. L. Rheingold, K. D. Karlin, *J Am Chem Soc*, **2003**, 125, 634–635.

49. M. J. Henson, M. A. Vance, C. X. Zhang, H-C. Liang, K. D. Karlin, E. I. Solomon, *J Am Chem Soc*, **2003**, 125, 5186–5192.

.

.

.

Chapter 2. L55Bu$_4$*

2. L55Bu$_4$*

2.1 Introduction

The topic of dioxygen activation, to promote oxidation of organic molecules, has been so far attractive for bioinorganic chemists. My research group has focused its interest in developing many different biomimetic systems, based on copper as metal center, varying the coordination environment to change the reactivity of the active intermediates.[1-4]

The dinuclear copper complex of the ligand labeled as L55 was extensively studied by this research group since 1993.[2e] This hexadentate nitrogen ligand consists in two amino-bisbenzimidazole three-coordinating units, connecteded by a m-xylyl bridge, to obtain the final skeleton. This ligand can host two copper ions. Each copper ion is coordinated to one amino-bisbenzimidazole arm, resulting in two five-membered chelate rings. The limited size of the chelate rings increases the reactivity of the copper complex toward dioxygen. The reason of this enhancement in reactivity could be found on the structure of the copper complexes. X-ray structure of the dicopper(II)-complex of

L55[2b] shows that the distance between the tertiary amine and the copper center is higher, resulting in a weaker bond. This weaker donor effect of the farther amine makes the dioxygen bound more electrophilic and this increases a lot the efficiency on catalytic reactions. Studies on the catalytic activity of the dinuclear copper complexes of L55 showed that this biomimetic system exhibited both simple catecholase activity, typical of catechol oxidases, and tyrosinase activity.[2c] The copper complex catalyzes the oxidation of 3,5-ditertbutyl catechol to 3,5-ditertbutyl quinone, and it was found to be the best model to mimic the catecholase activity.

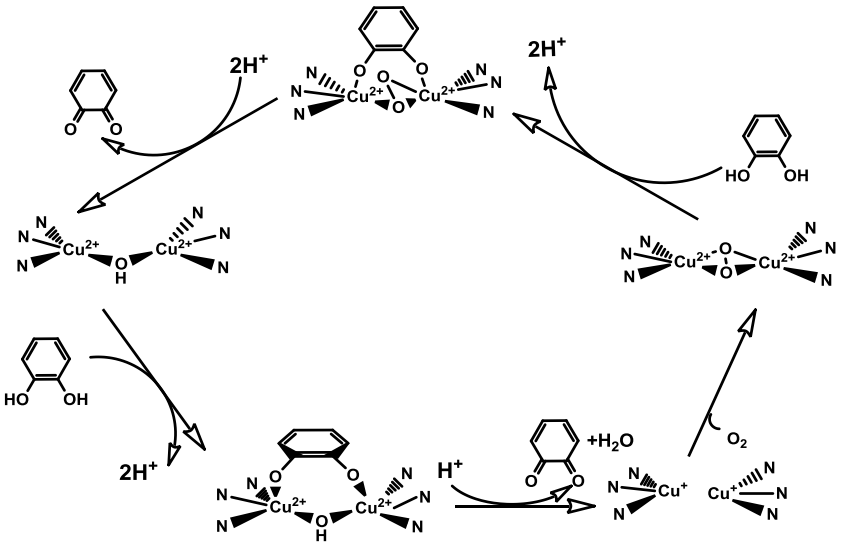

Scheme 2.1- Simplified catalytic cycle of catechol oxidases. Two molecules of catechol are oxidized in the catalytic reaction.

Cathecols have a double role in the catecholase activity (Scheme 2.1). When the first molecule of catechol is bound to the copper(II) complex, it promotes the reduction to copper(I). Dicopper(I) complex reacts with molecular oxygen, generating the reactive oxygen intermediate that can oxidize a second molecule of catechol. Many copper complexes, proposed as catechol oxidase mimetics, can replicate this kind of activity, but an important feature of $[Cu_2L55]^{4+}$ is that it is possible to separate the two reaction steps, allowing deeper insights in the catalytic cycle.

Studies on biomimetic systems can also help in having more information about the activity of the natural source of inspiration. In tyrosinase, the oxygenated complex was found to be a μ-η^2:η^2-peroxo species,[5] so studies to trap this putative intermediate were carried out also on the synthetic analogues. For the dinuclear copper complex of L55, the higher electrophilicity discussed above, that causes an enhanced catalysis,

compromises the stability of the Cu_2-O_2 complex, even at temperature below -80 °C. The studies on the nature of the oxygenated intermediate on bezimidazole-based systems were carried out by my research group on another synthetic analogue, the dinuclear copper complex of the ligand Me-L66.[2d] This system has the same skeleton, but the amino-bisbenzimidazole units has a further methylene group in the spacer, generating six-membered chelate rings. This increased flexibility of the structure accommodates the changes in coordination needs due to the reduction of copper(II) to copper(I) and increases the donor effect on metal ions. The stronger electrondensity on the copper ions stabilizes the μ-η^2:η^2-peroxo complex (Figure 2.1) at temperature below -60 °C in acetone, making a spectroscopic characterization possible. Even if this small changes in the structure of the ligand allowed to trap this intermediate, the similarity in coordination set of these two biomimetic complexes make it possible to attribute the same structure to the oxygenated intermediate of the catalytic cycle.

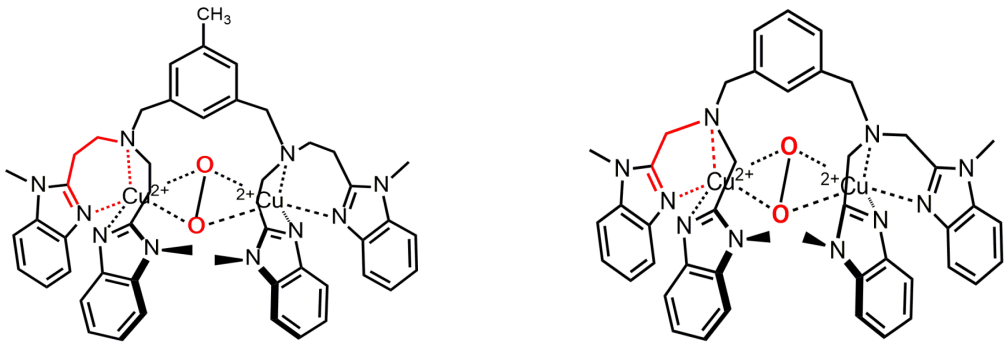

Figure 2.1- Structure of the oxygenated intermediate trapped in the dinuclear copper(I) complex of the ligand MeL66 (on the left) and supposed for the dinuclear copper complex of the ligand L55 (on the right).

Tyrosinase exhibits another kind of activity, the oxidation of sulfides to sulfoxides, where it acts as external monoxygenases.[6] This type of activity of the enzyme requires the presence of a sacrificial reducing agent: sulfides, unlike phenols, in fact, are two electron donors (Scheme 2.2):

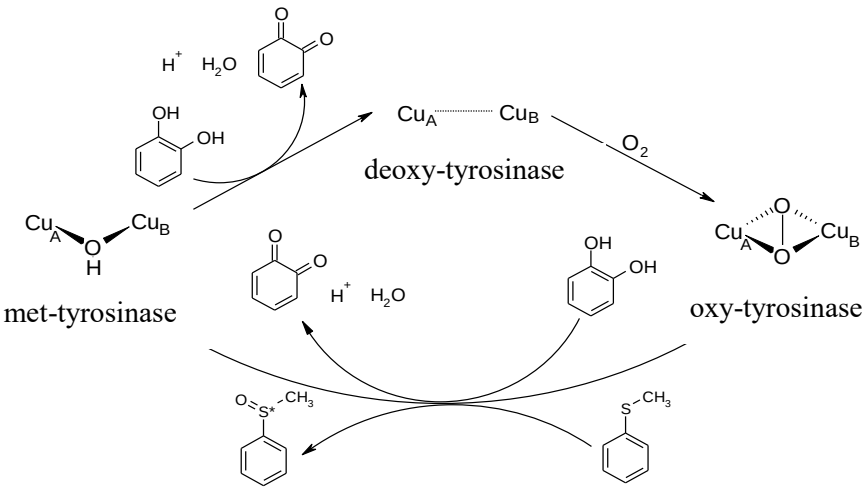

Scheme 2.2- Catalytic process for tyrosinase acting as external monoxygenase in the oxidation of thioanisole. L-Dopa is used as sacrificial catecholic cosubstrate to reduce the met form to the deoxy form.

The cosubstrate chosen to study the oxidation of thioanisole promoted by tyrosinase was L-Dopa, a typical substrate of the enzyme. In these conditions, the prostereogenic substrate is oxidized to a chiral sulfoxide with an enantiomeric excess up to 85 %, even if with moderate yield (around 20 %). The reason of these moderate yields could be attributed to the competition between the oxidation of L-Dopa and thioanisole. Enantioselectivity was further increased by adding a large excess of ascorbic acid, that reduces the quinones produced from the oxidation of Dopa, which inhibit tyrosinase. Experiments were repeated in presence of 18-O_2, showing an incorporation of the 18-isotope up to 95 %, confirming that the oxidation of this sulfide proceeded following the pathway of oxy-tyrosinase. Only few copper complexes were found to be able to oxidize sulfides to sulfoxides[2a] and in most cases the reaction requires the use of hydroperoxidic or peroxidic reagents instead of molecular oxygen as oxidant.[7] $[Cu_2(L55)O_2]^{2+}$ was found to be active in the hydroxylation of phenols[2f] and the copper(II) analogue is considered one of the best model for catechol oxidase,[2c] this biomimetic system was used in the oxidation of thioanisole and other sulfides.[2a] As sacrificial cosubstrate, the best performance was exhibited by hydroxylamine hydrochloride. This reducing agent also competed in the oxidation of sulfides, but molecular nitrogen was the only byproduct of the reaction and workup procedure was makedly simplified. Dinuclear copper complexes of L55 and L66 are, indeed, complete and efficient models to describe and mimic the activity of tyrosinase, but they cannot

induce stereoselective reaction on the substrates. Therefore, we decided to integrate the catalytic efficiency of the $[Cu_2(L55)]^{4+}$ with the possibility to promote stereoselective oxidation of substrates.

Asimmetry in the world of coordination compounds can be achieved in several ways. Chirality elements could be directly assigned to the metallic center, and in this case we define configurational chirality. Otherwise, asimmetry of the complex could arise by chirality of the ligand. This last case inspired the synthesis of the asymmetric analogue of the ligand L55, whose chirality was obtained by substituting the methyl group on the benzimidazolic core with 2-(S)-methyl-butyl chains. The catalysis promoted by the dinuclear copper complex was extensively studied with reference to catecholase activity on chiral catechols, and in the oxidation of sulfides to sulfoxides.

2.2. Results and discussion

2.2.1. Synthesis of the dinuclear copper complex of ligand L55Bu$_4$*

2.2.1.1. First attempt.

The chiral ligand L55Bu$_4$* was conceived by introducing asymmetric moieties (Scheme 2.3) on the well known skeleton of L55. Benzimidazoles are efficient mimetics for the histidine imidazoles of the active site of the enzyme. From this starting point, it became necessary to find the proper strategy to obtain the ligand with the higher possible yield and enantio-purity.

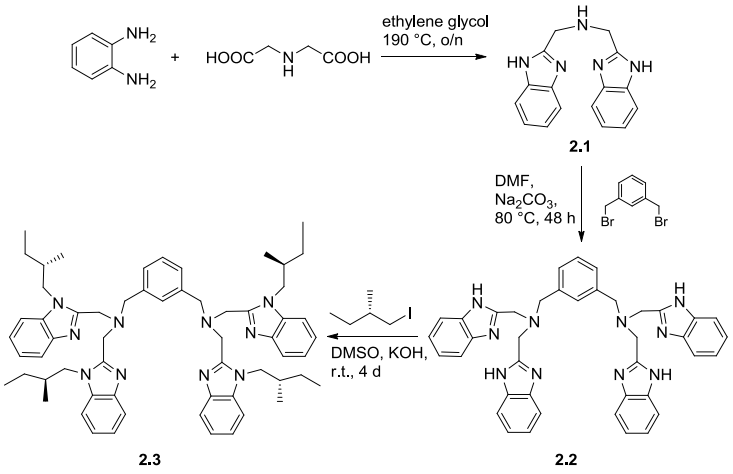

Scheme 2.3- First strategy devised for the synthesis of the ligand L55Bu$_4$*

The pathway started from the synthesis of the amino-bisbenzimidazole moiety **2.1**, the trisdentate unit required for the coordination of copper ions. The reaction consists in a direct condensation between the *ortho*-phenylendiamine and iminodiacetic acid, with slight modification of the procedure reported in the literature.[9] This condensation can be conducted in solvent-free condition, but the heating in non-homogeneous conditions induces an uncontrolled polymerization of the reagent, dramatically decreasing the reaction yield. To warrant a better reagents homogenization, ethylene glycol was added as high-boiling medium. Pure amino-bisbenzimidazole (BB5H) was obtained after recrystalization from hot methanol/water in 50 % yield. Two of these subunits were connected by reaction with *m*-xylyl bromide in DMF with heterogeneous basic condition promoted by an excess of K_2CO_3, providing **2.2**. The last reaction was the most critical part of the synthetic process. It consisted in four simultaneous SN2 reactions, so the steric hindrance tended to increase as long as the reaction proceeded to the tetra substituted product. The best condition to carry out the SN2 reaction was found in literature[10] and consisted in an initial deprotonation of the benzimidazolic N-H mediated by KOH in DMSO. The deprotonated species reacts faster with alkyl iodide. Despite a large excess of alkyl halide, the reaction gave a mixture of the four intermediates of the substitution reaction, as it can be highlighted by an ESI-MS analysis of the crude product (Figure 2.2).

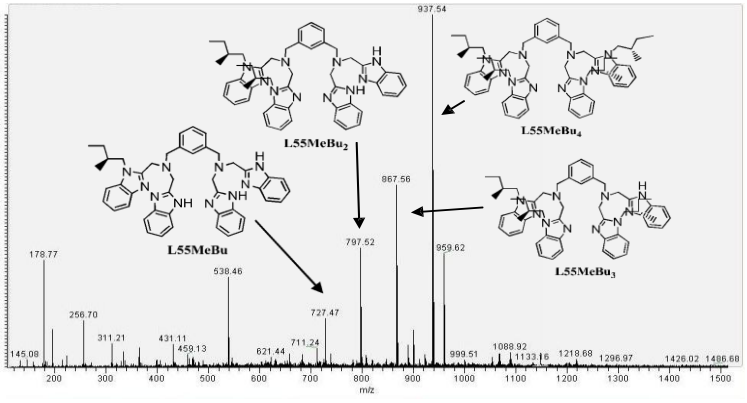

Figure 2.2- ESI-MS spectrum of the crude product from the alkylation of L55 with 2-methyl butyl iodide.

Purification of the crude proved to be difficult. It was not possible to separate the intermediates by common column chromatography, as it required reverse phase HPLC for purification. This kind of separation involved longer purification time and the

product **2.3**, recovered as quaternary trifluoroacetic salt, needed to be neutralized before reacting with copper. The copper complex was obtained easly by reaction of the ligand L55Bu$_4$* with the copper salt in 1:2 ratio.

2.2.1.2. Second attempt

The previously described synthetic strategy suffers many problems. The main aim of changing the pathway, modifying the synthetic intermediates, is to increase the reaction yield and to make the purifying processes less time-consuming.

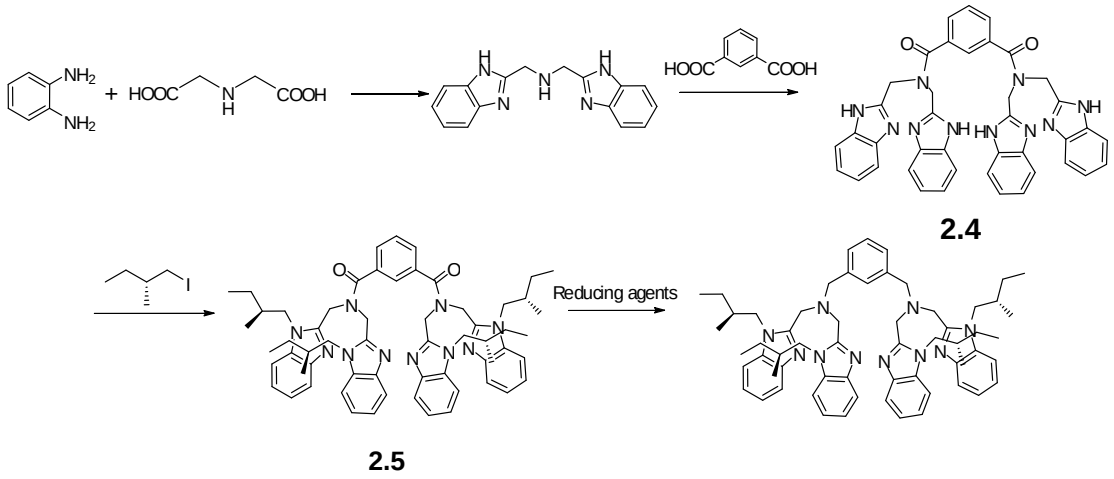

Scheme 2.4- Second synthetic pathway for the synthesis of L55Bu$_4$*

This second strategy followed an approach that involved a bis-amidic intermediate **2.4**. The diamide product is less polar than the diamine analogue and this peculiarity facilitates purification of the product, so that the tetra-alkylated ligand **2.5** could be isolated by simple column chromatography. Another relevant advantage of this synthetic procedure is that the diamide analogue of L55 did not require further purification techniques. Indeed, it precipitates as pure product when the crude reaction mixture is treated with ethyl acetate. When the diamide intermediate was obtained, the last step consisted of a reduction reaction. Unfortunately, this last step did not bring to the desired product, even if many reducing agents were been tested. The first synthetic procedure involved the use of borane with dimethylsulphide complex. In this case, the reduction did not bring to the desired product according to standard workup procedure, [11] probably because of difficulties in the cleavage of the borane-amine complexes, derived from the reaction.

Another more chemo-selective procedure was tested to reduce the bis-amide. This procedure is completely metal-free and implied the activation of the amidic function by trifluoroacetic anhydride, followed by reduction in mild condition (Scheme 2.5). I decided to test two different mild reducing agents.

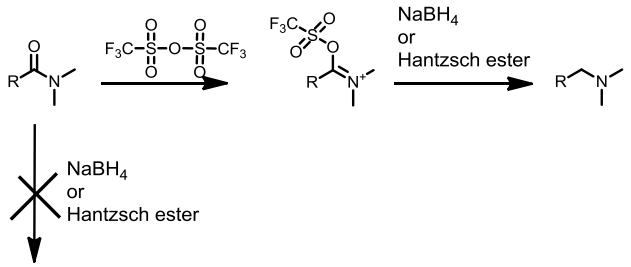

Scheme 2.5. Reaction mechanisms for the reduction of a general amide in mild conditions.

The first one was sodium borohydride.[12a] In normal condition, amides are not sensitive to reduction by sodium boroydride, but the imidium ions generated by activation is much more electrophilic and can react with not strong hydrides or other mild reducing agents. Unfortunately, it was not possible to achieve the desired bis-amine, because the activation with the anhydride generate stable imidium ions that were probably resistant to reducing agent. The same problem was found when Hantzsch ester was used as reducing agent, [12b] so these two chemo-selective and mild reductions were abandoned.

2.2.2. Spectroscopic characterization of the dinuclear copper complex of L55Bu$_4$*

2.2.2.1. Uv-Vis titration of [Cu$_2$(L55Bu$_4$)](ClO$_4$)$_4$ with hydroxide*

The dinuclear copper(II) complex of the ligand L55Bu$_4$* was obtained as described in the Experimental section.

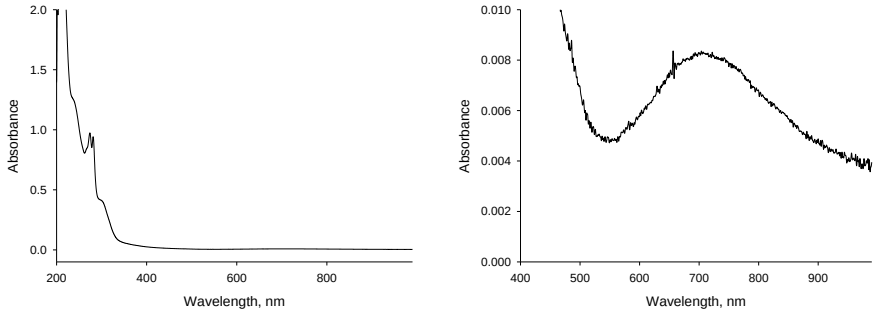

Figure 2.3- UV-Vis spectrum of $[Cu_2L55Bu_4*]^{4+}$, in methanol solution ($1.23x10^{-4}$ M) at 25 °C.

Comparing the electronic spectrum of $[Cu_2(L55Bu_4*)]^{4+}$ (Figure 2.3) with that of the parent complex derived from L55, is clear that the addition of methyl groups on the benzimidazole rings does not substantially affect the UV-Vis features of the systems. In the case of $[Cu_2L55]^{4+}$, it was found that the spectrum had pH dependent features, as on increasing the pH favored the dissociation of the metal coordinated water.[2e]

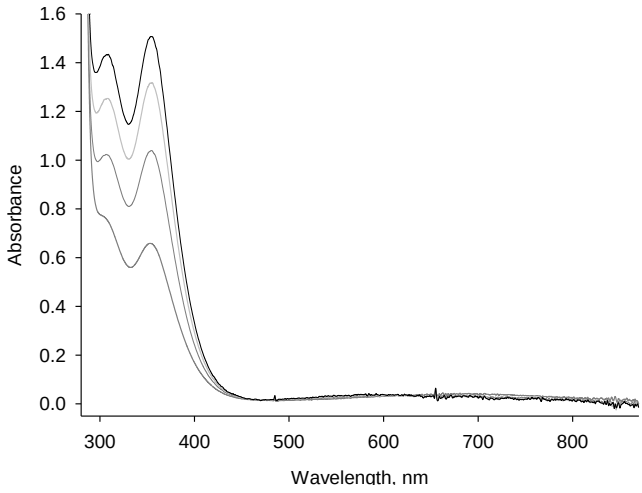

Figure 2.4- UV-Vis spectra upon titration of a solution 5.3 x 10^{-4} M of $[Cu_2(L55Bu_4)](ClO_4)_4$ with sodium hydroxide from 0 to 2 eqv. of OH^-.

Addition of hydroxide to $[Cu_2(L55Bu_4)]^{4+}$ generated a double effect. First, two near-UV absorption bands at 308 and 354 nm (ε = 5430 and 5700 $M^{-1}cm^{-1}$, respectively) developed, accompanied by the shift of the broad LF envelope from 690 to about 600 nm (Figure 2.4). These changes were due to the formation of a bis-μ-(hydroxo)dicopper(II) species in methanol.[2e]

2.2.2.2. ^{1}H-NMR coupling studies of [Cu$_2$(L55Bu$_4$)]$^{4+}$ with hydroxide*

The unpaired electron in d orbitals of copper(II) makes this ion paramagnetic. This effects the ^{1}H-NMR spectra of copper(II) complexes; broadening and significant shifts of protons resonance values are observed, due to the relaxation effect on hydrogen nuclei induced by the unpaired electron. For dinuclear copper complexes, the broadening effect can be reduced or even cancelled in some cases, when bridging molecules generate a strong coupling between the unpaired electrons of the two copper nuclei, that could even lead to strongly coupled diamagnetic centers. [2e]

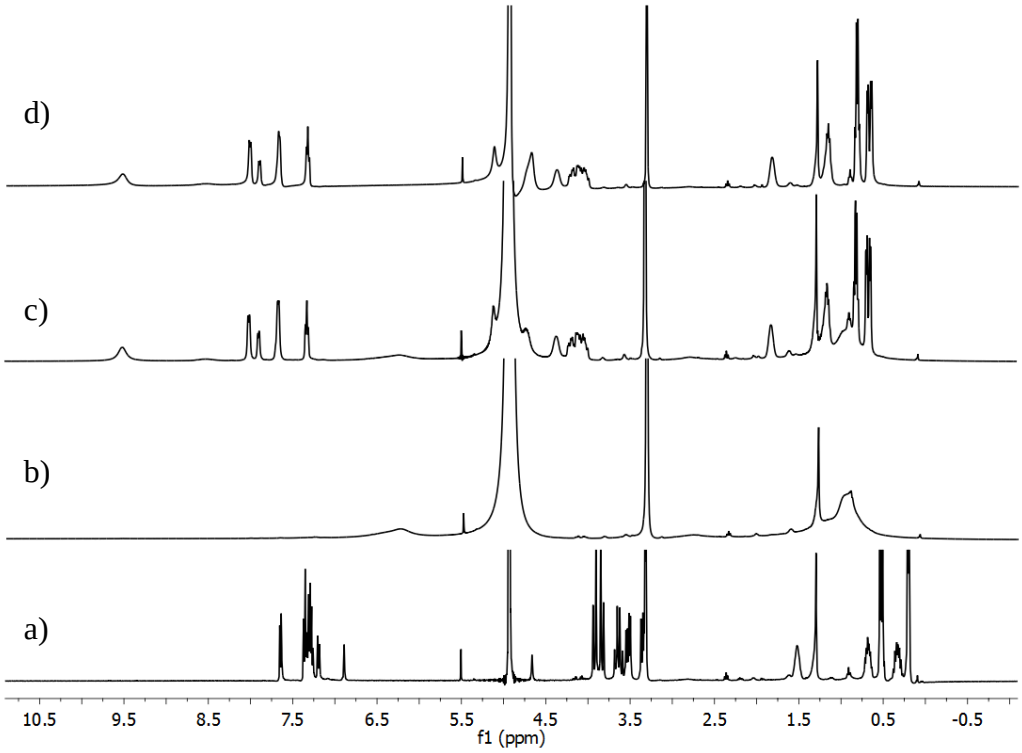

Figure 2.5- ^{1}H-NMR spectra of a) free ligand L55Bu$_4$*; b) [Cu$_2$(L55Bu$_4$*)]$^{4+}$; c) + 1 equivalent of OH$^-$; + 2 equivalents of OH$^-$ in MeOD.

Here an NMR study confirming the formation of a strong bridging bond induced by the addition of OH$^-$ to a deuterated methanolic solution of [Cu$_2$(L55Bu$_4$*)]$^{4+}$ is reported (Figure 2.5). It is evident that after the addition of the copper(II) salt and generation of the dinuclear copper complex, the spectrum changes from well-defined, sharp signals to broad signals. Upon addition of the first equivalent of OH$^-$, all signals re-acquired sharp shapes, with no further changes after the addition of the second equivalent of anion. Furthermore, the signals undergo changes in chemical shifts, compared with the free ligand, so that we can conclude is that the addition of OH$^-$ does not induce

demetallation of the complex, but rather strongly couples the two copper(II) ions, generating a diamagnetic species.

2.2.2.3. Uv-Vis titration of [Cu$_2$(L55Bu$_4$)]$^{4+}$ with azide anion*

2.2.2.4. Copper-azide binding studies

Azide is a small ligand extensively used to mimic the interaction of copper complexes (especially dinuclear complex with oxygen). Many biomimetic systems of enzymes belonging to the oxygenases and oxidases family contain dinuclear copper complexes, so azide-binding studies represent a powerful tool.[1,13] Copper(II)-azido interactions can be studied with a large variety of spectroscopic techniques. The nature of HOMO of azide (a set of filled degenerate π orbitals[14]) makes this ligand spectroscopically similar to peroxide[15] (Figure 2.6)[16]. Azide-copper(II) complexes were prepared for a series of biomimetic copper complexes of met- mollusk and arthropod hemocyanin[19] and met-tyrosinase. [20]

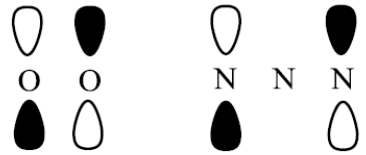

Figure 2.6- In-plane HOMO orbitals of peroxide and azide anions.

Azide can bind metal ions in different fashions, that can be differentiated by their spectroscopic features. Terminal azide adducts are 1:1 copper azide complexes (Figure 2.7). The absorption spectra tipically show an intense band around 400 nm. This band is attributable to a charge transfer transition from the HOMO of azide ($\pi_{nb\ \delta}$) to the $d_{x^2-y^2}$ orbital of copper, while the second interaction is weaker and derives from a π interaction between the orthogonal HOMO of the azide and copper $d_{x^2-y^2}$ orbital.

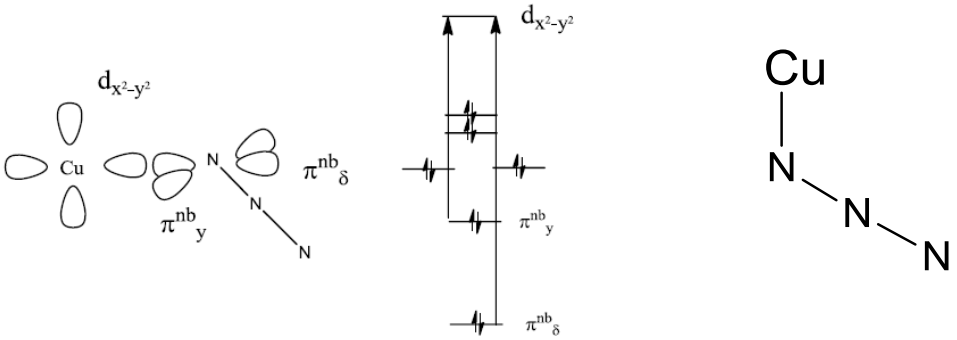

Figure 2.7- Left- Orbital energy diagram of azide and schematic representation of copper-azide interaction. Right- Terminal azide-copper adduct.

Azide can be also bind in a bridging fashion, in two different arrangments, yielding μ-1,3 and μ-1,1-adducts. In μ-1,3 azide-copper adduct, the charge transfer transitions responsible for the absorption features are the same as in the terminal mode. The better overlap of $d_{x^2-y^2}$ of copper and the orthogonal π_{nb} of azide increase the intensity of this weaker transition.

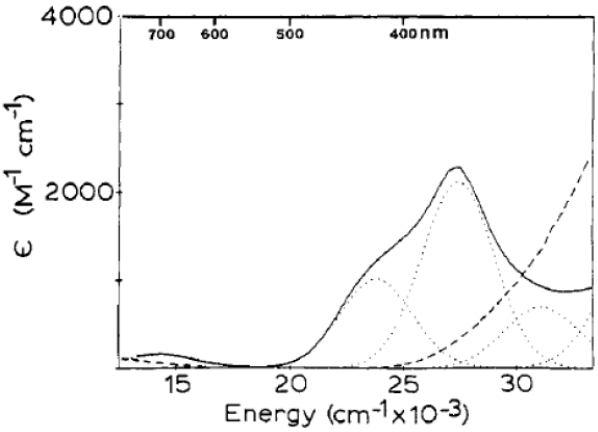

Figure 2.8- Absorption spectra of acetonitrile solutions of $[Cu_2(L\text{-}Et)(N_3)](BF_4)_2$ (solid line) and $[Cu_2(L\text{-}Et)(OAc)](ClO_4)_2$ (dashed line). L-Et: the anion of N,N,N',N'-tetrakis[2-(l-ethylbenzimidazolyl)]-2-hydroxy-l,3-diaminopropane. Gaussian components of the azide complex are indicated by dotted line.[17]

Spectroscopic studies on dinuclear copper(II)-azide complexes, reported by Pate ed al., [17] compared several complexes that binds azide in different fashions. $[Cu_2(L\text{-}Et)(N_3)](BF_4)_2$, forming a μ-1,3-azide adduct, shows an electronic spectrum consisting in an intense band at around 375 nm (ε = 2300 $M^{-1}cm^{-1}$), accompanied by a shoulder at 440 nm (ε 1200 $M^{-1}cm^{-1}$). Computation analysis resolved these features, attributing the resulting spectrum to two charge transfer bands, at 365 nm (ε = 2100 $M^{-1}cm^{-1}$) and 420

nm (ε = 1000 $M^{-1}cm^{-1}$). Comparison with the not-azide-cointaining $[Cu_2(L\text{-}Et)(OAc)](ClO_4)_2$ demonstrates that these bands are associated with the bound azide.

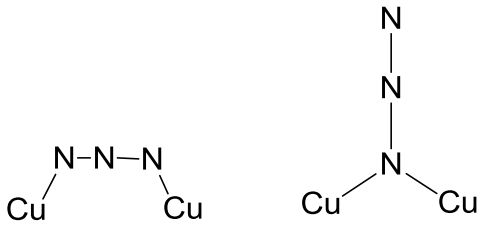

Scheme 2.6- Schematic representation of μ-1,3 and μ-1,1 azide adducts.

The arrangment of μ-1,1 azide adducts facilitates the binding of a second bridging molecule, such as hydroxide, phenolate or other oxo-ligands. This peculiarity complicates the assignment of the spectral transitions .

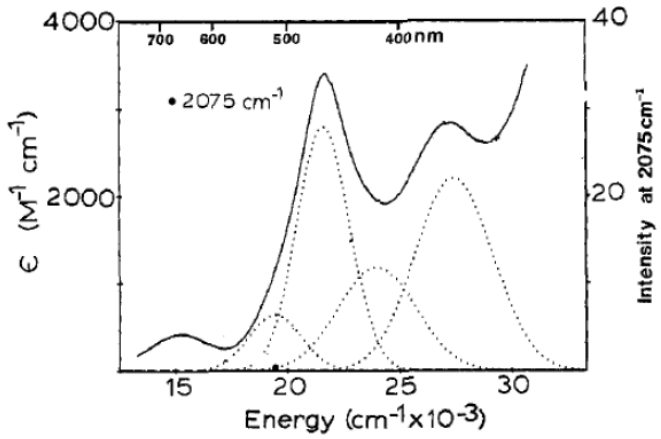

Figure 2.9- Absorption spectra of an acetonitrile solutions of $[Cu_2(L\text{-}O^-)(N_3)]$(solid line). $L\text{-}O^-$: the anion of 2,6-bis-[N,N-bis(2-pyridylethyl)aminomethyl]phenol. Gaussian components of the azide complex (dotted line).[17]

2.2.2.5. [Cu$_2$(L55Bu$_4$)]-azide adducts - UV-Vis characterization*

UV-Vis binding studies were performed with the dinuclear copper(II) complex of L55Bu$_4$*, by monitoring the spectral changes upon addition of a solution of sodium azide (Figure 2.10). As the structure is basically the same as the parent L55, the intramolecular binding of azide anion was expected to give the same spectral feature.[2e]

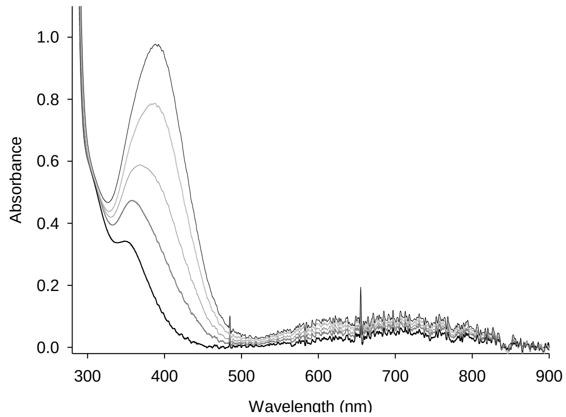

Figure 2.10- UV-Vis spectra of $Cu_2(L55Bu_4*)-N_3$ adducts: spectral changes upon addition of NaN_3 solution from 0 to 2 equivalents.

As shown before, the near-UV LMCT feature of a bridging μ-azido-dicopper(II) complex consists in a broad multicomponent absorption band, in the range 370-390 nm, due to the coupling of transition moments. The LMCT features of $[Cu_2(L55Bu_4*)]$-azido complex, almost superimposable to the $[Cu_2L55]$-azido analog, [2e] consist in a broad asymmetric band, centered at 370 nm, accompanied by a poorly defined shoulder. The band shifted from 370 to 390 nm as more azide solution was added, up to 2 equivalents (Figure 2.10). This behavior is attributable to the formation of a bis-μ-1,1-Cu_2-N_3 complex (Scheme 2.7).

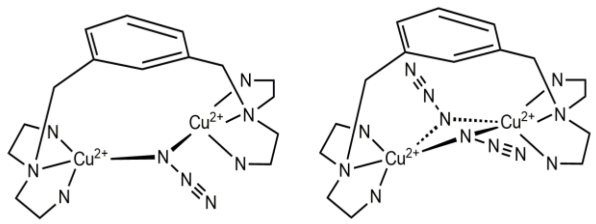

Scheme 2.7- Mono (left) and bis (right) azido-dicopper(II) adducts structure proposed for $Cu_2(L55Bu_4*)(N_3)_n$ with n= 1,2.

2.2.2.6. [$Cu_2(L55Bu_4)*$]-azide adducts - CD studies

Contrary to L55, the alkylated analogue $L55Bu_4*$ contains stereocenters in the ligand skeleton, so CD analysis of the dicopper complex and of the μ-azido dicopper complexes could give important information on the optical activity of the modeled oxygen intermediates (Figure 2.11).

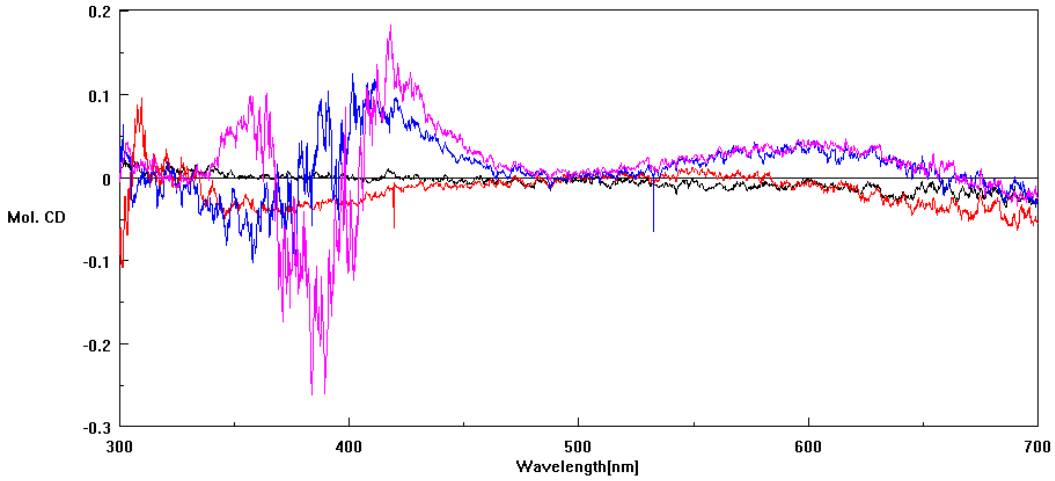

Figure 2.11- CD spectra of ligand L55Bu$_4$* (black), Cu_2(L55Bu$_4$*) (red), [Cu_2(L55Bu$_4$*)]N_3 (blue), [Cu_2(L55Bu$_4$*)](N_3)$_2$ (pink).

The CD spectrum of the μ-mono-azido-dicopper(II) complex exhibits two well resolved bands, a negative peak at 318 nm and a positive peak at 410 nm. These are related to a pair of azide LMCT→Cu(II) transitions. For the μ-bis-azido-dicopper(II) adduct, peculiar CD features were also observed. The higher energy band was reversed in sign, while a prominent negative band appeared at 387 nm, partially cancelling the positive component at 410 nm. These peculiarities are difficult to interpret. They probably arise from an exciton coupling of LMCT transitions, that are expected to increase the number of components in the optical absorption. Coordination of an azide anion also generated significant changes in lower energy d-d bands. The absorption maximum of the d-d envelope shifts to 650 nm, and is accompanied by CD changes. This transition was evidenced by a CD band at 610 nm of positive sign. It is also worth of notice that the coordination of a second azide anion does not change the CD features, indicating that the binding of this second molecule occurrs with no changes in coordination mode (Figure 2.11).

2.2.3. Stereoselective oxidation of chiral catechols- catecholase activity.

A set of enantiomeric catechols of biological interest was chosen to study the ability of the dinuclear copper complex of L55Bu$_4$* to promote enantio-discrimination in oxidation of catechols. The set of substrates (Figure 2.12) was previously used to test the enantiodifferentiating power in catechol oxidation of other dinuclear and trinuclear complexes. [3]

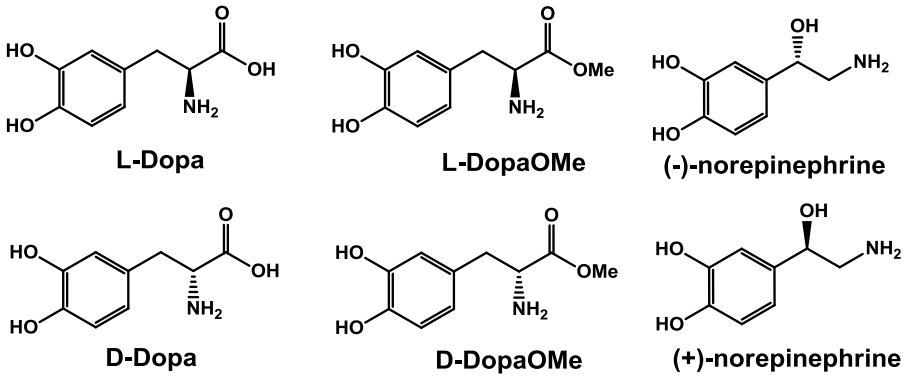

Figure 2.12. Enantiomeric pairs of chiral catechols used for the investigation of enantio-discriminating catecholase activity, promoted by $[Cu_2(L55Bu_4*)]^{4+}$.

Proposed mechanism for oxidation of these amino catechols suggests an initial formation of the quinone-intermediate, that acting as a Michael acceptor gives intramolecular cyclization to generate the related aminochrome.

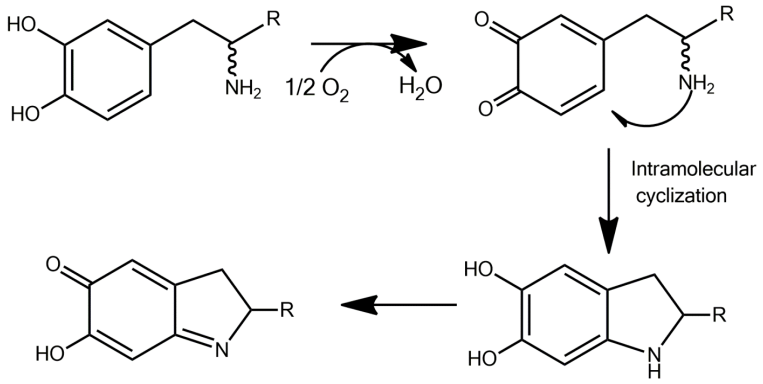

Previously, these studies were conducted in presence of MBTH, [3c-d, 4] a typical probe for quinones that generates a stable adduct, with high absorbance upon reaction with the quinone moiety. MBTH was subsequently abandoned as it was found to be non-redox innocent. Fortunately, the aminochrome intermediate, that spontaneously undergoes other polymerization reactions, is enough stable to be followed experimentally by UV-Vis techniques. The studies were, therefore, conducted by spectrophotometric analysis, following the increase of the band of aminochrome (around 475 nm) with time, and varying the substrate concentration. To slow down the following polymerization reaction, we chose to work in slightly acidic mixture, using acetate buffer at pH 5.1 in combination with methanol in 1:10 ratio. In these conditions, it was possible to perform the entire kinetic study, in order to extrapolate parameters of interest. The mechanism

involved in this reaction was extensively studied for $[Cu_2L55]^{4+}$, and can be briefly described as follow.[2c]

First Step:

$$[Cu^{II}\text{-OH-}Cu^{II}]^{3+} + CatH_2 \leftrightarrows [Cu^{II}\text{-Cat-}Cu^{II}]^{2+} + H_2O + H^+ \quad \text{(Ia)}$$

$$[Cu^{II}\text{-Cat-}Cu^{II}]^{2+} \rightarrow [Cu^{I}_2]^{2+} + Qui \quad \text{(Ib)}$$

Second Step

$$[Cu^{I}_2]^{2+} + CatH_2 + O_2 \leftrightarrows [Cu^{II}_2O_2/Cat]^{2+} + 2\,H^+ \quad \text{(IIa)}$$

$$[Cu^{II}_2O_2/Cat]^{2+} + 3\,H^+ \rightarrow [Cu^{II}\text{-OH-}Cu^{II}]^{3+} + Qui + H_2O \quad \text{(IIb)}$$

The reaction proceeds in two steps. During the first step, a molecule of catechol is oxidized by the dinuclear copper(II) complex, which is consequently reduced to copper(I). The reduced complex reacts with dioxygen, generating a reacting intermediate that is able to oxidize a second molecule of substrate. In the initial condition, the complex is supposed to contain a bridging hydroxide anion that pre-organizes the complex and favors the deprotonation of the catechol, a key step allowing its coordination to copper. $CatH_2$ represents the substrate, Qui the quinone, while $[Cu^{II}_2O_2/Cat]^{2+}$ is the tertiary intermediate. The mechanism studies on $[Cu_2L55]^{4+}$ used 3,5-ditertbutylcatechol as substrate, because the corrisponding quinone is stable in the reaction conditions. With this kind of electron-rich catechol, the reaction exhibits a biphasic kinetic behavior, and it was possible to separate the first step from the second one, and determine the related parameters.[2c] When the biogenic catechols are used as substrates, the kinetic profile is monophasic, so we were unable to separate the two steps, but the oxidation rate at increasing substrate concentration followed a typical hyperbolic trend. This behavior could be interpreted using the Michaelis-Menten equation as model. It was so possible to extrapolate two parameter, k_{cat} and K_M, using the following simplified reaction scheme:

$$Cu + C \underset{}{\overset{K_M}{\rightleftharpoons}} Cu\text{-}C \xrightarrow{k_{cat}} Cu + Q$$

The reaction could be analyzed with a pre-equilibrium kinetic model, and in this case the K_M has the meaning of a dissociation constant for the preequilibrium binding, while k_{cat} can be interpreted as the oxidation rate. K_M indicates substrate affinity (higher

values corresponding to lower affinity and *viceversa*), while k_{cat} was related to how the effective binding of the substrate facilitate the electron transfer reaction. The rate data are expressed as $v/[catalyst] = \left(\frac{(A/s)}{\varepsilon\ aminochrome}\right)/[complex]$, where A/s is the absorbance changes with time upon formation of the quinone and $\varepsilon\ aminochrome$ is equal to 3600 M^{-1} s^{-1}.[18] K_M and k_{cat} values are listed in Table 2.1.

Table 2.1- Kinetic parameters for the catalytic oxidation of catecholic substrates in methanol/50 mM aqueous acetate buffer, pH 5.1, 10:1 (v/v), at 25 °C.

Substrate	K_M (mM)	k_{cat} (s^{-1})	k_{cat}/K_M ($M^{-1}s^{-1}$)	R(k_{cat}) %	R(k_{cat}/K_M) %
L-Dopa	0.12 ± 0.02	(1.1 ± 0.1) ×10^{-3}	9.0	+ 4 %	- 21 %
D-Dopa	0.07 ± 0.015	(9.7 ± 0.5) ×10^{-4}	13.9		
L-DopaOMe	0.25 ± 0.03	(1.3 ± 0.1) ×10^{-2}	53.7	+70 %	- 36 %
D-DopaOMe	0.020 ± 0.007	(2.3 ± 0.1) ×10^{-3}	114.0		
L-norepinephrine	0.11 ± 0.01	(7.5 ± 0.2) ×10^{-4}	6.9	- 3 %	- 3 %
D-norepinephrine	0.11 ± 0.01	(7.9 ± 0.1) ×10^{-4}	7.3		

Enantiodifferentiation can be deduced by direct observation of K_M and k_{cat} values, but two more parameters were calculated to underline the differences among the series, R(k_{cat}) % and R(k_{cat}/K_M) %, as defined below.

$$R(k_{cat})\ \% = \frac{(k_{cat})^L - (k_{cat})^D}{(k_{cat})^L + (k_{cat})^D} \times 100$$

$$R(k_{cat}/K_m)\ \% = \frac{(k_{cat}/K_m)^L - (k_{cat}/K_m)^D}{(k_{cat}/K_m)^L + (k_{cat}/K_m)^D} \times 100$$

R % > 0 correspond to a preference for the L enantiomer, while R% < 0 is related to the opposite situation. R(k_{cat}) % is used to evaluate discrimination at high concentration of

substrate, while the term R(k_{cat}/K_M) %, containing K_M value, describes the enantioselectivity at low concentration of substrate. It can be explained by considering that in the second case, the affinity between the complex and the substrate plays an important role, as low concentration of substrate corresponds to a smaller fraction of bound catechol, while in the first case the saturating conditions makes the reaction depend only on the electron transfer rate. From the observation of the data in Table 1 and Figure S.I. 2.1 it is possible to deduce that no relevant enantiodifferentiation was found for the pair of L/D-Dopa and L/D-norepinephrine substrates, while a good selectivity was found for the couple L/D-Dopa methyl ester. The difference in discrimination between the two pairs L/D-Dopa and L/D-DopaOMe can be explained by supposing that the zwitterionic nature of Dopa interferes with the hydrophobic nature of the benzimidazolic complex. In norepinephrine, instead, the stereocenter is located closer to the catecholic ring, so the chiral information brought by the copper complex might not match with the one on the substrate. Another peculiarity can be deduced by the observation of the data in Table 1: selectivity in oxidation of L/D-DopaOMe is reversed passing from low to high concentration of substrate. An R(k_{cat}/K_M) % < 0 means that D enantiomer is strongly bound by the dicopper(II) complex, while a R(k_{cat}) % > 0 indicates a more efficient electron transfer of the L substrate. This could be explained by assuming that a stronger binding is not necessarily related to a more efficient electron transfer, which essentially depends on the correct orientation of the substrate in the complex "cavity" and, to a lesser extent, from the dissociation of the obtained quinone.

2.2.4. Catalytic sulfoxidation of thioanisole

Tyrosinase was previously found to act as external monoxygenase,[6] catalyzing the oxidation of sulfides, with moderate yields but high enantiomeric excess (up to 85 %). As sulfides have not the adequate redox potential to reduce the met-form (in which both copper are as copper(II)), the reaction was carried out with an external source of electrons (Scheme 2.8). L-Dopa was chosen as sacrifical reducing agent, but the high competition between the catecholic substrate and the sulfide could explain the low reaction yields.

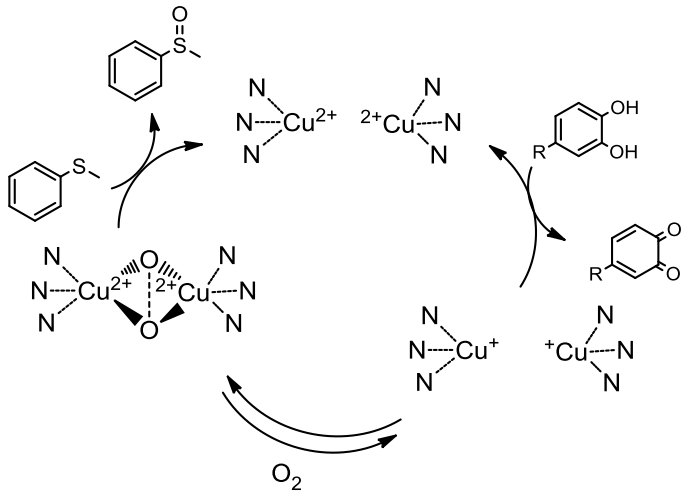

Scheme 2.8- Catalytic cycle proposed for the oxidation of sulfides promoted by tyrosinase.

This behavior was also found when the dinuclear copper complex of ligand L55 was used as catalyst, with hydroxylamine as reducing cofactor.[2a] From this starting point, due to the intrinsic chiral nature of the $[Cu_2(L55Bu_4*)]^{4+}$, we decided to replicate this kind of activity, focusing on the possibility to transfer the chiral information on the obtained sulfoxide. Thioanisole was used as substrate, and reaction conditions were maintained identical to those used for the achiral L55 complex analogue. Unfortunately, at least in the condition used, the oxidation of thioanisole to sulfoxide occurred, but did not show an efficient transfer of chiral information. S-methyl-phenylsulfoxide was, in fact, obtained with a modest enantiomeric excess of 12%. This result is not surprising: the orientation of aromatic sulfides inside the cavity of $[Cu_2(L55Bu_4*)]^{4+}$ can be guided by π-π stacking interaction with the benzimidazoles. In this arrangement, the chiral alkyl chain of benzimidazole cannot significantly interact with the sulfide. Also the reaction conditions may need further optimization as well as changing the reducing agent could improve the stereoselectivity.

2.3. Conclusions

The ligand L55Bu$_4$* was synthesized by modifying the skeleton of the well-known L55 analog, inserting chiral 2-methyl-butyl chains in substitution of the methyl groups on benzimidazoles. In the synthesis of the new ligand, two different synthetic pathways were undertaken, but only one of them brought to the final product. The dinuclear copper(II) complex of L55Bu$_4$* was analyzed with spectroscopic techniques, that

enabled to show its tendency to form hydroxo complexes. Its efficiency as biomimetic system was proved in catecholase activity, where it was found to appreciably discriminate the oxidation of L/D-Dopa methyl esters, favoring the L enantiomer. Studies on oxidation of sulfides in presence of hydroxylamine did not yield the expected results, but represent a good starting point for future studies. Changing reaction mixture or reducing agent could improve both yield and enantioselectivity.

2.4. Experimental section

Materials and methods

All reagents and solvents from commercial sources were of the highest purity available and were used as received. Elemental analyses were obtained at the Microanalysis service of the Milano CIMA department. CD spectra were obtained with a Jasco J500 spectropolarimeter, spectra were recorded in the range 300-700 nm, at 50 nm/min, with three scans acquired for each spectrum, and 0.2 nm resolution. NMR spectra were recorded on a Bruker AVANCE 400 spectrometer, operating at 9.37 T, with 400.13 and 100.6 MHz proton and carbon-13 frequencies, respectively. Data acquisition and processing were performed using a standard Bruker software package (Topspin 1.3). UV-Vis spectra were recorded on an Agilent 8453 spectrophotometer. HPLC analyses were performed on a Jasco HPLC instrument equipped with two PU-1580 pumps and a MD-1510 diode array detector (working range: 195–659 nm). Mass spectra were recorded using a Thermo-Finnigan LCQ ADV MAX spectrometer.

General procedures

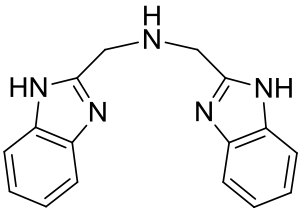

Synthesis of bis((1H-benzimidazol-2-yl)methyl)amine (**2.1-BB5H**): 4.05 g of 1,2-diaminobenzene (0.037 mol) and 2.5 g of iminodiacetic acid (0.019 mol) were intimately crushed and then suspended in ethylene glycol. The suspension was stirred overnight in a pre-heated oil bath, at 180 °C. The mixture was poured in cold water, until a pink, feathery solid precipitated. Three recrystallizations from methanol/water (1:1) gave the ligand as pink powder (5.3 g, 49%).

^{1}H-NMR (400 MHz, MeOD) δ 7.54 (dd, *J* = 6.0, 3.0 Hz, 4H), 7.22 (dd, *J* = 6.0, 3.0 Hz, 4H), 4.11 (s, 4H). MS (ESI): *m/z* +278 $[M+H]^+$

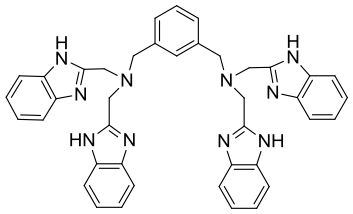

Synthesis of N,N-[1,3-Phenylenebis(methylene)]bis{N-[(1H-benzimidazol-2-yl)-methyl]-1-(1H-benzimidazol-2-yl)methanamine} (**2.2-L55H**): To a solution of BB5H (0.50 g, 1.8 mmol) in dry *N*,*N*-dimethylformamide (DMF, 70 mL) were sequentially added *m*-bromoxylene (0.238 g, 0.9 mmol) and solid Na_2CO_3 (0.191 g, 1.8 mmol), and the mixture was heated at 80 °C for 48 h. The solvent was removed by rotary evaporation to yield the crude product, which was purified by chromatography with silica gel as the stationary phase and a mixture of ethyl acetate/methanol (8:2) and 1.5% aqueous ammonia (30%) as the eluent, yield 41%. ^{1}H-NMR (MeOD): δ = 7.48 (dd, J = 6.0, 3.0 Hz, 8 H), 7.16 (m, 12 H), 3.95 (s, 8 H), 3.58 (s, 4 H) ppm. MS (ESI): m/z = 657 $[M + H]^+$.

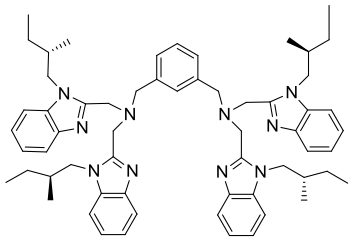

Synthesis of (S)-N,N'-(1,3-phenylenebis(methylene))bis(1-(1-((S)-2-methylbuthyl)-1H-benzimidazol-2-yl)-N-((1-((s)-2-methylbutyl)-1H-benzimidazol-2-yl)methyl)methanamine (**2.3-L55Bu$_4$***)*:* 0.205 g of L55H (0.3 mmol) were dissolved in 4 mL of DMSO, then 0.175 g of KOH (3 mmol) were poured into the solution, which was left stirring at r.t for an hour. The color of the solution turned from orange to brown, suggesting deprotonation of L55H. 0.162 mL of S-2-methyliodobutane (1.25 mmol) were then added and the reaction proceeded at r.t overnight. (*The flask was wrapped in aluminum foils in order to prevent the degradation of the photosensitive chiral iodide*) Further equivalents of chiral iodide were added until no more changes appeared in the reaction (5 mmol overall). The progress of the reaction was monitored by MS-spectrometry. The solution was diluted with 20 mL of distilled water to give a white suspension, that was extracted 10 times with dichloromethane. The reunited organic phases were washed twice with water, then dried on Na_2SO_4, filtered, and the solvent was eliminated by rotary evaporation, to yield the crude product. The mixture was separated by semi-preparative HPLC with C18 reverse-phase column using a gradient of acetonitrile:water, from 45:55 to 100:0, containing 0.1% of trifluoroacetic acid in 23 minutes (r.t. product = 15 min). The product was treated with concentrated ammonia solution, then extracted with dichloromethane in order to give the free amine. Yield: 11 %. Optical purity was confirmed by HPLC analysis using chiral column Lux 5u Amylose-2 (0.46 Φ x 25 cm), eluent: hexane:2-propanol = 60:40 flow rate: 0.8 ml min^{-1}. ^{1}H-NMR (400 MHz, $CDCl_3$) δ 7.74 (dd, J = 6.0, 3.0 Hz, 4H), 7.28 – 7.17 (m, 14H), 7.15 (d, J = 7.4 Hz, 2H), 6.97 (s,

1H), 3.92 (dd, *J* = 35.1, 13.5 Hz, 8H), 3.71 (dd, *J* = 35.0, 13.0 Hz, 4H), 3.47 (ddd, *J* = 22.9, 14.4, 7.7 Hz, 8H), 1.65 – 1.44 (m, 4H), 0.85 – 0.68 (m, 4H), 0.55 (t, *J* = 7.2 Hz, 12H), 0.48 – 0.31 (m, 4H), 0.25 (d, *J* = 6.6 Hz, 12H). ^{13}C-NMR (100 MHz, $CDCl_3$) δ 151.65 (Q), 142.77 (Q), 139.12 (Q), 135.89 (Q), 131.49 (CH), 129.61 (CH), 129.07 (CH), 123.03 (CH), 122.39 (CH), 120.14 (CH), 110.48 (CH), 59.54 (CH_2), 51.13 (CH_2), 49.83 (CH_2), 35.18 (CH), 26.90 (CH_2), 16.54 (CH_3), 11.59 (CH_3). UV (MeOH) λmax (ε, M^{-1} cm^{-1}): 280 (2700), 330 sh (350), 380 nm (150). CD (MeOH) λmax (Δε, M^{-1} cm^{-1}): 280 (-0.3), 320 nm (+0.02). MS: +937,61 $[M+H]^+$, +469,78 $[M+2H]^{2+}$.

Synthesis of the [Cu$_2$(L55Bu$_4$)](ClO$_4$)$_4$:* 10 mg of L55Bu$_4$* (0.010 mol) were dissolved in 500 μL of methanol, giving a pale yellow solution. 7.9 mg of $Cu(ClO_4)_2 \times 6H_2O$ (0.022 mmol) dissolved in 500 μL were added dropwise to the ligand solution, which turned from yellow to dark green. The solution was stirred for 15 minutes at r.t, then diethyl ether was added until a green precipitate appeared. The green solid was washed three times with diethyl ether, then dried under vacuum. (Yield 70%). UV (MeOH) λmax (ε, M^{-1} cm^{-1}): 315 sh (1700), 355 (840), 688 nm (200). CD (MeOH) λmax (Δε, M^{-1} cm^{-1}): 380 (-0.05), 560 (+0.01), 690 br nm (-0.04). Anal calcd for $C_{60}H_{76}Cl_4Cu_2N_{10}O_{16} \cdot 4H_2O$: C, 46.97; H, 5.52; N, 9.13; Found : C, 46.82, H, 5.50, N, 8.87.

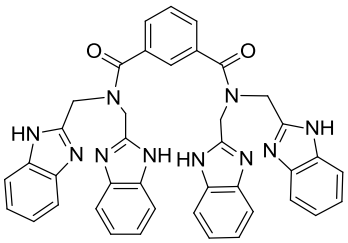

Synthesis of N^1,N^1,N^3,N^3-tetrakis((1H-benzoimidazol-2-yl)methyl)isophthalamide (**2.4**)*:* 0.045 g of isophtalic acid (0.27 mmol) were dissolved in 5.5 mL of DMF. 0.205 g of HBTU (0.54 mmol) were added to the solution, that was let stirring for 5 min. A solution of 0.152 g of BB5H (0.55 mmol) in 1.5 mL of DMF was then added dropwise, followed by the addition of 0.188 mL of triethylamine (1.35 mmol). The reaction mixture was bubbled with argon, that left under stirring overnight. DMF was removed by rotary evaporation, then ethyl acetate was added: with the use of ultrasound, a pale pink powder is obtained from the orange oil. The powder was collected and washed three times with ethyl acetate. Yield: 84 %; ^{1}H-NMR (400 MHz, CD_3CN) δ 7.77 (m, 8H), 7.38 (m, 9H), 7.17 (d, *J* = 7.6 Hz, 2H), 6.97 (t, *J* = 7.7 Hz, 1H), 5.06 (s, 4H), 4.88 (s, 4H). ; ESI-MS: +685 $[M-H^+]$

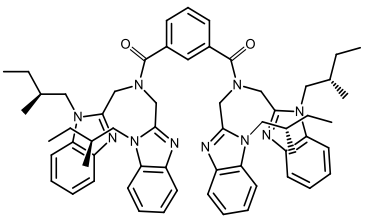

Synthesis of N1,N1,N3,N3-tetrakis((1-((S)-2-methylbutyl)-1H-benzo[d]imidazol-2-yl)methyl)isophthalamide (**2.5**)*:* 0.245 g of compound **2.4** (0.36 mmol) were dissolved in dimethylsulfoxide (DMSO). 0.200 g of KOH (3.6 mmol), opportunely minced, were added to the solution, that was left stirring for about 40 minutes. 0.186 mL of 2-(S)-methylbutyl iodide (4 equivalents) were added to the solution, that was stirred overnight at room temperature. Further 2-(S)-methylbutyl iodide were added until no changes appeared in TLC and mass spectrum. The reaction mixture was diluted with 25 mL of distilled water and extracted 11 times with 20 mL of dichloromethane. The reunited organic extracts were washed with water, then dried on sodium sulfate, filtered and evaporated by rotary evaporation. The crude product was purified by column chromatography with silica gel 230-400 mesh and a 95:5 ethyl acetate/methanol mixture + 1.5% of ammonia solution (30%) as eluent. The product requires further purification, by column chromatography with silica gel as stationary phase and 1:1 hexane/ethyl acetate as eluent. ESI-MS: +965 [M-H$^+$]; ^{1}H-NMR (400 MHz, $CDCl_3$) δ 7.96 – 7.52 (m, 6H), 7.43 – 6.98 (m, 13H), 5.13 (s, 4H), 4.94 (s, 4H), 4.28 – 3.93 (ddd, *J*= 23, 14.5, 7.6 Hz, 4H), 3.76 (ddd, *J* = 23.0, 14.6, 7.5 Hz, 4H), 1.89 (bm, 2H), 1.68 (bm, 2H), 1.19 (m, 8H), 0.95 – 0.71 (m, 18H), 0.63 (d, *J* = 6.3 Hz, 6H).

[Cu$_2$L55Bu$_4$]$^{4+}$- NMR spectroscopy.*

1.8 mg (1.92 x 10^{-6} mol) of L55Bu$_4$* was dissolved in 600 μL of CD_3OD and an NMR spectrum was recorded. This solution was used to dissolve 1.4 mg of copper(II) trifluoromethanesulfonate and another spectrum was recorded. 1.0 μL of NaOH 2 M in D_2O was added and the spectrum was recorded. Another 1.0 μL of NaOH 2 M in D_2O was added and the last spectrum was recorded. The spectra recorded in the presence of Cu(II) was recorded using 187 ppm as spectral with and centered at 35 ppm, 800 acquisitions were accumulated with 0.2 second delay because of the short relaxation time promoted by the copper.

Catalytic oxidation of o-catechols.

The catecholase activity of [Cu$_2$(L55Bu$_4$*)]$^{4+}$ was determined for the catalytic oxidation of a series of chiral catechols L-Dopa, D-Dopa, L-DopaOMe, D-DopaOMe, R-(-)-norepinephrine, and S-(+)-norepinephrine. The kinetic studies of the oxidation of the *o*-

diphenols were carried out spectrophotometrically by the method of initial rates monitoring the increase of each characteristic product absorption band over time, respectively at 475 nm (ε475 = 3600 M^{-1} cm^{-1} for L-/D-Dopa), at 468 nm for L-/D-DopaOMe, at 480 nm for R-/S-norepinephrine. The solvent used was a 10:1 (v/v) mixture of methanol/aqueous acetate buffer (50 mM, pH 5.1). The experiments were carried out over a 5×10^{-5} to 1×10^{-3} M substrate concentration range, at a constant temperature of 20±0.1 °C. To determine the dependence of rate on substrate concentration a constant 5×10^{-6} M solution of this complex was treated with at least 10 equiv of substrate and a maximum of 200 equiv so as to maintain the pseudo first order condition.

Supporting information

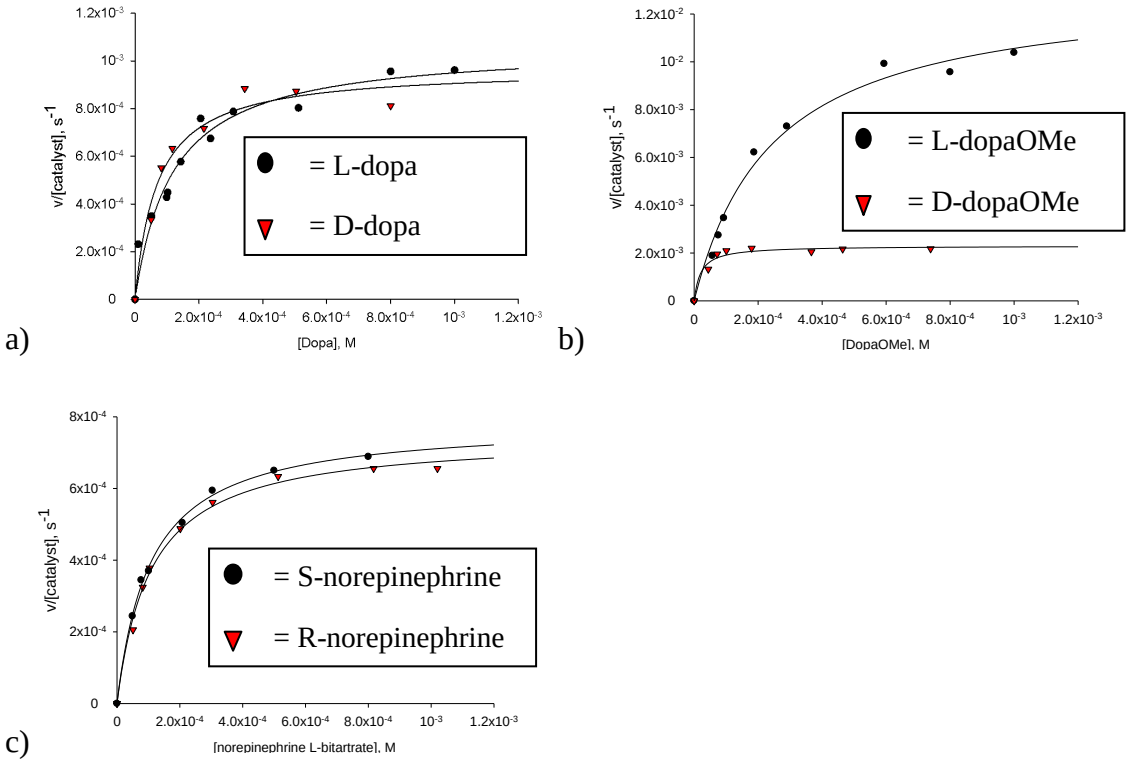

Figure S.I. 2.1- Effect of substrate concentration on initial rate of oxidation of a) L-/D-Dopa, b) L-/D-DopaOMe, c) R-/S-norepinephrine promoted by $[Cu_2(L55Bu_4*)]^{4+}$ 5 µM, in 10:1 MeOH:acetate buffer (50 mM, pH = 5.1), temperature: 25 °C.

a)

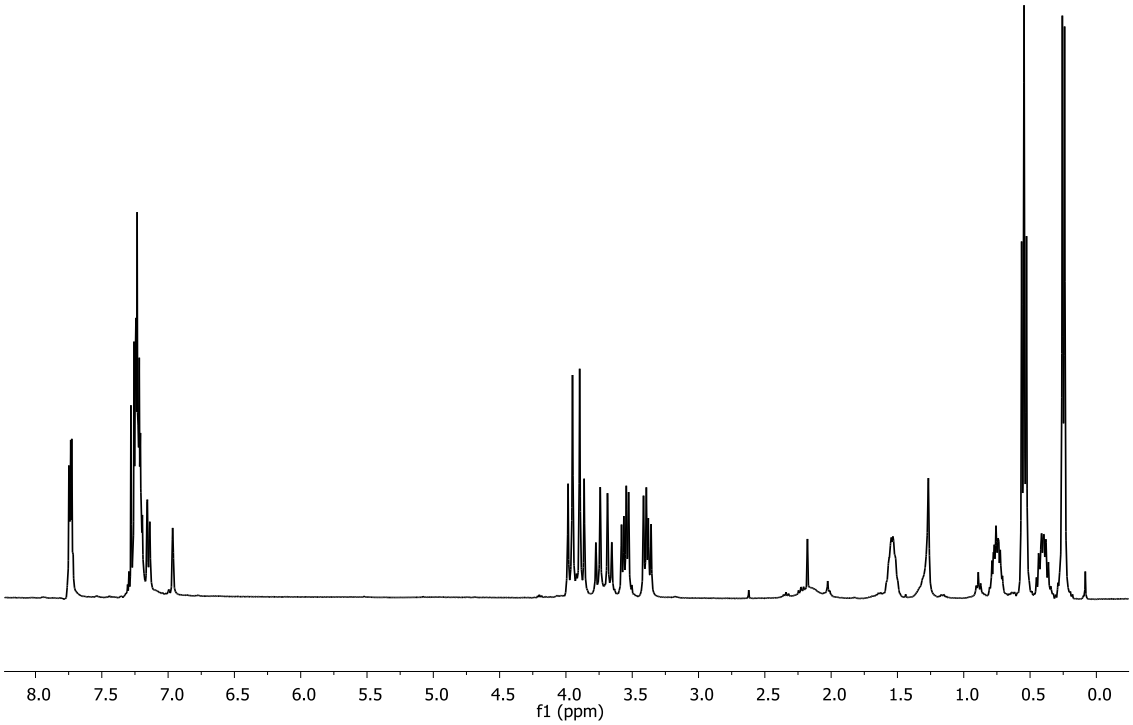
8.0
7.5
7.0
6.5
6.0
5.5
5.0
4.5
4.0
3.5
3.0
2.5
2.0
1.5
1.0
0.5
0.0
f1 (ppm)

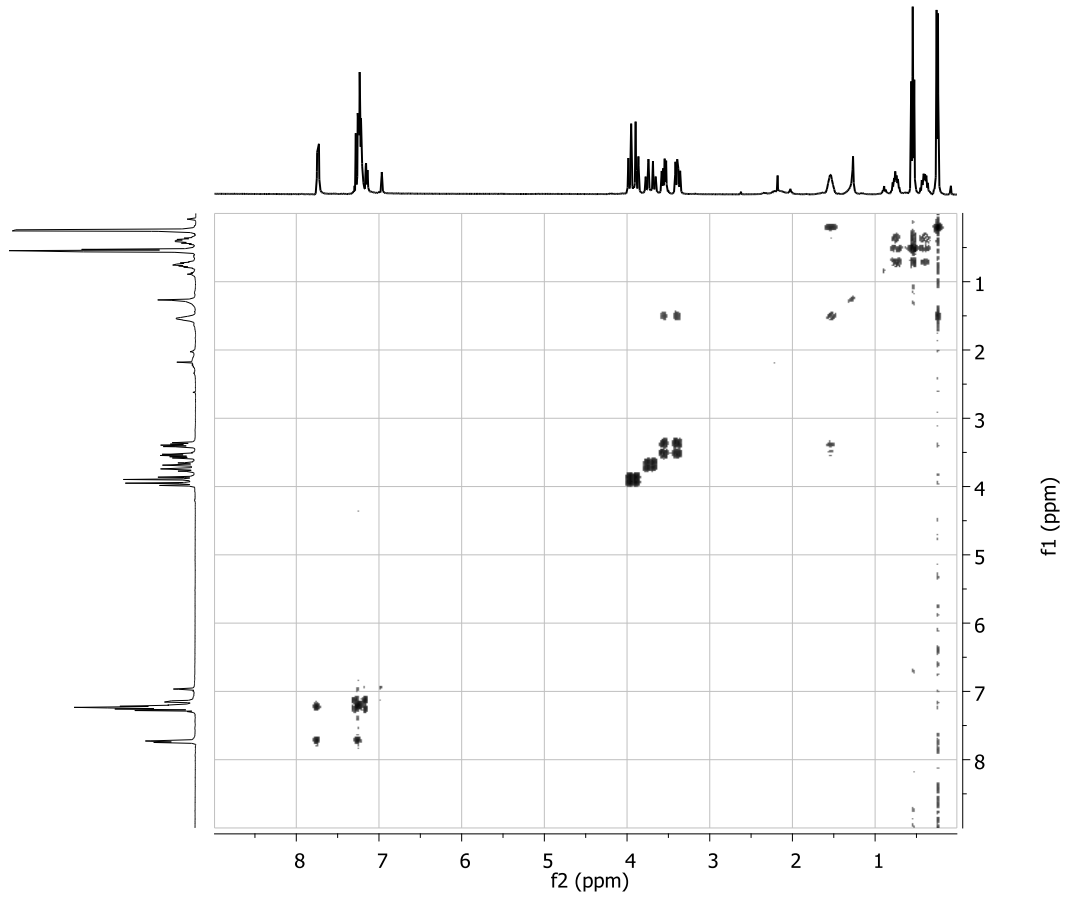
1
2
3
4
5
6
7
8
f1 (ppm)
8
7
6
5
4
3
2
1
f2 (ppm)

b)

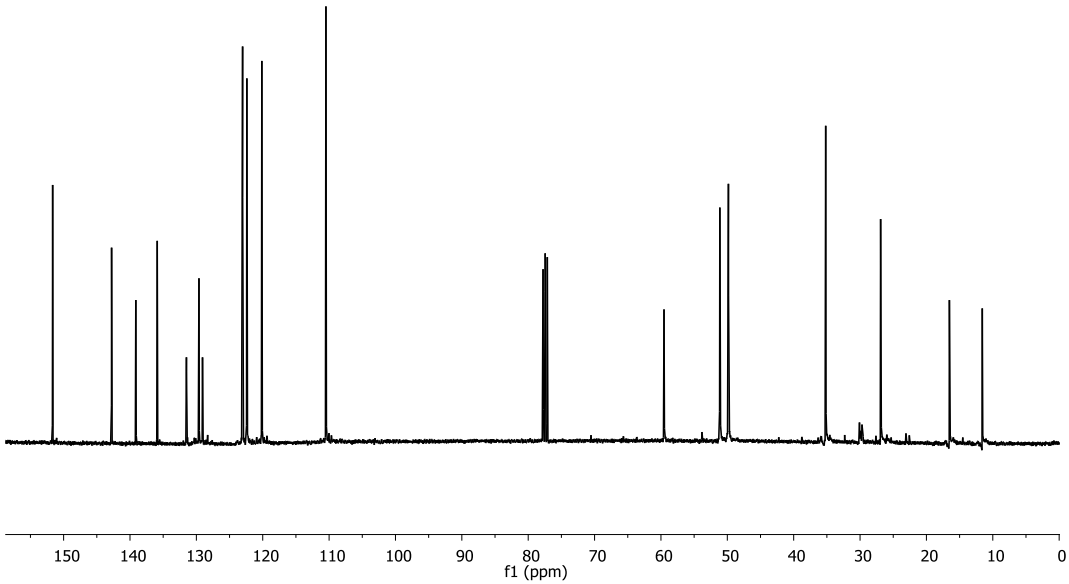

c)

Figure S.I 2.2- NMR characterization of L55Bu$_4$* a) ^{1}H-NMR, b) COSY, c) ^{13}CNMR recorded on a Brucker AVANCE 400 spectrometer, in $CDCl_3$.

References

1- G. Battaini, A. Granata, E. Monzani, M. Gullotti, L. Casella, *Adv. Inorg. Chem.* **2006**, 58, 185- 233.

2- (a) I. Gamba, S. Palavicini, E. Monzani, L. Casella, *Chem. Eur. J.*, 2**009**, 15, 12932-12936; (b) G. Battaini, L. Casella, M. Gullotti, E. Monzani, G. Nardin, A. Perotti, L. Randaccio, L. Santagostini, F. W. Heinemann, S. Schindler, *Eur. J. Inorg. Chem.*, **2003**, 1197-1205; (c) A. Granata, E. Monzani, L. Casella, *J. Biol. Inorg. Chem.*, **2004**, 9, 903-913; (d) S. Palavicini, A. Granata, E. Monzani, L. Casella, *J. Am. Chem. Soc.*, **2005**, 127, 18031-1836; (e) L. Casella, O. Carugo, M. Gullotti, S. Garofani, P. Zanello, *Inorg. Chem.*, **1993**, *32*, 2056–2067; (f) L. Casella, E. Monzani, M. Gullotti, D. Cavagnino, G. Cerina, L. Santagostini, R.Ugo, *Inorg. Chem.*, **1996**, *35*, 7516-7525.

3- (a) L. Santagostini, M. Gullotti, R. Pagliarin, E. Monzani, L. Casella, *Chem. Commun.*, **2003**, 2186-2187; (b) M. Gullotti, L. Santagostini, R. Pagliarin, S. Palavicini, L. Casella, E. Monzani, G. Zoppellaro, *Eur. J. Inorg. Chem.*, **2008**, 2081-2089; (c) M. C. Mimmi, M. Gullotti, L. Santagostini, G. Battaini, E. Monzani, R. Pagliarin, G. Zoppellaro, L. Casella, *Dalton Trans.*, **2004**, 2192-2201; (d) F. G. Mutti, M. Gullotti, L. Casella, L. Santagostini, R. Pagliarin, K. Kristoffer Andersson, M. F. Iozzi, G. Zoppellaro, *Dalton Trans.*, **2011**, 40, 5436-5457;

4- F. G. Mutti, G. Zoppellaro, M. Gullotti, L. Santagostini, R. Pagliarin, K. Kristoffer Andersson, L. Casella, *Eur. J. Inorg. Chem.*, **2009**, 554-566.

5- (a) M. E. Cuff, K. I. Miller, K.E. van Holde, W. A. Hendrickson, *J. Mol. Biol.*, **1998**, 278, 855–870; (b) E. I. Solomon., U. M. Sundaram, T. E. Machonkin, *Chem. Rev.*, **1996**, 96, 2563–2605.

6- R. Pievo, M. Gullotti, E. Monzani, L. Casella, *Biochemistry*, **2008**, 47, 3493–3498.

7- O'Mahony, G. E., Ford, A., Maguire, A. R., *Journal of organic chemistry*, **2012**, 77 (7), 3288-3296.

8- M. Perrone, E. Lo Presti, S. Dell'Acqua, E. Monzani, L. Santagostini, L.Casella, *Eur. J.I.C.* ,**2015**, 21, 3493–3500.

9- H. Adams, N. A. Bailey, J. Crane, D.F. Fentom, J.M. Williams, *J. Chem. Soc. Dalton Trans.*, **1990**, 1727–1735.

10- D. Chapman, C. Reed, *Tetrahedron Letters*, **1988**, 29, 3033-3036.

11- L. Santagostini, M. Gullotti, R. Pagliarin, E.Bianchi, L. Casella, E.Monzani, *Tetrahedron: Asymmetry*, **1999**, 10, 281–295.

12- (a) S. H. Xiang, J. Xu, H.Q. Yuan, P. Q. Huang, *Synlett*, **2010**; (b) G. Barbe, A. B. Charette, *J. Am. Chem. Soc.*, **2008**, 130, 18–19.

13- (a) E. A. Lewis, W. B. Tolman, *Chem. Rev.*, **2004**, *104*, 1047–1076; (b) L. Q. Hatcher, K. D. Karlin, *Adv. Inorg. Chem.*, **2006**, *58*, 131–184; (c) L. M. Mirica, X. Ottenwaelder, T. D. P. Stack, *Chem. Rev.*, **2004**, *104*, 1013–1045; (d) S. Itoh, S. Fukuzumi, *Acc. Chem. Res.*, **2007**, *40*, 592–600; (e) P. Gamez, P. G. Aubel, W. L. Driessen, J. Reedijk, *Chem. Soc.Rev.*, **2001**, *30*, 376–385.

14- (a) W. D. Closson, H. B. Gray, *J. Am. Chem. Soc.*, **1963**, *85*, 290-294. (b) J. R. McDonald, J. W. Rabalais, S. P. McGlynn, *J. Chem. Phys.*, **1970**, *52*, 1332-1340.

15- (a) U. Kaldor, I. Shavitt, *J. Chem. Phys.*, **1966**, 44, 1823-1829. (b) W. H. Fink, L. C. Allen, *J. Chem. Phys.*, **1967**, 46, 2261-2275. (c) W. H. Fink, L. C. Allen, *J. Chem. Phys.* **1967**, 46, 2276-2284. (d) B. M. Gimarc, *J. Am. Chem. Soc.*, **1970**, 92, 266-75.

16- J. E. Pate, P. K. Ross, T. J. Thamann, C. A. Reed, K. D. Karlin, T. N. Sorrell, E. I. Solomon, *J. Am. Chem Soc.* **1989**, 111,5198-5209.

17- J. E. Pate, P. K. Ross, T. J. Thamann, C. A. Reed, K. D. Karlin, T. N. Sorrel1, E. I. Solomon, *J. Am. Chem. SOC.*, **1989**, 111, 5198-5209.

18- Acta Biochimica polonica, vol 58, n 3, **2011**, 303-311.

19- (a) R. F. Ziolo, M. Allen, D. D. Titus, H. B. Gray, Z. Dori, *Inorg. Chem.* **1972**, 11 , 3044-3050. (b) K. D. Karlin, B. I Cohen, J. C. Hayes, A. Farooq, J. Zubieta, *Inorg. Chem.* **1987**, 26, 147-153.

20- R. S. Himmelwright, N. C. Eickman, C. D. LuBien, K. Lerch, E. I. Solomon, *J. Am. Chem. Soc.* **1980**, 102, 7339-7344.

Chapter 3. mXPhI

3. mXPhI

3.1. Introduction

The dinuclear copper complex of the ligand L55 is considered one of the most efficient biomimetic complex for catecholase activity. It is a dinucleating tetrabenzimidazole ligand, in which two amino bis-benzimidazolic units are interfaced by a m-xylyl bridge.[1] As explained in **Chapter 2**, the aim to progress toward biomimetic systems that can promote stereoselective oxidations prompted suitable modifications of the ligand skeleton. The alkylation of the benizimidazole nitrogens with 2-(S)-methyl-butyl iodide generates the chiral ligand L55Bu_4* discussed before. The related dinuclear copper complex displayed moderate efficiency in catalyze enantiodiscriminating catecholase activity, except for the pair of L/D-Dopa methyl ester.[2] In relation to other kind of enantioselective oxidations, for example sulfoxidations, no significant influence of the catalyst was found on the configuration of the obtained oxidation product.[2] These results could be explained by considering the structure of the ligand. In L55Bu_4*, the chiral information is brought by the four chiral chains on the benzimidazoles. The

stereocenters are therefore distant from metal ions, responsible for the coordination and the orientation of the substrates. Natural chiral molecules, such as amino acids, represents in most of cases favored hinges for active site structures. In tyrosinase, for example, each copper ion in the active site is coordinated by three histidine residues.[3] In amino acids, the position of the stereocenter is located close to the primary amine group, representing in many cases a good coordination site for metal ions. From the idea that the closer the stereogenic center, the larger is the chiral information that can be transferred, a new family of chiral biomimetic systems based on amino acid residues was conceived. The inspiration derived from the structure of $[Cu_2(L55)]^{4+}$, in which the catalytic efficiency is dictated by the strain of the five-memberered chelate ring between copper and coordinating nitrogens. The benzimidazole unit is also a common motif, but in this newly conceived strategy, the benzimidazole is built up on the carboxylic moiety of the amino acid, bringing many advantages. First of all, this coordinating unit is strictly bound to the stereocenter, potentially influencing the translation of the chiral information to an external substrate. Furthermore, this strategy is very versatile, as, in principle, it could be adapted to other amino acids, making it possible to vary the nature of the chiral center surrounding.

3.2. Results and discussion

3.2.1. Ligand synthesis- general synthesis of new L55-like systems

Amino acids were, therefore, chosen as chiral building blocks for the synthesis of new biomimetic systems. Here I report the general procedure for the synthesis of these new L55-like ligands, potentially applicable to all amino acids (Scheme 3.1).

The synthesis started from the N-Fmoc-protected amino acid, that was transformed in an α-amino-N-methyl benzimidazole analogue **3.1** *via* a two steps reaction that involved a coupling between the acidic portion of the amino acid and N-methyl-*ortho*-phenylenediamine, followed by ring closure with elimination of water, promoted by glacial acetic acid.[4]

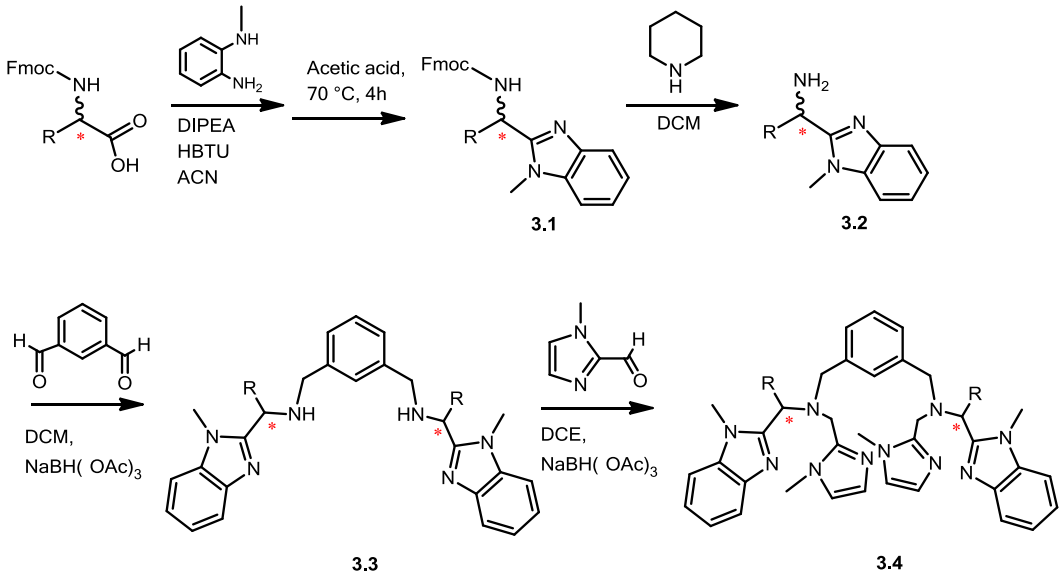

Scheme 3.1- General procedure for the synthesis of the new L55-like ligand based on amino acids.

Fmoc-deprotection of compound **3.1,** in dichloromethane with 20 % (v/v) of piperidine gave **3.2**, in quantitative yield. Two of these chiral *alpha*-aminobenzimidazoles were conncted by stepwise reductive amination with isophtaldialdehyde, giving compound **3.3**, that, after a subsequent reductive amination with 1-methyl-2-imidazolecarboxyaldehyde, gave the final ligand **3.4**.

First, the choice for starting amino acid fell on phenylalanine (Figure 3.1), due to the presence of an aromatic and hydrophobic side chain represented by a benzylic group. The flexible nature of the benzylic function could help in accommodating the substrate inside the "cavity" defined by the assembly of four heterocyclic donor groups in the dinuclear complex. This arrangement could take advantage of π-stacking interactions to align the substrate in a well-defined position.

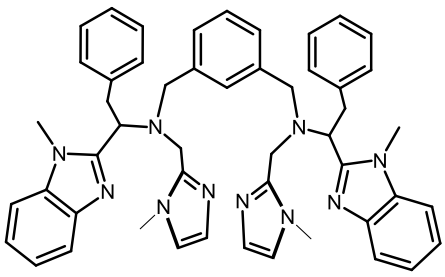

Figure 3.1. Structure of the ligand mXPhI, obtained when phenylalanine is the starting amino acid.

The dinuclear copper complex of mXPhI was easly obtained by reaction of the ligand with an appropriate copper salt.

3.2.2. Spectroscopic characterization of the dinuclear copper complex $[Cu_2(mXPhI)]^{4+}$

3.2.2.1. Uv-Vis and CD features of $[Cu_2(mXPhI)]^{4+}$

The electronic spectrum of $[Cu_2(mXPhI)]^{4+}$ in the UV region (Figure 3.2) is dominated by the typical absorption profile of the benzimidazolic moieties on the ligand skeleton around 288 nm. The visible region is mostly dominated by a broad non-symmetrical absorption band centered at 710 nm, attributable to d-d metal centered transitions. The d-d envelope feature is suggestive of a trigonal bypiramidal coordination geometry.[5]

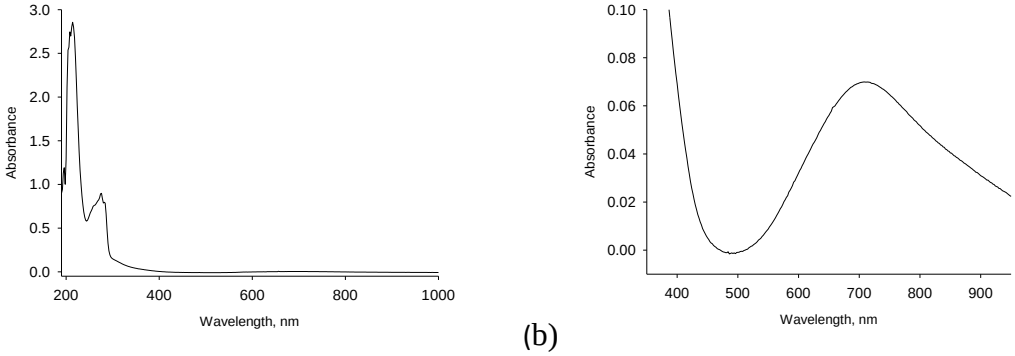

(a) (b)

Figure 3.2- UV-Vis spectrum of $[Cu_2(mXPhI)](ClO_4)_4$ in methanol. a) 0.1 mM; b) magnification of d-d bands of a 0.5 mM solution of complex

3.2.2.2. Spectroscopic characterization of the dinuclear copper complex- Azide binding studies

As previously stated, azide binding experiments to $[Cu_2(mXPhI)]^{4+}$ were performed to gain information about the mode of binding of small ligands to the copper(II) centers of the complex. UV-Vis spectral changes upon titration with N_3^- solution (Figure 3.3) basically consisted in an increase of an intense band at 398 nm, attributable to π(azido)→Cu(II) LMCT.[1e]

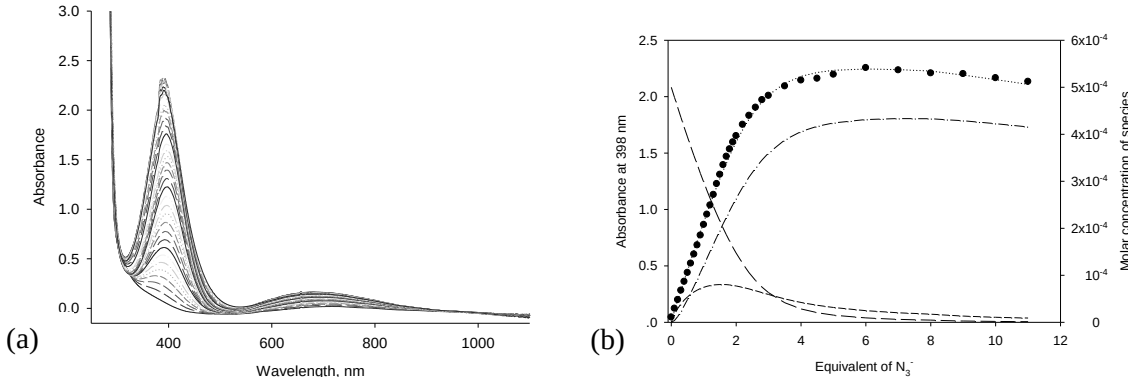

Figure 3.3- (a) Family of UV-Vis spectra taken upon addition of a concentrated solution of NaN_3 ($4x10^{-2}$ M) to $[Cu_2(mXPhI)]^{4+}$ in methanol solution ($5x10^{-4}$ M). (b) Distribution diagram (concentration *vs.* equivalent of N_3^-) of the species. Long dashed and short dashed lines: free $[Cu_2(mXPhI)]^{4+}$ and $[Cu_2(mXPhI)(N_3)]^{3+}$, respectively; dashed-dotted line: $[Cu_2(mXPhI)(N_3)_2]^{2+}$. The graph shows the experimental profile of absorbance *vs.* equiv. NaN_3 at 398 nm (diamonds) and the fitted curve (dotted line).

During the titration it was also possible to note a slight red shift to the LMCT band. By analyzing the optical data it was possible to extrapolate two binding constants, related to the following equilibria:

$$[Cu_2(mXPhI)]^{4+} + N_3^- \rightleftharpoons [Cu_2(mXPhI)(N_3)]^{3+}$$
$$[Cu_2(mXPhI)(N_3)]^{3+} + N_3^- \rightleftharpoons [Cu_2(mXPhI)(N_3)_2]^{2+}$$

$\log K_{b1}$ was found to be 3.11, while $\log K_{b2}$ is 3.96, which represent a moderate strength in binding of small ligand to this dinuclear copper complex.

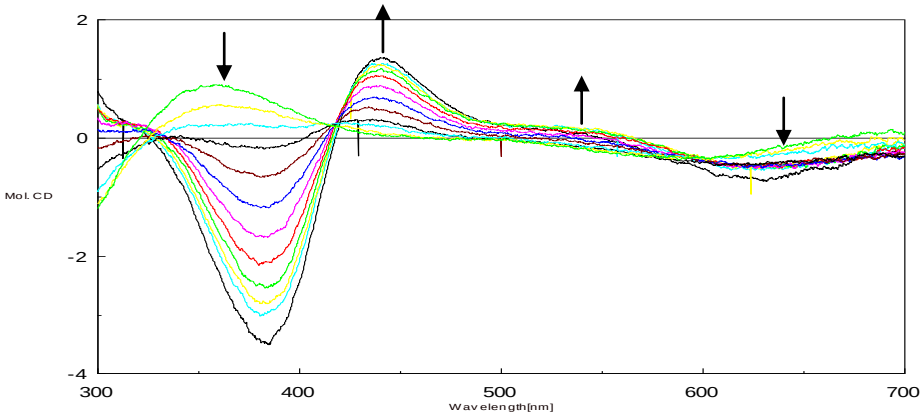

Figure 3.4- CD spectra upon titration of $[Cu_2(mXPhI)]^{4+}$ with azide, from 0 to 2 eqv by addition of 0.2 eqv and from 2 to 5 eqv with addition of 3 eqv.

The CD spectrum of $[Cu_2(mXPhI)]^{4+}$ shows a positive band at 356 nm and a negative band in the LF region at 597 nm. CD spectra changes upon addition of NaN_3 consist in the development of an intense negative band at 380 nm, accompained by an higher energy positive band at 444 nm. Similarly to $[Cu_2(L55Bu4*)]^{4+}$, they probably arise from an exciton coupling of LMCT transitions, that are expected to increase the number of components in the optical absorption. d-d envelope alfo shifts to lower energy upon addition of azide anion, to 630 nm. It is also noteworthy that the coordination of azide anion does not generate a change in CD features, indicating that the binding of a second N_3^- occurrs with no changes in coordination mode (Figure 3.4)

3.2.2.3. Spectroscopic characterization of the dinuclear copper complex- Hydroxide binding studies

Complex $[Cu_2(mXPhI)]^{4+}$, like $[Cu_2(L55)]^{4+}$ and $[Cu_2(L55Bu_4*)]^{4+}$, showed pH-dependent features in the electronic spectra. Changes in electronic spectrum upon titration with sodium hydroxide consisted in the development of a prominent near-UV absorption band at 354 nm, accompained by a weaker shoulder around 308 nm (Figure 3.5). These bands are due to coupled hydroxo→Cu(II)-LMCT transitions.

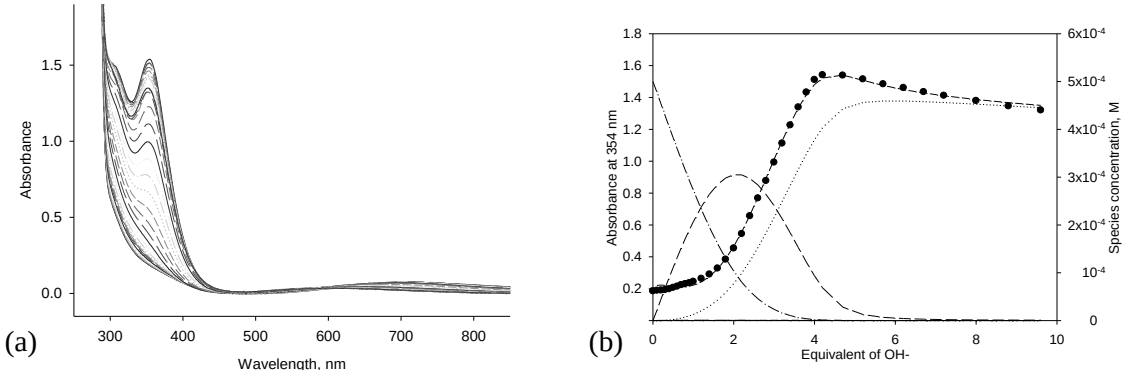

Figure 3.5- UV-Vis spectra upon titration of $[Cu_2(mXPhI)]^{4+}$ ($5x10^{-4}$ M) with sodium hydroxide ($4x10^{-2}$ M) (a), species distribution diagram (b). The graph shows the experimental profile of absorbance *vs.* equiv. NaOH at 354 nm (diamonds) and the fitted curve (dashed line). Dashed-dotted line: Free complex concentration. Medium dashed line: $[Cu_2(mXPhI)(OH)_2]^{2+}$ complex. Dotted line: $[Cu_2(mXPhI)(OH)_4]$.

Addition of hydroxide also generated a marked blue shift of the d-d envelope from 710 nm to about 600 nm, indicating a transition from trigonal bipyramidal (TBP) to square

pyramidal (SPY) coordination geometry. Titration with sodium hydroxide showed, in this case, an unattended profile. From 0 to 2 equivalents of added hydroxide, no significant spectral changes were shown, while in the range from 2 to 4 equivalents of added OH^- , the larges changes of the spectrum occurred.

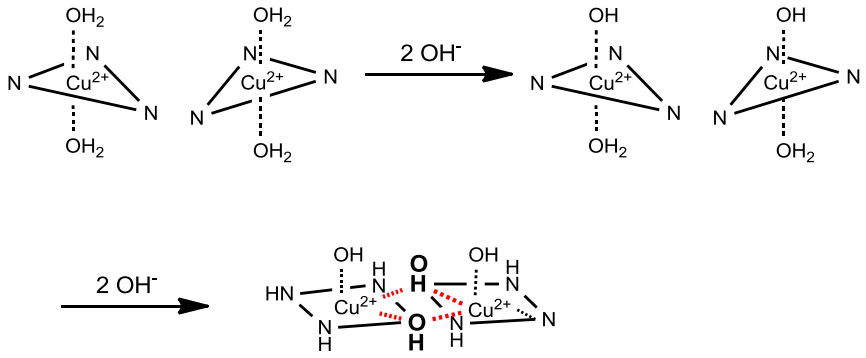

Scheme 3.2- Hypothesis on the nature of the involved species in hydroxide coordination.

Analysis of experimental data showed that four possible species were involved in the equilibrium. The hypothesis is that the coordination of the first two hydroxide anions generates a TBP species with one water and one OH^- coordinated in terminal arrangement. Further addition of hydroxide generates a transition from TBP to SPY of a bis-μ(OH) species (Scheme 3.2).[1e]

3.2.3. $[Cu_2(mXPhI)]^{n+}$ as biomimetic catalyst for oxidation reactions

3.2.3.1. Stereoselective oxidation of chiral catechols- catecholase activity

As previously described for $[Cu_2(L55Bu_4*)]^{4+}$, the possibility to induce enantio-discrimination in catechol oxidation was investigated on $[Cu_2(mXPhI)]^{4+}$. The same set of enantiomeric pairs of chiral catechols and experimental conditions were maintained. [2] Results of the study are reported in Table 3.1.

As previously reported,[2] to elucidate the enantio-differentiating capability in oxidation reaction, two more parameter were calculated, R(k_{cat}) % and R(k_{cat}/K_M) %, that represent the enantiodifferentiation in substrate-saturation condition and at low concentration of substrate respectively. R > 0 indicates a preference for the L enantiomer, while R < 0 shows a reversed preference for the D enantiomer.

Table 3.1. Kinetic parameters for oxidation of chiral catechols in methanol/50 mM acetate buffer, pH = 5.1, 10:1 v/v, at 25 °C.

Substrate	K_M (mM)	k_{cat} (s^{-1})	k_{cat}/K_M ($M^{-1}s^{-1}$)	R (k_{cat}) %	R (k_{cat}/K_M) %
L-Dopa	$(7.37 \pm 0.16) \times 10^{-2}$	$(2.20 \pm 0.13) \times 10^{-3}$	29.9	3 %	-3 %
D-Dopa	$(6.52 \pm 0.89) \times 10^{-2}$	$(2.14 \pm 0.07) \times 10^{-3}$	32.8		
L-DopaOMe	$(1.35 \pm 0.14) \times 10^{-1}$	$(3.93 \pm 0.13) \times 10^{-2}$	29.1		
D-DopaOMe	-	-	-		
R-(-)-norepinephrine	$(8.26 \pm 0.52) \times 10^{-2}$	$(2.29 \pm 0.04) \times 10^{-3}$	27.7	3 %	-10 %
S-(+)-norepinephrine	$(6.38 \pm 0.41) \times 10^{-2}$	$(2.17 \pm 0.04) \times 10^{-3}$	34.0		

From the data in Table 3.1, it is clear that no significant discrimination was shown when L/D-Dopa and R/S-norepinephrine were used as substrates. As for $[Cu_2(L55Bu_4*)]^{4+}$, for the two enantiomers of norepinephrine, this behavior could be explained by considering that the position of the stereogenic centre, located on the carbon atom directly bound to the catecholic moiety, did not match with the chirality of the ligand as they are too distant for significant interactions. For the two enantiomers of Dopa, an unfavorable electrostatic interaction between the zwitterionic side chain and the high hydrophobicity of the ligand mXPhI could explain the behavior. For L/D-Dopa methylester to the esterificated analogue, in fact, an interesting difference in oxidation rate of the two enantiomers of the substrate was found. While the rate data at increasing substrate concentration followed a typical Michaelis-Menten trend for the L-enantiomer, the D-enantiomer exhibited substrate inhibition (Figure 3.6).

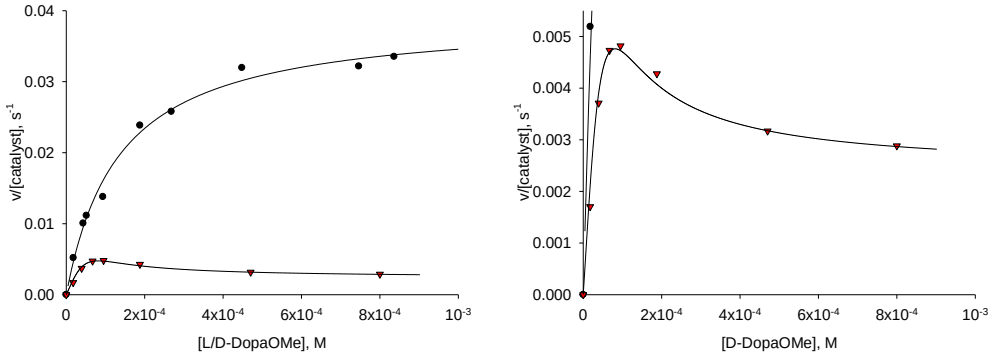

Figure 3.6- On the left: rate data at increasing substrate concentration for L-Dopa methyl ester (black circles), and D-Dopa methyl ester (red triangles). On the right: expansion of the graph to underline the behavior of the D-enantiomer.

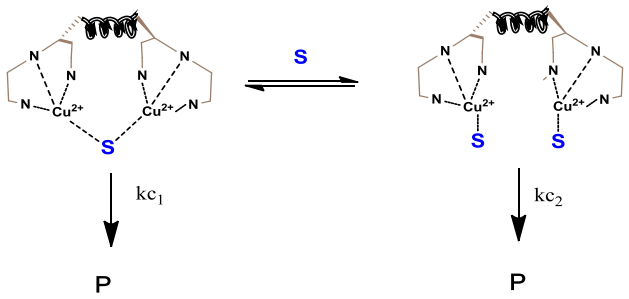

Scheme 3.3- Hypothesis on the nature of the reactive intermediates involved in the oxidation of D-dopa methyl ester. S: D-dopa methyl ester; P: oxidation product; k_{c1} and k_{c2} are the oxidation rates for the 1:1 complex:substrate and the 1:2 complex:substrate adduct respectively.

The inhibition was not complete, as the rate of oxidation did not drop to zero, and this could be explained by assuming that, in saturating condition, two molecules of substrate can be bound by the copper complex, and this form is less, but still reactive (Scheme 3.3). The equation used to interpolate these rate data is the following:

$$\frac{v}{[catalyst]} = \frac{k_{c1}[S] + k_{c2}K_{B2}[S]^2}{K_M + [S] + K_{B2}[S]^2}$$

The model used to interprete the behavior of D-Dopa methyl ester is adequate, as data trend is well represented (Figure 3.6), but it was not possible to extrapolate the four parameters due to the high intercorrelation of the experimental data.

3.2.3.2. Oxidation of phenols- monophenolase activity

Ortho-hydroxylation of phenols is considerable more interesting than catecholase activity from a synthetic point of view. Several attempts to mimic this feature of tyrosinase has been done in the past decades. Karlin and coworkers[6] designed a system based on *m*-xylyl-tetrapyridyl based copper complex, giving significant insight in chemical dioxygen activation by dinuclear copper(I) complexes. Furthermore, the oxygen activation and the ligand oxygenation steps were separated and studied. Our research group subsequently found that, by substituting pyridyl groups with benzimidazoles it was possible to generate even better tyrosinase biomimetic systems.[1f] Their activity was tested on different substrate and methyl-4-hydroxybenzoate was found to be the best candidate. Lower reactivity, due to the presence of an electron withdrawing group on the phenolic ring, could help in identify the involved intermediates. Following a similar procedure already used with the copper(I) complex of ligand L55,[1f] $[Cu_2(mXPhI)]^{2+}$ was also tested in its capability to hydroxylate carbomethoxyphenol. The dinuclear copper(I) complex of mXPhI was, in this case, generated in situ by addition of a proper quantity of $[Cu(I)(CH_3CN)_4]PF_6$ to a ligand solution of known concentration in acetonitrile. This solvent was chosen for the reaction as it stabilizes copper(I) oxidation state. Addition of substrate was followed by addition of sodium borohydride ($NaBH_4$), as it was previously found that *in situ* generation of phenolate in reductive conditions did not prevent phenol hydroxylation with di-copper complexes as catalysts.[1f] The reaction was left under stirring for two hours under inert atmosphere, then it was exposed to air oxygen for two more hours at room temperature. The crude product was recovered with a slightly modified work-up procedure, and direct ESI-MS analysis showed, in positive ions, just one major peak at $[M+Cu^{2+}]$ of +761, that was attributable to a fragment of the dinuclear copper complex (Figure 3.7), as it was found to have a characteristic copper-like isotopic distribution.

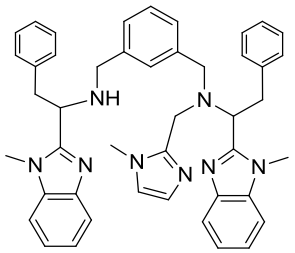

Figure 3.7- Hypothesis on the ligand fragment structure, detected after reaction of $[Cu_2(mXPhI)]^{2+}$ with 4-carbomethoxyphenol in reducing conditions and then exposed to air.

Negative peaks showed residual phenolic reagent as major product ($M\text{-}H^+$: -152) and a peak at -167 that could be attributable to the related catechol. Other minor relevance by-products have not been yet identified. The presence of catechol could be justified in two different ways. First, the reaction could have been stoichiometric, so phenol was oxygenated by the copper(I) complex, that terminated its catalytic activity with oxidation to copper(II). Studies from Sayre and Nadkarni reported that when phenol oxygenation is conducted in presence of $NaBH_4$, the observed catecholic product could be due to the reduction of the 4-carbomethoxy-1,2-benzoquinone, promoted by the excess of hydride.[7] Attempts of column chromatography purification were made, but only the unreacted starting phenol was recovered. The same reaction was conducted with tetrabutylammonium phenolate, as it was found that in nonreducing conditions the major product derived from the Michael addition of the unreacted phenol on the product quinone.[1f] Also in this case we were only able to recover the unreacted phenol with the same fragment derived from the ligand. Monophenolase activity was also tested on a phenol with more extended aromatic core, β-naphthol, as the nature of the substrate should match positively with the nature of the complex. This attempt was unsuccesful, as the only unreacted phenol was recovered.

The poor performance in the monophenolase activity promoted by $[Cu_2(mXPhI)]^{2+}$ could be explained by considering the extreme reactivity of the intermediate, i.e. the oxygenated Cu_2O_2 complex. Tested experimental conditions did not permit to accumulate this putative intermediate, that probably undergoes inactivation generating a Cu(II) complex.

3.2.3.3. Enantioselective oxidation of sulfides

As explained in **Chapter 2**, tyrosinase was found to catalyze stereoselective oxidation of sulfides in presence of L-Dopa as sacrificial cosubstrate.[8] Also the dinuclear copper complex of ligand L55 was found to catalyze the oxidation of thioanisole and other sulfides in presence of hydroxylamine hydrochloride as reducing agent.[1a] We decided to implement the efficiency of this system with the possibility to promote enantioselective oxidation of sulfides, by exploiting the dinuclear copper(II) complex of mXPhI. The reaction was carried out in a methanol/acetate buffer (50 mM pH= 5.1) 9:1 v/v as mixture, with 10 mM of substrate and 10 μM of $[Cu_2(mXPhI)]^{4+}$, varying the concentration of hydroxylamine from 0.3 to 20 mM, in order to evaluate the effect on both yield and enantiomeric excess. Due to the high volatility of sulfides and sulfoxides, the previously reported work-up procedure[1a] was slightly modified, separating the analysis of reaction yield from the analysis of enantiomeric excess. Reaction yield was determined before the work up, by taking an aliquot of reaction mixture and adding a proper quantity of an internal standard of known concentration, preventing the evaporation step that causes a reagent and product loss. Determination is made by reverse phase HPLC analysis, calculating the ratio between the area of the peak of sulfoxide and that attributable to the chosen internal standard. In order to determine the concentration of sulfoxide, this ratio is then compared with the one obtained at known concentrations of both sulfoxide and internal stardard. For determination of the enantiomeric excess, instead, the crude product for chiral HPLC analysis was recovered as described in literature.[1a]

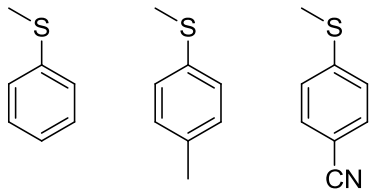

Figure 3.8- Thioanisole, p-tolylmethyl sulfide and 4-methylthiobenzonitrile are the three sulfides used in this study.

In these studies, we chose to investigate a set of aromatic sulfides (Figure 3.8), with different electronic characteristics. The aromatic ring of sulfides could, in fact, give positive interaction with the benzyl group of the ligand skeleton, favoring a preferential orientation and, consequently, a well defined oxygen insertion.

Table 3.2. Reaction yield, calculated on the reducing agent concentration, and enantiomeric excess for the studied sulfides.

$[NH_2OH]$, mM	Thioanisole		*p*-tolyl-methyl sulfide	
	Yield %	e.e. %	Yield %	e.e %
0.3	35 %	18 %	-	40 %
0.5	13 %	32 %	6	39 %
1	6 %	43 %	3	38 %
5	0.5 %	36 %	0.3	27 %
10	trace	19 %	trace	racemic

Data reported in Table 3.2 may not seem encouraging from the point of view of both yield and enantiomeric excess, but have to be considered as noteworthy. Most of the sulfoxidation reactions catalyzed by copper complexes exploit peroxides as oxidizing reagents,[9] so the main influence of the complex is on the enantioselectivity. This is the first case of a dinuclear copper complex that is both able to activate dioxygen in a catalytic fashion and to transfer the chiral information to the pro-stereogenic sulfide.

The initial experiment were conducted with thioanisol, which was previously studied using the dinuclear complex $[Cu_2(L55)]^{4+}$. In these studies, the reaction yield was evaluated varying the concentration of reducing agent, and it was found that the best turnover number (TON) corresponded to a $[NH_2OH]$ = 10 mM. In this case, obviously the product sulfoxide was racemic. The scope of maintaining the same ligand features, in term of coordination surrounding, implementing chirality inside the ligand skeleton was achieved with $[Cu_2(mXPhI)]^{4+}$. The oxidation of thioanisole was conducted according to the General procedure described in Experimental section, varying the concentration of reducing agent.

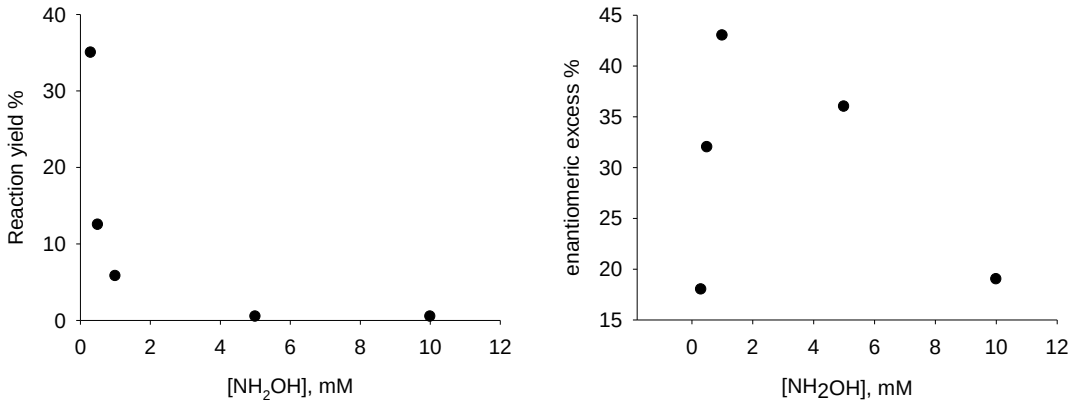

Figure 3.9- Reaction yield and enantiomeric excess trends in oxidation of thioanisole promoted by $[Cu_2(mXPhI)]^{4+}$

From the trend shown in Figure 3.9 and Table 3.2, it is evident that reaction yield decades exponentially when the concentration of reducing agent increases. The enantiomeric excess, instead, undergoes a rapid increase between 0 and 1 mM of hydroxylamine, followed by a sudden decay. The reason that could justify this behavior resides in the nature of the reducing agent, considering the potential competition between the reaction centered on the sacrificial reductant and the substrate monoxygenation. On increasing hydroxylamine concentration, a radical pathway of sulfur oxidation assumes prominent role, so the one-electron transfer prevails on the oxygen transfer from the active species, thus making negligible the influence of the chiral catalyst. It is noteworthy that, even if the yields are not very high, the reaction was still catalytic, as the catalyst makes from 2 to 10 turnover cycles before deactivation.

When methyl *p*-tolyl sulfide was used as substrate, low yields were detected in all experiments, but the study of the reaction gave interesting results. Reaction yield and enantiomeric excess have a parallel behavior and are related to the concentration of reductant, as lower concentration of hydroxylamine corresponds to higher values of both parameters (Figure 3.10).

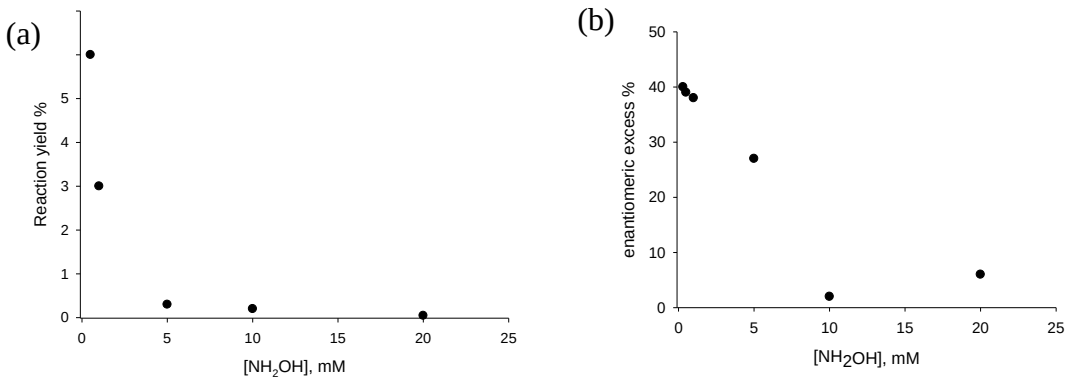

Figure 3.10- Effect of hydroxylamine concentration on yield (a) and enantiomeric excess (b)

The low yield of conversion of sulfide to sulfoxide may be attributed to the poor competition of this bulky substrate with oxydation of hydroxylamine. An appreciable enantiomeric excess of 40 % was detected with the lowest concentration of reductant investigated (0.3 mM), while when an equimolar concentration [substrate]:[hydroxylamine] was used, the resulting product was found to be almost racemic. Also in this case, radical pathways induced by oxidation of NH_2OH may favor a one-electron oxidation instead of an oxygen transfer to the substrate. With p-tolylmethylsulfide, the effect of other reducing agents was evaluated, choosing the effect of a combination of L-Dopa and sodium ascorbate. With tyrosinase, this combination was found to increase the reaction yield.[8] Quinones derived from oxidation of Dopa, in fact, inhibit the activity of tyrosinase, so a large excess of sodium ascorbate could help in eliminating these products. The reaction was conducted in presence of 1 mM of L-Dopa and 300 mM of sodium ascorbate and stirred overnight, without changing other conditions. Reaction yield increased to 36 % (calculated on L-dopa concentration), but enantiomeric excess dropped to about 0 %, making these conditions unfavorable for the reaction.

With 4-methylthio benzonitrile, the enantiomeric excess found in the reaction ranged from 0 to 20 % at all concentration of substrate, but the main problem is probably connected to general experimental conditions. After comparison with a "blank" reaction (conducted in the same conditions, but in the absence of catalyst), it was evident that the reaction was poorly catalyzed by $[Cu_2(mXPhI)]^{4+}$, that also did not have a relevant role in influencing enantioselectivity of the oxidation.

Oxidation of thioanisole- incorporation of 18-O

As previously reported, the sulfoxidation promoted by tyrosinase involves the introduction of an oxygen atom derived from molecular oxygen. To demonstrate that also $[Cu_2(mXPhI)]^{4+}$ is capable to follow the same kind of mechanism, the sulfoxidation of thioanisole was replicated in presence of oxygen-18. I chose the best conditions in terms of enantiomeric excess, in order to elude the competition with radicalic reactions (1 mM of hydroxylamine).

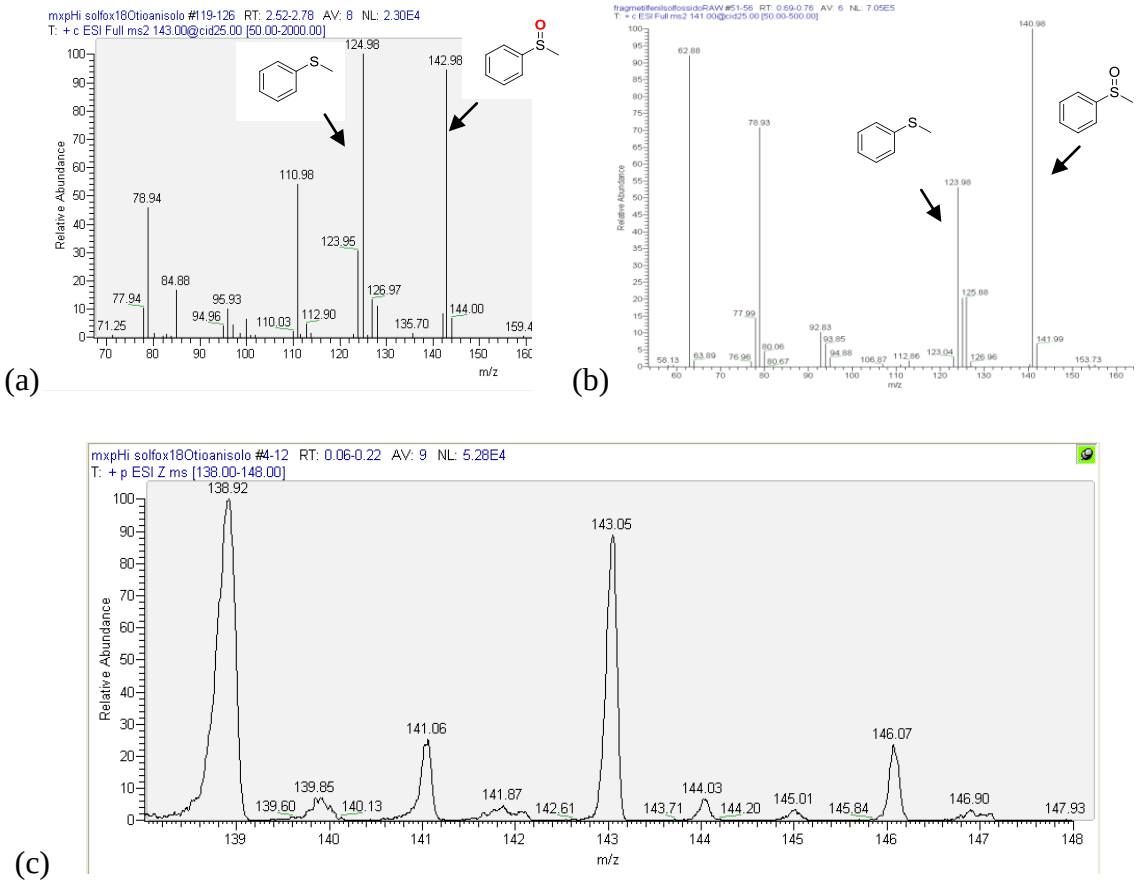

Figure 3.11- Sulfoxidation of thioanisole in presence of oxygen-18; (a) Fragmentation pattern of the methylphenyl sulfoxide including 18-O (18-O-methylphenyl sulfoxide: m/z = +143) ; (b) Fragmentation pattern of commercial methylphenyl suloxide (methylphenyl sulfoxide: m/z = +141); (c) Enlargement of the ESI-MS spectrum.

The catalytic oxidation in presence of $[Cu_2(mXPhI)]^{4+}$ provided the desired sulfoxide which incorporates the 18-O isotope (Figure 3.11-a). The similarities in fragmentation pattern of the commercial methylphenyl sulfoxide and the 18-O analog permitted an attribution of the same structure for these two products (Figure 3.11- a and b). From the enlargment of the ESI-MS spectrum of the methylphenyl sulfoxide it was possible to

determine the percentage of incorporation of 18-O, that was extimated around 77 %. These results are indicative that the reaction occurred with oxygen transfer from the Cu_2-O_2 intermediate to the sulphide, with negligible contribution from radical pathways.

3.3. Conclusions

With the synthesis of the ligand mXPhI, we developed a new versatile synthetic pathway for L55-like systems, exploiting the natural chirality of amino acids to generate biomimetic models for tyrosinase. We studied the oxidation of biogenic catechols and the best results were obtained for the couple L/D-Dopa methyl ester, in which the two enantiomers seemed to have a different approach to the active centre of the catalyst. Oxygenation of phenols and sulfoxidation reactions needs to be deeply investigated, as results are stimulating. Future perspective for this highly reactive asymmetric catalyst could be represented by its involvement in asymmetric oxidation of other not endogenous substrates, such as olephines, or in cross-coupling reactions.

3.4. Experimental section

Materials and methods

All reagents and solvents from commercial sources were of the highest purity available and were used as received. Elemental analyses were obtained at the Microanalysis service of the Milano CIMA department. CD spectra were obtained with a Jasco J500 spectropolarimeter, spectra were recorded in the range 300-700 nm, at 50 nm/min, with three scans acquired for each spectrum, and 0.2 nm resolution. NMR spectra were recorded on a Bruker AVANCE 400 spectrometer, operating at 9.37 T, with 400.13 and 100.6 MHz proton and carbon-13 frequencies, respectively. Data acquisition and processing were performed using a standard Bruker software package (Topspin 1.3). UV-Vis spectra were recorded on an Agilent 8453 spectrophotometer. HPLC analyses were performed on a Jasco HPLC instrument equipped with two PU-1580 pumps and a MD-1510 diode array detector (working range: 195–659 nm). Mass spectra were recorded using a Thermo-Finnigan LCQ ADV MAX spectrometer.

General procedures

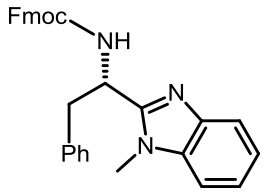

Synthesis of (9H-fluoren-9-yl)methyl(1-(1-methyl-1H-benzo[d]imidazol-2-yl)-2-phenylethyl)carbamate (**3.1**)*:* 0.173 g of HBTU (2-(1H-benzotriazol-1-yl)-1,1,3,3-tetramethyluronium hexafluorophosphate) (0.464 mmol) are dissolved in 5 mL di acetonitrile at 0 °C, bubbling Argon in the solution. 0.150 g of N-Fmoc protected L-phenylalanine (0.387 mmol) are added to the solution, followed by 0,073 g of N-methyl *orto*-phenylenediamine dihydrochloride (0.464 mmol) and 82.5 µL of diisopropylethylamine (0.464 mmol), continuing bubbling Argon for 15 min. The reaction is let go to room temperature, stirring overnight. After rotary evaporation of the solvent, 5 mL of acetic acid are added to the solution, that is heated to 70 °C for 4 hours. The reaction is stopped by evaporating the acetic acid and directly puridied by column chromatography with silica 230-400 mesh as stationary phase and hexane:ethyl acetate 6:4 mixture as eluent (Rf: 0.4). Obtained product: 0,026 g (yield 14 %). MS: + 474 ($M+H^+$), ^{1}H-NMR (400 MHz, $CDCl_3$) δ 7.79 (dd, *J* = 17.9, 7.4 Hz, 1H), 7.57 (dd, *J* = 13.8, 7.5 Hz, 1H), 7.40 (t, *J* = 7.3 Hz, 1H), 7.35 – 7.23 (m, 2H), 7.08 (d, *J* = 2.7 Hz, 1H), 6.48 (d, *J* = 8.4 Hz, 1H), 5.30 (t, *J* = 9.5 Hz, 1H), 4.38 (ddd, *J* = 17.6, 10.2 Hz, 1H), 4.20 (t, *J* = 7.1 Hz, 1H), 3.44 (ddd, 1H), 3.29 (s, 1H).

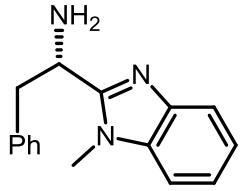

Synthesis of 1-(1-methyl-1H-benzo[d]imidazol-2-yl)-2-phenylethanamine - (**3.2**)*:* 0.026 g of compound **3.1** (0.056 mmol) is dissolved in1 mL of dichloromethane, then 200 µL of piperidine is added to the solution (20 % v/v). The reaction is stirred at room temperature for 30 min, then the solvent is removed by rotary evaporation and the obtained product is not further purified. Yield: quantitative. MS: + 252 ($M+H^+$).

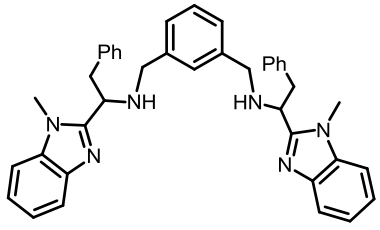

Synthesis of N,N'-(1,3-phenylenebis(methylene))bis(1-(1-methyl-1H-benzo[d]imidazol-2-yl)-2-phenylethanamine) - (**3.3**) 0.014 g of compound **3.2** (0.056 mmol) are dissolved in 1 mL of dichloromethane, then 0.0037 g (0.028 mmol) of solid isophtaldialdehyde are added to

the solution, that is subsequently stirred at room temperature overnight. The reaction is followed by mass spectroscopy, and further compound **3.2** is added until the disappearance of the starting material. 0.018 g of sodiumtriacetoxyborohydride (STABH, 0.084 mmol) are added to the solution, that is left stirring for three hours at room temperature. The reaction is stopped by removing the solvent by rotary evaporation, then is purified by column chromatography with silica 230-400 mesh as stationary phase and hexane:ethyl acetate:methanol 85:15:20 as eluent. Yield = 69%, MS: +605 ($M+H^+$).

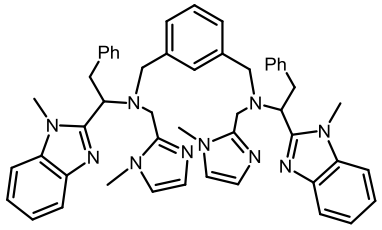

*Synthesis of N,N'-(1,3-phenylenebis(methylene))bis(1-(1-methyl-1H-benzoimidazol-2-yl)-N-((1-methyl-1H-imidazol-2-yl)methyl)-2-phenylethanamine)-(***3.4-mXPhI***):* 0.080 g of compound **3.3** (0.132 mmol) are dissolved in dichloroethane e brought to 0 °C. 0.036 g of 1-methyl-2-imidazole carboxyaldehyde (0.331 mmol) are added to the solution, that is left stirring for 30 minutes at this temperature. 0.084 g of STABH (0.397 mmol) are added and the solution is left stirring at low temperature for 1 hour. The reaction is followed by mass spectroscopy. After one hour, 0.331 further mmol of 1-methyl-2-imidazole carboxyaldehyde are added, the reaction is stirred for 30 min and then 0.084 g of STABH completes the reduction of the iminio intermediate. The reaction is stopped by removing the solvent by rotary evaporation, then the crude product is purified by column chromatography with silica 230-400 mesh as stationary phase and hexane: ethyl acetate 9:1 + 1.5 % of aq. ammonia solution 28 % as eluent. Yield: 8.3 % MS: + 793 ($M+H^+$), ^{1}H NMR (400 MHz, MeOD) δ 7.76 – 7.63 (m, 2H), 7.39 – 7.19 (m, 7H), 7.11 (m, 13H), 6.88 (s, 2H), 6.83 (s, 2H), 4.33 (dd, *J* = 9.1, 5.4 Hz, 2H), 4.08 (d, *J* = 23.4 Hz, 2H), 3.99 (d, *J* = 13.8 Hz, 2H), 3.87 (d, *J* = 13.8 Hz, 2H), 3.83 – 3.69 (d, *J* = 23.4 Hz, 2H), 3.62 – 3.47 (m, 4H), 2.87 (s, 6H), 2.76 (s, 6H).

Synthesis of the copper complex of mXPhI: an appropriate quantity of ligand is dissolved in methanol, then 2 eq of $Cu(ClO_4)_2$ x $6H_2O$, dissolved in methanol, are added to the ligand solution. After 15 minutes, the solution is poured in diethyl ether and the copper complex precipitate as a brilliant blue solid. The solid is then washed three times

with diethyl ether. Anal calcd for $C_{50}H_{52}Cl_4Cu_2N_{10}O_{16}x5H_2O$: C= 42.65; H= 4.44; N= 9.95; Found: C= 42.72, H= 4.58; N=10.51.

Spectrophotometric titration of $[Cu_2(mXPhI)]^{4+}$ with NaN_3: a $5x10^{-4}$ M methanolic solution of mXPhI was first added with 2 equivalents of copper triflate, to generate in situ the dinuclear copper complex (Initial volume: 2 mL). The resulting solution was titrated with a $4x10^{-2}$ M solution of sodium azide, until a ratio 1:11 [Cu_2mXPhI]: [N_3^-]. Data were analyzed with a not-linear least-square procedure,[10] to estrapolate the binding constants for the 1:1 and 1:2 adducts.

Spectrophotometric titration of $[Cu_2(mXPhI)]^{4+}$ with NaOH: a $5x10^{-4}$ M methanolic solution of mXPhI was first added with 2 equivalents of copper triflate, to generate in situ the dinuclear copper complex (Initial volume: 2 mL). The resulting solution was titrated with a $4x10^{-2}$ M solution of sodium hydroxide, until a ratio 1:10 [Cu_2mXPhI]: [N_3^-]. Data were analyzed with a not-linear least-square procedure,[10] to estrapolate the binding constants for the adducts.

Oxidation of chiral catechols: kinetics of oxidation of the chiral *ortho*-catechols L-Dopa, D-dopa, L-DopaOMe, D-DopaOMe, L-norepinephrine, and D-norepinephrine were studied by UV-Vis spectroscopy, using a magnetically stirred and thermostated (at 25.0 ± 0.1 °C) optical cell of 1-cm path length. A mixture of acetate buffer (50 mM, pH 5.1), and methanol (1:10 v/v) was used as solvent for the catalytic oxidation. The experiments were performed over the substrate concentration range between 5×10^{-5} and 1×10^{-3} M, while a constant concentration of 5×10^{-6} M of the copper complex was used. The experiments were initiated adding to a solution of the substrate in the mixed aqueous/methanol buffer a few microliters of a methanolic solution of the complex, (final volume was 2.5 mL). The formation of the corresponding aminochrome was followed through the development of the band at 475 nm for L/D-Dopa and L/D-norepinephrine, and 468 nm for L/D-DopaOMe. In all the experiments, the noise was reduced by reading the absorbance difference between the λ_{max} of the aminochrome and that at 820 nm, and the initial rates of the oxidation were obtained by fitting the absorbance *vs.* time curves in the first few seconds of the reactions. To convert the rate data from Δabsorbance/time to Ms^{-1}, the absorbance changes were divided by the molar extinction coefficient of the aminochrome (3600 $M^{-1}cm^{-1}$) and the molar catalyst concentration. The dependence of the reaction rates of the catalytic reactions as a

function of the substrate concentration exhibited hyperbolic behavior; therefore, the kinetic parameters (k_{cat}, K_m) were estimated, were possible, by fitting the data using a Michaelis-Menten equation. The enantio differentiating capability in the catalytic reaction was evaluated through the two parameters R(k_{cat})% and R(k_{cat}/K_m)%, defined above.

General procedure for asymmetric sulfoxidation: a solution of sulfide (10 mM) in 9:1 v/v methanol/acetate buffer 50 mM pH 5.1 (1 mL), $[Cu_2(mXPhI)]^{4+}$ (10 μM) was stirred a room temperature. The reaction was initiated with addition of the appropriate volume of a solution of hydroxylamine 0.3 M, prepared in the same acetate buffer. For the detection of the reaction yield, a proper internal standard was added (final concentration: 0.2 mM) and the reaction mixture was analyzed by HPLC without any previous workup in order to prevent the loss of both reagent and product. Separation was operated with a inverse phase coloumn, Ascentis express C18, 10 cm x 4.6 mm.

For thioanisole: Internal standard: p-nitro-acetophenone; Retention times: 9.5 min (methylphenyl sulfoxide), 12.5 min (p-nitroacetophenone), 14.2 min (thioanisole)

Time	H_2O:ACN (+0.1 %TFA)initial	H_2O:ACN (+0.1 %TFA)final
0--> 15 min	95:5	0:100
15--> 20 min	0:100	0:100
20--> 22 min	0:100	95:5
22 min	95:5	95:5

For p-tolyl-methylsulfide: Internal standard: benzophenone; Retention times: 11.3 min (methylp-tolylsulfoxide); 13.6 min (benzophenone); 14.1 min (p-tolylmetylsulfide).

Time	H_2O:ACN (+0.1 %TFA)initial	H_2O:ACN (+0.1 %TFA)final
0-->5 min	95:5	95:5
5-->12 min	95:5	0:100
12-->20 min	0:100	0:100
25-->25 min	0:100	95:5

Detection of enantiomeric excess was performed by HPLC analysis, with a column in direct phase (for thioanisole: Lux 5u amylose-2 250 x 4.60 mm, flux 0.8 mL/min, 85:15 hexane:2-propanol, r.t_1: 25 min, r.t_2: 27 min; for methyl p-tolyl sulfide: Lux 5u cellulose-1 250 x 4.60 mm, flux 0.8 mL/min, 9:1 hexane:2-propanol, r.t_1: 21 min, r.t_2: 22 min), but the reaction is previously quenched with the addition of $HClO_4$ 1 M. The organic fraction is removed by rotary evaporation, then the remaining water was extracted with three portions of dichloromethane, dried over sodium sulfate, filtered and evaporated to give the crude product for the HPLC analysis.

Supporting information

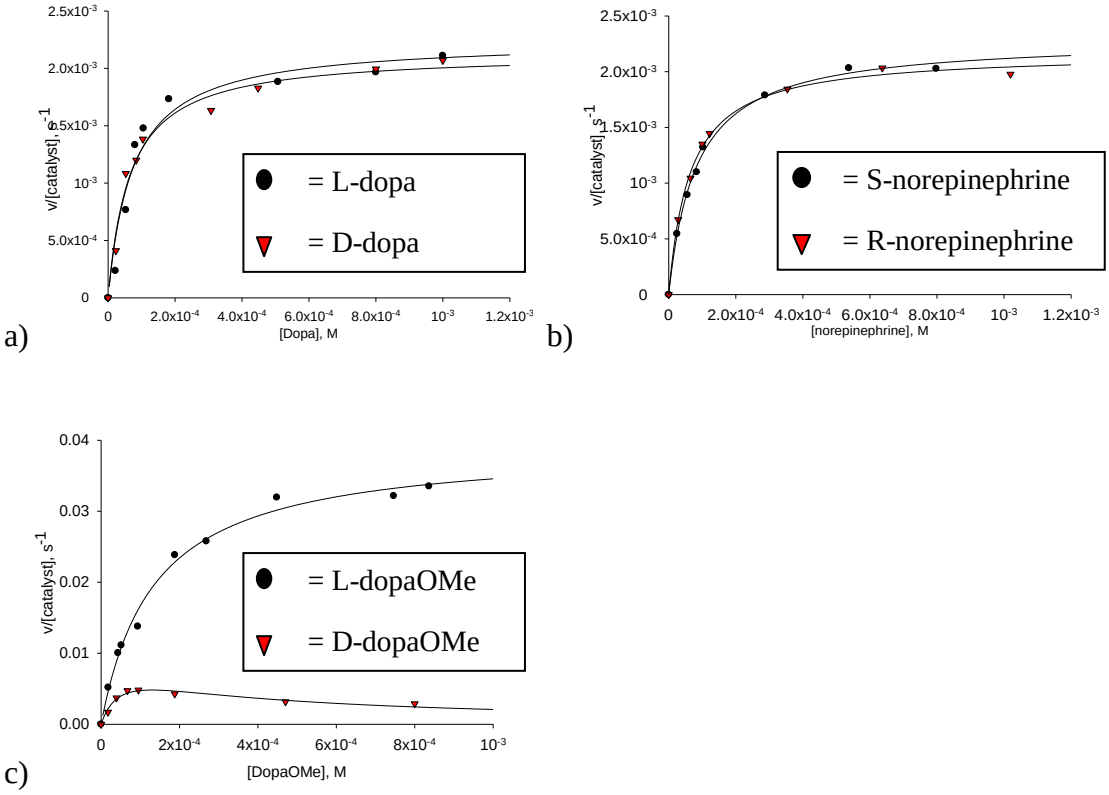

Figure S.I 3.1- Effect of substrate concentration on initial rate of oxidation of a) L-/D-dopa, b) R-/S-norepinephrine, c) L-/D-dopaOMe promoted by $[Cu_2(mXPhI)]^{4+}$ 5 μM, in 10:1 MeOH:acetate buffer (50 mM, pH = 5.1), temperature: 25 °C.

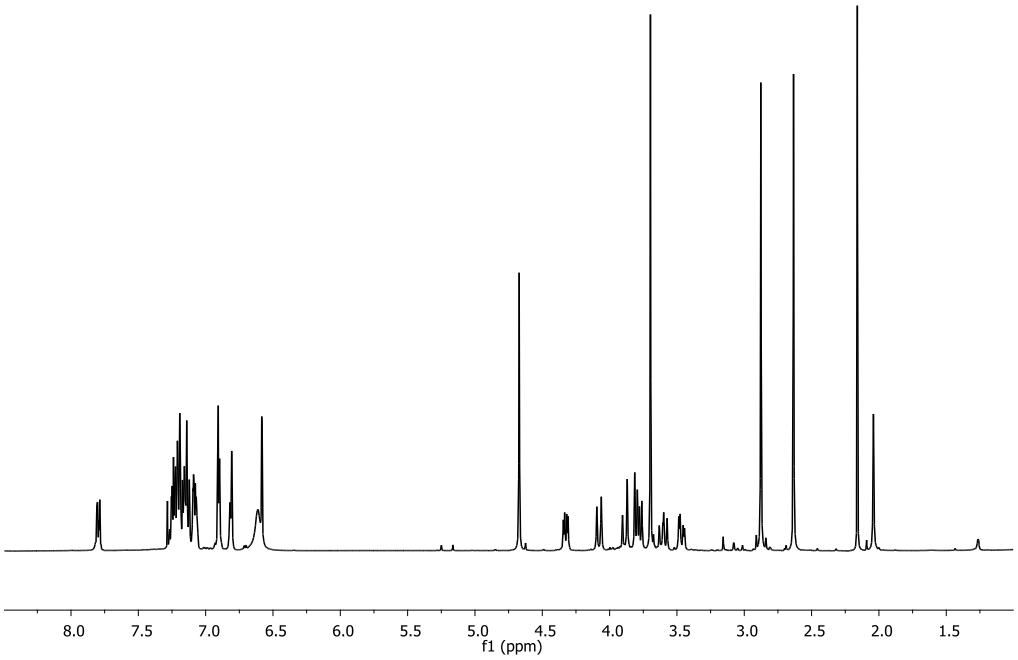
8.0
7.5
7.0
6.5
6.0
5.5
5.0
4.5
4.0
3.5
3.0
2.5
2.0
1.5
f1 (ppm)

a)

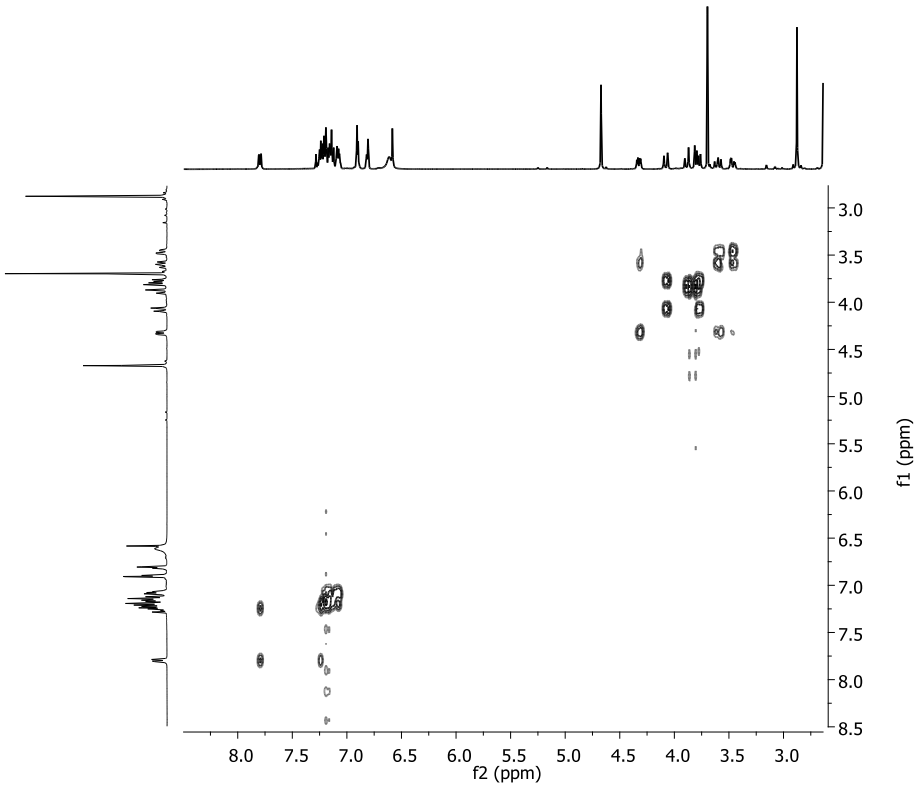
3.0
3.5
4.0
4.5
5.0
5.5
6.0
6.5
7.0
7.5
8.0
8.5
f1 (ppm)
8.0
7.5
7.0
6.5
6.0
5.5
5.0
4.5
4.0
3.5
3.0
f2 (ppm)

b)

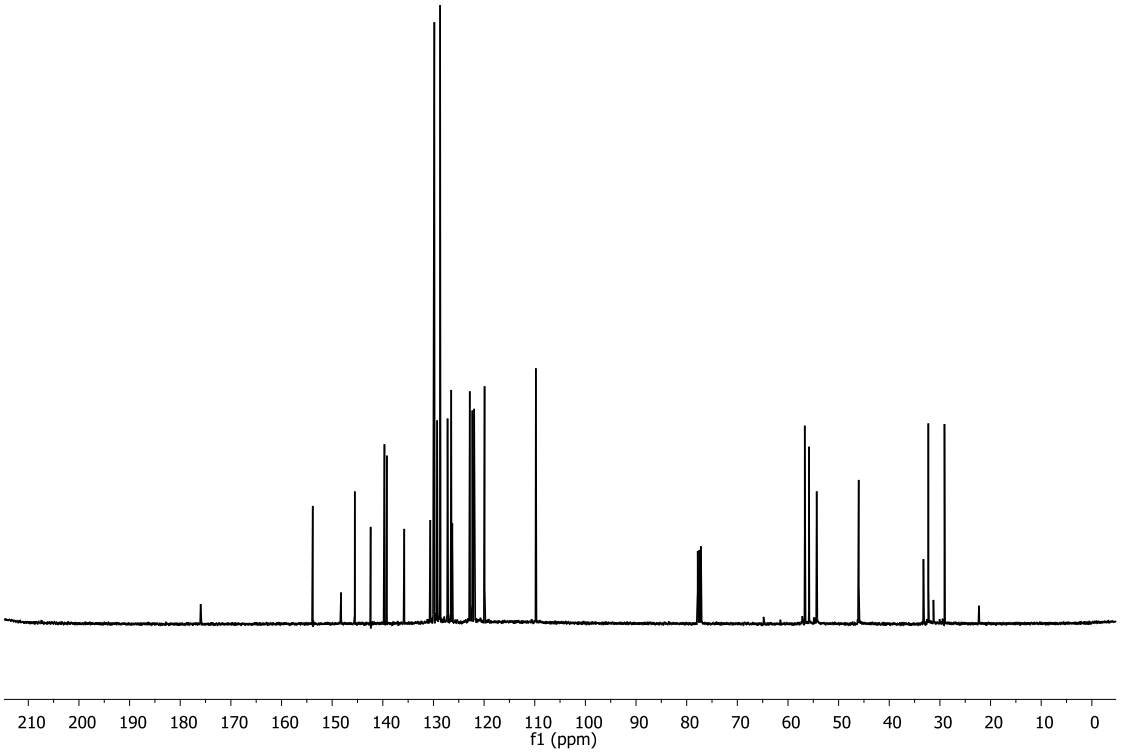

c)

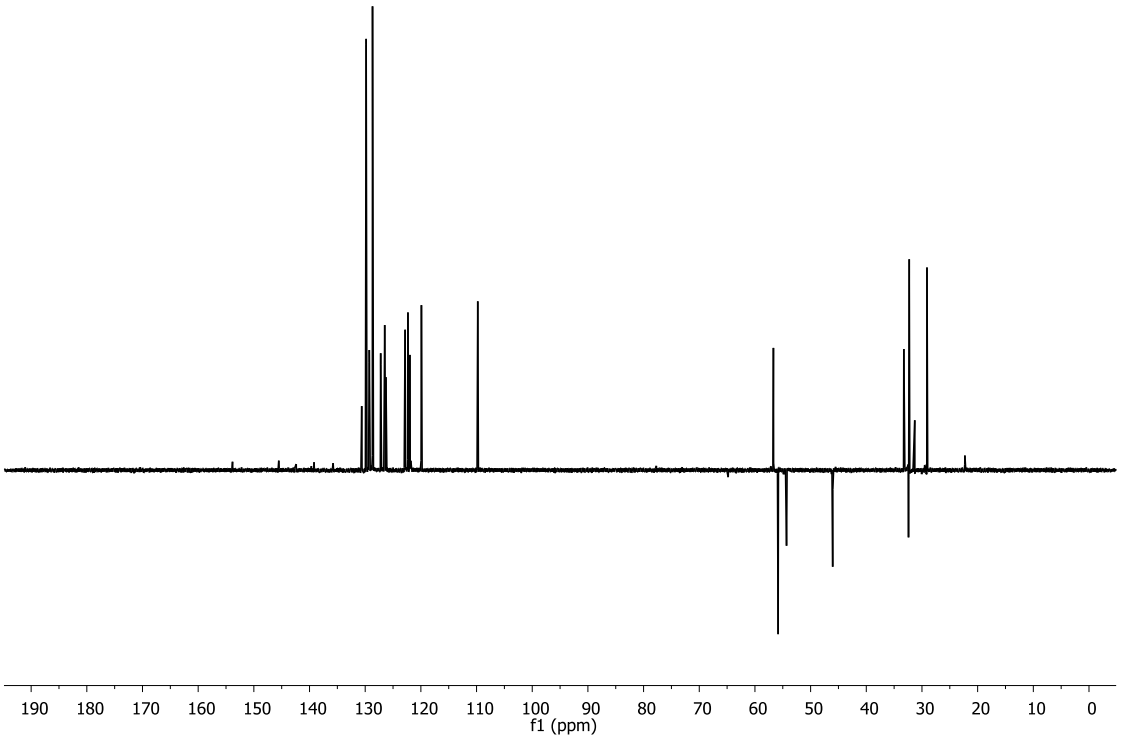

d)

Figure S.I. 3.2- ^{1}H-NMR and ^{13}C-NMR characterization of mXPhI in deuterated chloroform.

References

1- (a) I. Gamba, S. Palavicini, E. Monzani, L. Casella, *Chem. Eur. J.* 2**009**, 15, 12932-12936; (b) G. Battaini, L. Casella, M. Gullotti, E. Monzani, G. Nardin, A. Perotti, L. Randaccio, L. Santagostini, F. W. Heinemann, S. Schindler, *Eur. J. Inorg. Chem.* **2003**, 1197-1205; (c) A. Granata, E. Monzani, L. Casella, *J. Biol. Inorg. Chem.* **2004**, 9, 903-913; (d) S. Palavicini, A. Granata, E. Monzani, L. Casella, *J. Am. Chem. Soc.* **2005**, 127, 18031-1836; (e) L. Casella, O. Carugo, M. Gullotti, S. Garofani, P. Zanello, *Inorg. Chem.* **1993**, *32*, 2056–2067; (f) L. Casella, E. Monzani, M. Gullotti, D. Cavagnino, G. Cerina, L. Santagostini, R.Ugo, *Inorg. Chem.* **1996**, *35*, 7516-7525.

2- M. Perrone, E. Lo Presti, S. Dell'Acqua, E. Monzani, L. Santagostini, L.Casella, *Eur. J.I.C.* ,**2015**, 21, 3493–3500.

3- (a) M. E. Cuff, K. I. Miller, K.E. van Holde, W. A. Hendrickson *J. Mol. Biol.* **1998**, 278, 855–870; (b) E. I Solomon.; U. M. Sundaram,; T. E. Machonkin, *Chem. Rev.* **1996**, 96, 2563–2605.

4- A. J. Potter et all., *Bioorg. Med. Chem. Lett.*, **2010**, 20, 586-590.

5- B. J. Hataway, D. E. Billing, *Coord. Chem. Rev.*, 5, **1970**, 143-207.

6- (a) K. D. Karlin, J. C. Hayes, Y. Gultneh, R.W. Cruse, J. W. McKown, J. P. Hutchson, J. Zubiete, *J. Am. Chem. SOC.*, **1984**,106, 2128-2139; (b) Karlin et all., *J. Am. Chem. SOC.*,116, 4, **1994,** 1324-1336.

7- Sayre, L. M.; Nadkarni, D. V. *J. Am. Chem. Soc.* **1994**, *116*, 3157.

8- R. Pievo, M. Gullotti, E. Monzani, L. Casella, *Biochemistry*, **2008**, 47, 3493–3498.

9- O'Mahony, G. E., Ford, A., Maguire, A. R., *Journal of organic chemistry*, **2012**, 77 (7), 3288-3296.

10- P. Gans, A. Sabatini, A. Vacca, *Talanta*, **1996**, *43*, 1739-1753.

Chapter 4. EHI

4. EHI

4.1. Introduction

Bioinorganic chemists have been interested in synthesizing molecules whose structure and activity can be compared to those of natural systems. Enzymes represent a typical source of inspiration in this chemistry field. A peculiar class of enzymes is that containing a redox metal ion in the active site. In this case, the enzymes can exploit peculiar redox and coordination characteristics of the contained metal ions to perform their activity. Our research group has been interested in developing structural and functional models for enzyme active sites, focusing on those to the family of copper monooxygenases and oxidases, such as tyrosinase. As previously mentioned, tyrosinase active site consists in a dinuclear copper center in which each copper ion is coordinated to three histidine residues to give a six-coordinating nitrogen environment.[1] Previous works on biomimetic systems,[2] in which histidine was used as coordinating unit for copper, were focused on octadentate nitrogen ligands for three copper ions. In this system, where the ligand was known as PHI, the third metal ion has a different

coordination set, and it has the specific scope of anchoring the substrate in order to direct it to specific orientation for catalysis. PHI and other similar analogues are, of course, efficient systems for mimic the activity of munltinuclear enzymes, but ligands synthesis is time spending and not much efficient in term of yield. From this starting point we devised a new hexadentate nitrogen ligand based on histidine as hinges. Here I report the synthesis and studies performed on $[Cu_2(EHI)]^{n+}$ (n= 2+; 4+), a novel biomimetic system for tyrosinase. The ligand EHI is presented as a pair of tridentate amino-histidine-imidazole units, forming two adjacent chelating rings with copper, one five- and one six-membered. This peculiarity should confer to $[Cu_2(EHI)]^{n+}$ catalytic characteristics intermediate between those of $[Cu_2(L55)]^{n+}$ and $[Cu_2(L66)]^{n+}$ behaviors.[3]

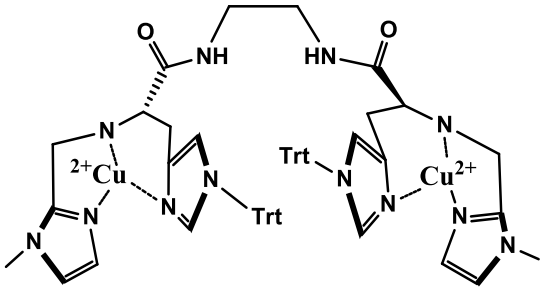

Figure 4.1- Structure of $[Cu_2(EHI)]^{4+}$; (Trt: trityl group)

4.2. Results and discussion

4.2.1. Synthesis of the ligand

The synthetic pathway followed for the synthesis of EHI is outlined in Scheme 4.1. The synthesis of this hexadentate ligand started from N-Fmoc-N(τ)-trityl histidine. Two molecules of histidine were interfaced by coupling with ethylendiamine. This reaction used PyBOP (benzotriazol-1-yl-oxytripyrrolidinophosphonium hexafluorophosphate), a common reagent for solid-phase peptide synthesis, as mediator for coupling.

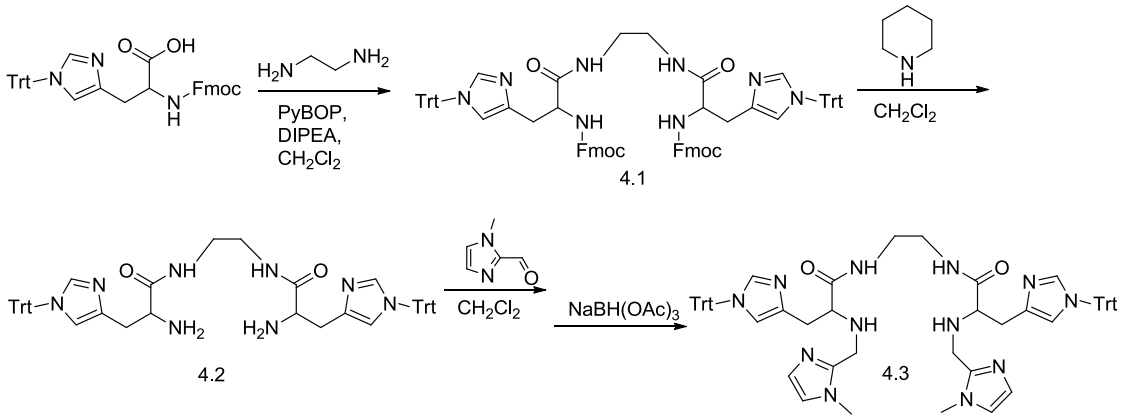

Scheme 4.1- Synthetic pathway followed for EHI

This coupling reaction provides the basis structure of the molecules. Primary amine groups were, subsequently, deprotected in basic condition with 20% of piperidine in dichloromethane, giving product **4.2** in quantitative yields. Then, **4.3**, labeled as EHI, was obtained by stepwise reductive amination with 1-methyl-2-imidazolecarboxyaldehyde and sodium triacetoxyborohydride as reducing reagent. Trityl groups have, in this context, a double effect. As chromogenic functions, trityl helps in chromatographic purifications due to its intense optical absorption. Furthermore, protection of imidazole nitrogens of histidine prevent from carbonatation, that could hinder copper coordination.

The dinuclear copper complex of EHI was synthesized by simply mixing a methanolic solution of EHI with a methanolic solution of the appropriate copper salt in 1:2 equivalent ratio.

4.2.2 Spectroscopic characterization of the dinuclear copper complex $[Cu_2(EHI)]^{4+}$

4.2.2.1 UV-Vis titration of EHI with copper triflate

EHI has a structure that differs from the ligands previously described. First, the spacer between the two tridentate units has a bis-amidic nature, which is more rigid than a *m*-xylyl bridge and this could influence the possibility to cooperate by the copper ions. In order to gain information about the strength of the coordination, titration of copper triflate with was performed. A diluted solution of copper(II) triflate ($9.97x10^{-4}$ M) was titrated with a concentrated solution of EHI ($2.45x10^{-2}$ M).

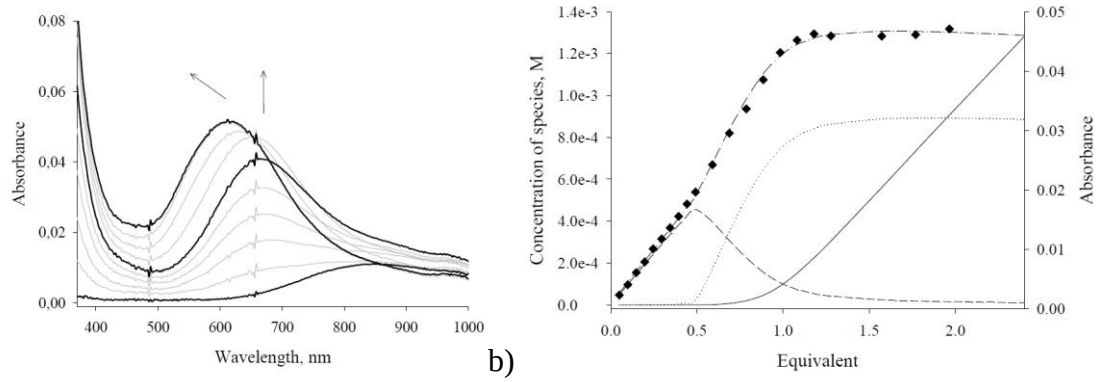

a) b)

Figure 4.2- a) Spectral changes upon titration of $Cu(OTf)_2$ with a methanolic solution of EHI, d-d bands magnification; b) Absorbance intensities at 572 nm superimposed to species distribution diagram. Diamond: experimental values of Absorbance. Dashed-Dotted line: Calculated Absorbance. Solid line: distribution of free [EHI]. Dashed line: distribution of $[CuEHI]^{2+}$. Dotted line: distribution of $[Cu_2EHI]^{4+}$.

The first event was the formation of the 2:1 copper:EHI adduct, followed by the formation of the 1:1 complex with excess ligand, accompanied by a spectral change of the band centered in the visible region. Absorption maximum associated with the 2:1 complex is located at 668 nm, while the 1:1 complex has higher energy, as its maximum is centered at 614 nm (Figure 4.1-a). Experimental evidences indicates that after addition of 0.5 equivalent of EHI, there was no free metal in the solution as it was all implied in the formation of $[Cu_2(EHI)]^{4+}$. Further addition until 1 equivalent of ligand per Cu, generated spectral changes associated with the formation of the 1:1 complex $[Cu(EHI)]^{2+}$ (Figure 4.2-b). Experimental titration data at 572 nm were interpolated with a minimum least square procedure, to gain information about stability constants.

$[EHI] + Cu^{2+} \rightleftharpoons Cu[EHI]^{2+}$ $\quad \text{Log } K_{b1} = 7.43 \pm 0.01$

$Cu[EHI]^{2+} + Cu^{2*} \rightleftharpoons Cu_2[EHI]^{4+}$ $\quad \text{Log } K_{b2} = 5.65 \pm 0.01$

$[EHI] + 2Cu^{2+} \rightleftharpoons Cu_2[EHI]^{4+}$ $\quad \text{Log } \beta_{b2} = 13.08 \pm 0.01$

4.2.2.2 UV-Vis and CD features of $[Cu_2(EHI)]^{4+}$

Optical characterization of $[Cu_2(EHI)]^{4+}$ showed an UV region mostly dominated by the absorption features of trityl groups, accompained by a weak shoulder at around 370 nm, attributable to the π(imidazole)→Cu(II) LMCT transitions.[2b] The visible region is

dominated by the d-d transitions, centered at around 630 nm, whose tail extends to near-IR.

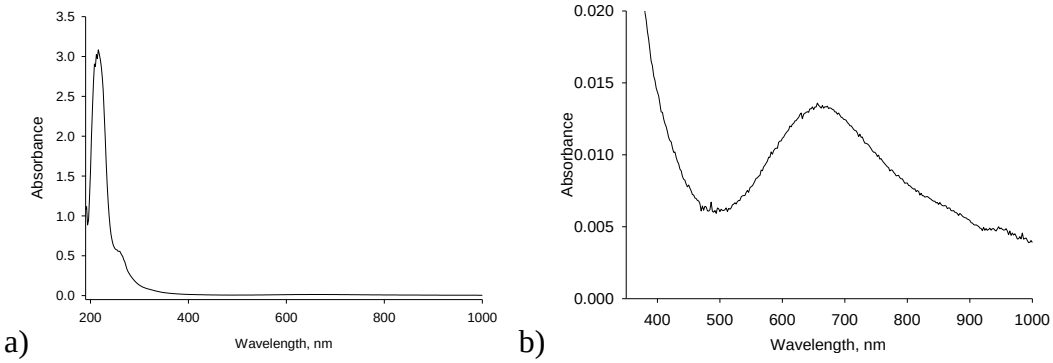

Figure 4.3- UV-Vis spectra of $[Cu_2(EHI)]^{4+}$ in methanol, 0.1 mM. b) shows a magnification of the dd region.

As for $[Cu_2(PHI)]^{4+}$,[2b] the CD spectrum, provides interesting details on the conformation of the chelate rings formed by histidine (Figure 4.4, Scheme 4.2). The visible region of the spectrum shows a positive band at 670 nm, accompained by a weaker negative band at about 550 nm. This pattern implies that for $[Cu_2(EHI)]^{4+}$ all three nitrogen donor atoms occupy equatorial coordination positions of Cu(II), preferring a δ chirality, while $[Cu_2(PHI)]^{4+}$ favors a λ conformation.[2b]

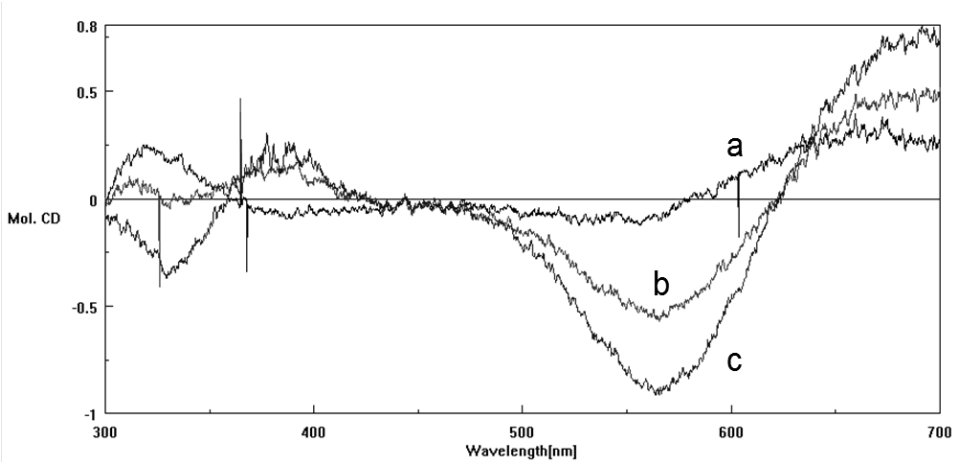

Figure 4.4. CD spectra in the near-UV and visible range of complex $[Cu_2EHI]^{4+}$ (a), and after the addition of 1 (b) and 2 (c) equiv. of azide in MeOH/MeCN 9:1 (v/v) solution.

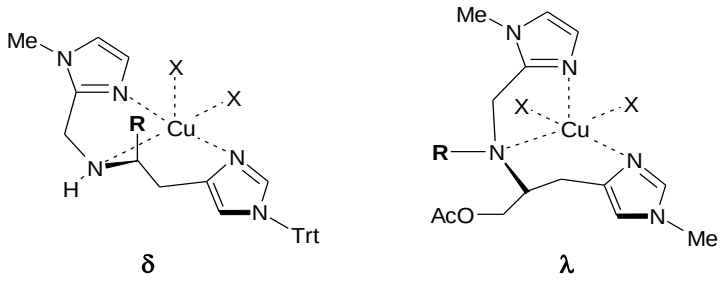

Scheme 4.2- Difference in conformation adopted by $[Cu_2(EHI)]^{4+}$ (left) and $[Cu_2(PHI)]^{4+}$

Conformational differences are mostly due to the position of the linker between the chelating arms. For $[Cu_2(PHI)]^{4+}$, this chain is directly linked on the coordinating nitrogen and this condition force an equatorial orientation. For $[Cu_2(EHI)]^{4+}$, instead, the connecting unit is farther from the coordination site and this let the ligand to occupy an axial position, with a δ conformation on the ring. These structural consideration could be important to rationalize catalysis outputs.

4.2.2.3. Azide binding studies- UV-Vis and CD titration

As previously described, titration with azide could be an interesting means to deduce information about the coordination of small molecules to the biomimetic metal complex. For $[Cu_2(EHI)]^{4+}$, the titration was carried out in a methanol/acetonitrile 9:1 v/v mixture, in the same experimental conditions used for $[Cu_2(PHI)]^{4+}$, to allow a direct comparison between these two biomimetic systems.[2b] Addition of NaN_3 to a solution of $[Cu_2(EHI)]^{4+}$ produced the development of the characteristic band at 382 nm (ε_{382} = 4600 M^{-1} cm^{-1}), due to the π(azido)→Cu(II) LMCT. This band is symmetric and increases with the addition of azide until 2:1 azide:$[Cu_2(EHI)]^{4+}$ molar ratio is reached, with only a slight change in the absorption maximum (Figure 4.5).

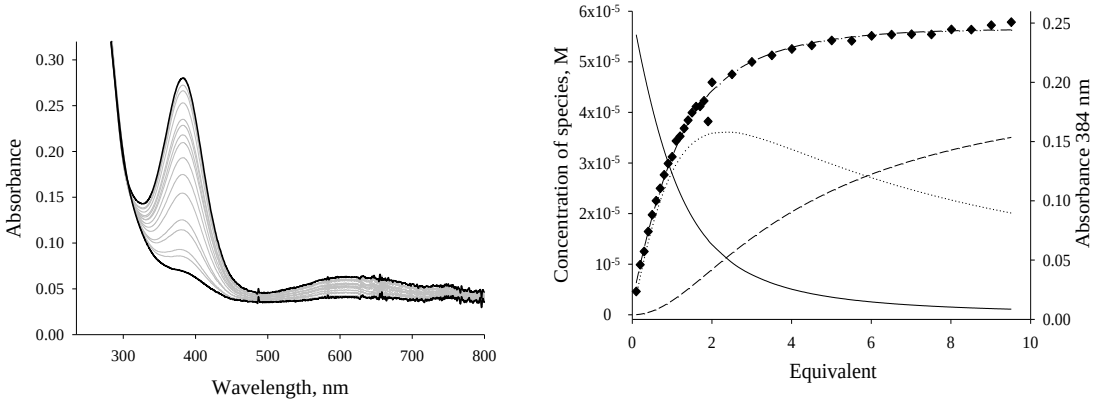

Figure 4.5. Left- Family of UV-vis spectra taken upon addition of a concentrated solution of NaN_3 to $[Cu_2EHI]^{4+}$ in 9:1 methanol/acetonitrile (v/v) solution. Solid black lines: initial and final spectra of the titration, corresponding to $[Cu_2EHI]^{4+}$ and the mixture of $[Cu_2EHI(N_3)]^{3+}$ and $[Cu_2EHI(N_3)_2]^{2+}$ species, respectively. Right- Calculated distribution diagram (concentration *vs.* equiv. of added NaN_3) of the species.

By analysis of the data obtained from UV-vis titration of $[Cu_2(EHI)]^{4+}$ it was possible to separate the two reactions involved and calculate the related binding constants.

$$[Cu_2EHI]^{4+} + N_3^- \rightleftharpoons [Cu_2EHI(N_3)]^{3+} \qquad \log K_{b1} = 4.61$$

$$[Cu_2EHI(N_3)]^{3+} + N_3^- \rightleftharpoons [Cu_2EHI(N_3)_2]^{2+} \qquad \log K_{b2} = 3.59$$

These values are comparable to those obtained with $[Cu_2(PHI)]^{4+}$ and indicate a moderate affinity for azide molecules.[2b]

The CD spectrum showed a weak positive band in the same position (Figure 4.4), indicating that each copper ion bound an azido ligand in terminal mode. For $[Cu_2(PHI)]^{4+}$, instead, the structure favoured the coupling between the LMCT transition moments, due to the spatial proximity of the two Cu-azido chromophores. Furthermore, in $[Cu_2(PHI)]^{4+}$, coordination of azide generated an inversion of conformation of L-histidine chelate ring, while $[Cu_2(EHI)]^{4+}$ this was maintained.

4.2.2.4. Determination copper coupling constant by NMR

4.2.2.5. Determination of magnetic moment with Evans' method- NMR study

When a magnetic substance is introduced in a magnetic field, it induces a variation of magnetic induction B (expressed in Tesla), generating a macroscopic magnetisation. The effective magnetic field results, in this case, is given by:

$B = \mu_0 (H + M) = B_0 + \mu_0 M$

where B_0 represents magnetic induction in vacuum, μ_0 the magnetic permeability of vacuum, and M the magnetisation, so $\mu_0 M$ is the magnetic contribution brought by the magnetic substance. The majority of substances exhibit a magnetization parallel to the applied magnetic field, with a proportionality constant known as magnetical susceptibility ($M = \chi H$). For paramagnetic substances, magnetical susceptibility is related to magnetic moments. With particles with quantic spin number S, the resulting magnetic moment is given by the sum of all substates m_{si}, calculated with Boltzmann statistic:

$$M_{molar} = \frac{M}{[Concentration]} = \frac{N_{av} g^2 \beta^2}{3\,k\,T} S(S+1)$$

where N_{av} is Avogadro constant, g is electronic "g factor", whose value is 2.0023 when there is no orbital contribution, β in Bohr magneton, k is Boltzmann constant and T the temperature expressed in Kelvin degrees.

Magnetic susceptivity can be calculated considering:

$$\chi_M = \frac{\chi}{[Concentration]} = \frac{M}{H\,[Concentration]} = \frac{M_M}{H} = \frac{M_M\,\mu_0}{B_0} = \frac{\mu_0 N_{av} g^2 \beta^2}{3\,k\,T} S(S+1)$$

Assuming that

$\mu_{eff} = g\beta\sqrt{S(S+1)}$

and substituting it in the previous equation, we obtain:

$\chi_M = \frac{\mu_0 {\mu_{eff}}^2 N_{av}}{3\,k\,T} = \frac{\beta_0 \mu_0 {\mu_{eff}}^2 N_{av}}{3\,k\,T}$ when it is expressed in Bohr magneton.

Real magnetic moment is so related to temperature by the following equation:

$$\mu_{eff} = \sqrt{\frac{3kT\chi_M}{N_{av}\mu_{0\beta_0}}}$$

As it can be deduced from the equation, real magnetic moment can be determined by magnetical susceptibility measurements. NMR represents a good and simple technique to measure magnetic susceptibility.[4a-c] The method is based on generating a macroscopic magnetization when the paramagnetic sample is introduced in the magnetic field, that varies the entity of magnetic field inside the test tube. This local variation generates a low-field shift of protons' NMR signals, depending on the magnitude of magnetic susceptivity, and this influence is extended to signals not directly belonging to the paramagnetic substance (for example, the solvent or other non-interacting molecules). This is the phenomenon on which Evans' method is based on.

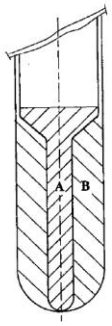

Figure 4.6- Coaxial test tube for magnetic susceptivity determination with Evans' method.

The experimental apparatus simply consists in two coaxial NMR tubes. From an experimental point of view, two diluted solutions are prepared, containing an identical and known concentration of diamagnetic standard, that does not interact with the paramagnetic substance. The internal tube contains the paramagnetic substance, while the external tube contains the same-solvent solution of the diamagnetic standard alone. When the NMR spectrum is recorded, the diamagnetic internal standard signals appear duplicated and the shift is directly related to the magnetic susceptivity of the paramagnetic center.

$$\chi = \frac{3 * \Delta\delta(ppm)}{concentration}$$

where $\Delta\delta(ppm)$ is the difference in ppm between the signal of the standard in the internal and in the external tube, concentration is expressed in mol/m^3.

Evans' method is useful when we want to study the interaction between two metal ions inside a dinuclear metal complex. In antiferromagnetic systems it is possible to determine the coupling constant of the two magnetic centers, by analyzing the variation of magnetic susceptivity with temperature. Temperature has a double effect: first, its increase tends to cancel the magnetic moment as it increases thermal motion, but a second effect is to enhance the excited triplet state population, which is paramagnetic. the effect is directly correlated to the value of coupling constant J. By interpolating magnetic susceptibility data at increasing temperature it is possible to determining the J value with the following equation:

$$\chi_M = \frac{\mu_0 N_{av} g^2 \beta^2}{3\,k\,T} * [1 + \frac{1}{3}\exp\left(\frac{-2J}{kT}\right)]$$

4.2.2.6. Determination of J coupling constant for[Cu_2(EHI)]$^{4+}$

Determination of magnetic susceptibility is, as previously mentioned, particularly useful for dinuclear complexes in which the metal ions can be coupled in their magnetic moments. The entity of coupling can be used as a means to measure the interaction between the two paramagnetic centers. It is affected by the distance between the metal ions and, consequently, it reflects the arrangement of the two metal ions in the complex. Measurments of magnetic susceptibility were performed on $[Cu_2(EHI)]^{4+}$ in deuterated methanol/deuterated acetate buffer (50 mM, pH = 5.1) 10:1 v/v, to replicate the conditions that were used to study catalytic oxidation of catechols. Acetone was chosen as internal standard, as it is poorly coordinating , diamagnetic and it does not interact with the copper complex. It was added in 10 % v/v, in order to be extremely more concentrated than the paramagnetic substance.

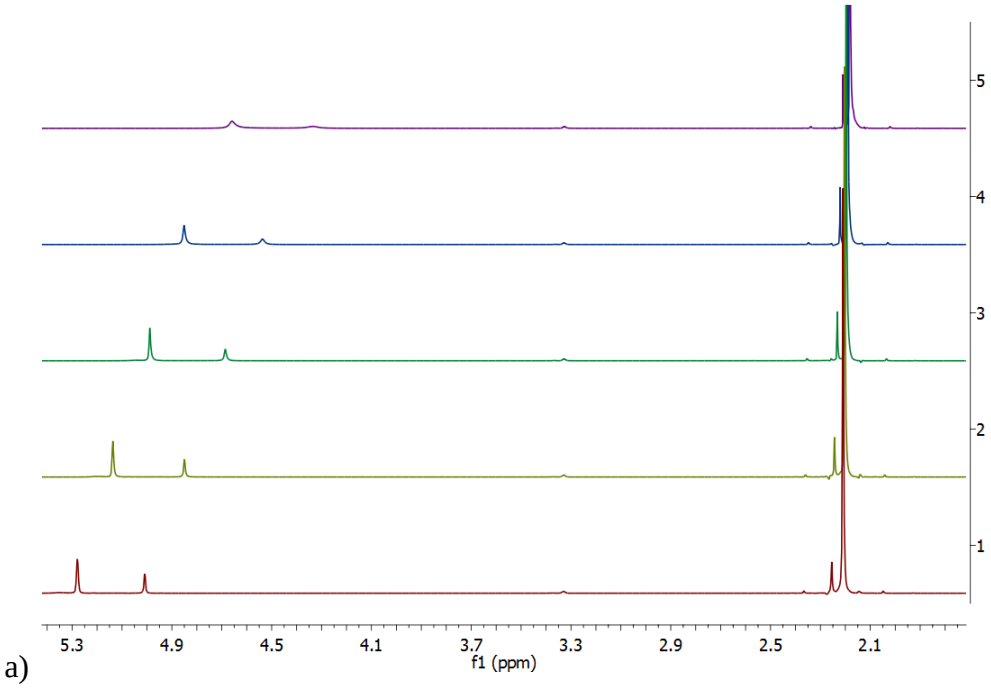

a)

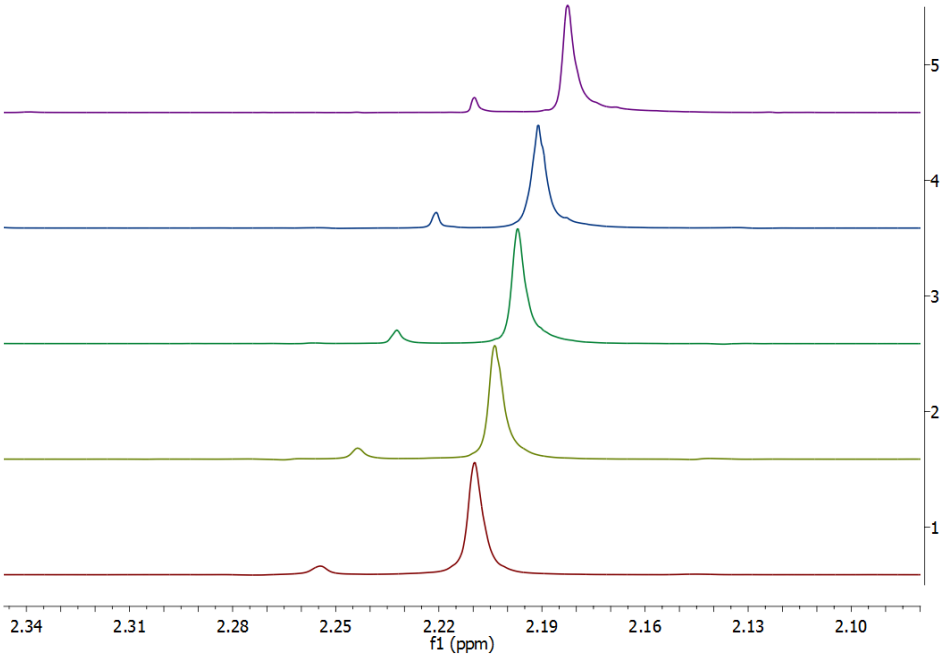

b)

Figure 4.7- a) ^{1}H-NMR collected at increasing temperature for $[Cu_2(EHI)]^{4+}$ in CD_3OD/deuterated acetate buffer (pH 5.1, 50 mM) 10:1 v/v + 10 % of acetone; b) Magnification, centered on acetone signals. 1: -15 °C; 2: 0 °C; 3: 15 °C; 4: 28 °C; 5: 45 °C.

The ^{1}H-NMR signal of acetone appears as a narrow singlet at around 2 ppm, depending on the solvent and the chemical surrounding. Furthermore it represents a valid choice because of its simple structure and the position in the NMR spectrum. Figure 4.7a and b

show that temperature variation generated a strong effect in both position and signal shape, but the most interesting parameter is the shift between the acetone signal of the internal and external solutions. Internal solution contained the dinuclear copper complex, so acetone signal was affected by interaction with the paramagnetic site. This proximity caused a low-field shift of the protons, so the signal of the standard belonging to the internal sample is less shielded than the external one. Experimental conditions covered a temperature range between -15 °C and 45 °C, as the mixture is stable in these conditions.

Table 4.1- Shifts (in Hz), magnetic susceptibility and magnetic moment (per copper) determined at different temperatures for $[Cu_2(EHI)]^{4+}$

Temperature (K)	Δδ (Hz)	χ	μ (β)
258	18.04	$1.6380x10^{-8}$	1.6405
273	15.98	$1.4510x10^{-8}$	1.5882
288	14.15	$1.2848x10^{-8}$	1.5350
301	11.94	$1.0841x10^{-8}$	1.4415
318	10.90	$9.8971x10^{-9}$	1.4157

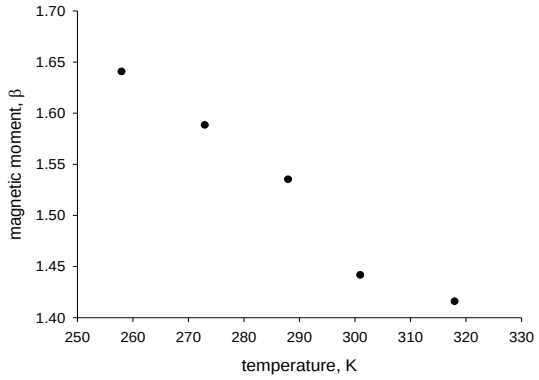

Figure 4.8. Magnetic moment *vs* temperature trend for $[Cu_2(EHI)]^{4+}$

The data in Table 4.1 show that the magnetic moment is only slightly reduced from the theoretical value (1.73 β). This is due to the weak interaction between copper ions, which poorly couples their spin moments, contrasting the paramagnetic effect of the

"free copper". Figure 4.8 shows that the magnetic moment further decreases as temperature increases. This trend could be explained by assuming a ferromagnetic behavior of the dinuclear copper complex, different from the typical antiferromagnetic properties of the majority of the previously studied dinuclear complexes.[4] Poor interaction between copper sites could be due to the rigidity of the system because the bis-amidic linker that connects the two tridentate chelating arms. Another explanation could reside in the steric hindrance of the trityl group that does not allow the two coordinating units to closely approach to each other.

The J value could be estimated interpolating the previously reported experimental data with the following equation:

$$\chi_M = \frac{\mu_0 N_{av} g^2 \beta^2}{3\,k\,T} * [1 + \frac{1}{3}\exp\left(\frac{-2\mathrm{J}}{\mathrm{kT}}\right)]$$

All parameters are known, so interpolation could permit determination of J value.

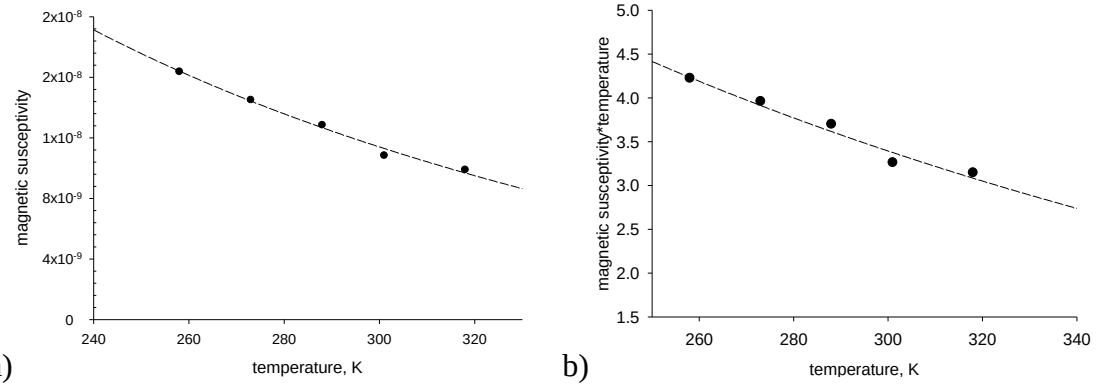

Figure 4.9- a) Dependence of magnetic susceptivity from temperature, measured for $[Cu_2(EHI)]^{4+}$ in 10:1 v/v MeOD/deuterated acetate buffer 50 mM; b) dependence of magnetic susceptivity x temperature from temperature.

Both graphs show a descending exponential-like trend, with a low slope. The descending trend is due to a ferromagnetic behavior between the two copper ions of the complex, but low slope values are imputable to a poor coupling between the unpaired electrons. Interpolation of data with the previously reported equation did not allowed a correct determination of J value. This deficiency could be imputable to not complete

solubility of the paramagnetic species, avoiding the magnetic susceptivity determination.

4.2.3. Oxidative activity of $[Cu_2(EHI)]^{n+}$

4.2.3.1. Oxidation of catechols promoted by $Cu_2(EHI)^{4+}$- catecholase activity

In order to study catalytic efficiency in catecholase activity promoted by $[Cu_2(EHI)]^{4+}$, we chose the same set of biogenic chiral catecholic pairs defined in **Chapter 2** and **3**. The rate dependence on substrate concentration was studied at pH 5.1 by keeping the catalyst concentration constant, varying that of substrate between 0.05 mM and 1.0 mM. For the oxidation of L-/D-Dopa and L-/D-DopaOMe (Figure S.I. 4.1), the plots of the initial rates exhibited a hyperbolic behavior and the kinetic parameters (k_{cat}, K_M) could be determined using simple Michaelis–Menten treatment. This enabled us to consider the same simplified reaction scheme used to explain the activity promoted by $[Cu_2(L55Bu^*)]^{4+}$ [5] and $[Cu_2(mXPhI)]^{4+}$. As previously described in **Chapter 2** and **3**, this implies fast initial copper(II) reduction by one molecule of catechol, followed by a complex series of events involving pre-equilibrium binding of a second catechol molecule, dioxygen binding to the dicopper(I) species, and finally substrate oxidation and irreversible release of quinone product. Data in Table 4.2 shows negligible enantiodifferentiation for L-/D-Dopa and only a modest preference for the L-enantiomer of DopaOMe. The enantioselectivity indexes $R_{kcat/KM}$ and R_{kcat}, expressed as percentages, are used as useful parameters to evaluate the discriminating effect observed in the catalytic oxidations at low and saturating substrate concentration, respectively. A different situation occurred for R-/S-norepinephrine (Figure S.I. 4.1-c), as rate data at increasing substrate concentration follows a sigmoidal trend. This tendency could be explained by considering a quadratic dependence of oxidation rate from substrate concentration, that could be due to a cooperative coordination of two molecules of substrate. The first molecule binds in an un-productive fashion (probably by the amino acidic portion), but this helps arranging the complex structure to give a more efficient oxidation. Unfortunately this effect does not discriminate between the two enantiomers.

Table 4.2. Kinetic parameters for the enantioselective oxidation of L-/D-Dopa, L-/D-DopaOMe and R/S-norepinephrine at pH 5.1 and 20 °C, using 1.0 and 5.0 μM concentration of $[Cu_2EHI]^{4+}$.

	K_M (mM)	k_{cat} (s^{-1})	K' (mM^2)	$R_{kcat/KM}$ %	R_{kcat} %
$[Cu_2EHI]^{4+}$	**1.0 μM**				
L-Dopa	$(2.10\pm0.58)\times10^{-1}$	$(9.93\pm0.96)\times10^{-3}$	-	-1	-4
D-Dopa	$(2.22\pm0.56)\times10^{-1}$	$(1.08\pm0.09)\times10^{-2}$	-		
L-DopaOMe	$(2.52\pm0.29)\times10^{-1}$	$(1.99\pm0.08)\times10^{-3}$	-	+15	+14
D-DopaOMe	$(2.55\pm0.52)\times10^{-1}$	$(1.50\pm0.11)\times10^{-3}$	-		
R-norepinephrine	-	$(2.84\pm0.01)\times10^{-3}$	$(4.15\pm0.01)\times10^{-2}$	$1.2^{a,c}$	$*1.2*^{b,c}$
S-norepinephrine	-	$(3.32\pm0.09)\times10^{-3}$	$(4.15\pm0.59)\times10^{-2}$		
$[Cu_2EHI]^{4+}$	**5.0 μM**				
L-Dopa	$(6.89\pm2.63)\times10^{-1}$	$(1.68\pm0.36)\times10^{-3}$	-	~0	+14
D-Dopa	$(5.18\pm0.82)\times10^{-1}$	$(1.27\pm0.09)\times10^{-3}$	-		
L-DopaOMe	$(3.89\pm0.01)\times10^{-2}$	$(5.36\pm0.01)\times10^{-4}$	-	$12.8^{a,c}$	$*0.9*^{b,c}$
D-DopaOMe	-	$(6.05\pm0.01)\times10^{-4}$	$(6.63\pm0.01)\times10^{-2}$		
R-norepinephrine	$(2.57\pm0.56)\times10^{-1}$	$(4.07\pm0.31)\times10^{-4}$	-	+3	-10
S-norepinephrine	$(3.34\pm0.75)\times10^{-1}$	$(4.98\pm0.39)\times10^{-4}$	-		

Experimental data for norepinephrine enantiomers could not be interpolated assuming a Michaelis-Menten model. Therefore kinetic equations to describe this behavior had to be derived. Catalytic oxidation of norepinephrine enantiomers by $[Cu_2(EHI)]^{4+}$ shows a substrate sigmoidal dependence suggesting the binding of two substrate molecules to the catalyst in order to observe catalysis. The reaction scheme describing the catalytic behavior is as follow:

$$C + 2S \overset{\beta_2}{\rightleftharpoons} CS_2 \xrightarrow{k_{cat}} \rightarrow\rightarrow C + S + P$$

where C is the catalyst, S is norepinephrine, CS_2 is the catalyst bound to two substrate molecules and P is the product of the reaction.

Assuming that:

a) Binding step I is faster than turnover cycle rate (as shown by the fast binding observed in the binding studies with $[Cu_2(EHI)]^{4+}$ and considering the slow reaction rates, i.e. moderate k_{cat} values)

b) Binding of two substrate molecules is needed to perform the reaction (i.e., the CS species is not catalytically efficient)

c) Only a minor fraction of 1:1 complex:substrate adduct accumulates during turnover (i.e., $[CS]<<[C]+[CS_2]$)

According to point a), binding of two substrate molecules occurs as a pre-equilibrium, allowing the use of the binding constant β_2 (equation 1), together with the mass balance on the catalyst (equation 2), to obtain the species concentration during turnover

$$C + 2S \overset{\beta_2}{\rightleftharpoons} CS_2 \qquad \beta_2 = \frac{[CS_2]}{[C]\cdot[S]^2} \tag{1}$$

$$[C]_0 = [C] + [CS_2] \tag{2}$$

where $[C]_0$ is the total concentration of the catalyst (free plus substrate bound)

$[CS_2]$ can be obtained from equation 1, $[CS_2] = \beta_2 \cdot [C] \cdot [S]^2$

The substitution of $[CS_2]$ in equation 2 gives the free (unbound) catalyst concentration:

$$[C] = \frac{[C_0]}{1 + \beta_2 \cdot [S]^2} \tag{3}$$

And then that of the CS_2 species is:

$$[CS_2] = \frac{[C_0]\cdot \beta_2 \cdot [S]^2}{1 + \beta_2 \cdot [S]^2} \tag{4}$$

The reaction rate depends on $[CS_2]$ through equation 5:

$$r = k_{cat} \cdot [CS_2] \tag{5}$$

The rate equation is obtained by combining equations 4 and 5:

$$r = \frac{k_{cat} \cdot [C_0] \cdot \beta_2 \cdot [S]^2}{1 + \beta_2 \cdot [S]^2} \quad (6)$$

and

$$\frac{r}{[C_0]} = \frac{k_{cat} \cdot \beta_2 \cdot [S]^2}{1 + \beta_2 \cdot [S]^2} = \frac{k_{cat} \cdot [S]^2}{1/\beta_2 + [S]^2} = \frac{k_{cat} \cdot [S]^2}{K' + [S]^2} \quad (7)$$

where $K' = 1/\beta_2$

It is inappropriate to make a direct comparison with the other enantiomeric pairs, so the discriminating power against the two enantiomers of norepinephrine was evaluated as a ratio between the oxidation rate (vR/vS) at high (0.8 mM) and low (0.015 mM) concentration of substrate. Another interesting result is the dependence of oxidation rate from $[Cu_2(EHI)]^{4+}$ concentration. Data in Table 4.2 show that higher concentration of catalyst corresponds to a decrease of an order of magnitude in k_{cat} values (Figure S.I 4.2).

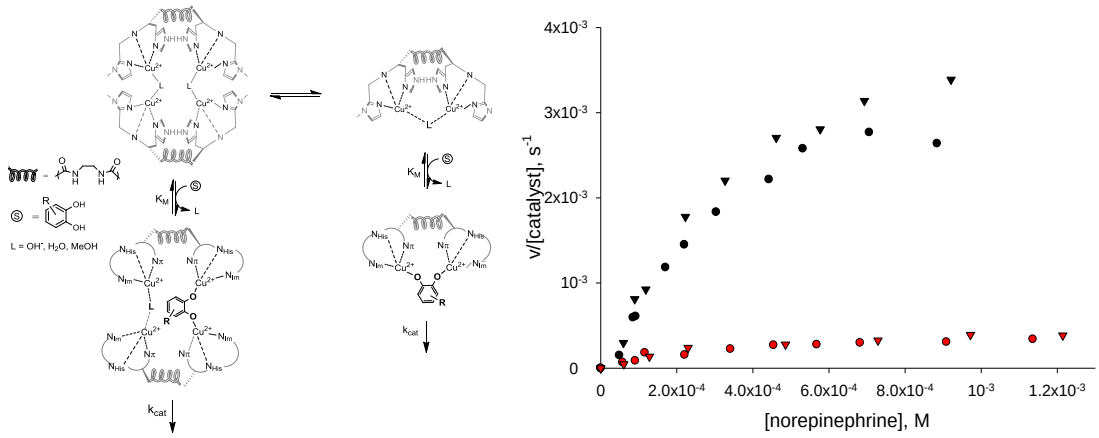

Figure 4.10- a) Hypothesis on the formation of a dimeric species, involved in catalysis. b) Effect of catalyst concentration on the initial rates of air oxidation of the enantiomers of norepinephrine by $[Cu_2EHI]^{4+}$ studied at pH 5.1 (black symbols: $[Cu_2(EHI)]^{4+}$ = 1 µM; red symbols: $[Cu_2(EHI)]^{4+}$ = 5 µM).

The hypothesis formulated to justify this behavior assumes the equilibrium between two active species, one monomeric and one dimeric, with the latter less but still active (Figure 4.10). It was therefore evident that the catalytic activity depends on the

concentration of $[Cu_2(EHI)]^{4+}$; to identify the nature of this dependence, a study of complex concentration dependence was performed.

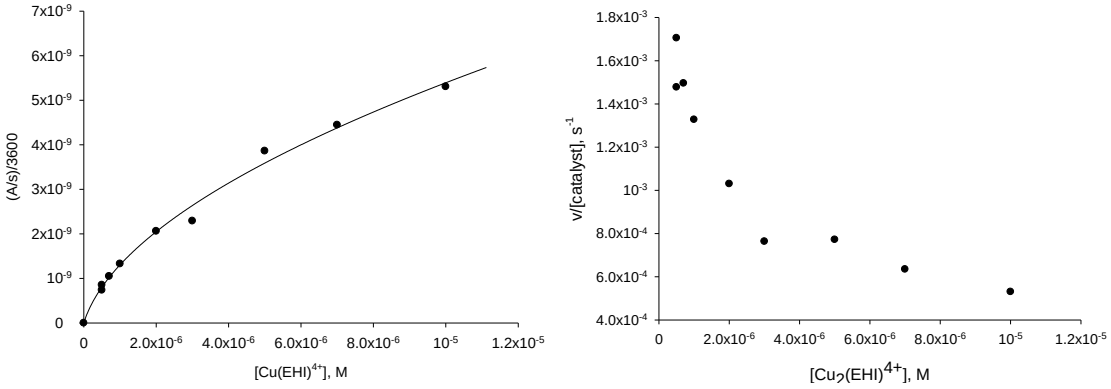

Figure 4.11- Dependence of oxidation rate of L-Dopa methyl ester (0.5 mM) from complex concentration. On the left: Rate data are expressed as Absorbance/time (A/s) divided for $\varepsilon_{aminochrome}$. On the right: Rate data are expressed as $((A/s)/3600)/[Cu_2(EHI)]^{4+}$.

Spectrophotometric kinetic studies were conducted in 10:1 methanol/acetate buffer 50 mM (pH=5.1) mixture, using a 0.5 mM L-Dopa methyl ester as substrate, and varying catalyst concentration between $5x10^{-7}$ and $1x10^{-5}$ M. As $[Cu_2(EHI)]^{4+}$ concentration increased, rate values decreased rapidly with a exponential decay, indicating a quadratic dependence from the catalyst concentration. In order to model this peculiar behavior, the kinetic equations were appropriately derived with the assumption that in substrate-saturating conditions, the oxidation rate depends only on complex concentration. We also assume that the complex exists in two form in dynamic equilibrium, the monomeric and the dimeric ones:

$2C \rightleftharpoons C_2$ ruled by $Kb = [C_2]/[C]^2$

Oxidation rate depends from both [C] and $[C_2]$

$v = k_1[C] + k_2[C_2]$

Considering the mass equation:

$[C_0] = [C] + 2Kb[C]^2$

appropriate substitution brings to the final equation, used for the interpolation:

$$v = k_1\left(\frac{-1+\sqrt{1+8Kb[C_0]}}{4Kb}\right) + Kbk_2(\frac{-1+\sqrt{1+8Kb[C_0]}}{4Kb})$$

However, we note that interpolating the data with the previously described equation, we did not obtained reliable data because of high standard deviation indicates high data intercorrelation, but the model (Figure 4.11) adequately represented the situation, reinforcing the initial hypothesis.

4.2.3.2. Oxidation of phenols- monophenolase activity

4.2.3.3. Binding of L-/D-tyrosine methyl ester $[Cu_2(EHI)]^{4+}$

Optical titration with either L- and D-tyrosine methyl ester is a useful mean to gain information about the difference in coordination preferences of endogenous phenols for $[Cu_2(EHI)]^{4+}$. The titrations were performed using their phenolate salts to improve the coordination to copper ions. Titrations were conducted in methanol, using the diazabicycloundecene salts of the tyrosine derivatives, in order to prevent solubility problems of both substrate and complex. The carboxylic function were protected as methyl esters, in order to disfavor the formation of the zwitterion form and also to direct coordination to the phenolic moiety of the molecule.

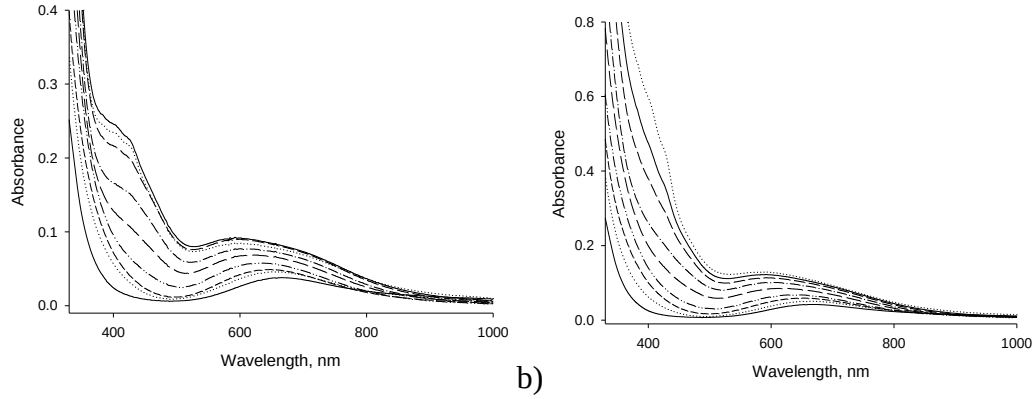

Figure 4.12- UV-Vis spectra recorded upon titration of $[Cu_2(EHI)]^{4+}$ (5×10^{-4} M) in methanol solution with the DBU salt of L-tyrosine methyl ester (a) and D-tyrosine methyl ester (b), from 0:1 to 10:1 [tyrosinate]:$[Cu_2]$ molar ratios. The spectra were recorded at 25±0.1 °C.

Spectral changes associated with addition of DBU salt of tyrosine methyl ester can be basically resumed as the development of a band at 430 nm, associated with a blue shift

of d-d bands to about 600 nm. The more intense band at 430 nm was attributed to a phenolate→copper(II) LMCT transition.[6] Experimental data were processed with a non-linear least procedure, and the obtained simplified model explained ligand binding as a sequence of two steps, which involved the formation of both 1:1 and 1:2 tyrosinato:complex adducts.

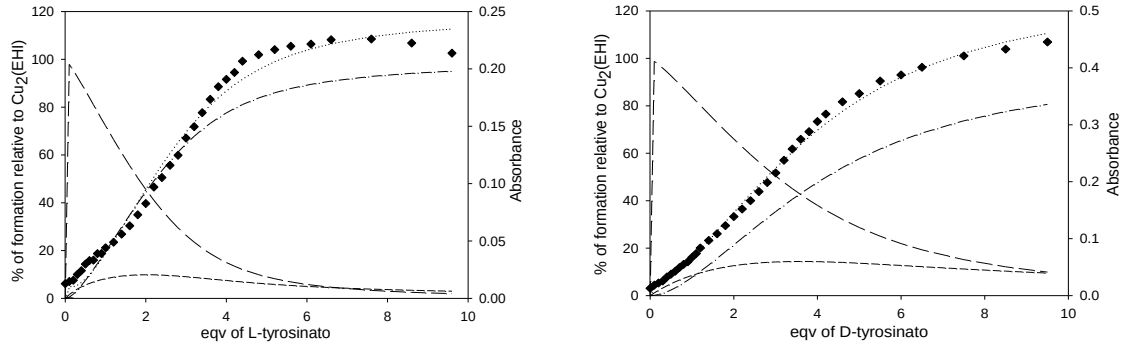

Figure 4.13- Absorbance profile at 428 nm during the titration of $[Cu_2(EHI)]^{4+}$ with methyl L-tyrosinate (left) and methyl D-tyrosinate (right), superimposed to species distribution diagram. Diamonds: experimental absorbance values; dotted line: calculated absorbance; long dashed line: distribution of free $[Cu_2(EHI)]^{4+}$; short dashed line: distribution of the 1:1 $[Cu_2(EHI)\text{-tyrosinato}]^{3+}$ complex; dashed and dotted line: distribution of the 1:2 $[Cu_2(EHI)(tyrosinato)_2]^{2+}$ complex.

Experimental absorption data (Figure 4.13) clearly showed that the system is more complicated, and the hypothesis is that the first phenolate was bound by the amino acidic portion, while the second one was bound throughout the phenolate moiety:

$$[Cu_2(EHI)]^{4+} + TyrOMe^- \rightleftharpoons [Cu_2(EHI)\text{-}N(TyrOMe)]^{3+}$$

$$[Cu_2(EHI)\text{-}N(TyrOMe)]^{3+} + TyrOMe^- \rightleftharpoons [Cu_2(EHI)\text{-}N(TyrOMe)\text{-}O(TyrOMe)]^{2+}$$

Even if we were not able to calculate reliable binding constants, plots of experimental absorption data (Figure 4.13) showed that formation of the 1:2 complex:tyrosinato adduct occurs at lower substrate concentration for L-enantiomer, and it could be rationalized assuming an higher affinity, in agreement with data for the corresponding catechols.

4.2.3.4. Oxidation of N-acetyl-L-/D-tyrosine ethyl ester- enantio-discriminating monophenolase activity

Phenol hydroxylation is, from a general point of view, a very interesting activity to mimic and tyrosinase, in Nature, exhibits a marked preference in oxidation of L-enantiomer.[7] Enantio-differentiating capability in oxidation of phenol was also tested with $[Cu_2(EHI)]^{2+}$ complex, chosing fully protected tyrosine derivatives in order to promote selective coordination of the phenolic moiety. Experiments were conducted with N-acetyl-L-/D-tyrosine as tetrabutyl ammonium salts, to favor substrate coordination as it occurs with the enzyme. The acetyl group on the amino group was introduced to prevent further cyclizations of the obtained quinone, that could complicate the interpretation of the product. Several attempts of low-temperature isolation of the oxygenated reactive intermediates were done, albeit unsuccessfully (down to -80 °C in dry acetone, -90 °C in dry dichlorometane, -120 °C in dry 2-methyl tetrahydrofuran), so characterization of this reactive intermediate was impossible. The hypothesis is that Cu_2O_2 complex did not accumulate because of its intrinsic high reactivity. Catalytic oxygenation of tyrosine derivatives was performed preparing the dinuclear copper(I) complex in dry acetone at -80 °C, then adding an excess of substrate, and finally exposing the mixture to atmospheric oxygen. After work-up (described in Experimental section), the complicated obtained mixture was purified to eliminate the oligomeric products derived from the oxidation. NMR and MS characterization (Fisure S.I 4.4-5) of the purified product showed that it cannot be attributable to pure monophenolase activity, as it could be considered deriving from C-O and C-C radical coupling of the modified substrate.

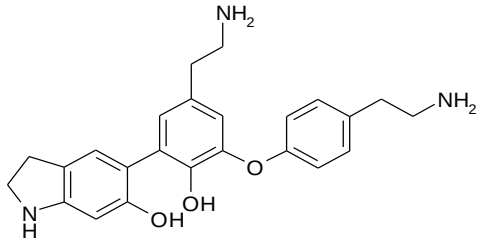

Figure 4.14- Hypothesis on the formation of the oxidation product, attributable to the oxidation of tyrosine derivative performed with $[Cu_2(EHI)]^{2+}$ as catalyst.

However, the main scope was not to investigate the real nature of the oxidation product, rather the enantiodifferentiation in oxidation of L-/D-enantiomers. We monitored the oxidation of the enantiomeric L-/D-tyrosine derivatives spectrophotometrically, after

exposing a solution of $[Cu_2(EHI)]^{2+}$ and excess phenolate salts of *N*-protected tyrosine ethyl esters (20 equiv.), initially prepared anaerobically, to air. In the initial part of the reaction, a broad absorption band centered around 400 nm, attributable to some quinone product(s), increases with time (Figure 4.15 and S.I. 4.6). The time profile of this band clearly shows a steeper increase for the L-tyrosinate substrate with respect to the D enantiomeric counterpart, indicating a faster reaction. The initial rates, in Δabsorbance/s units, are in fact 7.4×10^{-5} for ethyl *N*-acetyl-L-tyrosinate and 3.4×10^{-5} for ethyl *N*-acetyl-D-tyrosinate, that is in line with the binding preference for the L-tyrosinato ligand with respect to D-tyrosinato by $[Cu_2(EHI)]^{4+}$.

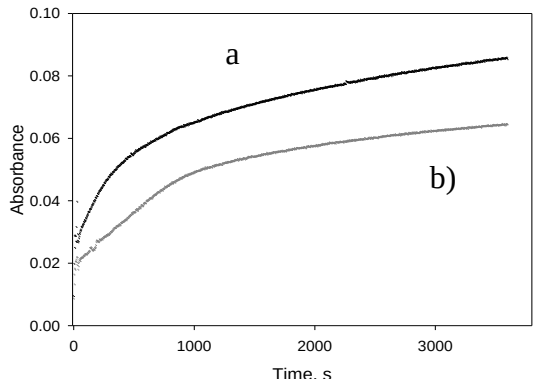

Figure 4.15. Time profile of the absorption at 400 nm during the oxidation of the tetrabutylammonium salts of ethyl *N*-acetyl-L-tyrosinate (a) and ethyl *N*-acetyl-D-tyrosinate (b) by $[Cu_2(EHI)]^{2+}/O_2$ in acetone solution at 25 °C.

4.2.3.5. Oxidation of β-naphthol

The oxygenation reaction was also performed on a more hydrophobic substrate, β-naphthol. Due to the more extended aromatic core, its oxidation products should be more manageable and easy to separate. The reaction was carried out in presence of an excess of substrate, that was used as its DBU salt in order to favor the coordination to the dicopper center. After exposure to air oxygen, the reaction turned to gold yellow after one night. The work-up procedure (described in Experimental section) permitted the crude product recovery. Unreacted phenol was separated by column chromatography and the pure product was recovered. NMR and MS analysis provided the identification of the structure, that corresponds to a Michael addition product of the unreacted phenol on the 1,2-naphthoquinone (Scheme 4.3). The same reaction was carried out in presence of $^{18}O_2$, so that we should notice 18-O insertion in the oxidation

product. Unfortunately, labeling experiment with $^{18}O_2$ did not show insertion of 18-O, suggesting a radical pathway instead of a tyrosinase like monoxygenation.

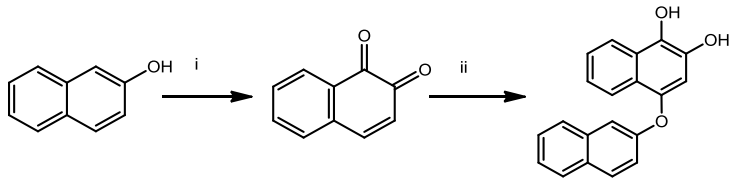

Scheme 4.3- The steps involved in the hydroxylation of β-naphthol (as DBU salt) by $[Cu_2(EHI)]^{2+}/O_2$, with the subsequent addition of β-naphtholate to the naphthoquinone product of the monooxygenase reaction.

4.3. Conclusions

A new chiral ligand based on histidine as building block was synthesized, starting from the parent ligand PHI and modifying either the linker between the two tridentate units and the number of coordination sites. EHI, and its related dicopper complex were fully characterized by NMR, MS, UV-Vis and CD spectroscopy. The dinuclear copper complex of EHI was also tested in its capability to mimic the activity of tyrosinase, both for catecholase and monophenolase activities. Studies of diphenolase activity showed an interesting dependence of the catalysis on the concentration of the complex. Monoxygenation reactions studies showed that obtained product derived from reactions. Determination of magnetic susceptivity and magnetic moment with Evans' method showed poor cooperation between copper centers, that could justify the tendency to favor radical reactions rather then tyrosinase-like pathways.

4.4. Experimental section

Materials and methods

All preparations were carried out using standard Schlenk techniques under an inert atmosphere of N_2 unless otherwise stated. Solvents were dried over standard drying agents and stored over 3-Å molecular sieves. All starting materials were of reagent grade and purchased from either Sigma-Aldrich Chemical Co. or VWR International and used without further purification. Nα-Fmoc-N(Im)-trityl-L-histidine was purchased from Novabiochem, and used without further purification. Elemental analyses were obtained at the Micro-analysis service of the Milano Chemistry Department. CD spectra were obtained with a Jasco J500 spectropolarimeter; the spectra were recorded at 0.2 nm

resolution in the range between 300 and 700 nm at 50 nm min^{-1} with three scans acquired for each spectrum. The NMR spectra were recorded with a Bruker AVANCE 400 spectrometer operating at 9.37 T with frequencies of 400.13 and 100.6 MHz for ^{1}H and ^{13}C NMR, respectively. The data acquisition and processing were performed with a standard Bruker software package (Topspin 1.3). The UV/Vis spectra were recorded with an Agilent 8453 spectrophotometer. Mass spectra were recorded with a Thermo-Finnigan LCQ 371 ADV MAX spectrometer.

General procedures

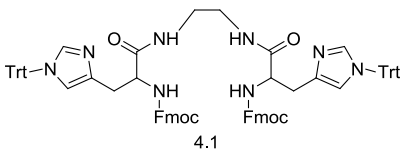

4.1

*Synthesis of bis[(9H-fluoren-9-yl)methyl]-[(2S,2'S)-(ethane-1,2-diyl-bis(azanediyl)]bis[1-oxo-3-(1-trityl-1H-imidazol-4-yl)propane-2,1-diyl)]dicarbamate (***4.1***).* Nα-Fmoc-N(Im)-trityl-L-histidine (2.00 g, 3.2 mmol) was suspended in dichloromethane (8 mL) and **(**benzotriazol-1-yloxy)tripyrrolidinophosphonium hexafluorophosphate (PyBOP**)** (1.66 g, 3.2 mmol) was poured into the solution. Ethylenediamine (108 μL, 1.6 mmol) was added to the solution and, finally, N,N-diisopropylethylamine (DIPEA, 2.2 mL, 12.8 mmol) was further added as a base. The reaction mixture was stirred for 3 h at room temperature. Then, the solvent was rotary-evaporated, yielding a highly viscous colorless oil, which was purified by silica chromatography using a mixture of dichloromethane-methanol (from 98:2 to 0:100, v/v) as eluent. A white foamy solid product (2.57 g, quantitative yield) was obtained, after treatment with diethyl ether. ^{1}H NMR (400 MHz, $CDCl_3$, 298 K): δ 9.72, (br. s), δ 7.75 (d, J = 7.0 Hz, 2H), δ 7.73 (d, J = 7.0 Hz, 2H), 7.55 (d, J = 7.0 Hz, 2H), 7.47 (d, J = 8.0 Hz, 2H), 7.44 – 7.30 (m, 24H), 7.25 (d, J = 7.0 Hz, 2H), 7.23 (d, J = 7.0 Hz, 2H), 7.19–7.11 (m, 12H), δ 7,01 (dd, 2H), 6.64 (s, 2H), 6.04 (d, J = 6.0 Hz, 1H), 4.53–4.44 (m, 2H), 4.33–4.06 (m, 6H), 3,5 (dd, 2H), 3.41 (d, J = 13.4 Hz, 2H). 13C NMR (100 MHz, 298 K): δ 170 (Q); 156 (Q), 144 (Q), 142 (Q), 138 (CH), 135 (Q), 130 (CH), 128,5 (CH), 125,6 (CH), 120,8 (CH), 120,31 (CH), 76 (Q), 67 (CH2), 53.5 (CH), 47,5 (CH), 38 (CH2), 31 (CH2). MS (ESI): m/z +1263 [$M+H^+$], +1285 [$M+Na^+$], +1302 [$M+K^+$].

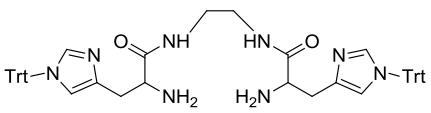

4.2

Synthesis of (2S,2'S)-N,N'-(ethane-1,2-diyl)bis(2-amino-3-(1-trityl-1H-imidazol-4-yl)propanamide) (**4.2**). Piperidine (2 ml, 20 mmol) was added to a solution of **4.1** (1.57 g, 1.2 mmol) in dichloromethane (10 ml). After stirring for 1.5 h at room temperature, the solvent was rotary-evaporated giving a yellow oil, which was washed with diethyl ether, affording a highly hygroscopic white powder (1.01 g, nearly quantitative yield). ^{1}H NMR (400 MHz, $CDCl_3$): δ 7.93–7.82 (s, 2H), 7.43–7.30 (m, 20H), 7.20–7.06 (m, 12H), 6.65 (s, 2H), 3.66–3.56 (m, 2H), 3.43–3.30 (m, 2H), 3.31–3.20 (m, 2H), 2.96 (dd, J = 14.4, 3.9 Hz, 2H), 2.75 (dd, J = 14.4, 8.0 Hz, 2H). MS (ESI): m/z +819 [$M+H^+$].

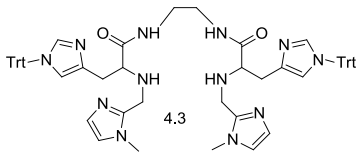

4.3

Synthesis of (2S,2'S)-N,N'-(ethane-1,2-diyl)bis(2-((1-methyl-1H-imidazol-4-ylmethyl)-amino)-3-(1-trityl-1H-imidazol-4-yl)propanamide) (**4.3-EHI**).

Compound **4.2** (612 mg, 0.75 mmol) was dissolved in dichloromethane (10 mL) under an inert atmosphere. A solution of 1-methyl-2-imidazole carboxaldehyde (230 mg, 2.09 mmol) in dichloromethane (1.5 mL) was slowly added. The reaction was stirred for 2 h at room temperature. The acid labile diimine could not be visualized by TLC, so the reaction was monitored by ESI–MS. Given the predominant formation of the disubstituted product, the material was transferred directly into the reduction reaction. Solid STABH (12 equiv in 4 portions) was added portion-wise and the suspension was stirred at room temperature for two more hours. The solvent was removed and the yellow oil was purified by column chromatography on silica gel, with eluent diethyl ether/2-propanol (5:3 v/v) and an increasing amount of aqueous ammonia (from 1% to 4%), to remove the reduced imidazole-carboxaldehyde (Rf= 0.86). The final product was recovered by chromatography on silica using a mixture of chloroform-methanol-aqueous ammonia (10:1:0.15 v/v) as eluent, giving EHI as a colorless oil (150 mg, 26 %). ^{1}H-NMR (400 MHz, $CDCl_3$): δ 7.42–7.22 (m, 20H), 7.15–7.02 (m, 12H), 6.74 (s, 2H), 6.69 (s, 2H), 6.60 (s, 2H), 3.82–3.67 (m, 4H), 3.58 (s, 6H), 3.47–3.15 (m, 6H), 2.91 (dd, J = 14.4, 5.7 Hz, 2H), 2.78 (dd, J = 14.4, 7.3 Hz, 2H). ^{13}C-NMR (100 MHz): δ 174.81 (Q), 146 (Q), 138.6 (CH), 137.8 (Q), 130.11 (CH), 128,5 (CH), 126.95 (CH), 121.6 (CH), 119.9 (CH), 75.6 (Q), 62.8 (CH),44.14 (CH2), 39.53 (CH2), 33.2 (CH3), 31.95 (CH2). MS (ESI): m/z +1007 [$M+H^+$].

Synthesis of $[Cu_2(EHI)][ClO_4]_4$. The ligand EHI (50 mg, 0.05 mmol) was dissolved in methanol (800 µL) yielding a pale yellow solution. Then, copper(II) perchlorate hexahydrate (37 mg, 0.10 mmol) in methanol (500 µL), from a stock solution, was added dropwise. The color of the solution changed from yellow to shining green, until a green solid precipitated. The solid was recovered by filtration, washed with diethyl ether (3×1 mL) and dried in air (yield: 65%). Anal. Calcd for $C_{62}H_{52}Cl_4Cu_2N_{12}O_{14}\cdot 4CH_3OH$ (1656.3): C 47.86, H 4.74, N 10.15; found C 47.17, H 4.34, N 9.87.

Synthesis of L- and D-tyrosine methyl ester The L- or D-tyrosine powder (100 mg, 0.552 mmol) was suspended in methanol and cooled in an ice/NaCl bath. Then, $SOCl_2$ (1.49 mmol) was slowly added under stirring and the solution was brought to room temperature and stirred overnight. The solvent was removed by rotary evaporation to give the pure product.

General procedure for the synthesis of the DBU salts of phenolic substrates The phenol was dissolved in 1 mL of methanol and an equimolar amount of diazabicycloundecene was added. The solution was stirred for 30 min at room temperature and the solvent removed by rotary evaporation, to give the pure product.

Azide binding studies Titrations with azide were performed by addition of a concentrated methanolic solution of sodium azide to the solution of $[Cu_2EHI]^{4+}$ in MeOH/MeCN 9:1 (v:v). All measurements were done at 25±0.1 °C and without any incubation of the mixtures, as the anion binding was found to be fast. Titration of $[Cu_2(EHI)]^{4+}$ (5.98×10^{-5} M) was performed by stepwise addition of equal amounts of the azide solution (1.00×10^{-3} M) from 0.1 to 2.0 [azide]:[Cu_2] ratios. It was possible to separate the titration steps for [N_3^-]:[Cu_2] between 0.1 and 1.0 (λmax = 389 nm) and between 1.1 to 2.0 (λmax = 382 nm). The spectral data were analyzed as previously described,[8] to deduce equilibrium constants and stoichiometry of formation of the adducts. CD spectra of the azide adducts were recorded after the addition of 1.0 and 2.0 equiv. of the ligand.

Determination of magnetic susceptivity with Evans method:
Solution A*:* 110 µL of 1 mM solution of $[Cu_2(EHI)]^{4+}$ in 10:1 MeOD: deuterated acetate buffer (pH= 5.1, 50 mM) were added with 10 % vol of acetone (11 µL);
Solution B: 660 µL of 10:1 MeOD: deuterated acetate buffer (pH= 5.1, 50 mM) were added with 10 % vol of acetone (66 µL).

Solution A was putted in the internal tube of a co-axial NMR tube system, while B is put in the external one (Figure 4.6). ^{1}H-NMR experiments were performed at different temperature (-15 °C, 0, 15 °C, 28 °C, 45 °C) and shifts between the Acetone (A) and Acetone (B) in Hz were recorded.

Catalytic oxidations of o-catechols. The catecholase activity of complex $[Cu_2(EHI)]^{4+}$ was determined by studying the oxidation of the chiral catechols L-Dopa, D-Dopa, L-DopaOMe, D-DopaOMe, R-(-)-norepinephrine, and S-(+)-norepinephrine. The kinetic studies were carried out spectrophotometrically by the method of initial rates by monitoring the increase of each characteristic aminochrome absorption band over time. The reading wavelengths were: 475 nm for L-/D-Dopa, 468 nm for L-/D-DopaOMe, and 480 nm for R-/S-norepinephrine. The solvent used was a 10:1 (v/v) mixture of methanol/aqueous acetate buffer (50 mM, pH 5.1), saturated with atmospheric dioxygen. To check the contribution of the autoxidation reaction of the catechols, we used the same solution without adding the catalyst as internal reference. The experiments were carried out over a substrate concentration range (from 5×10^{-5} to 1×10^{-3} M) at a constant temperature of 25±0.1 °C, to determine the dependence of the rate on substrate concentration. To maintain pseudo-first order conditions, a 5×10^{-5} M solution of $[Cu_2(EHI)]^{4+}$ was treated with a minimum of 10 equiv. of substrate, as the lowest concentration.

Kinetic studies of L-/D-dopa oxidation. Two stock solutions of 8×10^{-4} M of L- and D-dopa were prepared in a 1:1 (v/v) mixture of methanol/aqueous buffer. To favor the dissolution in the stock solution mixture, we found it useful to dissolve the substrates first in buffer solution and then in the remaining volume of methanol, with mild warming of the mixture. The exact substrate concentration was then controlled on the basis of the absorbance values measured at 283 nm, the wavelength of maximum absorbance for the catechols (εdopa = 2700 M^{-1} cm^{-1}). The kinetic measurements were performed diluting the stock substrate solution to the desired concentration; after recording the blank spectrum, the reaction was initiated by the addition of a small volume of a concentrated solution of the catalyst dissolved in methanol (final concentration $1x10^{-6}$ or 5×10^{-6} M). Absorption spectra of these solutions were recorded at a regular time interval of 1 s for 5 min in the wavelength range 200–800 nm. The reaction was followed by monitoring the increase in the absorbance at 475 nm (ε475 = 3600 $M^{-1}cm^{-1}$)[8] as a function of time.

Kinetic studies of L-/D-dopaOMe oxidation. These experiments were carried out following the same procedure described before. Due to their better solubility in organic solvents, the stock solutions of L- and D-dopaOMe were prepared in methanol, and their concentrations corrected on the basis of the absorbance measured at 283 nm (εdopaOMe = 2700 M^{-1} cm^{-1}). The catecholase activity was followed spectrophotometrically by monitoring the increase in the absorbance at 468 nm (the ε value used was assumed to be the same as that of dopachrome)[8] as a function of time.

Kinetic studies of R-/S-norepinephrine oxidation. Also for the oxidation of S-/R-norepinephrine L-bitartrate we followed the same general procedure described before. The initial solutions of the substrates were prepared in a 1:1 (v/v) mixture of methanol/aqueous buffer, and their concentrations corrected on the basis of the absorbance measured at 283 nm (εnorepinephrine =3070 M^{-1} cm^{-1}). The catechol oxidations were followed spectrophotometrically by monitoring the increase in the absorbance at 480 nm (the ε value used was assumed to be the same as that of dopachrome)[8] with time.

Binding of L- and D-tyrosine methyl ester to $[Cu_2(EHI)]^{4+}$. Spectrophotometric titration of $[Cu_2EHI]^{4+}$ (5×10^{-4} M) in methanol solution was performed by addition of successive amounts of a methanolic solution of the DBU salt of each enantiomer of tyrosine methyl esters, 0.05 M, from 0:1 to 10:1 [tyrosinate]:[Cu_2] molar ratios, maintaining a constant temperature of 25±0.1 °C. The spectral data were then analyzed with HypSpec,[9] considering the spectral changes in the range of wavelengths between 370 and 764 nm.

Low temperature hydroxylation of tetrabutylammonium N-acetyl-L-tyrosinate ethyl ester. An oven-dried 100 mL round bottom flask equipped with a stirring bar and a rubber septum was degassed and backfilled with Ar, then charged with anhydrous acetone (47 mL). Previously prepared solutions in dry acetone of tetrabutylammonium salt of the tyrosine derivative (1×10^{-5} mol in 1 mL) and EHI (5×10^{-7} mol in 1 mL) were cannulated into the reaction flask. The mixture was cooled at -80 °C with a cryostat and carefully degassed and kept under N_2. Separately, $[Cu(CH_3CN)_4]PF_6$ (1×10^{-6} mol) was dissolved in dry and degassed acetone (1 mL). This solution was cooled and added to the reaction flask, via cannula, under Ar. To the reactor was subsequently applied an O_2-filled balloon to assure an approximately constant pressure of O_2. At the end of the reaction, the vessel was opened to the atmosphere and the mixture was quenched at low temperature with 2 mL of 1 M $HClO_4$. The organic solvent was removed in vacuo and the aqueous phase was extracted with CH_2Cl_2 (3×10 mL). The combined organic

fractions were then dried over Na_2SO_4, filtered and rotary evaporated to afford an oil which was analyzed directly by ^{1}H-NMR. The crude reaction mixture was purified using column chromatography using silica gel and hexane as eluent.

Hydroxylation of N-acetyl-L/D-tyrosine ethyl ester- Spectrophotometric study. A solution of EHI (5×10^{-5} M) and the tetrabutylammonium salt of the tyrosine derivative (10^{-3} M) was prepared in freshly distilled and degassed acetone (2 mL) in a screw-cap thermostated optical cell, stoppered with a rubber setpum. A solution of $[Cu(CH_3CN)_4]PF_6$ in freshly distilled and degassed acetone (10^{-4} M, 1 mL) was added to the previous solution, through a cannula, maintaining the mixture under an inert atmosphere. The reaction was initiated by exposure to dioxygen and followed by spectrophotometry, monitoring the increase in intensity of the broad absorption band at 400 nm during 3600 s. The comparison of the reactivity of the two tyrosine enantiomers was made through the initial rates of development of the band at 400 nm.

Hydroxylation of β-naphthol. A solution of EHI (5×10^{-5} M) and the DBU salt of the naphthol (1×10^{-3} M) was prepared in degassed, dry acetone (20 mL), maintaining an argon atmosphere with the use of a Schlenk line. A solution of $[Cu(CH_3CN)_4]PF_6$ in freshly distilled and degassed acetone (1×10^{-4} M, 1 mL) was added to the above solution, with a gas-tight syringe. The reaction was initiated by the addition of dioxygen and was stirred at room temperature overnight; the color of the solution turned from colorless to pale-gold yellow. The solvent was removed by rotary evaporation, then the crude product was dissolved in dichloromethane and a few drops of distilled water were added, followed by a small amount of the disodium salt of EDTA. The organic phase was separated and evaporated to give the crude product. Purification by liquid chromatography, using silica gel (230-400 A mesh) and eluting with hexane/ethyl acetate 7:3 gives the final product (Rf= 0.38). ^{1}H-NMR (400 MHz, acetone-d6) δ 8.82 (s, 1H), 8.13 (d, J = 7.3 Hz, 1H), 7.97 (d, J = 9.0 Hz, 1H), 7.91 (d, J = 8.5 Hz, 1H), 7.77 (d, J = 7.6 Hz, 1H), 7.56 (dd, J = 11.6, 7.4 Hz, 2H), 7.44 – 7.21 (m, J = 7.1 Hz, 4H), 6.85 (d, J = 7.6 Hz, 1H), 6.46 (s, 1H).

Supporting information

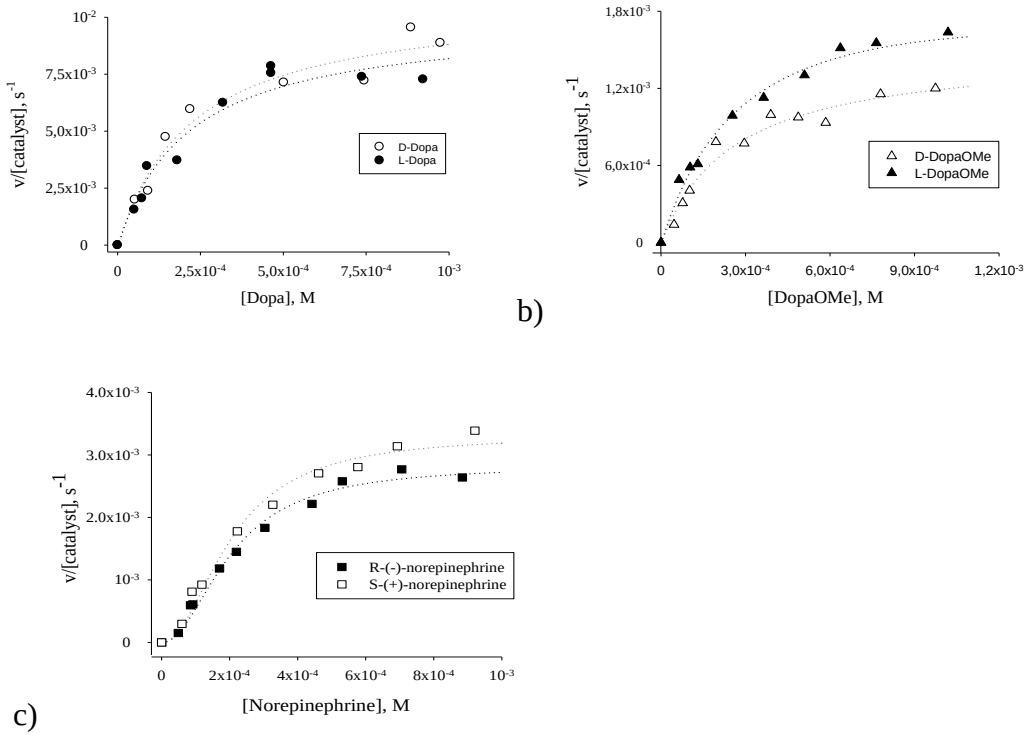

Figure S.I 4.1- Effect of substrate concentration on the initial rate of oxidation of L-/D-Dopa (a), L-/D-DopaOMe (b), and R-/S-norepinephrine (c) by $[Cu_2EHI](ClO_4)_4$ (1 μM) in a 10:1 (v/v) mixture of methanol/aqueous acetate buffer (50 mM) at pH=5.1.

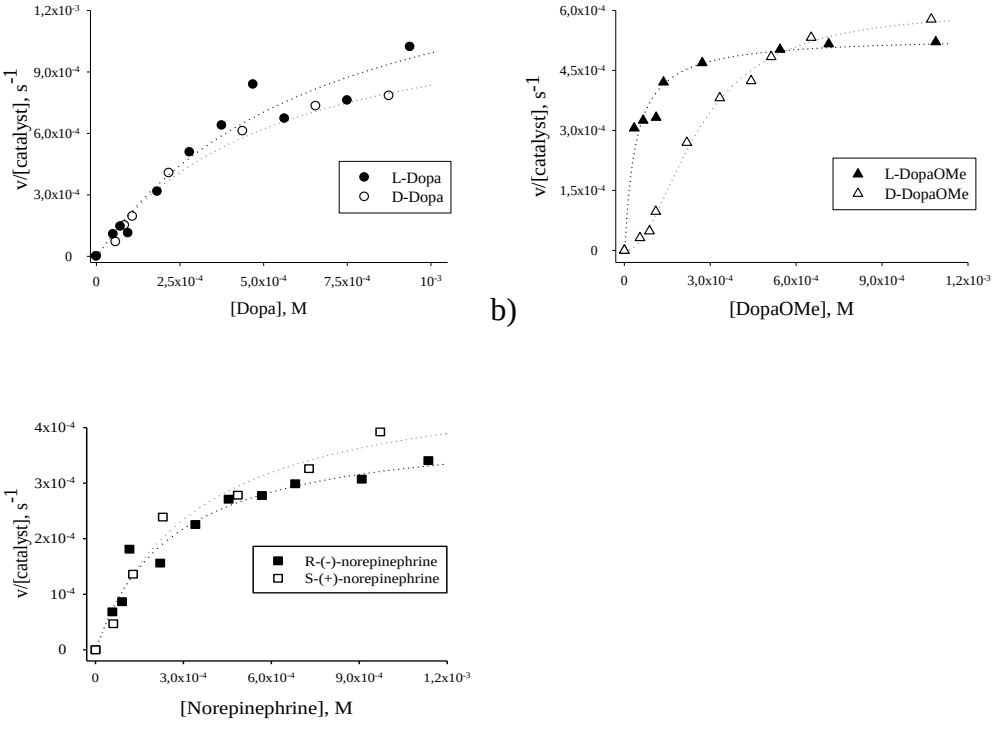

Figure S.I 4.2- Effect of substrate concentration on the initial rate of oxidation of L-/D-Dopa (a), L-/D-DopaOMe (b), and R-/S-norepinephrine (c) by $[Cu_2EHI](ClO_4)_4$ (5 μM) in a 10:1 (v/v) mixture of methanol/aqueous acetate buffer (50 mM) at pH=5.1.

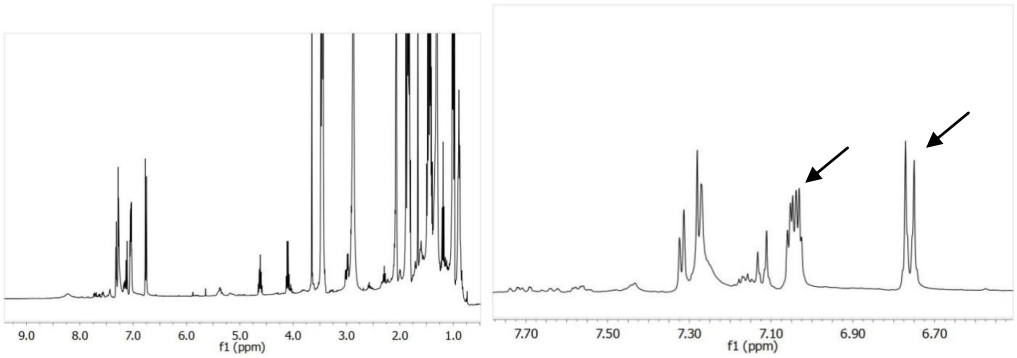

Figure S.I 4.3- ^{1}H NMR spectrum in acetone d-6 (δ values, ppm) of the crude product mixture of hydroxylation reaction of the TBA salt of L-tyrosine, with expansion of the aromatic region on the right. Unreacted phenol signals are indicated with arrows.

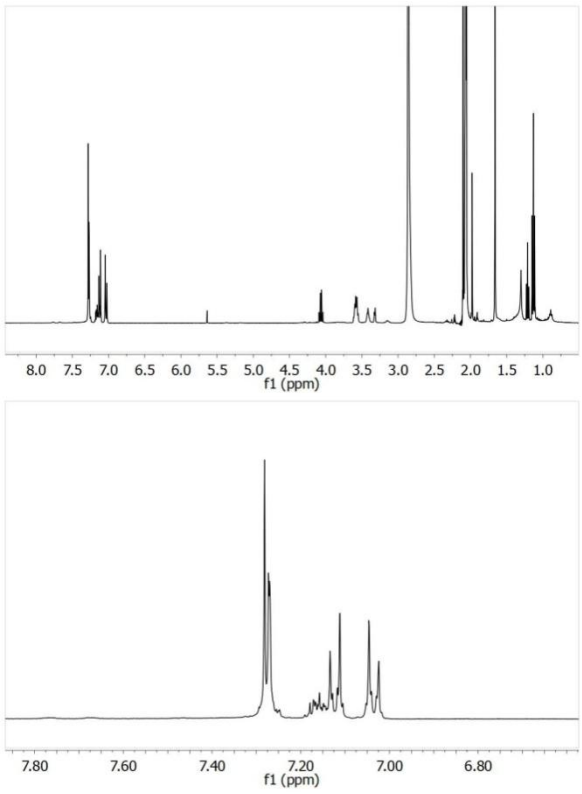

Figure S.I 4.4- ^{1}H NMR spectrum in acetone d-6 (δ values, ppm) of the pure product from the hydroxylation reaction of the TBA salt of L-tyrosine, with expansion of the aromatic region on the right.

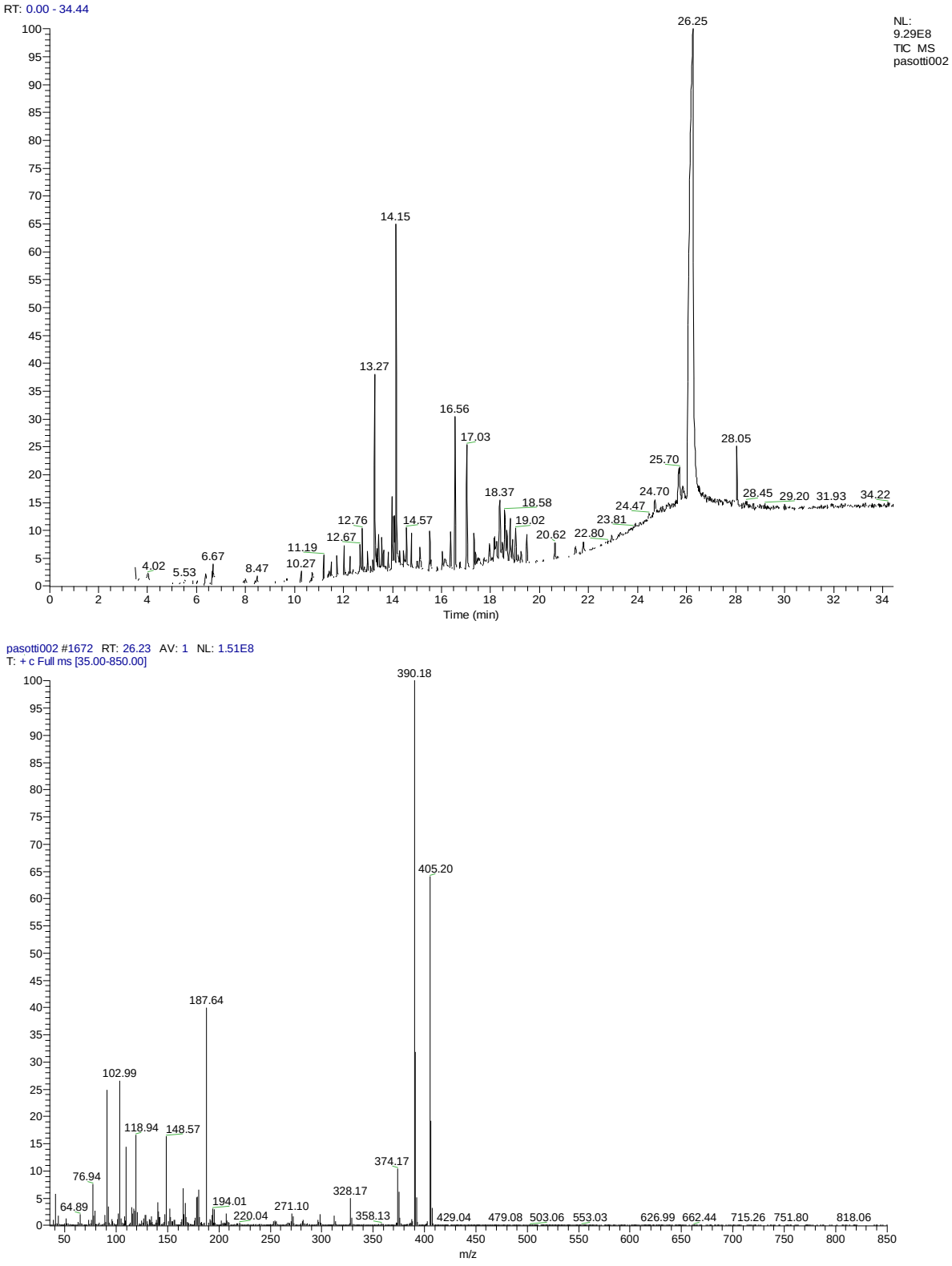

Figure S.I 4.5- GC-MS chromatogram of product mixture of the hydroxylation reaction of the TBA salt of L-tyrosine derivative (up) and fragmentation pattern of the main product (down), with retention time of 26.25 min.

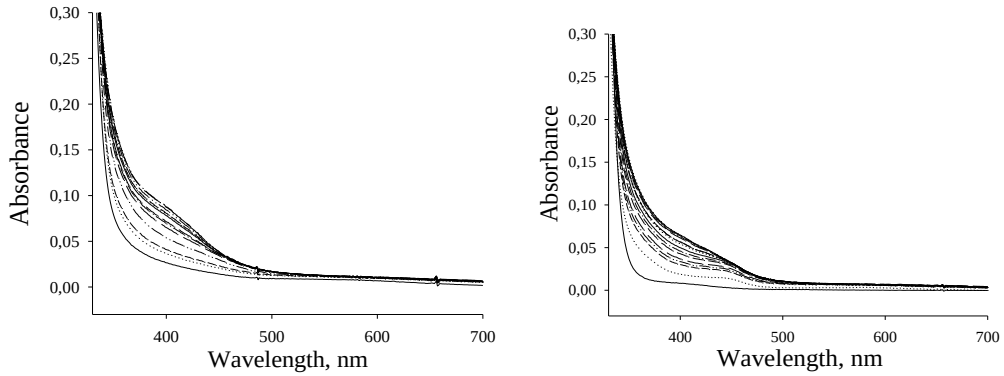

Figure S.I 4.6- Uv-Vis spectral changes observed during the oxidation of tetrabutylammonium salts of *N*-acetyl-L-tyrosine ethyl ester (left), and *N*-acetyl-D-tyrosine ethyl ester (right) by $[Cu_2(EHI)]^{2+}/O_2$.

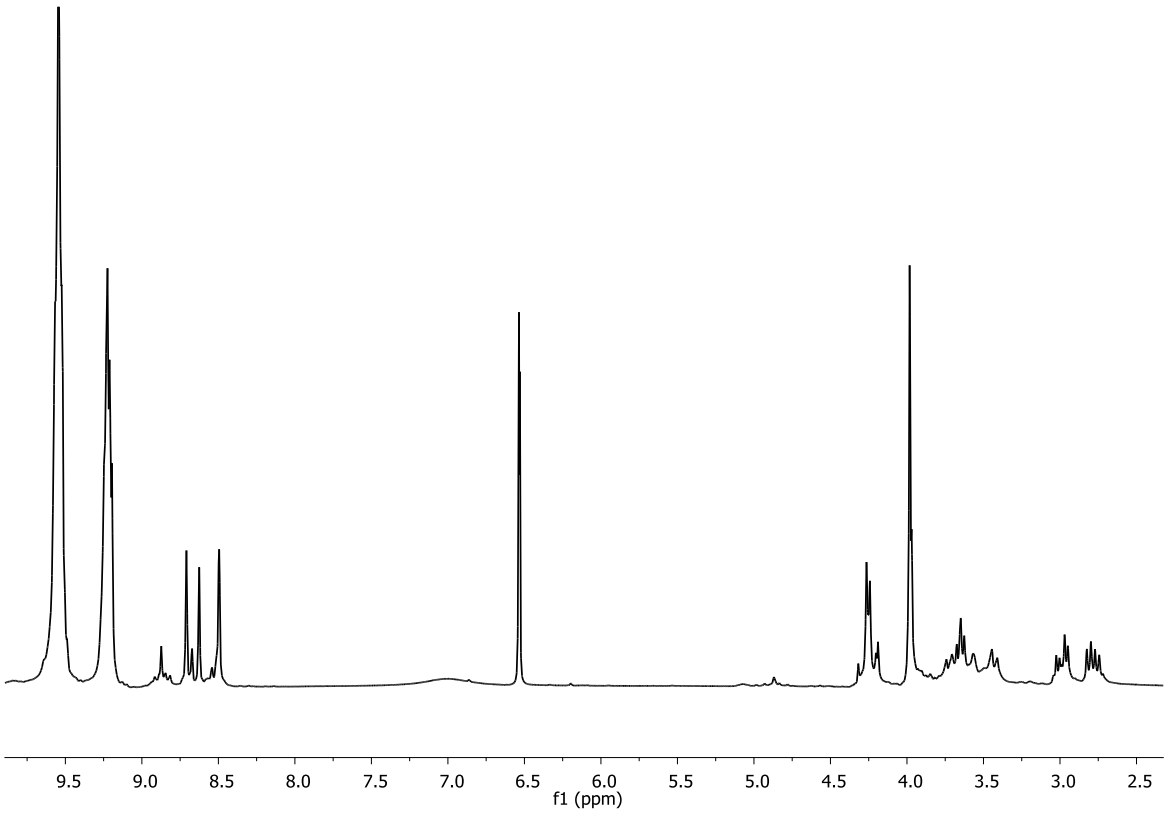

Figure S.I 4.7 ^{1}H-NMR of EHI in MeOD

References

1- (a) M. E. Cuff, K. I. Miller, K.E. van Holde, W. A. Hendrickson *J. Mol. Biol.* **1998**, 278, 855–870; (b) E. I Solomon.; U. M. Sundaram,; T. E. Machonkin, *Chem. Rev.* **1996**, 96, 2563–2605.

2- (a) L. Santagostini, M. Gullotti, R. Pagliarin, E. Monzani, L. Casella, *Chem. Commun.* **2003**, 2186-2187; (b) M. Gullotti, L. Santagostini, R. Pagliarin, S. Palavicini, L. Casella, E. Monzani, G. Zoppellaro, *Eur. J. Inorg. Chem.* **2008**, 2081-2089; (c) M. C. Mimmi, M. Gullotti, L. Santagostini, G. Battaini, E. Monzani, R. Pagliarin, G. Zoppellaro, L. Casella, *Dalton Trans.* **2004**, 2192-2201; (d) F. G. Mutti, M. Gullotti, L. Casella, L. Santagostini, R. Pagliarin, K. Kristoffer Andersson, M. F. Iozzi, G. Zoppellaro, *Dalton Trans.* **2011**, 40, 5436-5457.

3- (a) I. Gamba, S. Palavicini, E. Monzani, L. Casella, *Chem. Eur. J.* 2**009**, 15, 12932-12936; (b) G. Battaini, L. Casella, M. Gullotti, E. Monzani, G. Nardin, A. Perotti, L. Randaccio, L. Santagostini, F. W. Heinemann, S. Schindler, *Eur. J. Inorg. Chem.* **2003**, 1197-1205; (c) A. Granata, E. Monzani, L. Casella, *J. Biol. Inorg. Chem.* **2004**, 9, 903-913; (d) S. Palavicini, A. Granata, E. Monzani, L. Casella, *J. Am. Chem. Soc.* **2005**, 127, 18031-1836; (e) L. Casella, O. Carugo, M. Gullotti, S. Garofani, P. Zanello, *Inorg. Chem.* **1993**, *32*, 2056–2067; (f) L. Casella, E. Monzani, M. Gullotti, D. Cavagnino, G. Cerina, L. Santagostini, R.Ugo, *Inorg. Chem.* **1996**, *35*, 7516-7525.

4- a) R. C. Holz, J. M. Brink, *Inorg. Chem.*, **1994,** 33, 4609-4610; b) J. H. Satcher, Jr., A. L. Balch, *Inorg. Chem.*, **1995**, 34, 3371-3373; c) M. Maekawa, S. Kitagawa, M. Munakata, H. Masuda, *Inorg. Chem.*, **1989**, 28, 1904-1909. d) I. Bertini, C. Luchinat, "NMR of paramagnetic substances", Elsevier, Amsterdam, 1996, Chapter 5.

5- M. Perrone, E. Lo Presti, S. Dell'Acqua, E. Monzani, L. Santagostini, L.Casella, *Eur. J.I.C.* ,**2015**, 21, 3493–3500.

6- (a) R. C. Holz, J. M. Bradshow, B. Bennett, *Inorg. Chem.* **1998**, 37, 1219-1225; (b) C. Belle, C. Beguin, I. Gautier-Luneau, S. Hamman, C. Philouze, J. L. Pierre, F. Thomas, S. Torelli, *Inorg. Chem.* **2002**, 41, 479-491.

7- J. C. Espin, P. A. Garcia-Ruiz, J. Tudela, F. Garcia-Canovas, *Biochem. J.* **1998**, 331, 547-551.

8- Acta Biochimica polonica, vol 58, n 3, **2011**, 303-311.

9- P. Gans, A. Sabatini, A. Vacca, *Talanta,* **1996**, *43*, 1739-1753

Chapter 5. mXHI

5. mXHI

5.1 Introduction

Several attempts at mimicking the structure and the activity of tyrosinase has been done in the past few decades, to synthesize hexadentate ligand systems which contain several nitrogen donors for copper ions.[1] Natural tyrosinase presents six histidine residues as coordinating units for copper. In order to mimic these coordination features, our research group previously synthesized an octadentate ligand capable of bind two or three copper ions, labeled as PHI,[2] which was subsequently modified to obtain hexadentate analogue, based on histidine-amino-imidazole arms as coordinating tridentate subunits. Dinuclear copper complexes of EHI, whose structure and activity were described in **Chapter 4**, showed, however, negligible enantiodifferentiating capability in most of typical tyrosinase oxidation reactions. This poor stereoselectivity could be attributable to the rigidity of the system. To overcome this problem, the rigid bis-amidic moiety was substituted with a more flexible linker. As for L55 and L66 system, the *m*-xylyl group was found to be adequate in terms of flexibility and "bite-strength". This modification was used to design a new ligand for two copper ions,

labeled mXHI. Similarly to EHI, mXHI contains two tridentate histidine-amino-imidazole subunits able to chelate copper, but differs from this inspiring source under a few points of view. First, the bis-amidic linker was substituted with *m*-xylyl moiety and, furthermore, the central amine of the tridentate unite is a tertiary amine instead of a secondary amine. From the coordinative point of view, similarly to EHI, it generates two chelate rings of different size, one five-membered and one six-membered. Finally, the steric hindrance of the trytyl groups on the imidazole of histidine was reduced, substituting them with benzylic groups.

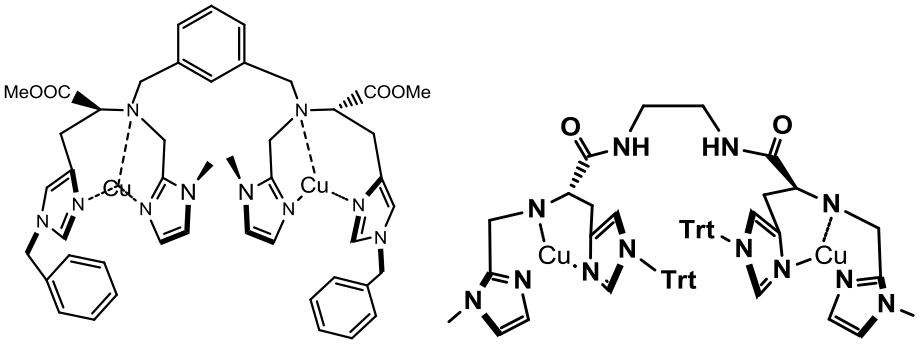

Figure 5.1: Structure of $[Cu_2(mXHI)]^{4+}$ (left) and $[Cu_2(EHI)]^{4+}$ (right)

5.2. Results and discussion

5.2.1. Synthesis of the ligand mXHI

The synthetic pathway for mXHI (Scheme 5.1) started from L-histidine methyl ester, which was regioselectively N(τ)-alkylated with benzyl bromide, following a literature procedure.[3] The steric hindrance of the trytyl group previously used to protect the imidazole nitrogen has been reduced to a smaller and more flexible moiety, maintaining the aromatic UV-Vis features, which guarantees easier chromatographic purification.

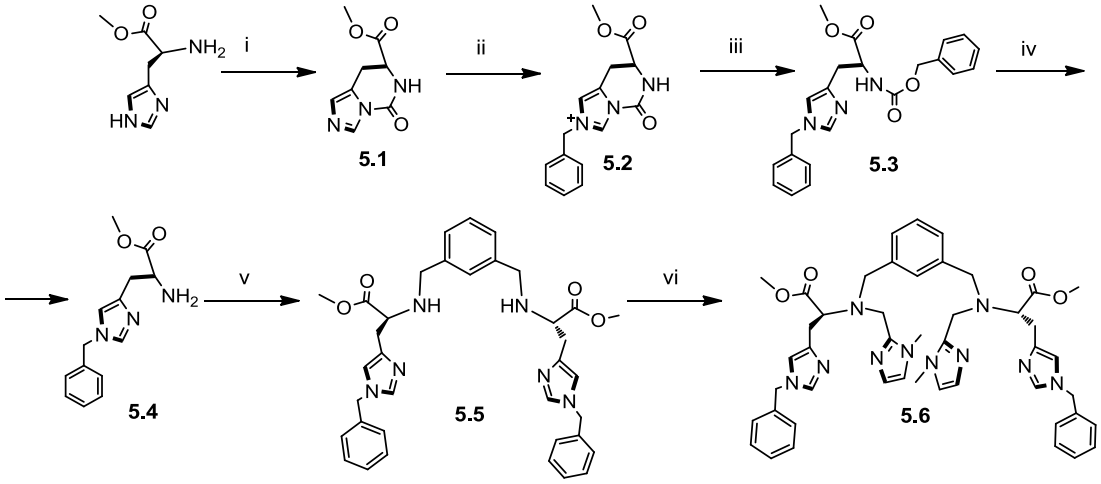

Scheme 5.1. Synthetic pathway for mXHI: i: carbonyldiimidazole, DMF, 60-70 °C; ii: benzyl bromide, CH_3CN, reflux; iii: benzyl alcohol, diisopropyl ethyl amine, CH_3CN, r.t; iv: H_2, Pd/C, EtOH, r.t; v: isophtaldialdehyde, sodiumtriacetoxyborohydride, DCM, r.t; vi: 1-methyl-2-imidazolcarboxyaldehyde, sodiumtriacetoxyborohydride, DCE, r.t.

Histidine methyl ester was reacted with carbonyldiimidazole, affording cyclic urea **5.1**, that was subsequently alkylated with benzyl bromide, giving **5.2**. The obtained quaternary salt, in basic conditions and in presence of benzyl alcohol as solvent, gave the N(τ)-benzyl histidine methyl ester, protected as carboxybenzyl (Cbz) derivative on the α-amine group (**5.3**), that was isolated with good yield (68%). Selective cleavage of the Cbz group by catalytic hydrogenation in presence of palladium (Pd/C) occurred quantitatively (**5.4**). Two of these histidine derivatives were, then, bound by stepwise reductive amination with isophtaldiadehyde and sodium triacetoxyborohydride (STABH) as the reducing agent,[4] affording **5.5** with good yield. Last step consisted in a further reductive amination with two equivalents of 1-methyl-2-imidazolecarboxyaldehyde and STABH as the reducing agent, giving **5.6** as final product with good yield (78 %).

The dinuclear copper complex of mXHI was simply prepared by mixing a methanolic solution of ligand (1 equivalent) with a methanolic solution of copper salt (2 equivalents). Copper complexes are, in most of cases, obtained in good yields.

5.2.2 Spectroscopic characterization of the dinuclear copper complex of mXHI

5.2.2.1 Titration of $[Cu_2(mXHI)]^{4+}$ with azide- UV-Vis and CD studies

As previously explained, optical titration of copper complexes with azide is an efficient way to mimic the interaction of these systems with small molecules, such as oxygen or, in particular, peroxide. UV-Vis titration with sodium azide is useful to determine the strength of binding.

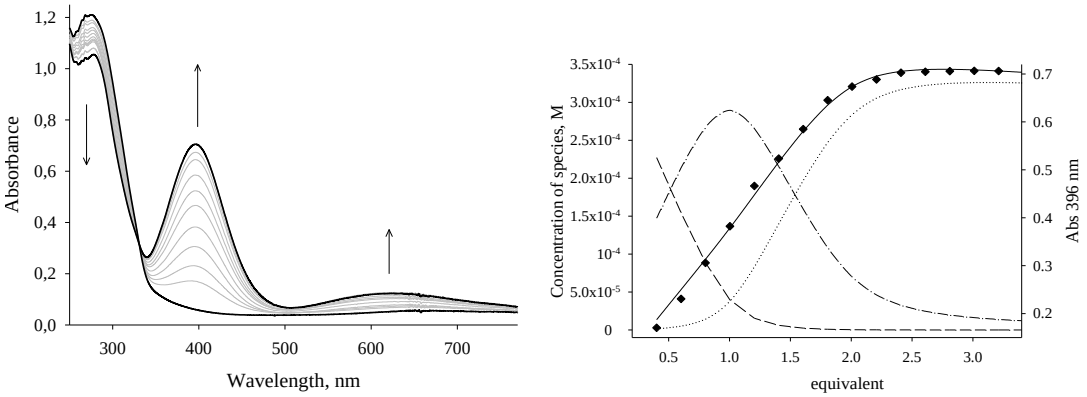

Figure 5.2- Left- Titration spectra of $[Cu_2mXHI]^{4+}$ with azide, showing the increase of two bands around 616 nm and 398 nm and the decrease of a band around 278 nm. Right- Titration at 396 nm superimposed to the species distribution diagram. Diamond: experimental values of absorbance *vs* equivalents. Solid line: calculated absorbance *vs* equivalents. Dashed solid line: distribution of free $[Cu_2mXHI]^{4+}$. Dashed-dotted line: distribution of $[Cu_2mXHI\text{-azide}]^{3+}$. Dotted line: distribution $[Cu_2mXHI\text{-}(azide)_2]^{2+}$.

As shown in Figure 5.2, upon addition of sodium azide an increase of a characteristic band around 396 nm, due to the π(azido)→Cu(II) LMCT is observed.[2c]
Fitting of absorbance data at 396 nm *vs* $[N_3^-]$ with a non-linear least square procedure makes possible to obtain dissociation constants for the 1:1 and 1:2 $[Cu(II)\text{-}N_3^-]$ adducts.

$[Cu_2(mXHI]^{4+} + Azide \rightleftharpoons [Cu_2mXHI\text{-}Azide]^{3+}$ Log Kb1 = 6.48 ±0.01

$[Cu_2mXHI\text{-}Azide]^{3+} + Azide \rightleftharpoons [Cu_2mXHI\text{-}(Azide)_2]^{2+}$ Log Kb2 = 4.74 ±0.01

$[Cu_2mXHI]^{4+} + 2\ Azide \rightleftharpoons [Cu_2mXHI\text{-}(Azide)_2]^{2+}$ Log β2 = 11.22 ±0.01

Due to the intrinsic chirality of this biomimetic copper complex, CD experiments can give further information. By observing the CD spectra (Figure 5.3), the d-d region showed higher intensity bands for the azide adduct, with an inversion of sign of the Cotton effects with respect to the corresponding $[Cu_2(mXHI)]^{4+}$.

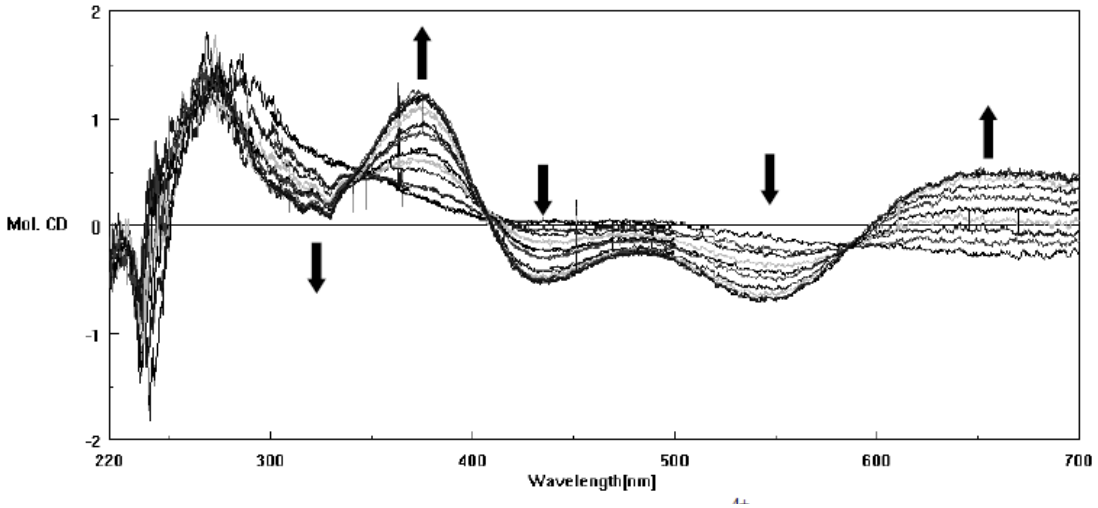

Figure 5.3. Circular dichroism spectra of $[Cu_2mXHI]^{4+}$ titrated with azide

This indicates, as previously reported for the di- and trinuclear copper complexes of PHI,[2a,c] that the azide binding reduces the conformational mobility of the ligand and induces a change from the slight preference exhibited by $[Cu_2mXHI]^{4+}$ for the conformation indicated as λ in Scheme 5.2 in favor of a stronger preference for the conformation δ in the adduct with azide. The sizeable intensity of the LMCT band implies a good overlap between the donor π (N_3^-) and the acceptor dx^2-y^2 (copper) orbital and therefore a coordination of azide in the Cu equatorial plane.

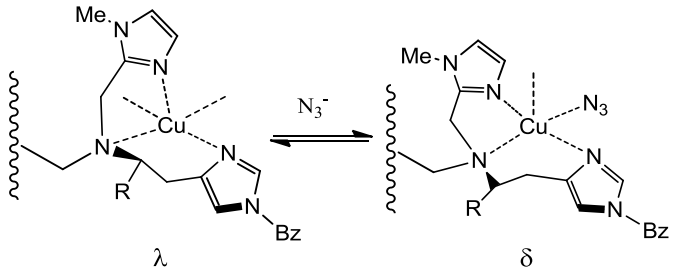

Scheme 5.2. Conformational changes caused the azide binding. R= –$COOCH_3$

The higher energy region of the CD spectrum features an exciton couplet that could be explained assuming that the coordination of two azide ions is necessary to couple the LMCT transition moments. These bands are visible also when the adduct stoichiometry

is 1:1, and this is consistant with the presence of a small amount of Cu-$(N_3^-)_2$ 1:2 (below 10 %), as confirmed by the calculated distribution diagram (Figure 5.2).

5.2.2.2 Titration of $[Cu_2(mXHI)]^{4+}$ with hydroxide- UV-Vis, CD and NMR studies

As previously cited, coordination of hydroxide anion is a good means to mimic natural cluster of some copper enzymes, as laccase, ascorbate oxidase and ceruloplasmin.[5-7] Here I report UV-Vis, CD and NMR studies on coordination of this anion to $[Cu_2(mXHI)]^{4+}$. UV-Vis spectral changes associated with the addition of sodium hydroxide to the complex solution consisted in the shift of the UV band from 278 to 296 nm (Figure 5.4), accompanied by the formation of a band around 350 nm. The LF region showed only a slight enhancement of the band at 630 nm. Shift of UV centered bands derives from the sum of the spectral features of three different coexisting species, whose molar extinction coefficients have been calculated.

$[Cu_2mXHI]^{4+}$ $\varepsilon 278 = 3100\ M^{-1}\ cm^{-1}$;

$[Cu_2mXHI\text{-}OH]^{3+}$ $\varepsilon 285 = 3100\ M^{-1}\ cm^{-1}$;

$[Cu_2mXHI\text{-}(OH)_2]^{2+}$ $\varepsilon 296 = 3300\ M^{-1}\ cm^{-1}$.

This band in the UV region could be attributed to σ(amino)→ Cu(II) LMCT transition,[1a] while the band developed at 350 nm is attributable to a OH^-→Cu(II) LMCT, that frequently occures in this spectral region.[8]

$[Cu_2mXHI\text{-}OH]^{3+}$ $\varepsilon 350 = 1050\ M^{-1}\ cm^{-1}$;

$[Cu_2mXHI\text{-}(OH)_2]^{2+}$ $\varepsilon 350 = 1200\ M^{-1}\ cm^{-1}$.

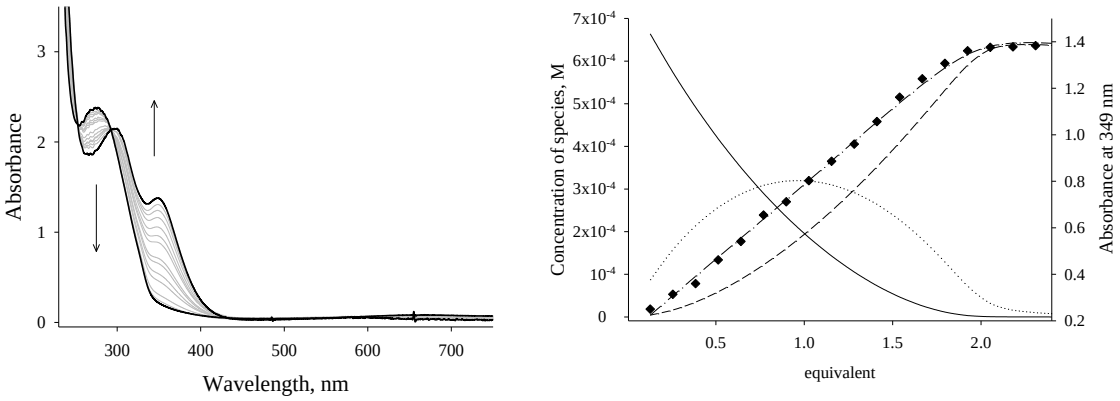

Figure 5.4- Titration of mXHI with sodium hydroxide. Representative spectra, normalized for dilution, refer to solution obtained after addition of successive and equal amounts of OH^- for $[OH^-]$:$[Cu_2]$ from 0.1 to 2. Titration at 349 nm superimposed to the species distribution diagram. Diamond: experimental values of absorbance *vs.*

equivalent of OH^-. Dashed-Dotted line: calculated absorbance vs. equivalent. Solid line: distribution of free $[Cu_2mXHI]^{4+}$. Dotted line: distribution of $[Cu_2mXHI\text{-}OH^-]^{3+}$. Dashed line: distribution $[Cu_2mXHI\text{-}(OH^-)_2]^{2+}$.

The spectral data at 349 nm were fitted with a non linear least square procedure, giving the following binding constants for the involved equilibria.

$[Cu_2mXHI(H_2O)_2]^{4+} + OH^- \rightleftharpoons [Cu_2mXHI(H_2O)OH]^{3+}$ Log Kb1 = 5.89 ±0.01

$[Cu_2mXHI(H_2O)OH]^{3+} + OH^- \rightleftharpoons [Cu_2mXHI(OH)_2]^{2+}$ Log Kb2 = 5.45 ±0.01

$[Cu_2mXHI(H_2O)_2]^{4+} + 2OH^- \rightleftharpoons [Cu_2mXHI(OH)_2]^{2+}$ Log βb2 = 11.34 ±0.01

In the CD spectra of Figure 5.5, addition of OH^- leads to the progressive development of a moderately intense negative Cotton effect around 300 nm and a weaker effect in the region around 360 nm, corresponding to two LMCT transitions $OH^- \rightarrow Cu(II)$. A positive Cotton effect is visible at 550 nm in the d-d band region.

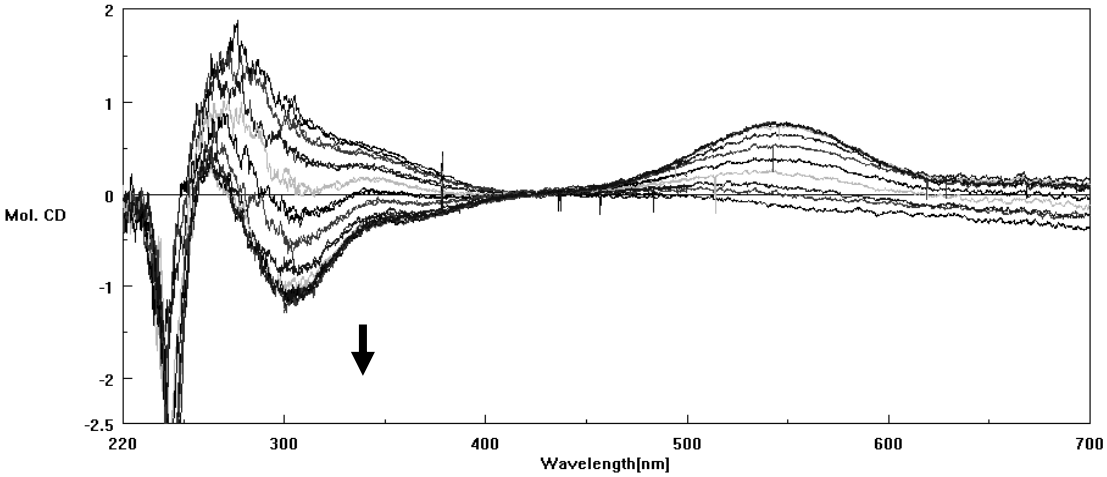

Figure 5.5- CD spectra of $[Cu_2mXHI]^{4+}$ upon titration with hydroxide.

To confirm the assumed bis(hydroxo)-bridged structure in solution, NMR spectra were recorded (Figure 5.6).

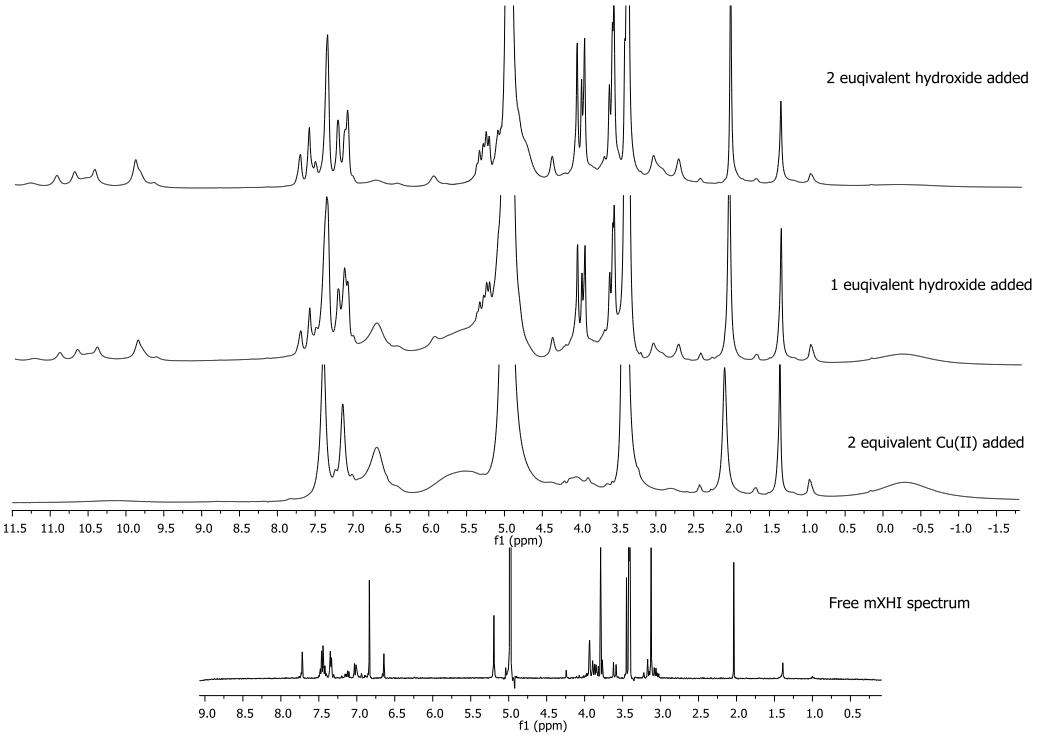

Figure 5.6- ^{1}H-NMR spectra in CD_3OD for the mXHI free ligand, after the addition of two equivalent sof copper(II) trifluoromethansulfonate, and after the addition of one and two equivalents of sodium hydroxide in D_2O (from bottom to the top).

NMR signals of $[Cu_2(mXHI)]^{4+}$, obtained *in situ*, adding of copper(II) triflate, are broad and cover a large range of chemical shifts. Coordination of OH^- induces coupling of magnetic moments of the two copper(II) ions, inducing diamagnetic properties to the dicopper complex (S=0). Signals appeared a little enlarged, because of the partial population of the excited triplet state, which is paramagnetic.

5.2.3. Biomimetic oxidation reactions promoted by $[Cu_2(mXHI)]^{n+}$

5.2.3.1. Stereoselective oxidation of chiral catechols- catecholase activity.

Also for $[Cu_2(mXHI)]^{4+}$, the capability in stereo-differentiation in oxidation of chiral catechols was evaluated, choosing the same set of enantiomeric couples of catechols of biological interest previously described. Experiments were conducted fixing the concentration of complex at 5 μM and measuring oxidation rates at increasing substrate concentration from 10^{-5} M to 10^{-3} M. The reaction were studied monitoring the increase of the band around 475 nm, due to the formation of the aminochrome obtained from the oxidation. The effect of two different buffers was evaluated, conducting the studies in

10:1 MeOH:acetate buffer (50 mM, pH 5.1) or in 10:1 MeOH:MES buffer (50 mM, pH 6). The rate data are expressed as $v/[catalyst] = \left(\frac{(A/s)}{\varepsilon\ aminochrome}\right)/[complex]$, where A/s is the absorbance change with time upon formation of the quinone and $\varepsilon\ aminochrome$ is equal to 3600 $M^{-1}s^{-1}$.[9] The rate constants k_{cat} and K_M are collected in Table 5.1.

Table 5.1- Kinetic parameters for the catalytic oxidation of catecholic substrates in methanol/50 mM aqueous acetate buffer, pH 5.1, 10:1 (v/v) or MES buffer, pH 6, at 25 °C.

	K_M (M)	k_{cat} (s^{-1})	k_{cat}/K_M ($M^{-1}s^{-1}$)	R k_{cat}/K_M %	R k_{cat}%
pH 5.1					
L-Dopa	$(3.13\pm0.83)\times10^{-4}$	$(1.01\pm0.87)\times10^{-3}$	3.3	-8.3	9.4
D-Dopa	$(3.09\pm0.78)\times10^{-4}$	$(1.22\pm0.12)\times10^{-3}$	3.9		
L-DopaOMe	$(4.43\pm0.82)\times10^{-4}$	$(7.89\pm0.61)\times10^{-2}$	179	-93.5	72.1
D-DopaOMe	$(5.23\pm1.95)\times10^{-6}$	$(1.28\pm0.04)\times10^{-2}$	2447		
R-(-)-norepinephrine	$(7.16\pm1.93)\times10^{-5}$	$(8.69\pm0.55)\times10^{-4}$	12.1	6.6	5.2
S-(+)-norepinephrine	$(7.42\pm0.16)\times10^{-5}$	$(7.84\pm0.37)\times10^{-4}$	10.6		
pH 6.0					
L-Dopa	$(1.67\pm0.23)\times10^{-4}$	$(2.01\pm0.09)\times10^{-4}$	1.2	14.3	7.2
D-Dopa	$(1.97\pm0.52)\times10^{-4}$	$(1.74\pm0.16)\times10^{-4}$	0.9		
L-DopaOMe	$(1.04\pm0.23)\times10^{-4}$	$(1.11\pm0.08)\times10^{-2}$	106.7	61.6	48.2
D-DopaOMe	$(1.54\pm0.55)\times10^{-4}$	$(3.88\pm0.59)\times10^{-3}$	25.2		
R-(-)-norepinephrine	$(4.47\pm1.82)\times10^{-5}$	$(4.64\pm0.39)\times10^{-4}$	10.4	49.6	7.0
S-(+)-norepinephrine	$(1.15\pm0.40)\times10^{-4}$	$(4.03\pm0.39)\times10^{-4}$	3.5		

In most cases, the rate data at increasing substrate concentration exhibited a typical hyperbolic behavior (Figure S.I. 5.1-5.2), so the fitting was performed with the Michaelis-Menten equation. Also in this case, even if it was not possible to separate the two involved phases, we assumed that the reactions carried out with a first fast *stoichiometric step*, concerning the formation of a copper-substrate adduct followed by the electron transfer.[10] The second step corresponds to the rate determining step of the catalytic cycle, involving Cu oxygenation and the electron transfer.

First Step:

$$[Cu^{II}\text{-}OH\text{-}Cu^{II}]^{3+} + CatH_2 \leftrightarrows [Cu^{II}\text{-}Cat\text{-}Cu^{II}]^{2+} + H_2O + H^+ \quad \text{(Ia)}$$

$$[Cu^{II}\text{-}Cat\text{-}Cu^{II}]^{2+} \rightarrow [Cu^{I}{}_2]^{2+} + Qui \quad \text{(Ib)}$$

Second Step

$$[Cu^{I}{}_2]^{2+} + CatH_2 + O_2 \leftrightarrows [Cu^{II}{}_2O_2/Cat]^{2+} + 2\,H^+ \quad \text{(IIa)}$$

$$[Cu^{II}{}_2O_2/Cat]^{2+} + 3\,H^+ \rightarrow [Cu^{II}\text{-}OH\text{-}Cu^{II}]^{3+} + Qui + H_2O \quad \text{(IIb)}$$

$CatH_2$ represents the substrate, while Qui is the corresponding quinone. Variation of the buffer from acetate (pH 5.1) to MES (pH 6) should increase the fraction of catecholate in solution, favoring the coordination to the dicopper site and, so, increasing the oxidation rate. Experimental rate data followed, also in these conditions, in most cases the hyperbolic behavior, except for D-Dopa methyl ester, which exhibited inhibition at high substrate concentration.

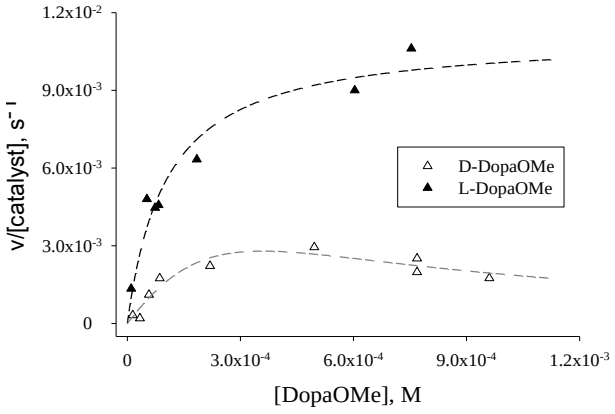

Figure 5.7- Plot of the rate of oxidation at increasing substrate concentration for L/D-DopaOMe at in methanol/MES buffer (pH= 6) 10:1.

The kinetic parameters reported in Table 5.1 were estimated from the portion of the rate *vs* substrate concentration plot in which inhibition could be neglected. The enantio-differentiating effects in the oxidation of the three couples of substrates were expressed, as previously described, in terms of Rk_{cat}/K_M % and Rk_{cat} % index. Data collected in Table 5.1 reveal, in both the working conditions explored, a larger reactivity towards DopaOMe (more than one order of magnitude higher) and an evident preference for the L-enantiomer. Nevertheless, at low substrates concentrations and at pH = 5.1 the complex showed an inversion of the selectivity with respect to that higher concentration. The contribution of K_M in the Rk_{cat}/K_M % expression resulted in a reversed enantioselection in favor of D-DopaOMe and this phenomenon could be explained by taking into account the greater binding affinity for this substrate, shown by its higher k_{cat}/K_M value. The hypothesis for this behavior could be a different binding fashion, where the amino acid moiety acts as a chelating agent, that can also justify a substrate inhibition at high concentration.

Another relevant evidence is that at pH = 6 oxidation rates are almost an order of magnitude lower than at pH 5.1. This was unexpected, as higher pH should increase the catecholate fraction, allowing an easier binding to the copper complex. This reversed behavior could be justified by the nature of the buffer MES; the morpholine derivative (Figure 5.8) could interfere with the coordination of the substrate, also due to the higher concentration of the buffer.

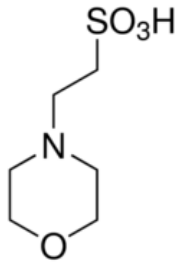

Figure 5.8- Methyl amino sulfonic acid (MES), molecule used for the pH 6 buffer.

On the other hand, the bidentate carboxylic group of acetate could bind the di-copper systems, pre-organizing the complex to favor the coordination of substrate.

In order to determine the effect of the buffers, further kinetic oxidation experiments were performed.

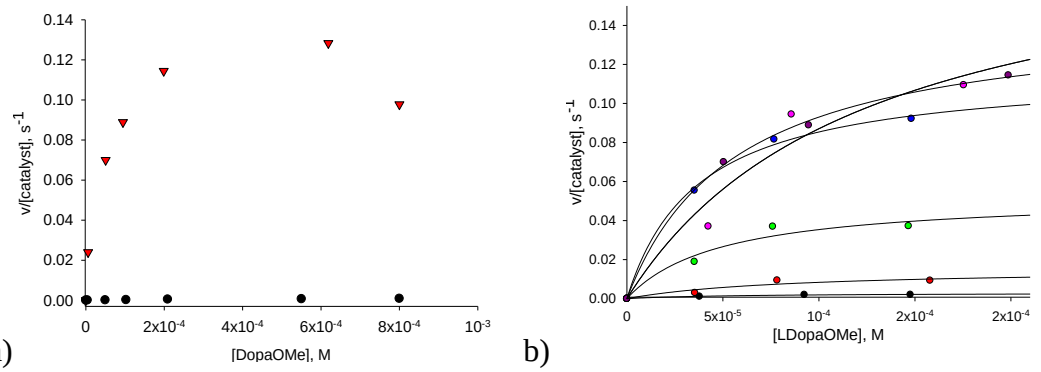

Figure 5.9- Dependence of oxidation rate. a) From buffer nature: red triangles for pH 5.1, acetate buffer 50 mM, black circles for pH 6.0, MES buffer 1 mM; b) From acetate buffer concentration: black circles: 1 mM; red circles: 2 mM; green circles: 5 mM; blue circles: 10 mM; pink circles: 20 mM; dark pink circles: 50 mM.

Figure 5.9-a outlined an evident dependence of oxidation rate from the nature of the buffer, showing that the presence of MES, even at lower concentration, negatively influenced the oxidation reaction. Figure 5.9-b shows that also acetate concentration deeply influence oxidation rate. When acetate is 1 mM, oxidation is slow, increasing until 10 mM concentration is reached, when it reaches a plateau. Acetate has a positive role in oxidation, probably arranging the complex in a feature that facilitates the coordination or the correct orientation of substrates. Rearrangement in complex structure, where acetate acts as a bridging ligand, could also couple the unpaired electrons of copper(II). Magnetic coupling, as explained in **Chapter 4**, can be detected by exploiting a simple and direct technique, NMR and using Evans' method for determination of magnetic susceptivity.

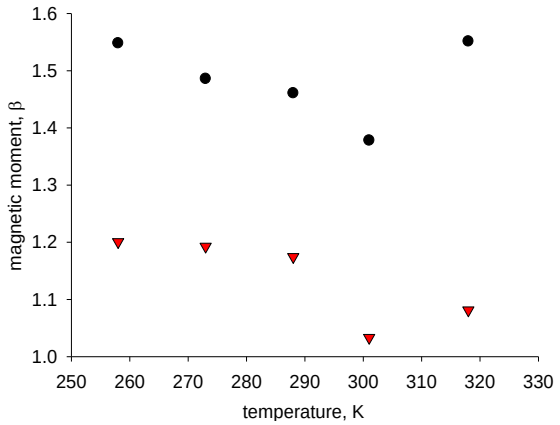

Figure 5.10- Dependence on temperature of the magnetic moment, measured with Evans' method on $[Cu_2(mXHI)]^{4+}$, with two different buffer concentrations. Black circles: deuterated acetate buffer 2 mM (pH 5.1); red triangles: deuterated acetate buffer 50 mM (pH 5.1).

The experiment was performed in a temperature range between -15 and 45 °C, with a 1.65 mM solution of $[Cu_2(mXHI)]^{4+}$ as paramagnetic molecule concentration. Complex concentration for the study is lower than for $[Cu_2(EHI)]^{4+}$, due to a different solubility. Acetone was found to be an excellent internal standard also in this case, as it does not interact with the complex. For $[Cu_2(mXHI)]^{4+}$, measured magnetic susceptivities and, consequently, magnetic moments are affected by acetate concentration, in particular Figure 5.10 shows that higher buffer concentration corresponds to a more strongly coupled system. Interpolation of the experimental data for determination of coupling constant does not give reliable data, but in this case the main purpose of the experiment was to compare the coupling at different acetate buffer concentration. Unfortunately, it was not possible to compare the experiment performed with 50 mM buffer with pure deuterated water, as it was found that the 10:1 MeOD/D_2O mixture freezes at -15 °C.

Another interesting behavior of the dinuclear copper complex of mXHI is represented by the dependence of the catechol oxidation rates from catalyst concentration.
Similarly to $[Cu_2(EHI)]^{4+}$ experiments (see **Chapter 4**), I evaluated the oxidation rate variation maintaining a fixed concentration of substrate (L-Dopa methyl ester, $5x10^{-4}$ M) and varying that of the catalyst between $5x10^{-7}$ and $5x10^{-5}$ M in 10:1 v/v MeOH/ acetate buffer (pH 5.1, 50 mM).

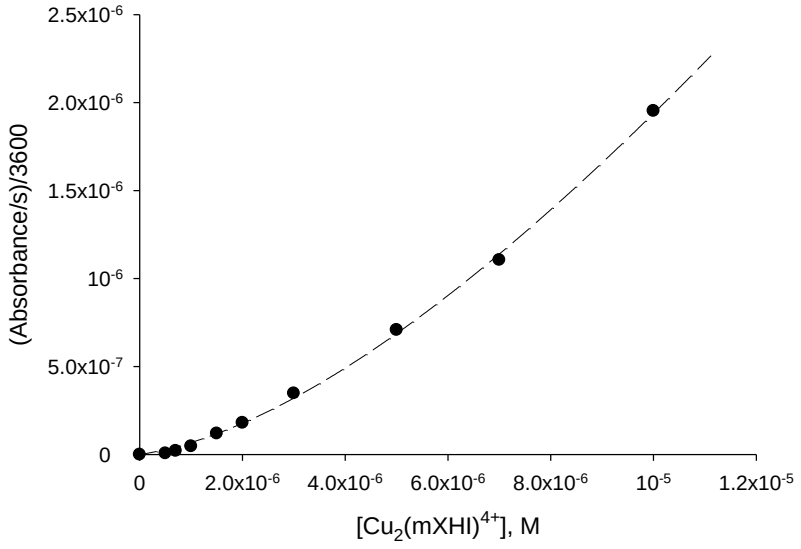

Figure 5.11- Dependence of oxidation rate from catalyst concentration for $[Cu_2(mXHI)]^{4+}$, in 10:1 MeOH/acetate buffer (50 mM, pH=5.1), 25 °C.

Rate data, expressed as absorbance variation *vs* time, divided for molar extinction coefficient of aminochrome, follow a pseudo-parabolic trend, which can be interpreted by considering a quadratic dependence of oxidation rate from catalyst concentration. Fitting of experimental data are based on the following assumptions. Working in substrate-saturating conditions, makes oxidation rate depending only on complex concentration. We also assume that the complex exists in two forms in dynamic equilibrium, a monomeric and a dimeric form:

$2C \rightleftharpoons C_2$ ruled by $Kb = [C_2]/[C]^2$

The oxidation rates depend from both [C] and $[C_2]$

$v = k_1[C] + k_2[C_2]$

Considering the mass balance:

$[C_0] = [C] + 2Kb[C]^2$

suitable substitution gives the final equation, used for the fitting:

$$v = k_1\left(\frac{-1+\sqrt{1+8Kb[C_0]}}{4Kb}\right) + Kbk_2\left(\frac{-1+\sqrt{1+8Kb[C_0]}}{4Kb}\right)$$

The kinetic and thermodynamic parameters k_1, k_2 and Kb were obtained through an adequate fitting of experimental oxidation rate data.

Table 5.2- Kinetic and thermodynamic parameters determined assuming a quadric dependence of oxidation rate of L-dopaOMe from $[Cu_2(mXHI)]^{4+}$ concentration

Parameter	Value
Kb	20000 ± 10000
k_1	$4.5x10^{-2} \pm 1.6\ x10^{-2}$
k_2	1.4 ± 0.4

Interpolating experimental data with the previously described equation, we did not obtained reliable data because of the high standard deviations due to high data intercorrelation, but the proposed model adequately represents the situation, reinforcing the initial hypothesis.

5.2.3.2. Phenolate hydroxylations by $[Cu_2(mXHI)O_2]^{2+}$

Due to the presence of two chelate rings, one five-membered and one six membered, $[Cu_2(mXHI)]$ complex is expected to have an intermediate behavior between $[Cu_2(L55)]$, characterized for its high reactivity, and $[Cu_2(L66)]$, known for the higher stability of the $Cu_2(I)$-O_2 complex. Even though several attempts of isolation of the oxygenated Cu(I) complex were inconclusive (acetone -80 °C, propionitrile -80 °C, dichloromethane -90 °C, 2-methyl-tetrahydrofurane -110 °C), phenol hydroxilation was studied with various salts of a series of *p*-substituted phenols. The first studied substrate was the DBU salt of 2-*tert*-butyl-4-methoxyphenol. The choice was due to the unsymmetrical substitution on the phenolic ring, that should guide the oxygen insertion to the only available *ortho* position of the ring. ^{1}H-NMR and GC-MS characterizations on the crude and the purified products indicate a C-C coupling, so under this condition $[Cu_2(mXHI)]$ reproduced the activity of another class of enzymes, peroxidases, which exploit hydrogen peroxide as oxidizing agent. Also the unsubstituted analogue *p*-methoxy phenol gave the C-C coupling product, as confirmed by ^{1}H-NMR, COSY and mass experiments (see Supporting info). Even if this is not the expected tyrosinase-like

activity, coupling of phenolic rings, especially C-C coupling, could be considered noteworthy. Coupling reactions, in fact, occur in most of cases with a previous activation of the phenolic ring, or with the use of further reagents. Furthermore, regioselectivity is a parameter of great interest, as in most of oxidative coupling it is not easy to direct the attack in a well-defined position. With this aim and with further refinement of design of the complex, future perspectives could involve the use of this system to mediate oxidative coupling in mild conditions.

When β-naphthol, used as DBU salt, was chosen as substrate, hydroxylation occurs. As both ligand and naphtholate were dissolved in dry degassed acetone under inert atmosphere, a solution of $[Cu(CH_3CN)_4]PF_6$ in dry degassed acetone was added to the mixture and the reaction was immediately initiated by exposing to air and stirring overnight at room temperature. The reaction, that turned from colorless to pale gold yellow, was stopped by removing the solvent by rotary evaporation and removing the copper residues as described in the Experimental Section. The product derived from the oxygenation was isolated by column chromatography and characterized by NMR (Figure 5.12 and Figure S.I 5.7). The resulting product indicates a monophenolase activity.

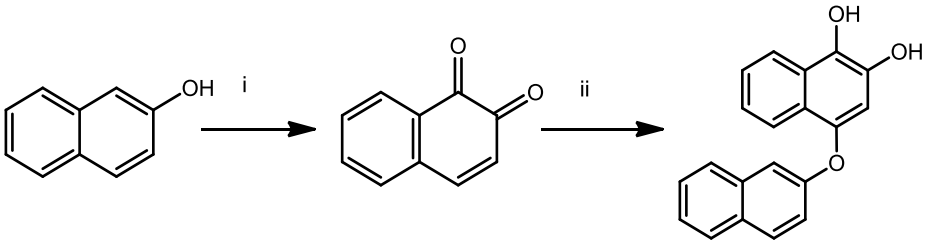

Scheme 5.3- Proposed mechanism for oxygenation of β-naphthol

The first step of the reaction gave the quinone product, but due to high electrophilicity undergoes conjugate addition with unreacted phenolate to generate the adduct. From the ^{1}H-NMR analysis of the crude product, information about the conversion could be obtained. The ratio between the NMR signals, equal to 1:10, suggested that the catalyst can perform two catalytic cycles in 16 h, then the reactivity is quenched.

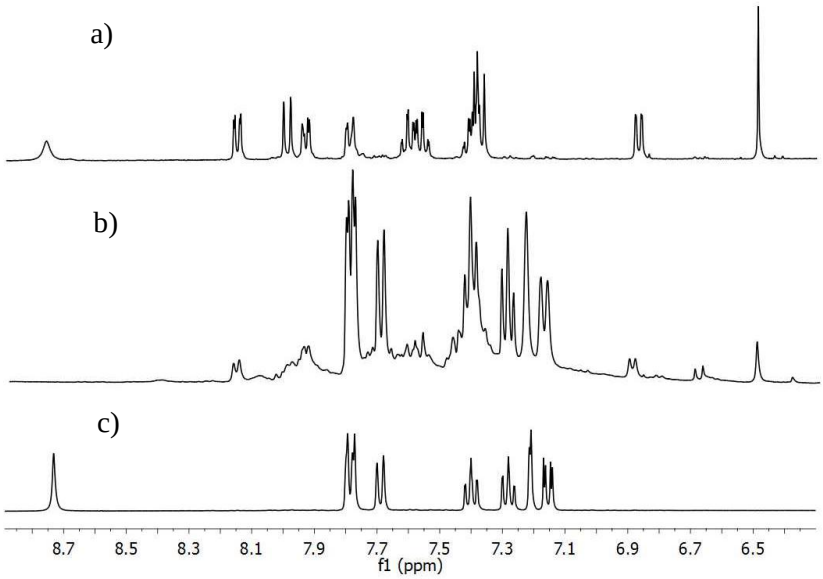

Figure 5.12- NMR spectra in acetone D-6 of a) pure product, b) crude product, c) starting material.

The mass spectrum of the purified product (*m/z* = +301, +623 amu) suggested the formation of the quinone of the previously described product, but both the NMR chemical shifts and the base-dependence of the UV-Vis spectrum confirmed the formation of the catechol derivative.

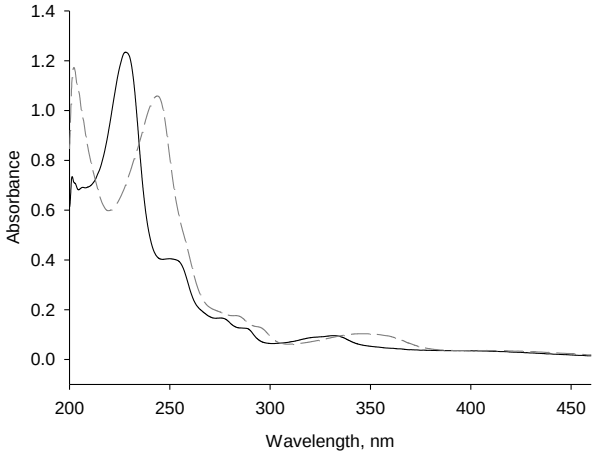

Figure 5.13- Dependence of the Uv-vis spectra upon the addition of OH^-. Solid line: methanolic solution of the pure product; Dashed line: Uv-vis spectrum after the addition of OH^-.

To obtain information on the mechanism, a $^{18}O_2$ incorporation experiment was performed. The reaction was conducted according to the previously described

procedure, but it was initiated by addition of $^{18}O_2$. The resulting purified product showed incomplete incorporation of oxygen-18, but a relevant increase of the related isotopic peak was identified by mass spectrometry and it represented almost 50% of the oxygen-16 related peak. This could suggest the coexistence of two mechanisms, one tyrosinase-like and the other of radical type.

5.2.3.3. Stereoselective oxyidation of chiral phenols: L/D-tyrosinate derivatives as substrates

As the main aim of this project is to introduce chirality into biomimetic systems, to promote stereoselective oxidations, the capability to distinguish between the oxidation of the two enantiomers of tyrosine has been evaluated. The tyrosine derivatives are N-acetylated, while the carboxylic groups are protected as ethyl ester. These protections have the scope to prevent coordination of amino acid group and also hinder intramolecular Michael addition after oxidation to quinone. The reactions of catalytic amounts of $[Cu_2(mXHI)O_2]^{2+}$ with TBA (tetrabutyl ammonium) phenolates of L- and D-tyrosine at 25 °C ([complex] = 0.1 mM, [substrate] = 5, 10 and 20 equiv) were optically monitored for 2 hours in dry acetone solution, until no change in the absorption spectrum was evident. Reactions were carried out by adding a $[Cu(CH_3CN)_4]PF_6$ solution in dry acetone to the same solvent solution of both ligand and substrate. Oxygenation was initiated with O_2 supply. Oxidation rates, obtained by fitting absorbance *vs* time values at increasing substrate concentration, collected in the first 200 seconds of reaction, and exhibited for both enantiomers a hyperbolic behavior. The kinetic parameters k_{ox} and Keq derived from the fitting, are listed in Table 5.3.

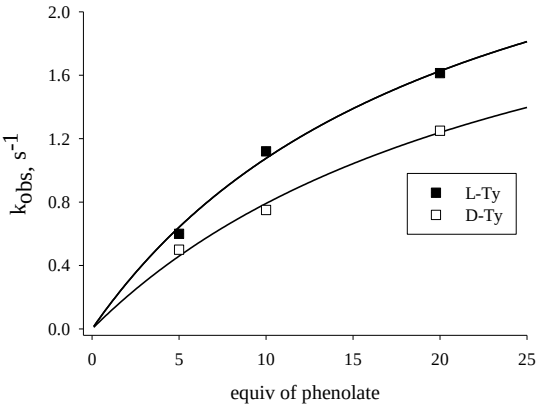

	K_{eq} (M^{-1})	k_{ox} (s^{-1})
L-enantiomer	0.047±0.014	3.33±0.58
D-enantiomer	0.038±0.015	2.85±0.74

Figure 5.14 and Table 5.3- Hydroxylation reactions with L- and D- tyrosinate; Values of kinetic parameters K_{eq} and $k_{ox.}$

To gain insight into the nature of the products, oxidation was replicated in larger scale for both enantiomers. The reaction was performed with 0.01 mM solution of $[Cu_2(mXHI)]^{2+}$ in dry acetone, and an excess of 20 equivalents of tetrabutylammonium salt of the tyrosine derivatives. The temperature was kept at -80 °C, to prevent collateral polymerization reactions, with a slight modification of a procedure reported in the literature.[1c] After 16 h reaction time, after stopping with an acidic quenching, the crude and pure products, obtained by column chromatography, were analyzed by MS and ^{1}H-NMR.

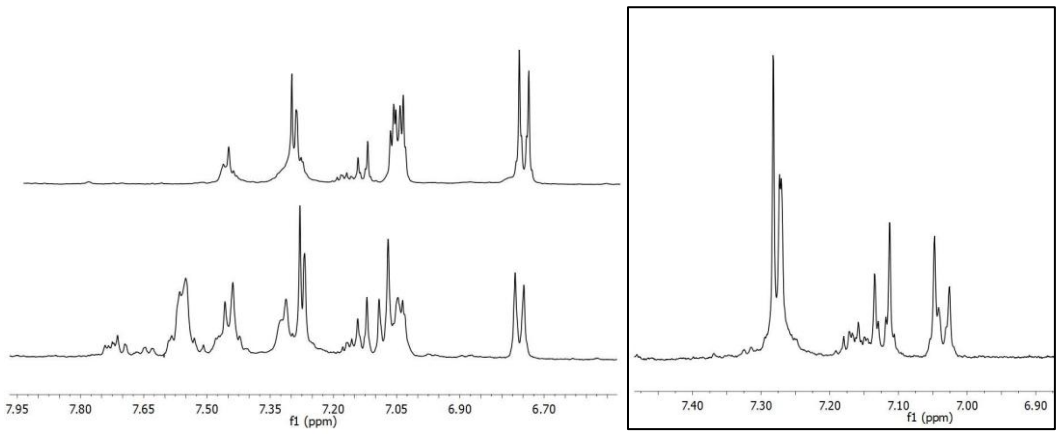

Figure 5.15. On the left, crude product obtained by the oxidation of; up: L-enantiomer; bottom: D-enantiomer; On the right: ^{1}H-NMR spectrum of the pure product of L-enantiomer of N-acetyl tyrosine ethylester as TBA salt.

Comparison with the product obtained with $[Cu_2(EHI)]^{2+}$ as oxidizing complex (see **Chapter 4**), showed that results are associated to a radical pathway, consisting in C-C and C-O coupling reactions. Differences between the two enantiomers oxidation rates could, so, derive from a favorable binding of L-tyrosinate compared with D-tyrosinate.

5.2.3.4. Titration of $[Cu_2(mXHI)]^{4+}$ with tyrosine

Titration of $[Cu_2(mXHI)]^{4+}$ with tyrosine is a good mean to evaluate differences in binding affinity between L- and D- enantiomers. The carboxylic group was protected as methyl ester, while the primary amine was left unprotected as there is no possibility for the substrates to be oxidized. Binding studies were carried out in methanol, using the DBU salts of L- and D- tyrosine methyl ester, to favor the coordination of the phenolic moiety.

Absorption data upon addition of phenolate were fitted with a non linear least square procedure to get an estimate of the affinity of tyrosine to the copper centers. Here the values of Log Kb calculated for each equilibrium are reported:

$[Cu_2mXHI]^{4+} + Tyr\text{-}O^- \rightleftharpoons [Cu_2mXHI\text{-}Tyr\text{-}O^-]^{3+}$ Log $Kb1_D$ = 3.94 ±0.01,Log $Kb1_L$ = 5.29 ±0.01

$[Cu_2mXHI\text{- }TyrO^-]^{3+} + Tyr\text{-}O^- \rightleftharpoons [Cu_2mXHI\text{-}(TyrO^-)_2]^{2+}$ Log $Kb2_D$ = 2.01 ±0.01 Log $Kb2_L$ = 2.69 ±0.01

Below the absorbance intensities, measured and calculated, respectively (Figure 5.16), superimposed to the species distribution diagram for L-tyrosine methyl ester are shown.

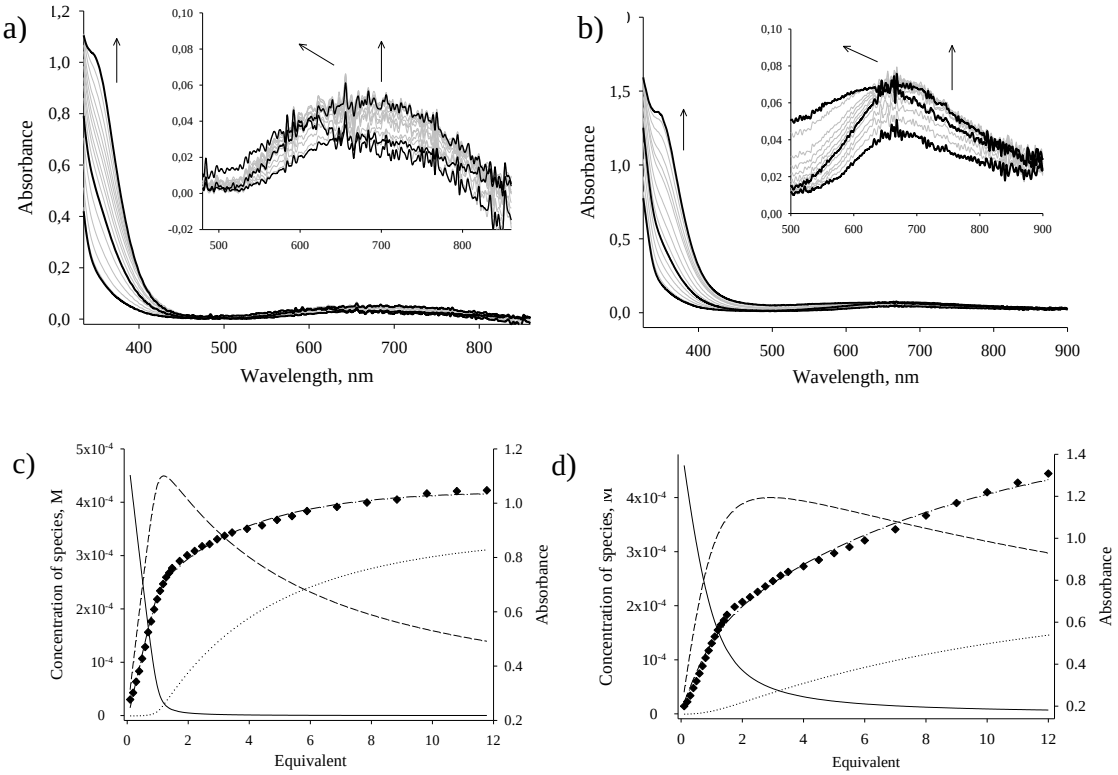

Figure 5.16- a) Absorption spectra of the titration of $[Cu_2mXHI]^{4+}$ by L-tyrosine methyl ester and b) D-tyrosine methyl ester; c) Titration at 350 nm with L-tyrosine methyl ester, superimposed to species distribution diagram and d) Titration profile at 352 nm with D-tyrosine methyl ester, superimposed to the species distribution diagram Diamond: experimental values of absorbance. Dashed-Dotted line: calculated absorbance. Solid line: distribution of free $[Cu_2mXHI]^{4+}$. Dashed line: distribution of $[Cu_2mXHI\text{-}TyrO^-]^{3+}$. Dotted line: distribution of $[Cu_2mXHI\text{-}(TyrO^-)_2]^{2+}$.

With both substrates, a two-step behavior can be envisaged: up to the addition of one equivalent, the principal event is the increase of two bands around 350 nm and 675 nm; gradually, the band at 675 nm stops growing and begins to shift to 637 nm, while the band around 350 nm continues to increase. This behavior suggests a first coordination of a phenolate, terminally bound or bridging the two copper centers, followed by the binding of a second molecule of phenolate. The larger binding constants calculated for L-tyrosine methyl ester reflect the higher oxidation rate reported for this substrate, confirming that the increased reactivity exhibited by the complex towards the L-enantiomer is related to an appreciable selectivity in the binding of this preferred substrate.

5.2.3.5. Catalytic sulfoxidation of thioanisole

As tyrosinase exhibits the capability to promote asymmetric oxidation of thioanisole in presence of Dopa as sacrificial reducing agent,[12] we replicated this activity exploiting the dinuclear copper(II) complex of mXHI as catalyst. Hydroxylamine was chosen as reducing agent, as N_2 is the only byproduct that derives from its oxidation.[13] Preliminary results were collected by analyzing both yield and enantiomeric excess at increasing reducing agent concentration (Figure 5.17).

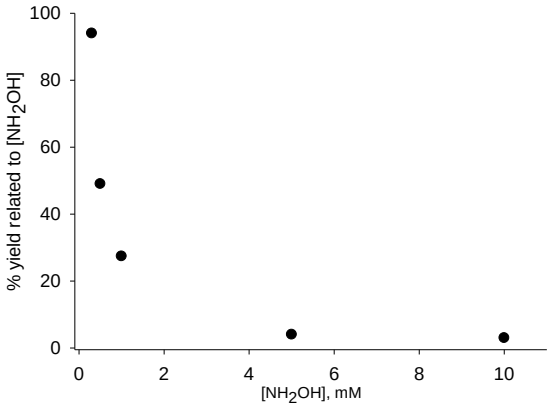

Figure 5.17- Sulfoxidation reaction yield calculated on the basis of the concentration of hydroxylamine.

As it is possible to see, reaction yield decreases exponentially, while there is no significant relationship between concentration of hydroxylamine and enantiomeric excess. However, in all cases, enantioselectivity was very low (entantiomeric excess from 8 to 16 %). The reaction proceeds in catalytic way, performing around 25 cycles in 16 h.

5.3. Conclusion

The design of ligand mXHI sums-up the coordination characteristics of the previously described EHI, integrated with a different linker between the two coordinating arms, changing the more rigid bis-amide moiety with the more flexible *m*-xylyl connecting unit. Tyrosinase-like activity promoted by the corresponding dinuclear copper complex was tested. $[Cu_2(mXHI)]^{4+}$ attitude to promote stereo-differentiating oxidation of chiral catechols was investigated on a set of enantiomeric catechol pairs of biological interest. The best results were obtained with the L-/D-DopaOMe pair, as the L-enantiomer was oxidized preferentially when compared with the D-enantiomer (Rk/k % = -72 %).

Mono-oxygenation reactions of achiral phenols show that electron-rich phenols tends to follow radical pathways to give coupling products. In the presence of phenols with more extended aromatic structure (β-naphthol), oxidation occurs with a monophenolase mechanism, as confirmed by 18-O insertion experiments. Stereoselective oxidation of tyrosine derivatives was also performed and kinetic experiments showed a preference for the L-enantiomer. $[Cu_2(mXHI)]^{4+}$ was also found to catalyze oxidation of organic sulphides in presence of hydroxylamine as reducing agent, but the sulfoxide was obtained as a racemic mixture.

5.4. Experimental section

Materials and methods

All preparations were carried out using standard Schlenk techniques under an inert atmosphere of N_2 unless otherwise stated. Solvents were dried over standard drying agents and stored over 3-Å molecular sieves. All starting materials were of reagent grade and purchased from either Sigma-Aldrich Chemical Co. or VWR International and used without further purification. UV-Vis spectra were recorded on Agilent HP 8453 diode-array spectrophotometers. Elemental analyses were obtained at the Micro-analysis service of the Milano CIMA department. CD spectra were obtained with a Jasco J500 spectropolarimeter; the spectra were recorded at 0.2 nm resolution in the range between 300 and 700 nm at 50 nm min^{-1} with three scans acquired for each spectrum. The NMR spectra were recorded with a Bruker AVANCE 400 spectrometer operating at 9.37 T with frequencies of 400.13 and 100.6 MHz for ^{1}H and ^{13}C nuclei, respectively. The data acquisition and processing were performed with a standard Bruker software package (Topspin 1.3). Mass spectra were recorded with a Thermo-Finnigan LCQ 371 ADV MAX spectrometer.

General procedures

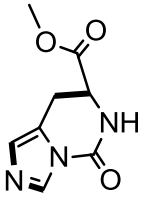

Synthesis of (S)-methyl 5-oxo-5,6,7,8-tetrahydroimidazo[1,5-c]pyrimidine-7-carboxylate (**5.1**) was prepared according to a procedure described in the literature. [3] ^{1}H-NMR (400 MHz, $CDCl_3$) δ 8.25 (s, 1H), 6.93 (s, 1H), 6.73 (s, 1H), 4.41 (ddd, J = 7.9, 5.4, 2.2 Hz, 1H), 3.83 (s, 3H), 3.41 (dd, J = 15.8, 5.3 Hz, 1H), 3.19 (dd, J= 16.2, 8.4 Hz, 1H); MS (ESI) $[M+H^+]$ +196 *m/z.*

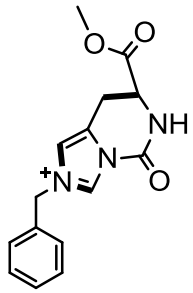

Synthesis of 2-benzyl-7-(methoxycarbonyl)-5-oxo-5,6,7,8tetrahydroimidazo[1,5-c]pyrimidin-2-ium.(**5.2**) The product was synthesized with a modification of a procedure known in literature.[3] To a suspension of **5.1** (1.0 g, 5.33 mmol) in 15 mL of acetonitrile 3 equivalents of alkyl bromide (1.9 mL, 16 mmol) were added. The reaction mixture was heated at reflux for 2 h, when the product precipitated as a white powder. The solution was cooled and the solid filtered, separated and washed with diethyl ether (3 x 30 ml). 1.8 g of the final product were obtained, corresponding to a yield of 93%. ^{1}H-NMR (400 MHz, MeOD) δ 9.77 (d, *J* = 1.6 Hz, 1H), 7.54 (d, *J* = 1.4 Hz, 1H), 7.52 – 7.42 (m, 5H), 5.49 (d, *J* = 1.7 Hz, 2H), 4.63 (t, *J* = 5.4 Hz, 1H), 3.77 (s, 3H), 3.47 – 3.39 (m, 2H). MS (ESI) [M+H+] +286 *m/z*.

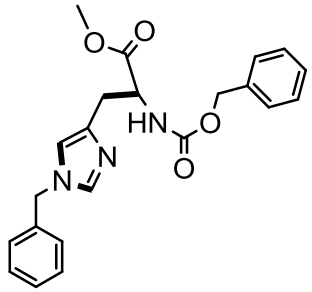

Synthesis of N-a-(benzyloxycarbonyl)-1-benzyl-L-histidine methyl ester (**5.3**). To a solution of **5.2** (1 g, 2.80 mmol) in acetonitrile (100 mL) was added benzyl alcohol (1.45 mL, 14 mmol) and diisopropylethylamine (0.98 mL, 5.6 mmol). The solution was stirred overnight at room temperature. The progress of the reaction was followed by TLC and ESI-MS The solvent was removed by rotary evaporation, obtaining a highly viscous yellow oil, which was dissolved in the minimum amount of dichloromethane and precipitated with diethyl ether. The crude product was purified by silica chromatography with eluent hexane-ethyl acetate 1:1 (v/v), with a yield of 68%. ^{1}H-NMR (400 MHz, $CDCl_3$) δ 7.45 (s, 1H), 7.40-7.30 (m, 8H), 7.16 – 7.08 (m, 2H), 6.65 (s, 1H), 6.37 (d, J = 8.1 Hz, 1H), 5.12 (s, 2H), 4.63 (dt, J = 8.2, 5.0 Hz, 1H), 3.66 (s, 3H), 3.08 (ddd, J = 19.2, 14.6, 4.9 Hz, 2H). MS (ESI) [M+H+] +393 *m/z*.

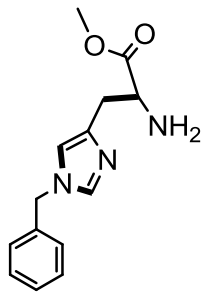

Synthesis of 1-Benzyl-L-histidine methyl ester (**5.4**). The mixture of the substrate **5.3** (0.65 g, 1.65 mmol) and 10% Pd/C (10 wt % of the substrate) in ethanol (10 mL) was vigorously stirred at room temperature (ca. 20 °C) under ordinary hydrogen pressure (balloon) for 24 h. The reaction mixture was filtered using Celite, the filtrate was washed several times with ethanol and concentrated to provide the product (yellow oil, quantitative yield). *Caution!* The product is highly photosensitive and should be protected from light. ^{1}H-NMR (400 MHz, $CDCl_3$) δ 7.42

(s, 1H), 7.38 – 7.21 (m, 3H), 7.11 (d, J = 6.7 Hz, 2H), 6.68 (s, 1H), 5.02 (s, 2H), 3.89 – 3.71 (m, 1H), 3.64 (s, 3H), 3.00 (dd, J = 14.4, 4.6 Hz, 1H), 2.88 – 2.77 (m, 1H), 2.46 (s broad, 2H), 1.18 (t, J = 7.0 Hz, 1H). MS (ESI) [M+H+] +260 *m/z*.

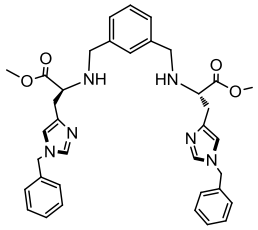

*Synthesis of dimethyl 2,2'-((1,3-phenylenebis(methylene))bis(azanediyl))bis(3-(1-benzyl-1H-imidazol-4-yl)propanoate)(***5.5, isophtalHis$_2$***).* In an amber-coloured round-bottom flask 1.2 mmol of **5.4** were dissolved in 5 mL of dichloromethane and under stirring solid isophtaldialdehyde (80 mg, 0.6 mmol) was added at room temperature under N_2. After 24 h 1.2 more mmol of **5.4** were poured into the solution and the mixture was left stirring overnight. Sodium triacetoxyborohydride was added until the complete reduction of the diimino product (3.6 mmol, 760 mg). The reaction mixture was quenched by removing the solvent and treating the borate salts obtained with dichloromethane. The suspension was centrifugated to allow sedimentation of the white salts, while the solvent was rotary-evaporated to give a viscous green oil. The final product was recovered by chromatography on silica using a mixture of hexane-ethyl acetate-methanol aqueous ammonia (1:9:1:0.3 v/v) as eluent, affording **5.5** as a colorless oil (98% yield).

^{1}H-NMR (400 MHz, $CDCl_3$) δ 7.42 (s, 2H), 7.33 – 7.25 (m, 6H), 7.15 (t, *J* = 7.3 Hz, 2H), 7.09 (dd, *J* = 6.7, 5.0 Hz, 6H), 6.64 (s, 2H), 6.23 (d, *J* = 44.9 Hz, 11H), 5.01 (d, *J* = 5.8 Hz, 4H), 3.79 – 3.69 (m, 2H), 3.63 – 3.53 (m, 10H), 2.96 – 2.82 (m, 4H). ^{13}C-NMR (101 MHz, $CDCl_3$) δ 175.44 (q), 140.14 (q), 138.90 (q), 137.26 (q), 129.45 (CH), 128.64 (CH), 128.64 (CH), 128.51 (CH), 127.63 (CH), 127.27 (CH), 117.34 (CH), 61.21 (CH), 52.26 (CH2), 52.08 (CH2), 51.16 (CH3), 32.46 (CH2), 22.96 (CH2).

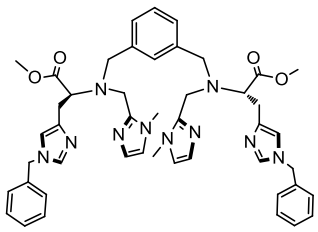

*Synthesis of dimethyl 2,2'-((1,3-phenylenebis(methylene))bis(((1-methyl-1H-imidazol-2-yl)methyl)azanediyl))bis(3-(1-benzyl-1H-imidazol-4-yl)propanoate)(***mXHI, 5.6***)* Compound **5.5** (430 mg, 0.70 mmol) was dissolved in dichloroethane (5 ml) under an inert atmosphere. A solution of 1-methyl-2-imidazole carboxaldehyde (186 mg, 1.73 mmol) in dichloroethane (1 ml) was slowly added. The reaction was stirred for 30 min at room temperature. Solid sodiumtriacetoxyborohydride (440 mg, 2.10 mmol) was added and the suspension was stirred at room temperature for 8 h. 1.73 mmol of aldehyde and an equivalent amount of

solid sodiumtriacetoxyborohydride were added to the reaction mixture, which was left stirring overnight. ESI-MS monitoring revealed uncomplete reduction of the diimino intermediate, so a new addition of equimolar aldehyde and reducing agent (1.73 mmol) was made to the reaction, which was then left stirring for 24 h at room temperature. The reaction was stopped by removing the solvent and the mixture of salts obtained were washed with dichloromethane. After centrifugation the solvent was separated and evaporated to get the crude product as a yellow oil. The final product was collected by chromatography on silica using a mixture of ethyl acetate-methanol-aqueous ammonia (80:20:3 v/v) as eluent, giving mXHI as a colorless oil (Rf= 0.23, 430 mg, 78 %). ^{1}H-NMR (400 MHz, $CDCl_3$) δ 7.42 (s, 2H), 7.29 (t, *J* = 5.0 Hz, 6H), 7.12 – 7.05 (m, 4H), 7.05 – 6.90 (m, 4H), 6.80 (d, *J* = 2.9 Hz, 2H), 6.59 (s, 2H), 6.40 (s, 2H), 4.96 (d, *J* = 2.8 Hz, 4H), 3.86 – 3.70 (m, 8H), 3.63 (t, *J* = 4.0 Hz, 6H), 3.51 (dd, *J* = 13.8, 2.3 Hz, 2H), 3.20 – 2.85 (m, 10H). ^{13}C-NMR (101 MHz, $CDCl_3$) δ 172.76 (q), 145.24 (q), 139.34 (q), 139.10 (q), 136.81 (CH), 136.58 (q), 130.35 (CH), 129.32 (CH), 128.65 (CH), 128.30 (CH), 128.26 (CH), 127.72 (CH), 126.68 (CH), 122.11 (CH), 116.91 (CH), 63.01 (CH), 55.28 (CH2), 51.76 (CH2), 51.18 (CH3), 47.86 (CH2), 32.93 (CH3), 28.44 (CH2). MS (ESI) [M+H+] +809 *m/z*.

Synthesis of [Cu$_2$mXHI][ClO$_4$]$_4$. To a solution of mXHI (10 mg, 1.24×10^{-5} mol) in methanol (0.6 mL) copper(II) perchlorate hexahydrate (9.1 mg, 2.47×10^{-5} mol) dissolved in the same volume of methanol was added. The resulting blue solution was poured in 5 mL of diethyl ether to induce precipitation of the complex. The suspension was centrifuged and the blue solid was separated, washed with diethyl ether (3×3mL) and dried under vacuum (68%). MS (ESI) [M+2Cu^{2+}+2ClO_4^-] +566 *m/z* (detected as double charged). Anal. Calcd. for $C_{46}H_{52}C_{l4}Cu_2N_{10}O_{20}$(1333.88): C 41.42, H 3.92, N 11.50. Found: C 41.31, H 3.52, N 11.23.

Titration of [Cu$_2$(mXHI)]$^{4+}$ with azide. The binding of azide to $[Cu_2(mXHI)](ClO_4)_4$ was studied spectrophotometrically by adding concentrated methanolic solutions of sodium azide to solutions of the complexes dissolved in MeOH/MeCN, 9:1 (v/v). All measurements were performed in a thermostated optical cell, with magnetic stirring, at 20 ±0.1 °C. In all cases, it was found that binding of the anion is fast, so it was not necessary to incubate the mixtures before the spectroscopic measurements were performed. Titration of 0.9 mL $[Cu_2(mXHI)]^{4+}$ solution (3.82×10^{-4} M) was performed by the addition of successive and equal amounts (13 μL) of an azide solution (0.01 M) until further addition of azide did not produce appreciable spectral changes.

Titration of $[Cu_2(mXHI)]^{4+}$ with hydroxide. The binding of hydroxide to $[Cu_2(mXHI)]^{4+}$ was studied spectrophotometrically by adding concentrated methanolic solutions of sodium hydroxide to solutions of the complexes dissolved in MeOH/MeCN, 9:1 (v/v). All measurements were performed in a thermostated optical cell, with magnetic stirring, at 20 ±0.1 °C. In all cases, it was found that binding of the anion is fast, so it was not necessary to incubate the mixtures before the spectroscopic measurements were performed. Titration of 1.0 mL $[Cu_2(mXHI)]^{4+}$ solution (3.82×10^{-4} M) was performed by the addition of successive and equal amounts (9.8 μL) of a hydroxide solution (0.01 M) until further addition of hydroxide did not produce appreciable spectral changes.

$[Cu_2(mXHI)]^{4+}$ NMR spectroscopy. An NMR spectrum was recorded of a solution containing 3.1 mg of mXHI, dissolved in 600 μL of CD_3OD. This solution was used to dissolve 2.8 mg of copper(II) trifluoromethansolfonate and to record a new spectrum. Two consecutive spectra were performed after each of the two additions of a 2 M NaOH (1.9 μL) solution in D_2O. The spectra in the presence of Cu(II) were recorded using a spectral width of 187 ppm, centered at 30 ppm. 800 acquisitions were performed with a 0.3 second delay because of the short relaxation time induced by the copper ions.

Titration of mXHI dicopper complex with L/D-tyrosine methyl ester. The binding of L- and D-tyrosine methyl ester to $[Cu_2(mXHI)]^{4+}$ was studied spectrophotometrically by adding concentrated methanolic solutions of tyrosine to a solution of $[Cu_2(mXHI)](ClO_4)_4$ dissolved in methanol. All measurements were performed in a thermostated optical cell, with magnetic stirring, at 25 ±0.1 °C. In all cases, it was found that the binding is fast, so it was not necessary to incubate the mixtures before the spectroscopic measurements were performed. Titration of 2.2 mL $[Cu_2(mXHI)](ClO_4)_4$ solution (5.0×10^{-4} M) was performed by the addition of successive amounts (from 2.0 to 20 μL) of a tyrosine solution (0.055 M) up to 12 equivalent of ligand.

Catalytic oxidation of o-catechols. The catecholase activity of Cu(II) complex $[Cu_2(mXHI)]^{4+}$ has been determined by the catalytic oxidation of a series of chiral catechols L-Dopa, D-Dopa, L-DopaOMe, D-DopaOMe, R-(-)-norepinephrine, and S-(+)-norepinephrine. The kinetic studies of the oxidation of the *o*-diphenols were carried out spectrophotometrically by the method of initial rates by monitoring the increase of each characteristic quinone absorption band over time, respectively at 475 nm (ε475 = 3600 $M^{-1}cm^{-1}$ for L-/D-Dopa), at 468 nm for L-/D-DopaOMe, at 480 nm for R-/S-norepinephrine. The solvent used was a 10:1 (v/v) mixture of methanol/aqueous acetate buffer (50 mM, pH 5.1) or MES (2-(*N*-morpholino)ethanesulfonic acid) buffer (50 mM,

pH 6) saturated with atmospheric dioxygen. The experiments were carried out over a substrate concentration range (5×10^{-5} to 1×10^{-3} M) at a constant temperature of 20±0.1 °C, to determine the dependence of rate on substrate concentration and various kinetic parameters a 5×10^{-5} M solution of these complexes was treated with at least 10 equiv of substrate and a maximum of 200 equiv. so as to maintain the pseudo first order condition. A stock solution of 5×10^{-4} M $[Cu_2(mXHI)](ClO_4)_4$ was prepared, by dissolving 3.3 mg of complex in 5 ml of methanol, and used for the kinetic measurements with all the substrates, in order to guarantee reproducibility to the experiments.

Oxidation of Phenols- General Procedure for the Aerobic Functionalization of Phenols.

Note: Reaction prepared using standard inert atmosphere techniques, not requiring a glove box. An oven-dried 100 mL round bottom flask equipped with a teflon-coated stir bar and a rubber septum was degassed and backfilled with N_2, then charged with anhydrous and acetone (47 mL). Previously prepared solutions in acetone of phenolate (1×10^{-5} mol in 1 mL) and mXHI (5×10^{-7} mol in 1 mL) were cannulated into the reaction flask. The reactor flask was cooled at -80°C with a cryostat and thermostated at the appropriate temperature. In a separate, oven-dried 3 mL microwave vial, $[Cu(CH_3CN)_4]PF_6$ (1×10^{-6} mol) was dissolved in dry and degassed acetone (1 mL). The colourless solution was then refrigerated and added to the reactor, formerly degassed to remove N_2, via cannula to afford a final volume of 50 mL and a phenolate excess of 20 eq with respect to the complex $[Cu_2(mXHI)]^{2+}$. The reactor was then supplied with an O_2-filled balloon to assure an approximately constant pressure of O_2. At the end of the reaction, the vessel was depressurized by opening to the atmosphere and the mixture was quenched with 2 mL of 1 M $HClO_4$. The organic solvent was removed *in vacuo* and the aqueous phases were extracted with CH_2Cl_2 (3×10 mL). The combined organic fractions were then dried over Na_2SO_4, filtered and concentrated to afford an oil which was analyzed directly by ^{1}H-NMR. The crude reaction mixture was in some cases purified using column chromatography.

Hydroxylation of DBU 2-tert-butyl-4-methoxyphenolate. DBU salt of 2-tert-butyl-4-methoxyphenolate was prepared by the reaction of phenol (50 mg, 0.28 mmol, 1 eq) with substoichiometric amount of DBU solution (0.034 mL, 0.25 mmol, 0.9 eq) in CH_2Cl_2 and subsequent removal of the solvent. ^{1}H-NMR (400 MHz, acetone-D6): δ 6.77 (d, *J* = 3.1 Hz, 1H), 6.74 (d, *J* = 8.6 Hz, 1H), 6.56 (dd, *J* = 8.6, 3.1 Hz, 1H), 5.62 (s, 1H), 3.69 (s, 3H), 3.30-3.23 (m, 6H), 1.92–1.70 (m, 2H), 1.66-1.60 (m, 6H), 1.41 (s,

9H). The reaction was carried out in accordance to General Procedure using DBU salt of 2-tertbutyl-4-methoxyphenolate (3.3 mg, 1×10^{-5} mol), mXHI (0.4 mg, 5×10^{-7} mol), $[Cu(CH_3CN)_4]PF_6$ (0.38 mg, 1×10^{-6} mol) and acetone (50 mL). The reaction was quenched after 2 h at room temperature and analyzed. ^{1}H-NMR (400 MHz, acetone-D6): δ 6.89 (d, *J* = 3.1 Hz, 2H), 6.66 (d, *J* = 3.1 Hz, 2H), 5.63 (s, *2*H), 3.78 (s, 6H).

Hydroxylation of DBU 4-methoxyphenolate DBU (1,5-diazabiciclo(5.4.0)undec-5-ene) salt of 4-methoxyphenolate was prepared by the reaction of p-methoxyphenol (50 mg, 0.40 mmol, 1 eq) with substoichiometric amount of DBU solution (0.050 mL, 0.36 mmol, 0.9 eq) in CH_2Cl_2 and subsequent removal of the solvent. ^{1}H-NMR (acetone-d6): δ 6.71 (s, 4H), 3.69 (s, 3H), 3.32-3.29 (m, 3H), 3.23-3.21 (m, 3H), 1.87-1.75 (m, 2H), 1.69-1.60 (m, 6H). The reaction was carried out in accordance to General Procedure using DBU salt of 4-methoxyphenolate (2.8 mg, 1×10^{-5} mol), mXHI (0.4 mg, 5×10^{-7} mol), $[Cu(CH_3CN)_4]PF_6$ (0.35 mg, 1×10^{-6} mol) and acetone (50 mL). The solution was rotary-evaporated and the yellow oil obtained was dissolved in 1 mL of dichloromethane and extracted three times with water (1 mL), containing EDTA. The yellowish oil was analyzed and purified with column chromatography on silica gel (7:3 hexane/ethyl acetate). ^{1}H-NMR (400 MHz, acetone-D6): δ 6.94 (d, *J* = 8.7 Hz, 2H), 6.88 (d, *J* = 3.1 Hz, 2H), 6.85 (dd, *J* = 8.7, 3.1 Hz, 2H), 3.79 (s, 6H).

Hydroxylation of β-naphthol A solution of mXHI ($5x10^{-5}$ M) and the DBU salt of the naphthol ($1x10^{-3}$ M) was prepared in degassed acetone (volume: 20 mL), maintaining an argon gas atmosphere with the use of a Schlenk line. A solution of $[Cu(CH_3CN)_4]PF_6$ in freshly distilled and degassed acetone ($1x10^{-4}$ M, 1 mL) was added to the previously described solution, with a gas-tight syringe. The reaction was initiated by the addition of molecular oxygen and was stirred at room temperature overnight, turning from colorless to pale gold yellow. The solvent was removed by rotary evaporation, then the crude product was dissolved in dichloromethane and few drops of distilled water were added, in order to dissolve a small amount of the sodium salt of ethylendiamino tetracetic acid, used to remove the copper from the reaction mixture. The organic phase was separated and evaporated to give the crude product. Purification by liquid cromatography, using silica gel (230-400 A mesh) and hexane:ethyl acetate 7:3 gives the purified product (Rf; ^{1}H NMR (400 MHz, acetone-D6) δ 8.82 (s, 1H), 8.13 (d, *J* = 7.3 Hz, 1H), 7.97 (d, *J* = 9.0 Hz, 1H), 7.91 (d, *J* = 8.5 Hz, 1H), 7.77 (d, *J* = 7.6 Hz, 1H), 7.56 (dd, *J* = 11.6, 7.4 Hz, 2H), 7.44 – 7.21 (m, *J* = 7.1 Hz, 4H), 6.85 (d, *J* = 7.6 Hz, 1H), 6.46 (s, 1H).

Hydroxylation of β-naphthol: incorporation of $^{18}O_2$ The experiment set is the same described above, but to initiate the reaction, pure $^{18}O_2$ is added with a gas-tight syringe.

Hydroxylation of TBA salt of N-acetyl-L-tyrosine ethyl ester TBA (Tetrabutylammonium) salt of N-acetyl-L-tyrosinate ethyl ester was prepared by the reaction of equimolar amounts of phenol (50 mg, 0.33 mmol, 1 eq) and tetrabutylammonium hydroxide x 30 H_2O solution (0.037 mL, 0.33 mmol, 0.9 eq) in CH_2Cl_2 (2 mL). The oil obtained was then dissolved in 2 mL of toluene to help the removal of water from the solution. The solvent was rotary-evaporated to obtain a colourless oil. The reaction was carried out in accordance to General Procedure using TBA salt of N-acetyl-L-tyrosine ethyl ester (3.9 mg, 1×10^{-5} mol), mXHI (0.4 mg, 5×10^{-7} mol), $[Cu(CH_3CN)_4]PF_6$ (0.38 mg, 1×10^{-6} mol) and acetone (50 mL). The reaction was quenched after 16 h and analyzed. The crude product was then purified using silica gel column cromatography (hexane). The same procedure was used for the synthesis of the D- enantiomer.

Spectrophotometric oxidation of catalytic amounts of exogenous substrates. This method is analogous to that reported by Tuczek in 2010.[14] To a mixture containing TBA salt of N-Acetyl-L-tyrosine ethyl ester (3×10^{-6} mol) in anhydrous acetone (100 µL) and mXHI (1.5×10^{-7} mol) in 50 µL of acetone was cannulated a solution of $[Cu(CH_3CN)_4]PF_6$ (3×10^{-7} mol in 1 mL) in dry acetone. To preclude the autoxidation to copper(II), a stock solution of copper(I) salt was first prepared in acetonitrile, then the correct volume of solution was withdrawn and evaporated *in vacuo*. The solid was then redissolved in dry acetone and rapidly poured into the solution. The reaction was monitored by UV-Vis spectroscopy at 25 °C for 2 h. Upon injection, an intense 400 nm feature develops, typically associated to the the formation of the quinone, and followed by the rapid increase of an absorption band at 440 nm, probably due to a degradation product of the quinone, promoted by the catalyst. The same experiment, also replicated for the D-enantiomer, was repeated with two other different substrate concentrations (5-10 equiv respect to the catalyst concentration) and the initial rates of oxidation were obtained by fitting the absorbance versus time curves in the first few minutes of the reactions.

Catalytic sulfoxidation of thioanisole. A 10 mM solution of thioanisole in 1 mL of 9:1 methanol/acetate buffer 50 mM (pH 5.1) was added first with a methanolic solution of $[Cu_2(mXHI)]Cl_4$ (final concentration 10 µM), followed by the addition of the appropriate volume of a solution of hydroxylamine hydrochloride in acetate buffer. The

reaction was stirred overnight at room temperature. The study was conducted by varying the concentration of hydroxylamine from 0.3 to 10 mM. For the determination of the yield, 100 µL of the reacted mixture was added with 1 µL of a 0.05 M solution of p-nitroacetophenone, used as internal standard. The so obtained mixture was directly analyzed by HPLC, using a Ascentis Express C18 10 cm x 4.6 mm as column, in a gradient of Acetonitrile +0.1% of TFA/Water +0.1% of TFA, flux 0.8 mL/min.

Time	H_2O:ACN (+0.1 %TFA) initial	H_2O:ACN (+0.1 %TFA) final
0--> 15 min	95:5	0:100
15--> 20 min	0:100	0:100
20--> 22 min	0:100	95:5
22 min	95:5	95:5

Retention times: methylphenylsulfoxide: 9.5 min; p-nitroacetophenone: 12.5 min; thioanisole: 14.2 min. For the determination of the enantiomeric excess, the reaction was quenched by the addition of 1 mL of 1 M solution of $HClO_4$. After the evaporation of the methanolic portion, the residual water was extracted 3x3mL of dichloromethane. The collected organic extract was dried over sodium sulphate, filtred and evaporated (thioanisole is partially lost during rotary evaporation). This crude product was analyze by HPLC, (chiral column: Lux 5u amylose-2 250 x 4.60 mm, flux 0.8 mL/min; Eluent: 85:15 hexane:2-propanol, Retention times: $r.t_1$: 25 min, $r.t_2$: 27 min.)

Supporting information

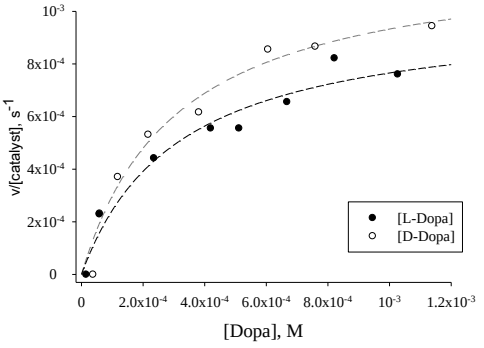

a)

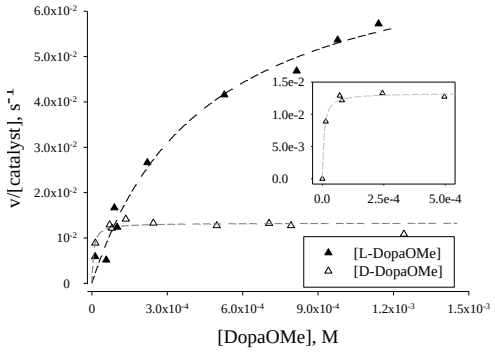

b)

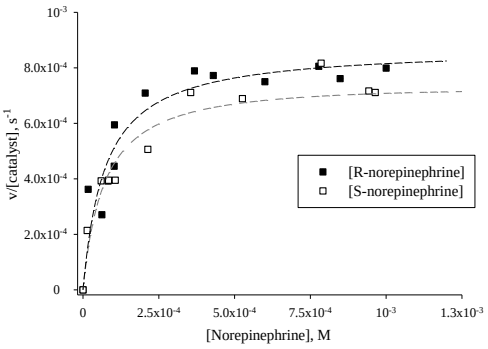

c)

Figure S.I 5.1. Effect of substrates concentrations on the initial oxidation rate of L-/D-Dopa (a), L-/D-DopaOMe (b) and R-/S-Norepinephrine (c) by complex $[Cu_2mXHI](ClO_4)_4$ at pH=5.1.

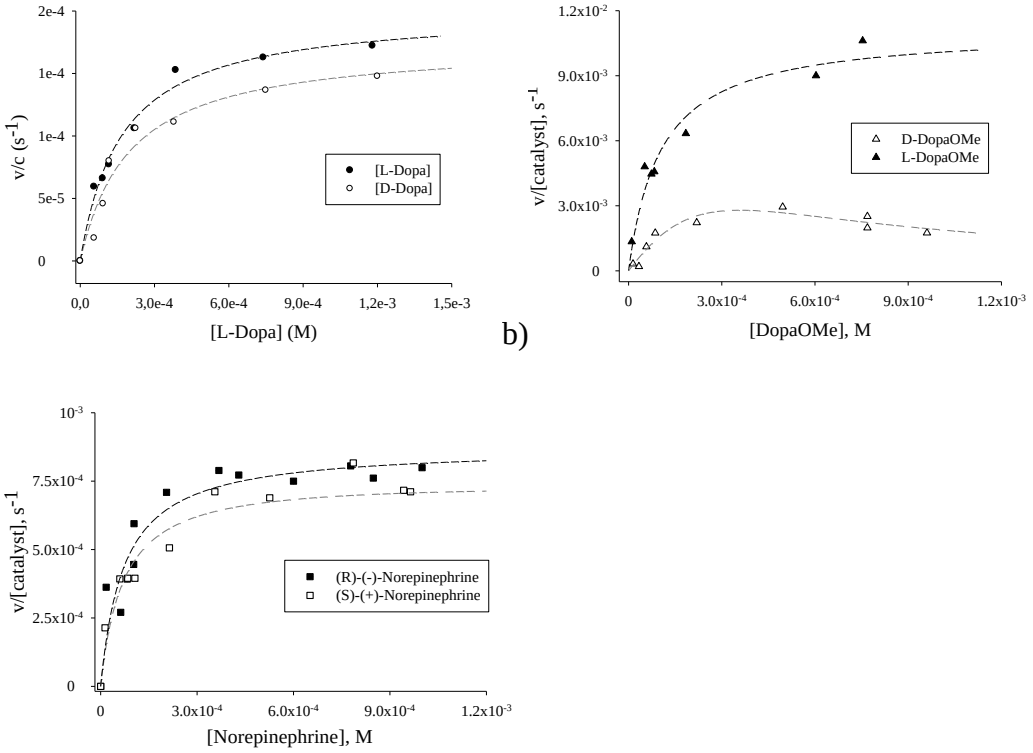

Figure S.I. 5.2 Effect of substrates concentrations on the initial oxidation rate of L-/D-Dopa (a), L-/D-DopaOMe (b) and R-/S-Norepinephrine (c) by complex $[Cu_2mXHI](ClO_4)_4$ at pH=6.

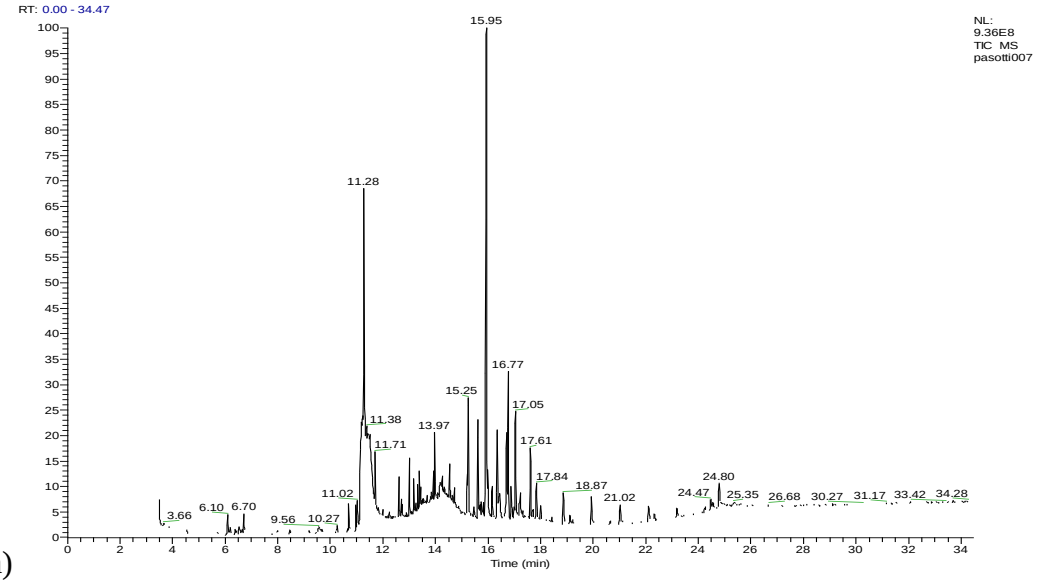

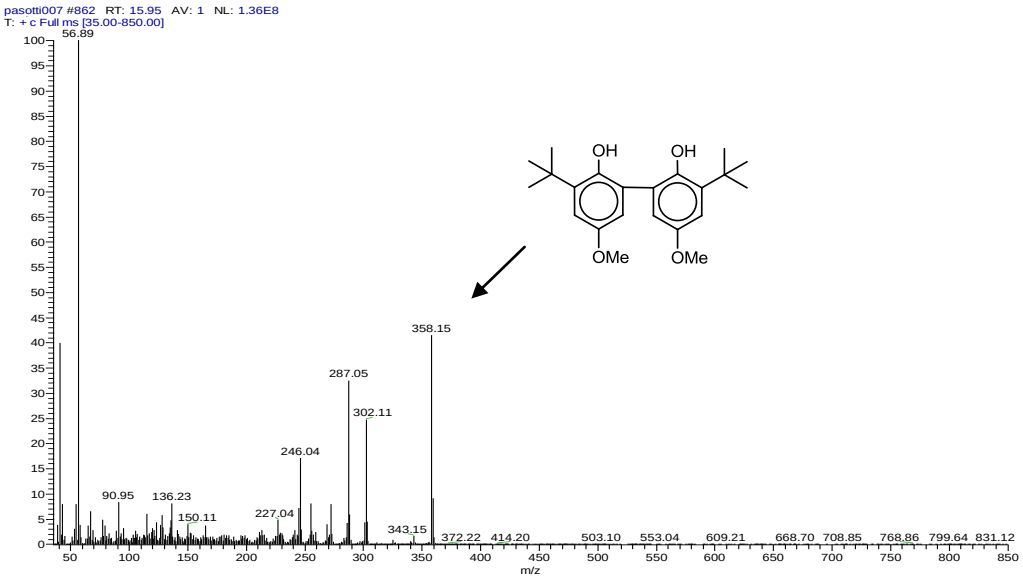

b)

Figure S.I 5.3. GC-MS analysis of the crude product derived from oxidation of 2-tert-butyl-4-methoxy phenol. a) GC-MS chromatogram. 11.28 min: reagent peak with molecular mass 180 *m/z*, 15.95 min: product peak with molecular mass of 358 *m/z*. Molecular mass and fragmentation of the product are shown in section b). Other peaks are recorded in database and belong to fragmentation patterns, typical of poliyisloxanes coming from the GC column.

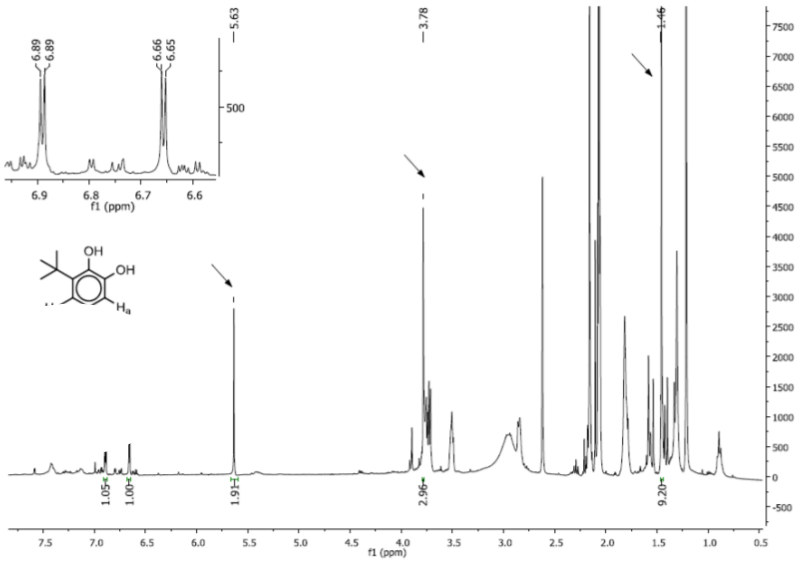

Figure S.I. 5.4- Crude ^{1}H-NMR spectrum (δ values, ppm) in acetone D-6 of the hydroxylation reaction of 2-*tert*-butyl-4-methoxyphenol. A zoomed view of the aromatic region is shown for clarity. The NMR signals, attributed to the product, are marked with arrows.

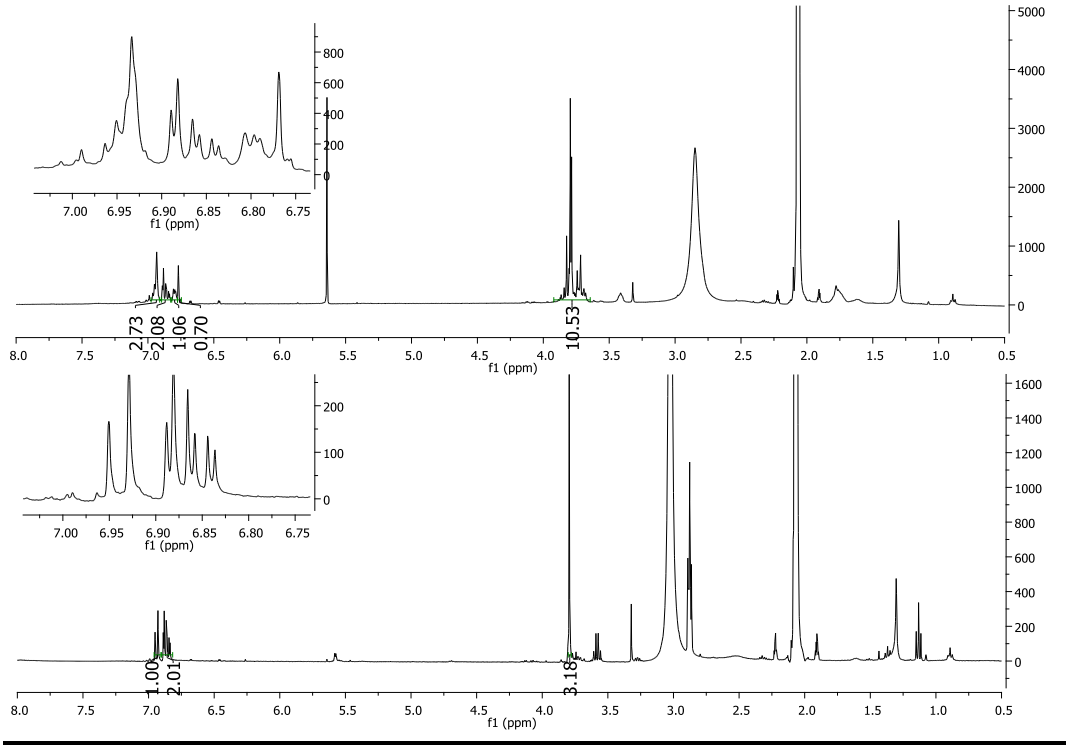

Figure S.I. 5.5- ^{1}H NMR analysis of the product obtained from oxidation of 4-methoxy phenol. Crude (top) and pure (bottom) ^{1}H NMR spectra (δ values, ppm) in acetone D-6. Zoomed view of the aromatic region are shown for clarity.

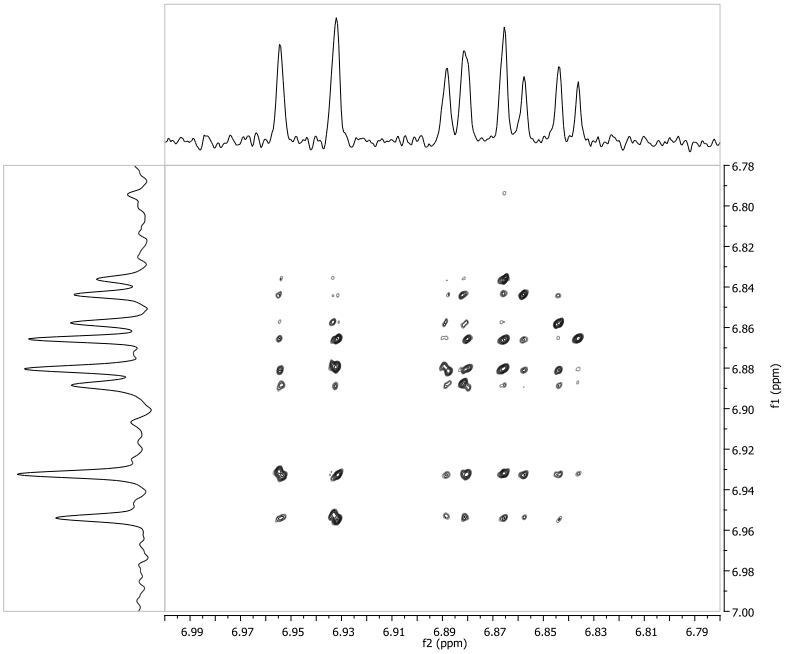

Figure S.I. 5.6- Aromatic region expansion of the COSY spectra of the pure product obtained from oxidation of 4-methoxy phenol.

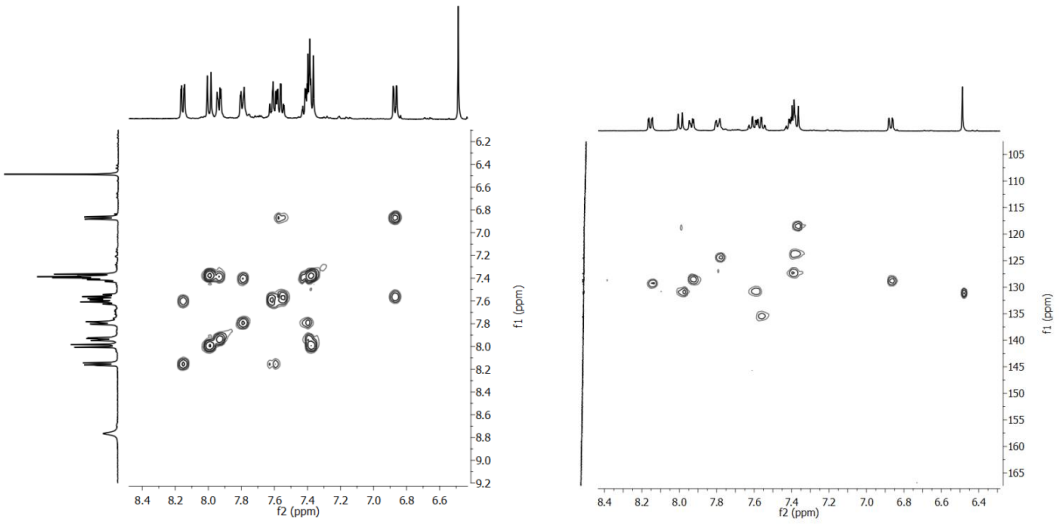

Figure S.I 5.7- COSY and HMQC 2D-NMR of the pure product obtained from oxidation of β-naphthol as DBU salt.

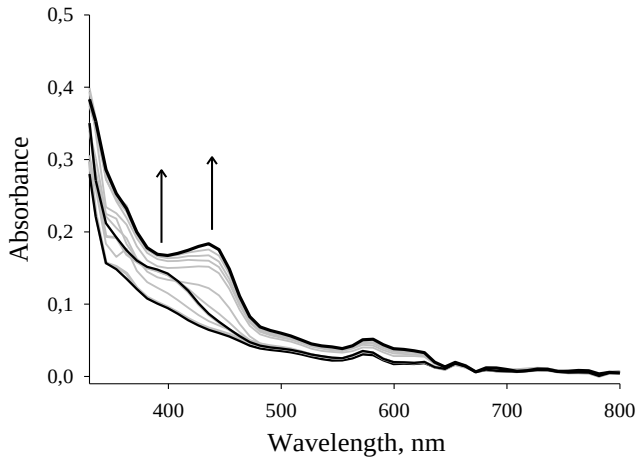

Figure S.I 5.8- Representative spectra recorded during the initial phase of the reaction involving $[Cu_2(mXHI)]^{2+}$, TBA salt of N-acetyl-L-tyrosine ethyl ester (20 equiv), and dioxygen at 25 °C in dry acetone.

Experimental details

Kinetic studies of L-/D-Dopa oxidation.

Two initial solutions of 8×10^{-4} M L- and D-Dopa were prepared in a 1:1 (v/v) mixture of methanol/aqueous buffer. The substrate concentration in cuvette was progressively corrected on the base of the absorbance values measured at 283 nm, the wavelenght of maximum absorbance for the catechols (εDopa =2700 M^{-1} cm^{-1}). To favor the solubility in the stock mixture, it is recommended to dissolve the substrates first in buffer solution and then in the remaining volume of methanol, under a moderate warming. A solvent

blank was first recorded, then the spectrum of increasing concentrations of catechols was employed to correct the substrate concentration, often susceptible of precision errors. A new blank was then repeated and the reaction was initiated by the addition of a constant volume of complex in methanolic solution (final concentration 5×10^{-6} M). Absorbance vs. wavelength (wavelength scans) of these solutions were recorded at a regular time interval of 1 s for 5 min in the wavelength range 200–800 nm. The reaction was followed by monitoring the increase in the absorbance at 475 nm (ε_{475} = 3600 $M^{-1}cm^{-1}$) as a function of time (time scan).

Kinetic studies of L-/D-DopaOMe oxidation.

The same procedure has been repeated for the couple L-/D-DopaOMe. Due to their improved solubility in organic solvents, the stock solutions of the substrates were prepared in methanol, and their concentrations corrected on the base of the absorbance measured at 283 nm (εDopaOMe=2700 $M^{-1}cm^{-1}$). The catecholase activity was followed spectrophotometrically by monitoring the increase in the absorbance at 468 nm (quinone band maxima, the ε value used was the same reported in literature at 475 nm ε_{475} = 3600 $M^{-1}cm^{-1}$) as a function of time (time scan).

Kinetic studies of S-/R-norepinephrine-L-bitartrate.

The same procedure has been replicated for the couple S-/R-norepinephrine-L-bitartrate. The initial solutions of the substrates were prepared in a 1:1 (v/v) mixture of methanol/aqueous buffer, and their concentrations corrected on the base of the absorbance measured at 283 nm (εNorepinephrine =3071 M^{-1} cm^{-1}) The catechol oxidations were followed spectrophotometrically by monitoring the increase in the absorbance at 480 nm (quinone band maxima, the ε value used was the same reported in literature at 475 nm ε_{475} = 3600 $M^{-1}cm^{-1}$) over the time.

References

1- (a) L. Casella, O. Carugo, M. Gullotti, S. Garofani, P. Zanello, *Inorg. Chem.* **1993**, *32*, 2056–2067; (b) S. Palavicini, A. Granata, E. Monzani, L. Casella, *J. Am. Chem. Soc.* **2005**, 127, 18031-1836; (c) A. Hoffmann, C. Citek, S. Binder, A. Goos, M. Rübhausen, O. Troeppner, I. Ivanović-Burmazović, E. C. Wasinger, T. D. P. Stack, S. Herres-Pawlis, *Angew. Chem.* **2013**, *125*, 5508 - 5512; (d) M. Perrone, E. Lo Presti, S. Dell'Acqua, E. Monzani, L. Santagostini, L.Casella, *Eur. J.I.C.* ,**2015**, 21, 3493–3500.

2- (a) Santagostini L., Gullotti M., Pagliarin R., Bianchi E., Casella L., Monzani E. *Tetrahedron: Asimmetry*, **1999**, 10, 281-295; (b) L. Santagostini, M. Gullotti, R. Pagliarin, E. Monzani, L. Casella, *Chem. Commun.* **2003**, 2186-2187; (c) M. Gullotti, L. Santagostini, R. Pagliarin, S. Palavicini, L. Casella, E. Monzani, G. Zoppellaro, *Eur. J. Inorg. Chem.* **2008**, 2081-2089; (d) M. C. Mimmi, M. Gullotti, L. Santagostini, G. Battaini, E. Monzani, R. Pagliarin, G. Zoppellaro, L. Casella, *Dalton Trans.* **2004**, 2192-2201; (e) F. G. Mutti, M. Gullotti, L. Casella, L. Santagostini, R. Pagliarin, K. Kristoffer Andersson, M. F. Iozzi, G. Zoppellaro, *Dalton Trans.* **2011**, 40, 5436-5457.

3- R. Jain, L. A. Cohen, *Tetrahedron*, **1996**, 52, 15, 5363-5370.

4- A. F. Abdel-Magid and S. J. Mehrman, *Org*. *Process Res*. *Dev*., **2006**, 10, 971-1031.

5- (a) C. F. Thurston, *Microbiology* **1994**, *140*, 19; (b) L. Marzullo; R. Cannio; P. Giardina; M. T. Santini; G.Sannia, *J. Biol. Chem*. **1995**, *270*, 3823; (c) J.M. Bollag *Met. Ions Biol. Syst*. **1992**, *28*, 205.

6- (a) P. M. H. Kroneck; F. A.Armstromg; H.Merckle; A Marchesini. *Adv. Chem. Ser*. **1982**, *200*, 223; (b) G.Chichiriccò; P. Cerù; A. M. D'Alessandro; A. Oratore; L. Avigliano, *Plant Sci*. **1989**, *64*, 61.

7- (a) A. Messerschmidt; R. Huber *Eur. J. Biochem*. **1990**, *187*, 341; (b) G.Musci; M. Carbonaro; A. Adriani, A. Lania; A. Galtieri; L. Calabrese, *Biochem. Biophys.* **1990**, *279*, 8.

8- (a) Karlin, K. D.; Farooq, A,; Hayes, **J.** C.; Cohen, B. I.; Rowe, T. M.; Sinn, E**.;** Zubieta, *J. Inorg. Chem.,* **1987,** 26, 1721. b) Solomon, **E. I.;** Penfield, K. W.; Wilcox, D. E. *Strucf. Bonding (Berlin)* **1983**, *53*, 1.

9- Acta Biochimica polonica, vol 58, n 3, **2011**, 303-311.

10- A. Granata, E. Monzani, L. Casella, J Biol Inorg Chem, **2004**, 9, 903–913.

11- R. Pievo, M. Gullotti, E. Monzani, L. Casella, *Biochemistry*, **2008**, 47, 3493–3498.

12- I. Gamba, S. Palavicini, E. Monzani, L. Casella, *Chem. Eur. J.* 2**009**, 15, 12932-12936.

13- M. Rolff, J. Schottenheim, G. Peters, F. Tuczek, *Angew. Chem.*, **2010**, 122, 6583-6587; *Angew. Chem., Int. Ed.,* **2010**, 49, 6438-6442.

Chapter 6. Chiral L66-like complexes

6. Chiral L66-like complexes

6.1 Introduction

As extensively elucidated in **Chapter 1**, Tyrosinase has a double mechanism of action to generate melanic polymers. Catecholase activity consists, in fact, in oxidation of catechols to *ortho*-quinones, and it is considerate "simpler" to be mimicked by synthetic functional models. Only few genuine tyrosinase models, in fact, are able to reproduce monophenolase activity,[1] which consists in a copper mediated *ortho*-hydroxylation of phenols, with a concomitant oxidation to quinones. Tyrosinase active site, similarly to hemocyanins and catechol oxidases, consists of a dinuclear type-3 copper center and it is able to reversibly bind molecular oxygen as peroxide in a μ-η^2:η^2 fashion.[2] This reactive intermediate of the catalytic cycle showed a typical electrophilic reactivity,[3] as phenol hydroxylation could be considered from the chemical point of view as an aromatic electrophilic substitution reaction.

Several attempts to create a suitable coordination surrounding for copper has been done in the last decades, as it emerged that stability of the oxygenated intermediate is directly related to the electron-donating capability of the coordinating nitrogens.[4]

Our research group ideated different systems capable to generate low temperature (below -80 °C) stable side-on μ-η^2:η^2 Cu_2-O_2 complexes, exploiting amino-bisbenzimidazole moieties as coordinating subunits.[5, 1a, 6] These systems are able to reversibly bind oxygen, generating the previously described copper-dioxygen complex that was also found to hydroxylate phenols to generate catechols. What differentiate these biomimetic systems from other ones described in literature is the flexibility of the six-member chelate rings formed between copper ions and the three-dentate chelating arms conjugated with the donor effect of the benzimidazolic nitrogens.

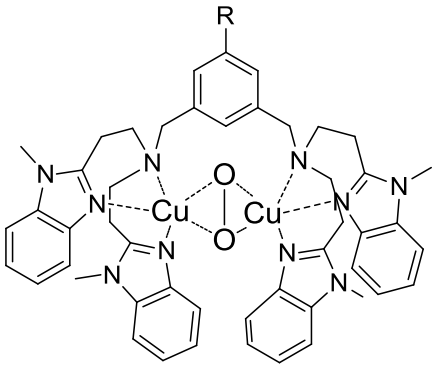

Figure 6.1- μ-η^2:η^2 Cu_2-O_2 complexes formed with our research group dinuclear amino-bisbenzimidazolic ligands. R= H, methyl.

This well optimized geometry represents a favorable starting point to new chiral ligands, with the possibility to perform enantio-discriminating *ortho*-hydroxylation of chiral phenols (especially tyrosine).

Here I report the synthesis of a dinucleating chiral ligand for copper, designed with the aim to replicate those favoring coordination features. The source of chirality was given by histidine, that was chosen by direct inspiration from the active site structure of tyrosinase.

6.1. Results and discussion

6.1.1. Ligand synthesis

6.1.1.1. Synthesis of 66-like dinucleating chiral ligand for copper

The source of inspiration for this dinucleating ligand derive from a combination between the structure of the previusly reported L66 (or MeL66) and the use of histidine as building block. I decided to introduce a *m*-xylyl moiety between the two tri-dentate units and for this purpose, the synthetic pathway needed appropriate modifications.

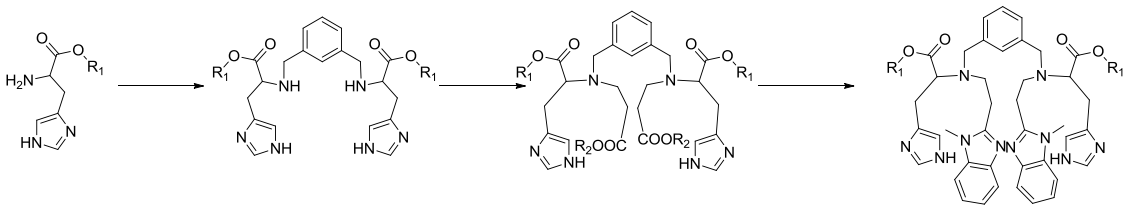

Scheme 6.1- General synthetic pathway for the synthesis of the dinucleating 66-like chiral ligands.
R_1: $-CH_3$, $-CH_2-CH_3$; R_2: $-CH_3$, *t*-Butyl.

6.1.1.1a. First attempt

I chose to start the synthesis from the methyl ester of histidine as hinge for the dinucleating structure. Two histidine molecules are interfaced by stepwise reductive amination, following the same procedure described for **mXHI** in **Chapter 5**, to afford compound **6.1** (yield = 47 %).

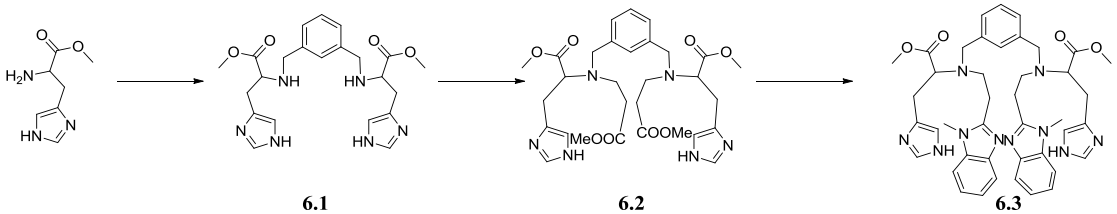

Scheme 6.2- First attempt for the synthesis of the dinucleating 66-like ligand.

Aza-Michael addition was performed using methylacrylate as both reagent and solvent, heating at moderate reflux overnight. The lacking protection on the N(τ) of histidine let this amino acid able to act as a nucleophile in Michael addition, so the use of methyl acrylate as solvent encouraged further addition to the imidazole group, decreasing

reaction yield. Compound **6.2** was obtained with 31 % yield. The last step consisted in a condensation reaction with N-methyl *ortho*-phenylenediamine in 6 M hydrochloric acid. The use of such high concentration of acid is necessary to increase the boiling point of the solution, promoting water elimination during the condensation, but it represented a disadvantage as it hydrolyzed also the methyl ester of histidine. Compound **6.3** was obtained in poor yield and low purity after esterification in methanol with thionyl chloride of the hydrolyzed intermediate.

6.1.1.1b. Second attempt

The first synthetic pathway suffers from two main problems that drastically reduced reaction yield. First, the absence of protection on the imidazole nitrogen of histidine makes this nucleus much more liable to aza-Michael conjugate addition. Furthermore, R_1 and R_2 have an identical reactivity in **6.2** so it is impossible to selectively hydrolyze the methyl esters on the newly inserted chains rather than those linked to histidine. Orthogonal deprotections were so introduced in the strategy in order to guarantee a selective cleavage of the introduced esters.

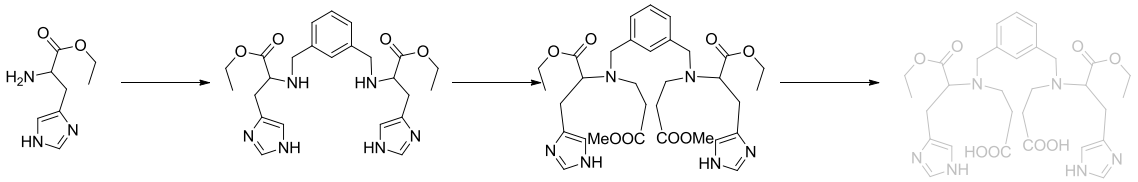

6.4 **6.5** **6.6** **6.7**

Scheme 6.3- First orthogonal protection proposed strategy

Scheme 6.3 outlined the first protection strategy proposed to provide selective cleavage of the introduced methyl esters. Compound **6.4** was synthesized by esterification in ethanol with thionyl chloride of histidine hydrochloride. Synthesis of **6.5** and **6.6** followed the same procedure described for **6.1** and **6.2** respectively. As suggested by Torò et al.,[7] methyl ester could be selectively removed in presence of ethyl ester in basic conditions at moderately low temperature, but by following the proposed experimental procedure, I obtained the total deprotection of all esters. This could be due to steric hindrance around the pending chains, preventing the deprotection reaction, mitigating the differences in reactivity between the methyl and the ethyl ester. In any case, procedure did not provide the desired **6.7** intermediate.

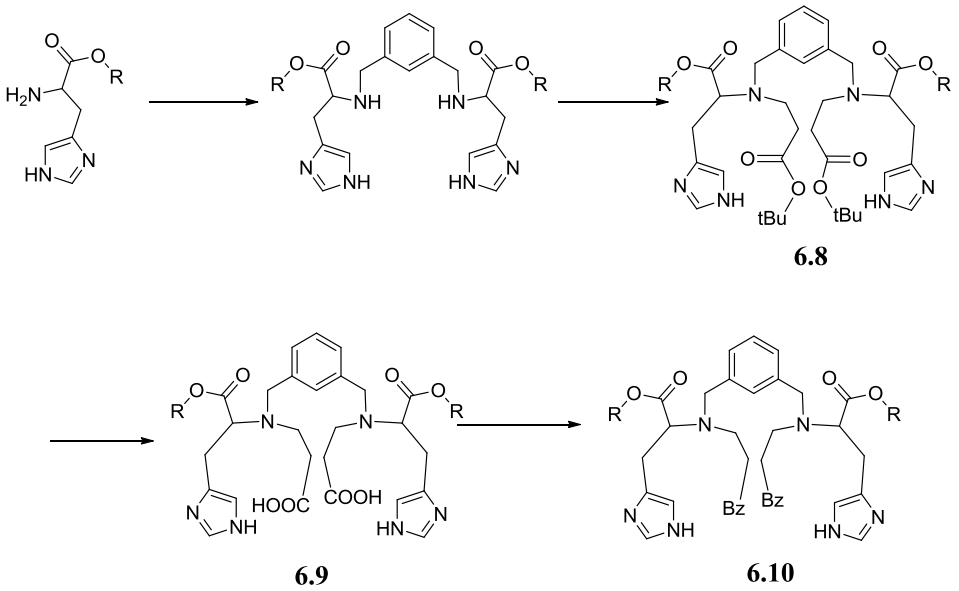

Scheme 6.4- Second orthogonal strategy proposed for the synthesis of the dinucleating chiral 66-ligand. (6.10a: R= -CH_2-CH_3, 6.10b: R= -CH_3; Bz= N-methyl benzimidazole).

The second strategy proposed for the synthesis, outlined in Scheme 6.4, follows a different orthogonal approach, based on the possibility to selectively deprotect tert-butyl ester in presence of other esters, as they are sensitive to aprotic acidic conditions. Conjugate addition with tert-butyl acrylate required the addition of a co-solvent, methanol in this case, because of the low solubility of **6.1/6.5** in the acrylate medium. Compound **6.9** was obtained quantitatively by treating **6.8** in a 1:1 v/v mixture of dichloromethane:trifluoroacetic acid and subsequently underwent a condensation reaction with N-methyl *ortho*-phenylenediamine to give **6.10**. Condensation was not conduced in 6 M HCl to prevent cleavage of the hisitidine esters, but the coupling procedure used for the synthesis of **3.1** (see **Chapter 3**) was followed. This approach was applied on two different histidine derivatives, methyl ester and ethyl ester, but only the ethyl ester compound **(6.10a)** provided the final ligand in adequate purity and yield.

6.1.2. Uv-Vis studies of oxygenation of Cu(I) complex

*6.1.2.2. Oxygenation of dinuclear complex of ligand **6.10a***

Oxygenation of the dinuclear copper(I) complex of the dinucleating ligand **6.10a** was performed in freshly distilled dry acetone, using an optical fiber apparatus (HELLMA) as spectrophotometric probe. The reaction was conducted in a Schlenck flask, preparing

a solution of ligand (as describe in the Experimental section) and removing oxygen from the reaction vessel with five cycles of vacuum/Ar purging before adding two equivalents of solid $[Cu(CH_3CN)_4]PF_6$ with subsequent exposure to air oxygen.

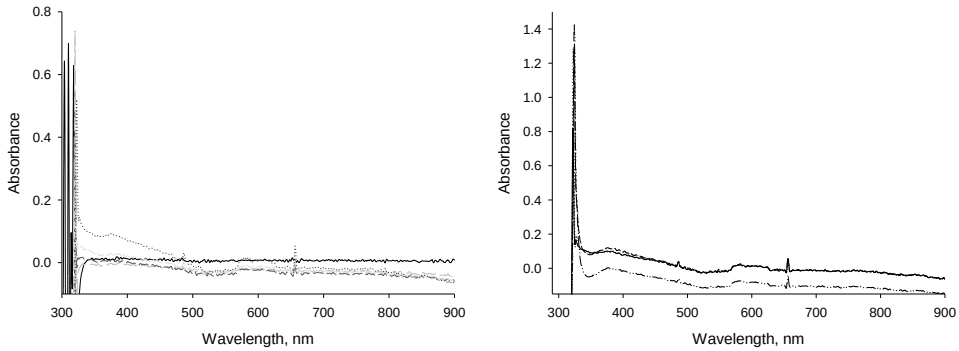

Figure 6.2- Left: Spectral changes upon addition of two equivalents of $[Cu(tetrakis)]PF_6$ to a ligand **6.10a** solution at -88 °C; Right: Effect of temperature increase on the spectum.

Spectrophotometric binding studies were performed with the ligand **6.10a**. In this case, after the addition of the Cu(I) salt, a poorly defined broad should appeared in the region between 330 and 360 nm even when the temperature was kept at -88 °C. The oxygenation reaction was monitored overnight, but no spectral changes occurred. This spectral variations were not affected by temperature increase, as the spectra did not show any changes when the mixture was brought to -30 °C. This band is so attributable to charge transfer transition attributable to some Cu(II) species.

6.2. Conclusions

Attempts of synthesizing novel chiral copper complexes, able to stabilize the side-on μ-η^2:η^2 Cu(I)-O_2 complex, were done, using histidine as starting amino acid. Dinucleating ligand, inspired by L66/MeL66 ligand, was not able to stabilize enough the Cu(I) complex, which underwent oxidation rather than oxygenation. Optimization of the ligand structure could improve the donating effect of involved nitrogens, making the characterization of the peroxo-complex possible.

6.3. Experimental section

Materials and methods

All reagents and solvents from commercial sources were of the highest purity available and were used as received.. NMR spectra were recorded on a Bruker AVANCE 400

spectrometer, operating at 9.37 T, with 400.13 and 100.6 MHz proton and carbon-13 frequencies, respectively. Data acquisition and processing were performed using a standard Bruker software package (Topspin 1.3). UV-Vis spectra were recorded on an Agilent 8453 spectrophotometer. Mass spectra were recorded using a Thermo-Finnigan LCQ ADV MAX spectrometer.

General procedures

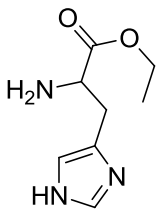

*Synthesis of ethyl 2-amino-3-(1H-imidazol-4-yl)propanoate (***6.4**) Histidine dihydrochloride (1.3 mmol) was suspended in absolute ethanol and cooled at 0 °C, then thionyl chloride was added (13 mmol) slowly. The reaction was refluxed for six hours, then uenched removing the solvent by rotary evaporation. The product was used without further purification.
ESI-MS: +184 [M-H^+].

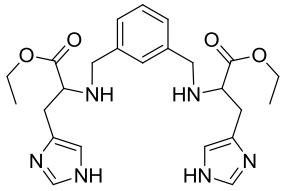

*Synthesis of diethyl 2,2'-((1,3-phenylenebis(methylene))bis(azanediyl))bis(3-(1H-imidazol-4-yl)propanoate) (***6.5***)* **6.4** (0.9 mmol) was dissolved in 6 mL of dichloromethane, then triethylamine was added (1.1 mmol), followed by isophtaldialdehyde (0.5 mmol). The reaction was left stirring overnight at room temperature, then sodiumtriacetoxyborohydride was added (1 mmol), stirring two more hours at room temperature. The reaction was monitored by mass spectroscopy, until disappearance of starting material, then was quenched by removing the solvent by rotary evaporation. Crude product was purified by column chromatography with silica as stationary phase and 95:5 dichloromethane:methanol + 0.5% of aqueous ammonia solution (30 %). ESI-MS: + 465 [M-H^+], 2+ 233 [M-$2H^+$].

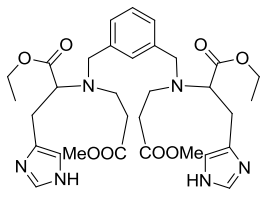

*Synthesis of ethyl 2-((3-(((3-(1H-imidazol-4-yl)-1-methoxy-1-oxopropan 2-yl)(3-methoxy-3-oxopropyl)amino)methyl)benzyl)(3-methoxy-3-oxopropyl)amino)-3-(1H-imidazol-4-yl)propanoate (***6.6***)* **6.5** was dissolved in methylacrylate and heated to bland

reflux overnight. The reaction was queched by removing the solvent by rotary evaporation, then purified with 95:5 dichloromethane:methanol + 0.5 % of aqueous ammonia solution (30 %). ESI-MS: + 641 [M-H$^+$].

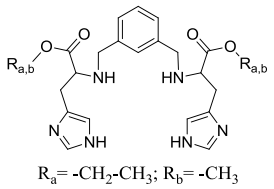

*Synthesis of dimethyl 2,2'-((1,3-phenylenebis(methylene))bis(azanediyl))bis(3-(1H-imidazol-4-yl)propanoate) (***6.1***)* The followed synthetic pathway was identical to **6.5** one. ESI-MS: + 437 [M-H$^+$].

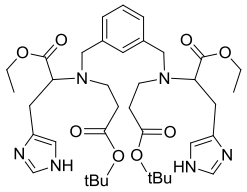

*Synthesis of diethyl 2,2'-((1,3-phenylenebis(methylene))bis((3-(tert-butoxy)-3-oxopropyl)azanediyl))bis(3-(1H-imidazol-4-yl)propanoate) (***6.8a**) Compound **6.5** (0.109 g) was dissolved in 1 mL of tert.butyl acrylate ad 1 mL of methanol, then heated to bland reflux overnight. Solvent was eliminated by rotary evaporation then crude product was purified by column chromatography using silica as stationary phase and a gradient of 85:15:10 +1 % of aqueous ammonia solution (30 %) ethyl acetate:hexane:methanol to 85:15:20 ethyl acetate:hexane:methanol +1 % of aqueous ammonia solution (30 %).
ESI-MS: + 725 [M-H$^+$].

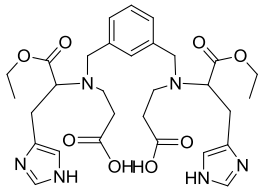

*Synthesis of 3,3'-((1,3-phenylenebis(methylene))bis((1-ethoxy-3-(1H-imidazol-4-yl)-1-oxopropan-2-yl)azanediyl))dipropanoic acid (***6.9a**) Compound **6.8a** (0.021 g) was dissolved in a 1:1 mixture of dichloromethane:trifluoroacetic acid (1 mL) and stirred at room temperature for one hour. Reaction was stopped removing solvent by rotary evaporation. ESI-MS: + 613 [M-H$^+$]; 2+ 307 [M-2H$^+$].

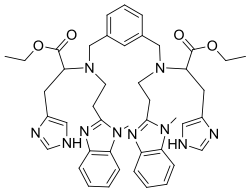

*Synthesis of diethyl 2,2'-((1,3-phenylenebis(methylene))bis((2-(1-methyl-1H-benzoimidazol-2-yl)ethyl)azanediyl))bis(3-(1H-imidazol-4-yl)propanoate) (***6.10a***)* 2-(1H-benzotriazol-1-yl)-1,1,3,3-tetramethyluronium hexafluorophosphate (HBTU, 0.024 g) was suspended in acetonitrile (0.7 mL) and cooled at 0 °C. A solution of **6.9a** (0.018 g) in 0.3 mL of acetonitrile was added, then the mixture was left stirring for 15 minutes at 0 °C, bubbling argon. After this time, N-methylorthophenylendiamine (0.0078 g, 7.2 µL) and diisopropylethylamine (11 µL) were added, then the reaction was left stirring

overnight at room temperature under air-oxygen atmosphere. Acetonitrile was removed by rotary evaporation, and 1 mL of glacial acetic acid was added to the crude product, refluxing for 4 h. Reaction was stopped by removing acetic acid by rotary evaporation and crude product was then purified by column chromatography using silica as stationary phase and 95:5 dichloromethane:methanol + 0.5 % of aqueous ammonia solution (30 %) as eluent. Purified product was then treated with ethyl acetate to give a pale brown oil as final pure product.

ESI-MS: + 785, ^{1}H NMR (400 MHz, MeOD) δ 7.61 (dd, 2H), 7.50 (s, 2H), 7.46 – 7.38 (m, 2H), 7.34 – 7.21 (m, 7H), 6.84 (s, 2H), 4.50 (m, 4H), 4.02 (q, 4H), 3.75 (d, 2H), 3.65 – 3.53 (m, 10H), 3.41 (m, 4H), 2.86 (dd, 4H), 1.13 (t, 6H).

References

1- (a) S. Palavicini, A. Granata, E. Monzani, L. Casella, *J. Am. Chem. Soc.* **2005**, 127, 18031-1836; (b) J. Schottenheim, N. Fateeva, W. Thimm, J. Krahmer, F. Tuczek. *Z. Anorg. Allg. Chem.* **2013**, 639, (8-9), 1491–1497. (c) C. Wilfer, P. Liebhäuser, A. Hoffmann, H. Erdmann, O. Grossmann, L. Runt, E. Paffenholz, R. Schepper, R. Dick, M. Bauer, M. Dìrr, I. Ivanovic´-Burmazovic´, S. Herres-Pawlis, *Chem. Eur.J.*, **2015**, 21,17639 –17649. (d) A.E.-M.M. Ramadan, M. M. Ibrahim, S. Y. Shaban, *Journal of Molecular Structure*, **2011**, 1006, 348–355. (e) C. Wilfer, P. Liebhäuser, A. Hoffmann, H. Erdmann, S. Herres-Pawlis, *Eur. J. Inorg. Chem.* **2015**, 494–502. (f) For a review: J. N. Hamann, B. Herzigkeit, R. Jurgeleit, F. Tuczek, *Coordination Chemistry Review*, **2016**, in press.

2- E. I Solomon.; U. M. Sundaram,; T. E. Machonkin, *Chem. Rev.* **1996**, 96, 2563–2605.

3- L. Q. Hatcher, K. D. Karlin, *J. Biol. Inorg. Chem.* **2004**, 9: 669–683.

4- P. L. Holland, W. B. Tolman, *Coordination Chemistry Reviews*, 190–192, **1999**, 855–869.

5- G. Battaini, M. De Carolis, E. Monzani, F. Tuczek, L. Casella, *Chem. Commun.*, 2003, 726–727.

6- (a) L. Casella, O. Carugo, M. Gullotti, S. Garofani, P. Zanello, *Inorg. Chem.* **1993**, *32*, 2056–2067; (b) L. Casella, E. Monzani, M. Gullotti, D. Cavagnino, G. Cerina, L. Santagostini, R.Ugo, *Inorg. Chem.* **1996**, *35*, 7516-7525.

7- A. Torò, P. P. Nowak, P, Deslongchamps, *J. Am. Chem. Soc.*, **2000**, 122, 4526-4527.

Chapter 7. General conclusions

7. General conclusions

Activation of small molecules to promote oxidation reactions is still considered a hot topic, as its potential role in substituting polluting and dangerous reactants with mild and available dioxygen. Inspired by natural enzymes, which are able to promote this activation, bioinorganic chemists have been so far focusing their attempts in developing synthetic analogues. Most of enzymes, due to their intrinsic nature, accompany their efficiency with stereo-selective activity. To this aim, my research project was focused on developing chiral dinucleating ligands for copper, whose complexes could activate oxygen and promote stereodiscriminating oxydation of chiral substrates. Design for ligand L55Bu$_4$*, reported in **Chapter 2** derived from the aim to introduce chirality in the skeleton of a previously studied biomimetic system, Cu$_2$L55. Ligand L55 consists of a tetrabenzimidazole core, symmetric from the coordinative point of view. Asymmetry was introduced by substituting the methyl groups on the benzimidazole with 2-methyl-butyl chains. The dinuclear copper(II) complex was studied in its capability to discriminate oxidation of chiral catechols (catecholase activity) using a set of enantiomeric pairs of substrates of biological relevance. The best performance was achieved with the enantiomeric pair of L-/D-dopa methyl ester. As $[Cu_2(L55)]^{4+}$ was found to catalyze sulfoxidation of aryl sulphides, the similarities of $[Cu_2(L55Bu_4*)]^{4+}$

with this system aimed the purpose to integrate enantioselection in this activity, but thioanisole sulfoxidation gave both poor yield and negligible enantiomeric excess.

In **Chapter 3** with the synthesis of the ligand mXPhI (acronym for m-xylyl-phenylalanine-imidazole), I devised a new versatile synthetic pathway for L55-like systems, exploiting the chirality of amino acids to generate efficient systems for catecholase activity. We studied the oxidation of biogenic catechols and the best results were obtained for the couple L/D-dopa methyl ester, in which the two enantiomers also seemed to have a different approach to the catalyst. Oxygenation of phenols needs to be more extensively investigated. Studies on asymmetric oxidation of aryl sulfide showed this system to be the first one capable to promote oxygen-mediated sulfoxidation with significant enantiomeric excess (~ 40 %). Future perspective for this highly reactive asymmetric catalyst could be directed to asymmetric oxidation of other substrates, such as olefines, or in cross-coupling reactions.

A new chiral ligand based on histidine as building block was synthesized, starting from the more complex precursor PHI and modifying either the linker between the two tridentate units or the number of coordination sites. EHI (acronym for ethylendiamide-hisitine-imidazole), and its related dicopper complexes were fully characterized by NMR, MS, Uv-Vis and CD spectroscopy, as reported in **Chapter 4**. The dinuclear copper complex of EHI was also tested in its capability to mimic the activity of tyrosinase, both in catecholase and monophenolase activities. Studies of diphenolase activity showed an interesting dependence of the catalysis from the concentration of the complex. Mono-oxygenation reaction studies showed that obtained product are derived from radical reactions. Determination of magnetic susceptibility and magnetic moment with Evans' method showed poor cooperation between the two copper sites, that could justify the tendency to favor radical reactions rather then tyrosinase-like pathways.

In **Chapter 5**, I reported the synthesis of ligand mXHI (acronym for m-xylyl-histidine-imidazole), which summarized the coordinating characteristics of the previously described EHI, integrated with a different linker between the two coordinating arms, replacing the rigid bis-amide moiety to the more flexible *m*-xylyl residue. $[Cu_2(mXHI)]^{4+}$ attitude to promote stereo-differentiating oxidation of chiral catechols was investigated on a set of enantiomeric catecholic pairs of biological interest. Best results were obtained with the pair L-/D-DopaOMe, as L-enantiomer was oxidized with

large preference compared with the D-enantiomer (Rk/k% = 72 %). Mono-oxygenation reactions of achiral phenols showed that oxidation of electron-rich phenols follows radical pathway to give coupling products. With less polar phenols (β-naphthol), oxidation occurs according to monophenolase pathway, as confirmed by 18-O insertion experiments. Stereoselective oxidation of tyrosine derivatives was also performed and kinetic experiments showed a preference for the L-enantiomer. $[Cu_2(mXHI)]^{4+}$ was also found to catalyze oxidation of organic sulphides in the presence of hydroxylamine as reducing agent, but sulfoxide was obtained as a racemic mixture.

Starting from the analysis of the relationship between the structure and the activity of these biomimetic complexes, the our group archetype $[Cu_2(L66)]^{n+}$ inspired, in **Chapter 6**¸ the synthesis of new chiral congeners. The flexibility of the six-membere chelate rings, with the high donor effect of benzimidazole is related to an higher stability of reactive catalytic intermediates. A new synthetic pathway has been ideated to replicate this attitude, integrated with asymmetry of the ligand skeleton, devising a dinuclear L66-like system. Unlikely to $[Cu_2(L66)]^{2+}$, Cu(I) complex of this ligand was not able to generate a stable μ-η^2:η^2-peroxo species, reacting with air oxygen. This low stability could be due to the increased acidity of imidazolic hydrogen after coordination to copper, which could protonate the unstable $Cu\text{-}O_2$ species, degrading it. Following the same strategy, further studies could be centered on N(τ)-protected histidine as starting amino acid.